Université catholique de Louvain
Faculté des Sciences
Département de Physique

A Relativistic BCS Theory of Superconductivity

**An Experimentally Motivated Study
of Electric Fields in Superconductors**

Damien BERTRAND
Dissertation présentée en vue de l'obtention
du grade de Docteur en Sciences

Composition du jury:

Prof. Jean-Pierre Antoine, président
Prof. Jan Govaerts, promoteur
Prof. François Peeters (Univ. Antwerp)
Prof. Jean-Marc Gérard
Prof. Ghislain Grégoire
Prof. Luc Piraux
Prof. Philippe Ruelle

Juillet 2005

Petit bout d'Homme qui se construit,
Ce travail, je te le dédie.

Acknowledgements

<div style="border: 1px solid black; padding: 1em; text-align: center;">

CONTENTS

</div>

LIST OF FIGURES

Introduction

Initially motivated by the realisation of a novel kind of particle detector, whose principle of detection is based on the quantum coupling between the magnetic moment of particles with the quantised magnetic field trapped inside small superconducting loops, we study in detail some of the properties of conventional superconductors at the nanoscopic scale, that is, for samples whose dimensions are comparable to the characteristic lengths associated to the superconducting phenomena.

The realisation of such a detector device requires a precise understanding of the superconducting mechanisms at nanometric scales and, in particular, their dynamic behaviour in a range of time scales characteristic of the relativistic domain. From that perspective, given that the phenomenological Ginzburg-Landau theory of superconductivity has often been proved to be successful for describing conventional Type-I superconductors, it is therefore considered as a natural starting point for the present study.

A natural framework for extending this theory to the relativistic domain is the U(1) local gauge symmetry breaking of the Higgs model, which provides a Lorentz-covariant extension of the well-known Ginzburg-Landau equations of motion. Even in a stationary situation, this covariant extension leads to the prediction of specific properties, naturally associated to the electric field, which plays a role dual to that of the magnetic field in Maxwell's equations.

That in the presence of electric fields a relativistic formulation of superconductivity may be called for is also motivated by the following argument. In physical units, the quantities $\mathbf{E}/c$ and $\mathbf{B}$ have the same dimensions, $\mathbf{E}$ and $\mathbf{B}$ being of course the electric and magnetic fields. Hence one could expect that in the non-relativistic limit $c \to \infty$, all electric field effects would decouple. It thus appears that a study of superconductivity involving electric fields must rely from the outset on a relativistic formulation.

In particular, the covariant formulation of the Ginzburg-Landau model suggests the penetration of an external electric field inside the sample, over a finite penetration length whose numerical value is identical to the well-known magnetic penetration length. The immediate consequence is a modification of the phase diagram associated to the critical points of such systems, with the apparition of a critical electric field whose features are similar to those of the usual critical magnetic field, and which retains finite values over the whole range of temperatures between $T = 0$ K and the critical temperature T_c.

On basis of this phase diagram, a specific criterion has been identified for a given geometry of a mesoscopic sample in properly oriented external electric and magnetic fields in a stationary configuration; as a matter of fact, numerical simulations for that particular configuration show a possible experimental discrimination between the usual and the covariant formulations of the Ginzburg-Landau theory.

The manufacturing of sub-micrometric devices requires lithography techniques: the experimental set-up was therefore realised in collaboration with UCL's Microelectronics "DICE" Laboratory, which has the appropriate infrastructure and extensive know-how in that field. Several successive prototypes were developed and a final set-up consisting of an aluminum slab equipped with the appropriate electric contacts, to be subjected to a normal electric field as well as a tangential magnetic field, was finally selected for its correspondence with the parameters considered for the aforementioned numerical simulations. Experimental measurements at very low temperatures were then carried out using a 3He cryostat. The superconducting-normal phase transition was monitored in various conditions of electric and magnetic fields applied onto the device. After a complete series of measurements, it was established that no apparent dependence on the electric field arises for any critical parameter, suggesting that an external electric field does not affect

significantly the superconducting state, in total contradiction not only with the simulations of the covariant theory, but also with the usual Ginzburg-Landau framework.

The results of the experimental measurements suggest that the external electric field is actually prevented from entering the sample not by the super-conducting condensate, but by a rearrangement of *other* charge carriers into the sample. This hypothesis calls naturally for a microscopic understanding of the superconducting mechanisms through a detailed study of the BCS theory in a relativistic covariant framework. This complete study was developed in the functional integral formalism of Finite Temperature Field Theory: after the identification of the relevant coupling between electrons, which reproduces the usual BCS scalar coupling in the nonrelativistic limit, we gave a second-order perturbative expansion of the effective action for the density of electron pairs in the saddle-point approximation, allowing to identify the relativistic generalisation of the magnetic penetration length and the superconducting extension of the electrostatic Thomas-Fermi screening length. Numerical calculations of these two characteristic lengths fully explain the experimental results and emphasize the specific aspects that are not taken into account in the Ginzburg-Landau theory or its covariant extension.

This thesis is organised as follows. After an introductory chapter presenting the standard features of Superconductivity, the second chapter is devoted to the Lorentz-covariant generalisation of the Ginzburg-Landau theory, and discusses some novel ring-like magnetic vortex solutions to the stationary Ginzburg-Landau equations, whose stability properties remain an open issue. The next chapter describes the technical realisation of the appropriate experimental set-up as well as the measurement procedure at very low temperatures, and concludes with the unexpected results. The three following chapters constitute the second part of the present work, devoted to the relativistic extension of the BCS theory: a first chapter motivates the choice of the appropriate ingredients and the methods specific to the functional approach which was followed. The next chapter is more technical and presents the detailed results for the lowest order, the first and second order perturbative expansions of the effective action. Finally, the last chapter contains the formal derivation and numerical analyses of the relevant characteristic penetration lengths.

The present thesis has a strong theoretical orientation, although containing a fully original and complete experimental procedure, and it is therefore aimed at the same time both to experimentalists and theoreticians alike. It also combines concepts from Condensed Matter Physics and from Field Theory. Therefore, in order not to overcrowd the text with solid state basics and mathematical interludes, these elements have been grouped at the end of the work in a series of appendices. A first appendix has also been added to summarize all conventions and notations used throughout this thesis. The main text should however be fully understandable without turning to the appendices for readers who are familiar with all the concepts used.

1

Introduction to Superconductivity

Progress of Science depends on new techniques, new discoveries and new ideas.
Probably in that order.

Sydney Brenner, biologist.

This chapter introduces in a rather conventional way the basics on super-conductivity, with a slightly more detailed description of the phenomenological Ginzburg-Landau and the microscopic BCS models, as the purpose of this work is to provide a generalised formulation for these theories.

Superconductivity is a wide ranging and active field in which experimental as well as theoretical improvements are published every day in numerous papers. A global summary of all the aspects and the current status of the knowledge of superconductivity is therefore well beyond the scope of this chapter, and we shall restrict to a pedagogical presentation of so-called Type-I superconductors and their general properties.

1.1 Early discoveries

The phenomenon of Superconductivity was discovered in 1911 by H. Kamerlingh Onnes, whose "factory" for producing liquid helium had provided a considerable advance in experimental low temperatures physics. In his quest for the *intrinsic* resistance of metals, he surprisingly observed that the electrical resistance of mercury drops abruptly to zero around 4 K [1].

He called this unexpected feature *superconductivity*, as a special and unknown way of carrying electric currents below that *critical temperature*. This was the beginning of one of the most exciting adventures in physics throughout the 20th century, having seen the award of numerous Nobel prizes[1].

For the next decades, several other metals and compounds were shown to exhibit superconductivity under very low temperatures, always below 30 K. Soon after his discovery, H.K. Onnes noticed that superconductivity was influenced by an external magnetic field, bringing back a sample to its normal resistive state at sufficiently high values. A superconductor was thus characterised by a spectacular feature – the total loss of resistivity – and two critical parameters – a temperature and a magnetic field.
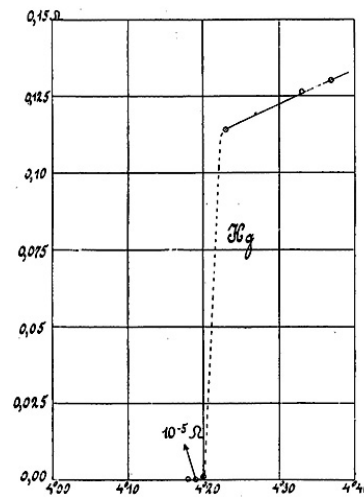
Figure 1.1: Resistivity of mercury as a function of temperature [3].

In 1933, W. Meissner and R. Oschenfeld discovered that superconductors also have the property of expelling a magnetic field, this perfect diamagnetism being further named the *Meissner effect* [4]. As a matter of fact, the magnetic field disappears as perfectly as the resistivity drops to zero below the critical temperature, but this new feature can by no means be explained by the loss of resistivity: both features are independent and provide the experimental twofold definition of the superconducting state.

---

[1]H.K. Onnes himself received the prestigious prize in 1913 for "his investigations into the properties of substances at low temperatures", but with a particular insistence on the liquefaction of helium and only a few words about superconducting Hg [2].
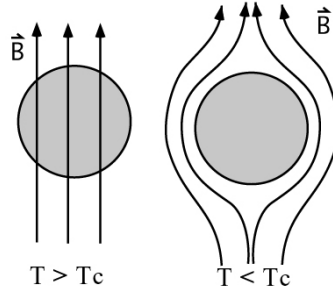
Figure 1.2: The Meissner effect for a superconducting sample.

1.2   London theory

The superconducting transition was so surprising that many theorists, including famous names such as Einstein or later Feynman, immediately tried to understand the phenomenon. At that time, amongst all audacious theories making their first steps, the only well-established theoretical framework was Maxwell's unified view of electromagnetism: for fields in vacuum,

$$\boldsymbol{\nabla} \cdot \mathbf{E} = \frac{\rho}{\varepsilon_o} \, ,$$
$$\boldsymbol{\nabla} \times \mathbf{E} + \partial_t \mathbf{B} = 0 \, ,$$

$$\boldsymbol{\nabla} \cdot \mathbf{B} = 0 \, ,$$
$$\boldsymbol{\nabla} \times \mathbf{B} - \frac{1}{c^2} \partial_t \mathbf{E} = \mu_o \mathbf{J} \, , \tag{1.1}$$

where **E** and **B** are respectively the electric and magnetic field, ρ is the density of source charges and **J** is the current density[2]. H. and F. London searched for a constitutive relation, different but somewhat related to Ohm's law, which couples to Maxwell's equations and reproduces the experimental facts of superconductivity. To this end, they considered the Drude model (see Appendix B) for a perfect conductor, namely with an infinite mean free path [6]. They obtained a system of coupled relations for the current density **J**:

$$\mathbf{E} = \partial_t \left(\Lambda \mathbf{J} \right) \, ,$$

$$\mathbf{B} = -\boldsymbol{\nabla} \times \left(\Lambda \mathbf{J} \right) \, , \tag{1.2}$$

---

[2]The Maxwell equations are given in MKSA units of the International System, for which $\mu_o \varepsilon_o = c^{-2}$. In a medium, they also take a slightly different form, that will not be described here; see for example [5].

with $\Lambda = \frac{m}{n_s q^2}$, m and q being respectively the mass and the electric charge, and n_s the density of the mysterious (for that time) superconducting carriers[3]. The first relation is nothing but the mathematical expression of the perfect conductivity, while the second leads to the Meissner effect. Both equations state that the so-called *supercurrent* can exist only at the surface of the superconducting sample in order to screen any external magnetic field, and dies off exponentially inside this material so that the magnetic field vanishes essentially over a *penetration length* λ_L such that

$$\lambda_L^2 = \frac{m}{\mu_o n_s q^2}.$$ (1.3)
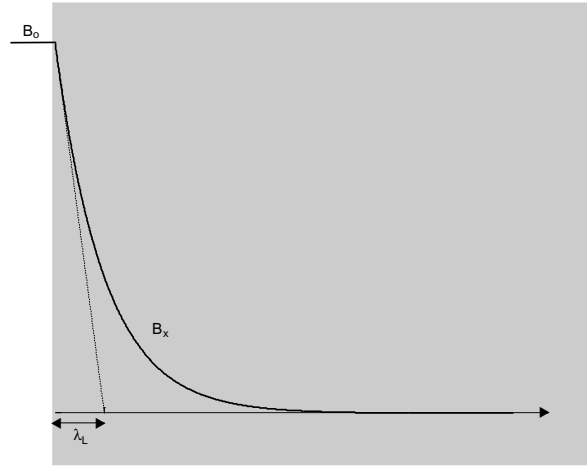
Figure 1.3: The applied magnetic field B_o enters the superconducting sample and decreases exponentially over the London penetration length λ_L.

It is important to note that when H. and F. London published their theoretical results, this exponential decay of the field had been observed experimentally, and an empirical dependence of that characteristic length with temperature was given by C. Gorter and H. Casimir [8]:

$$\lambda(T) \approx \frac{\lambda(0)}{\sqrt{1 - \left(\frac{T}{Tc}\right)^4}}$$ (1.4)

---

[3]There has been a historical confusion in the exact values of *m* and *q*, which were considered as the mass and charge of the electron until the introduction of Cooper pairs. At the time the Londons published their model, precise values of the parameters could not be assigned, and they obtained orders of magnitudes that matched with Gorter and Casimir's experiments [7].

where T_c is the critical temperature for superconductivity. While the Londons did not know exactly how to identify the density of "super-electrons", they naturally considered that all the conduction electrons should take part in the mechanism at least at absolute zero, identifying the limiting value[4]

$$\lambda_L(0) = \sqrt{\frac{m}{\mu_o n q^2}} \,.$$ (1.5)

The London equations involve a density of superconducting charged particles which is uniform and constant in the sample. Reproducing Gorter and Casimir's measurements along the different crystallographic axes of a tin sample, Pippard showed a manifest anisotropy of the penetration length and emphasised the need for a local theory [9]. However the next successful theory still provided only a macroscopic picture of the phenomenon.

1.3 Phenomenological Ginzburg-Landau theory

In the late 1940s, L. Landau elaborated a thermodynamic classification of phase transitions. *First-order transitions* involve a latent heat, that is, a fixed amount of energy which is exchanged between the system and its environment during the phase transition. Since this energy cannot be exchanged instantaneously, first-order transitions are characterised by a possible mixing of different phases; one typical example is boiling water, for which liquid and vapour phases can coexist. The free energies of the two phases are identical at the transition point, since the energy which is gained or released only operates the change in the structure of the material. However, the first derivatives of the free energy are discontinuous.

In *second order transitions*, one phase evolves into the other so that both phases never coexist. Their first derivatives are continuous, and second derivatives are discontinuous. They generally admit one ordered phase and a disordered one: for example in the ferromagnetic transition, spins have a random orientation in the paramagnetic phase and are aligned in a preferred direction in the ferromagnetic phase. This observation led Landau to assume that the order of the transition depends on the form of a thermodynamic free-energy functional expressed in terms of an *order parameter*. At the critical point, the free energy for a first-order transition hence exhibits two simultaneous

---

[4]This relation remains valid when one considers electrons pairs instead of individual electrons, as it is easily seen when substituting $n_s = n/2$, $q = 2e$ and $m = 2m_e$.

minima corresponding to the two phases, while the free energy of a second-order transition has only one minimum associated to one given phase.

In 1950, L. Landau and V. Ginzburg applied this successful framework and achieved a powerful phenomenological theory that could explain superconductivity as a second order phase transition [10].

The theory relies on a space dependent *order parameter* ψ which is supposed to vanish in the normal state, but to take some finite value below the critical temperature; it is usually normalized to the density of supercharge carriers n_s already introduced in the London theory[5]:

$$\psi(\mathbf{x}) = \sqrt{n_s(\mathbf{x})}\, e^{i\theta(\mathbf{x})}.$$

It is further assumed that the thermodynamic free energy F of the system is an analytic function of n_s, so that its value F_s in the superconducting state can be expanded in power series[6] around its value in the normal state F_n, close to the critical temperature,

$$F_s = F_n + \alpha n_s + \frac{\beta}{2} n_s^2 + \dots \quad . \tag{1.6}$$

It follows that the Ginzburg-Landau (GL) theory is strictly valid only close to the critical temperature[7]. A dynamical approach requires the introduction of gradients of the order parameter, which are combined with the electromagnetic field in such way that local U(1) gauge invariance is preserved. Finally, the free energy of the normal state can involve different definitions, and may always be shifted by a constant, so that in general one is interested in the *condensation energy $F_s - F_n$*:

$$F_s - F_n = \alpha|\psi|^2 + \frac{\beta}{2}|\psi|^4 + \frac{\hbar^2}{2m}\left|\left(\boldsymbol{\nabla} - \frac{iq}{\hbar}\mathbf{A}\right)\psi\right|^2 + \frac{(\mathbf{B} - \mathbf{B}_{ext})^2}{2\mu_o} \tag{1.7}$$

where $\mathbf{A}$ is the electromagnetic vector potential. It is now admitted that superconductivity involves paired electrons, so that we may identify the electric charge $q = 2e = -2|e| < 0$ in the term accompanying the gradient. For the same

---

[5]At the time when the Ginzburg-Landau theory was being developed, the nature of the superconducting carriers was yet to be determined.

[6]At this stage, no definite statement has to the radius of convergence of such a series expansion can be made; this issue depends on the values of the successive coefficients α, β, $\dots$

[7]In our local research group, G. Stenuit developed a computer analysis of lead nanowires directly built on the GL theory; in particular he showed that at least for such superconducting states the theory remains valid even far from the critical temperature [11].

reason, one generally considers $m = 2\,m_e$ as the mass of one pair of electrons[8]. Assuming the superconducting state to be energetically more favourable than the normal state below the critical temperature, this energy difference must be kept negative. The quantities α and β are phenomenological parameters whose signs are fixed by analysis of the power expansion: β must be positive, otherwise the minimal energy would be obtained for arbitrary large values of the order parameter, and the only way to get a nontrivial value of the order parameter which minimizes the energy is to assume that α is negative (Fig. 1.4). In principle both parameters are temperature dependent: one can show that α varies as $1 - t$, with $t = T/Tc$, close to the critical temperature, and β as $(1 - t^2)^{-2}$ and is usually taken to be constant [13].
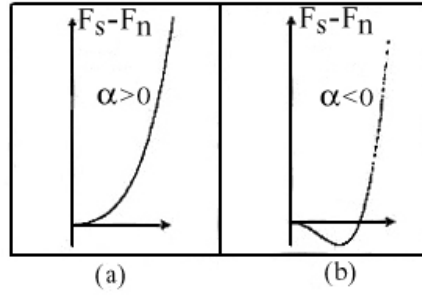
Figure 1.4: The shape of the potential term in the GL free energy depends on the sign of the parameter α: below the critical temperature, a minimum obtained for a non-zero density of charge carriers can be observed only if α is negative (b-graph).

Minimizing the free energy with respect to fluctuations of the order parameter and the vector potential respectively, leads to the celebrated *Ginzburg-Landau equations*

$$\alpha\psi + \frac{\beta}{2}|\psi|^2\psi - \frac{1}{2m}\left(\nabla - \frac{iq}{\hbar}\mathbf{A}\right)^2\psi = 0\,,$$

$$(1.8)$$

$$\mathbf{J} = \frac{1}{\mu_o}\nabla \times \mathbf{B} = -\frac{iq\hbar}{2m}(\psi^*\nabla\psi - \psi\nabla\psi^*) - \frac{q^2}{m}|\psi|^2\mathbf{A}\,,$$

---

[8]Actually, the identification of m as twice the electron mass assumes a model involving free electrons; to be more accurate, we should consider an effective mass m^* which takes into account possible effects due to the crystal lattice. However, it has been proved experimentally that the ratio e/m remains unchanged within 100 ppm, so that hypothesis of free electrons may be retained for most typical (Type I) superconductors, allowing to consider $m = 2m_e$ [12, 13].

with the additional boundary condition

$$\left(\boldsymbol{\nabla} - \frac{iq}{\hbar}\mathbf{A} \right) \psi \bigg|_{\partial\Omega} = 0 \qquad (1.9)$$

where the subscript $\partial\Omega$ refers to the component normal to the sample surface. The first relation is recognized as the Schrödinger equation for the superconducting carriers; the second generalizes London's constitutive relation including possible spatial variation of ψ. They allow for the identification of two characteristic lengths: the penetration length λ is obtained by comparing the second GL equation with the London equations (1.2) and a second parameter, called the *coherence length* ξ, measures the extension in space where the variation of ψ is significant. The two characteristic lengths are given by

$$\begin{aligned}
\lambda_{GL} &= \sqrt{\frac{m\beta}{\mu_o q^2 |\alpha|}} \quad \propto \frac{1}{\sqrt{1-t^4}} \ , \\
\xi_{GL} &= \sqrt{\frac{\hbar^2}{m|\alpha|}} \quad \propto \frac{1}{\sqrt{1-t}} .
\end{aligned} \qquad (1.10)$$

They can further be combined into a dimensionless ratio which is known as the *Ginzburg-Landau parameter*

$$\kappa = \frac{\lambda}{\xi}$$

which is essentially constant close to T_c. One must take care of the temperature variations of the GL characteristic lengths, since it has been shown to be strongly influenced by the purity of the sample; this is not the purpose of the current analysis, but the interested reader is referred to Ref. [13] for a complete description.

As a consequence of the GL formalism, one can evaluate numerically the limiting values for the supercurrent and the external magnetic field, namely the values at which the energy difference becomes positive. Qualitatively, critical temperature, current and magnetic field are correlated in the the *phase diagram* depicted in Fig. 1.5.

	T_c	$B_c(0)$	λ_o	ξ_o	$gN(0)$
	(K)	gauss	(nm)	(nm)	N/A
Pure materials					
Al	1.175	100	50	1600	0.18
Sn	3.721	300	51	230	0.25
In	3.405	280	64	440	0.30
Pb	7.19	800	39	83	0.39
Nb	9.25	1270	44	40	0.30
Compounds					
Nb_3Ge	23		3		
Ceramic cuprates					
$YBa_2Cu_3O_7$	93	10 000	130	1.5	0.66

Table 1.1: Experimental values of superconducting parameters for some typical substances: T_c is the critical temperature, B_c is the critical magnetic field, λ_o and ξ_o are the extrapolated penetration and coherence lengths at zero temperature, $gN(0)$ is the BCS coupling constant (see section 1.5)[14].
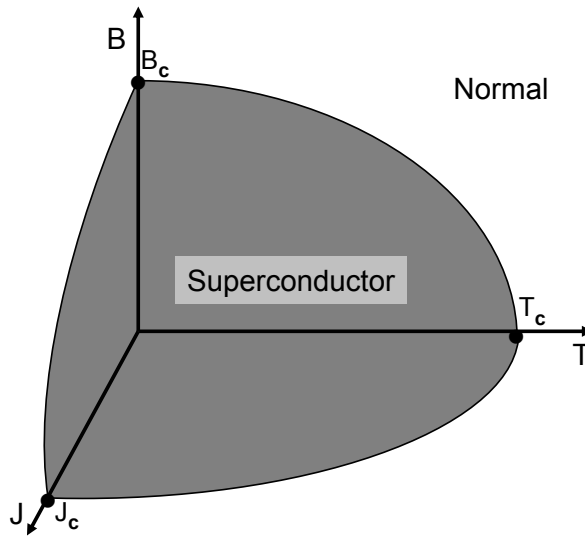
Figure 1.5: Phase diagram of a superconducting material: inside the quarter of sphere delimited by the critical temperature, current and magnetic field, the sample is in the superconducting state; outside it recovers the normal phase.

1.4   Abrikosov vortices

An additional consequence of the GL theory is the possibility of classifying the superconductors into two classes with different behaviours when subjected to an external magnetic field. Materials with a parameter $\kappa < 1/\sqrt{2}$ are named *type I* superconductors, those with $\kappa > 1/\sqrt{2}$ belonging to the *type II* family. The complete description of type II materials was given in 1957 by A.A. Abrikosov, who predicted the possibility for the magnetic field to penetrate samples along flux lines in a periodic arrangement [15]. He was rewarded with the 2003 Physics Nobel prize for that work. When raising the external magnetic induction from zero, surface currents appear to keep the material diamagnetic, up to a first critical value denoted H_{c1}. For higher values, the magnetic field starts entering the sample through vortices, named from the fact that they are surrounded by circular super-currents which develop in order to screen the magnetic field. Since the Meissner effect excludes the presence of a magnetic field inside a superconductor, one must conclude that vortex cores are in the normal state, with a vanishing value of the order parameter: this is therefore called the "mixed state", where the two phases coexist. Still increasing the magnetic field, the vortices progressively occupy the whole sample until a second critical value H_{c2} where the normal state is completely recovered. Such a *vortex lattice* was first observed in 1967 by U. Essmann and H. Träuble, who sputtered a ferromagnetic powder on a sample of NbSe$_2$ in order to exhibit the lattice pattern [16].

Type II superconductors present a hysteretic behaviour as a function of the external magnetic field: the nucleation of vortices is not identical in increasing or decreasing magnetic fields and occurs somewhat later in the latter case.

In the GL formalism, a direct consequence of the U(1) local gauge symmetry of the wavefunction ψ which describes the order parameter is that the magnetic field entering a type II superconductors is quantized: each vortex carries one *flux quantum* with value

$$\Phi_o = \frac{2\pi\hbar}{q} = 2.07\,10^{-15}\ \text{Wb (SI)} = 2.07\,10^{-7}\ \text{gauss/cm}^2. \qquad (1.11)$$

A regular pattern of vortices each carrying one flux quantum is only one class of solutions to the Ginzburg-Landau equations however. Depending on the size and the shape of the sample, both affecting the boundary conditions to which the equations are submitted, an energically more favourable configuration is sometimes provided by a single *giant vortex* located in the centre
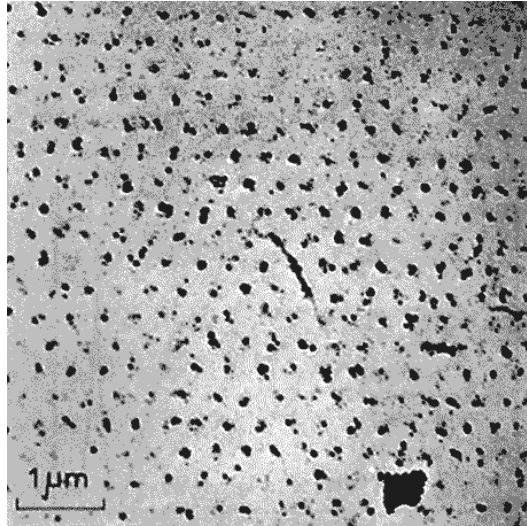
Figure 1.6: Abrikosov lattice of magnetic vortices in a type II superconducting sample [16].

of the sample, which can carry more than one flux quantum. To identify the exact configuration, a flux line is generally called a *fluxoid* and the number of flux quanta it carries the *vorticity*.

The gain in the values of the critical parameters as well as different properties associated to the structure and the dynamics of vortices opened the door to obvious technological challenges; they also initiated a totally specific approach to the study of superconductivity, which is beyond the scope of this work.

1.5 BCS theory

One had to wait until 1957 to see a microscopic model of superconductivity elaborated by J. Bardeen, L.N. Cooper and J.R. Schrieffer[9] [17]. Even if it has been proved to fail in explaining the mechanisms of superconductivity in high-Tc and other exotic superconducting materials, it is still a widely applied formalism to interpret experimental results and a reference basis for other spe-

---

[9]Bardeen, Cooper and Schrieffer earned the Physics Nobel prize for that work in 1972, making Bardeen the first man ever to be awarded the prestigious prize twice in physics, since he had already received the distinction for the discovery of the transistor effect, together with Schottky.

cific theories. Since a substantial part of this work aims at providing a generalised formulation of their theory, it is worth giving here a extended summary of it (see Refs. [13, 14] for a complete description and mathematical details).

The BCS theory is based on the idea of an attractive interaction between electrons due to phonons. It is well known that the Coulomb interaction between two identical electric charges is repulsive. However, in certain circumstances and when described in momentum space, *effective* attraction can bind electrons due to their motion through the ionic lattice. The best intuitive way of understanding this fact is given by the picture of a thick and soft mattress on which heavy balls are thrown rolling: the trajectory of one ball leaves a depression in which a second ball moving on the mattress would fall as if the balls would attract each other. The microscopic picture of superconducting metals is identical: electrons slightly deform the crystal lattice by attracting ion cores, creating an area of greater positive charge density around itself; this excess of positive charge attracts in turn another electron. At a quantum level, those distortions and vibrations of the crystal lattice are called phonons. Provided the binding energy is lower than the thermal excitations of the lattice which would break them up, the electrons remain paired; roughly, this explains why superconductivity requires very low temperatures. Cooper also showed that the optimal pairing is obtained by electrons with opposite spins and momenta.

The attractive interaction between electrons through lattice phonons has been verified experimentally through the isotope effect. When the number of nucleons is increased by addition of neutrons, then the atomic nuclei are obviously heavier, resulting in a greater inertia against the deformation due to the passing of electrons: the consequence for superconductivity is a lower critical temperature. Qualitatively, the critical temperature varies with the mean atomic mass M as $T_c \propto M^{-\alpha}$ with α close to $1/2$. Actually, this dependence had been observed some years before and Cooper's work followed Fröhlich's suggestion that superconductivity might be related to an electronic interaction mediated by the lattice ions [18].

Cooper first introduced the concept of electron pairs –further called *Cooper pairs*– by showing that the Fermi sea of conducting electrons was unstable in the presence of an attractive interaction; he demonstrated the possibility of bound states solutions, with negative energy with respect to the Fermi state, involving two electrons whose momenta belong to a thin shell above the Fermi level. At a quantum level, since the formed pairs have a bosonic character,

nothing prevents them from condensing in the same quantum state: hence the attractive interaction leads to a condensation of paired electrons close to the Fermi level until an equilibrium is reached. The usual picture of BCS super-conductivity is a twofold electron scattering by phonons. In its simplest reali-sation, which we shall also consider in the present study, it is assumed that the process is dominated by exchanges which do not flip the electron spin, hence the so-called s-wave pairing channel[10].

In the second quantisation formalism, we can represent the ground state of a normal metal at zero temperature by

$$\prod_{\mathbf{k} \leq \mathbf{k}_F} c_{-k\downarrow}^\dagger c_{k\uparrow}^\dagger |0\rangle \ ,$$

that is, for normal metals with a spherical Fermi surface, all energy states are completely filled up to the Fermi level and none are occupied above that level. In presence of an attractive interaction however, the BCS ground state becomes

$$|BCS\rangle = \prod_{\mathbf{k}} (u_k + e^{i\theta} v_k c_{-k\downarrow}^\dagger c_{k\uparrow}^\dagger) |0\rangle \tag{1.12}$$

where the parameter v_k (resp. u_k) can be interpreted as the probability that a pair of electrons with momenta $\pm\mathbf{k}$ and opposite spins is occupied (resp. empty). At $T = 0$, v_k is shown to have a behaviour as displayed on Fig. 1.7: some electron states just outside the Fermi level are occupied, and some just below are empty. Since the interaction between electrons is mediated by lattice phonons, the width of the shell around the Fermi level in which the occupa-tion is modified cannot exceed the characteristic energy cutoff for the phonons at the Debye frequency, and is therefore of the order of $2\omega_D$.

In order to identify the energy levels of the ground state and excited states, one considers an interaction term of the form

$$\sum_{k,k'>k_F} g_{kk'} c_{k'\uparrow}^\dagger c_{-k'\downarrow}^\dagger c_{-k\downarrow} c_{k\uparrow} \tag{1.13}$$

where the matrix elements $g_{kk'}$ characterise the scattering of an electron from the momentum state $\mathbf{k}$ to $\mathbf{k}' = \mathbf{k} - \mathbf{q}$ with the simultaneous scattering of another

---

[10]Different attractive interactions with a p-wave or d-wave character involving other types of exchanges may be responsible for high-Tc superconductivity and experimental evidences in favour of d-wave pairing have been found in layered cuprates. These and other so-called "exotic mechanisms" will not be discussed here.
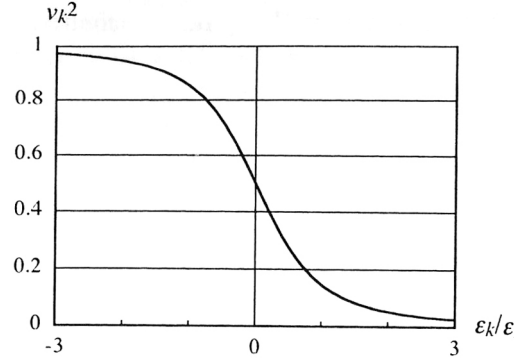
Figure 1.7: Energy dependence of the probability v_k^2 that an electron pair $(\mathbf{k}, +s; -\mathbf{k}, -s)$ is occupied in the BCS ground state at zero temperature near the Fermi level ε_F [14].

electron from $-\mathbf{k}$ to $-\mathbf{k}' = -\mathbf{k} + \mathbf{q}$; here $\mathbf{q}$ is the momentum of the phonon responsible of the interaction. In this expression, we have already omitted all pairs that do *not* include electrons with opposite spins and momenta, which are shown not to contribute to the BCS condensation. Practically, the interaction term is usually simplified by assuming a constant coupling parameter over the whole range of phonon momenta:

$$g_{kk'} = \begin{cases} -V & \text{for } q \text{ such that } \hbar q < \hbar\omega_c \\ 0 & \text{otherwise.} \end{cases} \tag{1.14}$$

As already mentioned, the cutoff energy $\hbar\omega_c$ is taken to be the Debye energy which characterises the range of the phonon energy spectrum. Inserting the simplified expression of the interaction (1.14) into the interaction term and replacing the momentum sum by an energy integration, one obtains energy states of the form

$$E_k = \sqrt{\varepsilon_k^2 + \Delta_k^2} \tag{1.15}$$

with

$$\Delta_k = \begin{cases} \Delta & \text{for } |\varepsilon_k| < \hbar\omega_c \\ 0 & \text{otherwise.} \end{cases} \tag{1.16}$$

In the above expressions, ε_k denotes the single-electron energy relative to the Fermi level; the quantity Δ_k plays the role of an energy gap between the ground state and the lowest excited states for the electrons. In a later reformulation of BCS theory, Bogoliubov interpreted E_k as the energy of *quasiparticles*

$\gamma_k^\dagger = u_k c_{k\uparrow}^\dagger + e^{i\theta} v_k c_{-k\downarrow}$ which create electron-like excitations above the Fermi level or correspondingly hole-like excitations below the Fermi surface [19]. The value of the gap Δ at zero temperature $T = 0$ K is shown to be

$$\Delta(0) \approx 2\hbar\omega_D \, e^{-1/gN(0)} \tag{1.17}$$

where ω_D is the Debye frequency and $N(0)$ is the density of energy states at the Fermi level.

At finite temperature, excitations above the ground state must be taken into account and a physical state will take the form

$$\prod_{\text{occ. states}} \gamma_k^\dagger |BCS\rangle \tag{1.18}$$

which expresses the fact that the quasiparticles progressively fill the excited states according to the Fermi-Dirac probability distribution

$$f(E_k) = (1 + e^{\beta E_k})^{-1} \, , \quad \beta = 1/kT. \tag{1.19}$$

The BCS treatment of the electron pairing allows for the identification of the gap equation at any temperature:

$$\frac{1}{gN(0)} = \frac{1}{2} \int_{-\hbar\omega_D}^{\hbar\omega_D} d\varepsilon \, \frac{\tanh \frac{\beta E_k}{2}}{E_k} \, . \tag{1.20}$$

In particular, the critical temperature is defined as the temperature at which the gap is completely closed; analysis of the previous integral yields

$$kT_c \approx 1.13 \, \hbar\omega_D \, e^{-1/gN(0)}. \tag{1.21}$$

Finally, the temperature dependence of the gap can be obtained by numerical analysis of (1.20) and is shown in Fig. 1.8; close to the critical temperature, the curve can be approximated by

$$\Delta(T) \approx 1.74 \, \Delta(0) \, \left(1 - \frac{T}{T_c}\right)^{1/2} \, , \quad \text{at } T \sim T_c. \tag{1.22}$$

Summarising the main results of the original BCS theory, it is possible to create bound states of electron pairs around the Fermi surface due to their interactions through lattice phonons. This attractive s-wave pairing gives rise to a modified energy spectrum of the conduction electrons, with a gap between
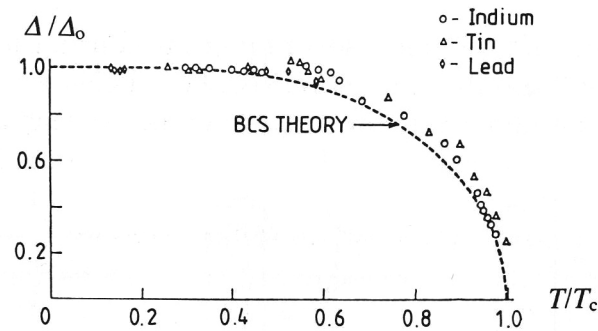
Figure 1.8: Temperature dependence of the energy gap according to the BCS theory, compared to some experimental data for typical superconductors [14].

the ground state and the first excited states corresponding to the minimal excitation energy of Bogoliubov's *quasiparticles*, which correlate electrons with opposite momenta and spins close to the Fermi level. This energy gap has a definite temperature dependence, and the temperature at which it vanishes –hence restituting the original energy spectrum of non-paired electrons– gives the critical temperature for the superconducting transition. The coherence and penetration lengths can also be recovered within this framework and they match with those of the Ginzburg-Landau formalism.

1.6   High Tc superconductors

The next experimental revolution occurred in 1986 when A. Müller and J. Bednorz discovered a superconducting compound with unexpectedly high critical temperature around 30K, while the BCS theory predicted a limit for the critical temperature around 25K [20]. Bednorz and Müller not only received immediately the Physics Nobel prize, they also initiated a galloping quest for superconducting materials with higher and higher critical temperature, offering a manifest interest for industrial applications. Nearly all these materials are layered cuprates and belong to the Type II family, allowing various configuration of vortex lattices.

The discovery of high temperature superconducting (HTSc) materials showed the limits of the BCS theory, which is apparently valid for describing the Type I superconductors, while Type II materials seem to obey different

mechanisms. An even more puzzling discovery was made recently, when a Japanese team announced magnesium diboride becomes superconducting under 39K [21]: the biggest surprise was not the critical temperature itself –the record being far above 100 K– but the fact that MgB_2 behaves as a Type I superconductor, suggesting that the BCS theory could still contain many hidden subtleties.
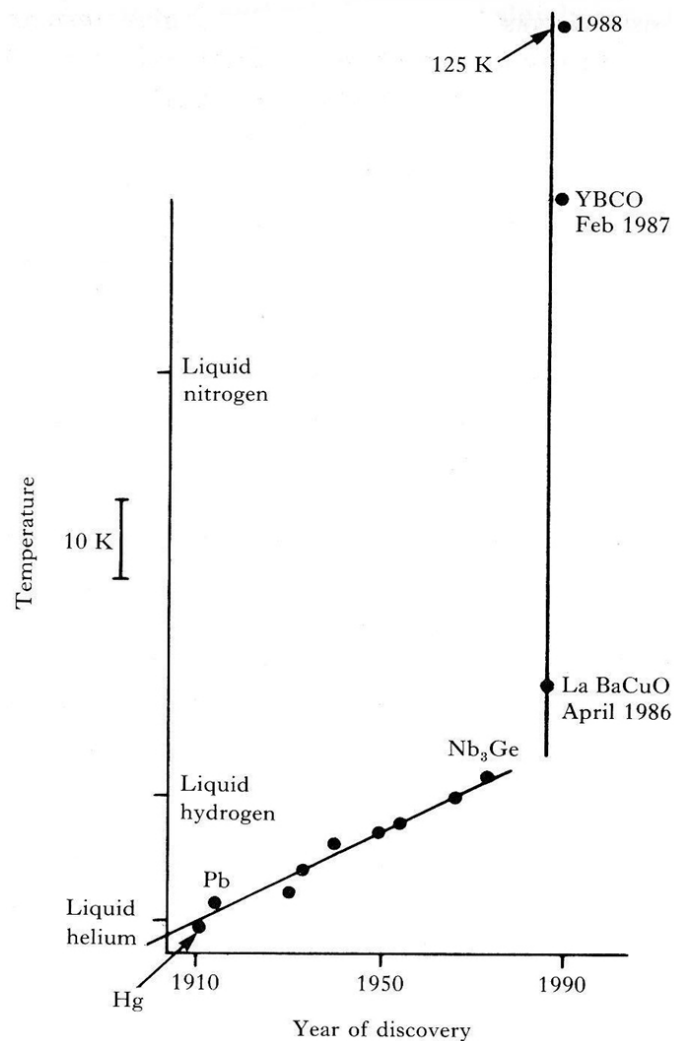
Figure 1.9: Timeline of the discovery of superconducting materials with increasing critical temperatures [3].

1.7 Mesoscopic superconductivity

With growing interest for physics at reduced dimensions, recent works have revealed a variety of interesting phenomena affecting the original subdivision between type I and type II superconductors at $\kappa = 1/\sqrt{2}$. When one considers *mesoscopic* superconducting structures (whose dimensions are comparable to the characteristic lengths), their behaviour in an external magnetic field is strongly affected by the boundary conditions and may exhibit new thermodynamic features, namely a manifest dependence of the order of the phase transition on the size of the superconducting sample [22, 23]. One example of such behaviour is presented in Fig. 1.10.

For the last decade, this subject has attracted a particularly great interest and resulted in very fruitful projects mixing numerical simulation specialists and talented experimentalists. In particular, experiments carried out in this University on lead nanowires were successfully reproduced by numerical simulations based on the Ginzburg-Landau equations [24, 25, 26]. Other original solutions arising from the analysis of the Ginzburg-Landau equations in nanoscopic structures are discussed in the next chapter.
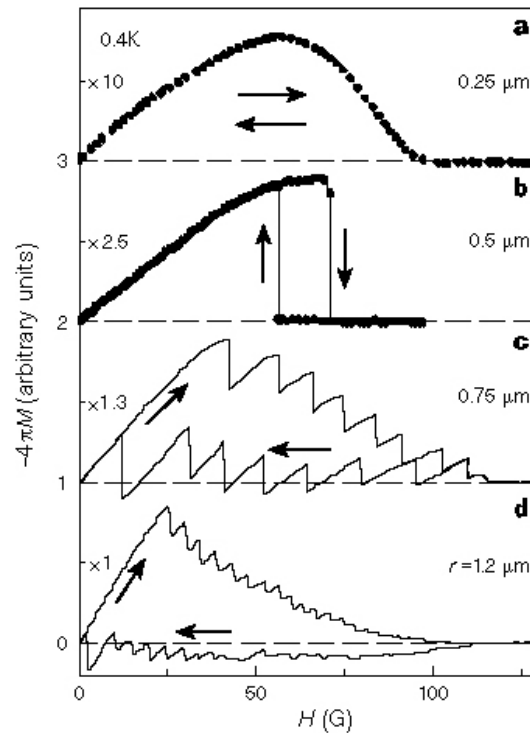
Figure 1.10: Magnetisation curves for small Al disks of various radii as a function of the external magnetic induction *H*; direction of magnetic sweep is indicated by the arrows. For small radius (a) the magnetisation operates a smooth continuous transition between superconducting and normal states, a characteristic behaviour of a second order phase transition as in type I superconductors. For a sample with higher radius in (b), the transition unexpectedly exhibits first order features, with one discontinuous complete loss of the magnetisation and an hysteretic response which is typical of type II superconductors. When the sample radius is increased further in (c) and (d), one recovers a progressive decay of the magnetisation typical of a second order transition, but presenting discrete jumps within the superconducting state [22].

2

New solutions to the
Ginzburg-Landau equations

Initially motivated by the quest for a new kind of particle detector based on the quantum properties of nanoscopic loops, a novel exploration of the usual Ginzburg-Landau (GL) equations was developed and led to the identification of new solutions extending the well-known Abrikosov configuration.

Pioneering studies of mesoscopic superconductors with cylindrical shapes were first carried out by W. Little and R. Parks in the early 1960s: they measured oscillations in the critical temperature $T_c(\mathbf{B})$ of a small-sized Sn loop in an axial magnetic field [27]. Those *Little-Parks oscillations* were predicted a few years later in mesoscopic disks [28], but the experimental verification was only made possible after the development of nanofabrication technologies, in particular e-beam lithography, together with highly sensitive measurement devices such as sub-micrometric Hall probes. This has revived the interest for mesoscopic superconducting loops and disks on theoretical and experimental levels. After Geim *et al.* measured the magnetization of superconducting disks and reported various kinds of phase transitions depending on the disk radii [22], a number of numerical studies were conducted by solving GL equations either self-consistently or by linear approximation close to the phase transition. F.M. Peeters *et al.* obtained simulations in agreement with Geim's results [29, 23]. Analyzing the phase diagram of the free energy as a function of the external magnetic field, they identified possible transitions between an

array of Abrikosov vortices and a centred *giant vortex* with more than one flux quantum [30]. A completely different approach was used by J.J. Palacios, who expanded the order parameter in an appropriate basis and directly minimized the free energy; his results were in agreement with experiments as well [31, 32]. E.H. Brandt developed specific numerical simulations capable of identifying the vortex structure of type II superconductors in various magnetic field and geometric configurations, see [33] and references therein for a detailed description. In the meantime, V.V. Moshchalkov *et al.* started numerical and experimental investigations towards the understanding of the mechanisms through which vortices enter or leave mesoscopic rings, see [34] and its extensive list of references for an overview.

After showing that the GL formalism constructed from the thermodynamic free energy is equivalent to the equations of motion resulting from the least action principle in classical field theory, we will highlight a new range of solutions to the GL equations with a static axial magnetic field, characterized by the order parameter vanishing along concentric circles [35, 36].

In a second stage, a covariant extension of the GL equations will be presented and the resulting modifications of the phase diagram in presence of an external electric field will be discussed. Actually, this question of electric field penetration has been addressed in the early days of superconductivity, and then later discarded on account of the argument of perfect conductivity. The Londons suspected the presence of an electric field inside superconductors in a steady state as a consequence of a non-uniform distribution of the superconducting current, but they finally modified their theory after their experiments failed to observe such effects [37]. In the thirties, Bopp [38] discussed the presence of a nonvanishing electrochemical potential inside superconductors following early approaches by the Londons; in particular, he obtained an expression for the electrostatic potential which follows the Bernoulli potential $e\Phi \sim mv^2/2$, where v is the velocity of the superfluid. Later, van Vijfeijken and Staas [39] extended the formulation of the electrostatic potential using the two-fluid model, and first introduced the notion of *quasiparticle screening*. Assuming that the electric screening at the surface of a superconductor is the same as in normal metals, Jakeman and Pike [40] showed that an electrostatic potential of the Bernoulli type may be recovered in the limit of strong screening, that is for a vanishing Thomas-Fermi screening length. The question of the electric field has also been raised within the framework of the BCS the-

ory, in particular by Rickayzen [41], who introduced some corrections to the Bernoulli potential. Recently, Lipavský *et al.* [42] gave a complete historical review of the study of the electrostatic potential in superconductors, and developed a modern formulation by evaluating the electrostatic and the thermodynamic potentials within the framework of the Ginzburg-Landau theory.

From an experimental point of view, the first experiments trying to observe an electric field inside a superconductor using direct contacts failed [43, 44]; it was later understood that these experiments measured the electrochemical potential instead of the electrostatic potential. Bok and Klein [45] reproduced similar experiments using an indirect capacitive coupling –known as the Kelvin method– and reported fluctuations of the surface electrostatic potential over a thickness of about 400 Å. Similar experiments have later been performed by Brown and Morris [46] and recently by Chiang and Shevchenko [47]. However, it is important to emphasize the very specific nature of the observed electrostatic potential: these experiments were performed in a magnetic field normal to the sample surface, hence inducing a surface charge to be identified as a Hall effect. Consequently, this analysis is not purely electrostatic in the sense that it is in fact related to magnetic phenomena.

Another way of investigating the electrostatic potential inside a superconductor is related to the electric charge and screening inside and around magnetic vortices. Forces acting on vortices due to the electrostatic potential of the Bernoulli type were identified by van Vijfeijken and Staas [39]. More recently, it was shown that vortices in high-Tc materials can accumulate electric charge due to the difference in the electrochemical potential between superconducting and normal phases [48]. Experimental evidences for such charged vortices were reported after very sensitive NMR measurements performed by Kumagai *et al.* [49]. An extensive review of related works for bulk superconductors as well as an extension to mesoscopic samples was given recently by Yampolskii *et al.* [50], who studied the distribution of electric charge in mesoscopic disks and cylinders within the Ginzburg-Landau theory. Again in this situation however, the analysis does not consider the superconductor in a purely electrostatic situation, since it is related to non-uniform supercurrents around magnetic vortices.

The change in the critical temperature was studied for the case of superconducting thin films subjected to an electric field: an enhancement of the critical temperature of about 10^{-4} K was observed experimentally in 70 Å-thick indium and tin superconducting films [51]. The origin of this shift lies

in a modification of the free electron gas density due to the direct voltage contact on the superconducting film, justifying the name of *charge modulation model* given to it. These electric effects were later predicted and then observed in high-Tc materials with increased change of the critical temperature, see Refs. [52, 53, 54] and references therein. Indeed, cuprate materials may be considered as stacks of alternating layers of insulating and metallic materials whose thickness is typically of the order of magnitude of the Thomas-Fermi screening lengths; they also have an intrinsic charge concentration which is lower than normal metals, making them more sensitive to the modification of charge density. Such systems were studied within the framework of the Ginzburg-Landau or the BCS theories, considering the Thomas-Fermi approximation for the screening of the electric field at the film surface. In all cases, the electric effects may not be attributed to some specific superconducting phenomena: they are due to the change of the free electron density as a direct consequence of the electric contacts on the sample, whose theoretical manifestation is through a realignment of the respective Fermi levels.

As a conclusion to the present review, to the best of our knowledge, all attempts to take electric fields into account in superconducting phenomena have always been considered in the limit of a Thomas-Fermi screening, that is, by decoupling the treatment of the electric field in superconductors and simply assuming it to be vanishing.

One purpose of the covariant extension of the Ginzburg-Landau theory is to provide a self-consistent approach describing the coupling of an electron gas to the electromagnetic field. In particular, it will be shown that the extended GL model considered for the case of a superconducting slab with specific configurations of the external electromagnetic fields exhibits some unrevealed features that could allow for an experimental discrimination between the two models.

2.1   Ginzburg-Landau-Higgs mechanism

A covariant extension of the GL equations is provided by the U(1) Higgs model of particle physics [55]: indeed, their solutions with an integer winding number L for the phase dependency of the scalar field have proven to be associated either to an Abrikosov lattice of L vortices or to a giant vortex carrying L magnetic flux quanta.

In this section we first show that the variational principle applied to the action of the Higgs model is equivalent, for stationary configurations, to the GL equations obtained by minimizing the thermodynamic energy. Then in a second step we study the case of mesoscopic superconducting samples, and in particular we identify particular solutions for which the order parameter –or equivalently the modulus of complex field– vanishes on closed surfaces within the bulk volume of the sample. Because of this particular topology, we refer to these solutions as *annular vortices* of order *n* and vorticity *L, n* referring to the number of cylindrical domains on which the order parameter vanishes and *L* to the usual fluxoid quantum number. These solutions define extrema of the free energy, but in our study we could not discriminate between maxima, minima or saddle points, thus leaving open the question of the stability of these solutions and the possibility of observing them in microscopic devices.

The Higgs model of particle physics, whose construction itself was motivated by GL theory in the late 1950s, provides a natural covariant extension of the GL equations[1]; the corresponding lagrangian density for a gauge covariant coupling of a complex scalar field $\psi(x)$ to the electromagnetic potential A_μ is given by [56]

$$\mathcal{L} = \frac{1}{2}\varepsilon_0 c \left(\frac{\hbar}{q\lambda}\right)^2 \left\{ \left(\partial^\mu - i\frac{q}{\hbar}A^\mu\right)\psi^* \left(\partial_\mu + i\frac{q}{\hbar}A_\mu\right)\psi - \frac{1}{2\xi^2}\left(\psi^*\psi - 1\right)^2 \right\} - \frac{1}{4}\varepsilon_0 c F_{\mu\nu}F^{\mu\nu}.$$

(2.1)

In this expression, the order parameter ψ is already normalised to the density of electron pairs in a bulk sample $\psi(x) = \Psi(x)/\Psi_o(x)$. Gauge invariance suggests the expression of the covariant derivative $(\partial_\mu + i\frac{q}{\hbar}A_\mu)$ in the kinetic term and the "double-well" form of the potential has been taken in order to reproduce the GL quartic potential (1.7). From the above expression one already notices that the penetration length $\lambda(T)$ weighs the relative contribution of the electromagnetic field energy and the condensate energy, while the coherence length $\xi(T)$ weighs the contributions to the condensate energy of the spatial inhomogeneities –through the covariant gradient– and the deviations from the bulk value $|\psi|^2 = 1$ –through the potential term. Assuming that an observable solution defines a local extremum in the energy spectrum, a variational method applied on the action $S = \int d^4x\,\mathcal{L}$ provides the following equations of motion for the scalar field ψ and the vector field A^μ respectively:

---

[1]The reader is referred to Appendix C for an introduction to relativistic formalisms and covariant theory.

$$\frac{1}{c}(\partial_t + i\frac{q}{\hbar}\Phi)^2\psi - (\nabla - i\frac{q}{\hbar}\mathbf{A})^2\psi = -\frac{1}{2\xi^2}\psi(\psi^*\psi - 1) \ ,$$

$$J_{em}^0 = c\rho_{em} = \frac{1}{2}\varepsilon_0 c\frac{iq}{\hbar}\left(\frac{\hbar}{q\lambda}\right)^2\left(\psi^*\partial_t\psi - \psi\partial_t\psi^* + 2i\frac{q}{\hbar}\Phi\psi^*\psi\right) , \qquad (2.2)$$

$$\mathbf{J}_{em} = -\frac{1}{2}\varepsilon_0 c^2\frac{iq}{\hbar}\left(\frac{\hbar}{q\lambda}\right)^2\left(\psi^*\nabla\psi - \psi\nabla\psi^* - 2i\frac{q}{\hbar}\mathbf{A}\psi^*\psi\right)$$

where the current density J_{em}^μ has been defined in such way that it agrees with the covariant form of the inhomogeneous Maxwell equations $\partial_\nu F^{\mu\nu} = \mu_o J_{em}^\mu$, which take the explicit form

$$\nabla \cdot \mathbf{E} = \frac{\rho_{em}}{\varepsilon_o} \quad , \quad \nabla \times \mathbf{B} - \frac{1}{c^2}\partial_t\mathbf{E} = \mu_o\mathbf{J} \ . \qquad (2.3)$$

The first equation of the set (2.2) generalises the GL equation (1.8) for the order parameter by considering a non-vanishing electrostatic potential Φ inside the superconductor. Considering spatial and time derivatives of the two other relations leads to generalised London equations:

$$\mathbf{E} = \nabla\left(\frac{\lambda^2}{|\psi|^2}J_{em}^0\right) + \frac{\partial}{\partial t}\left(\frac{\lambda^2}{|\psi|^2}\mu_o\mathbf{J}_{em}\right) \quad , \quad \mathbf{B} = -\nabla \times \left(\frac{\lambda^2}{|\psi|^2}\mu_o\mathbf{J}_{em}\right) \ . \qquad (2.4)$$

The relevant boundary conditions are

$$\left(\partial^\mu + i\frac{q}{\hbar}A^\mu\right)\psi\Big|_{\partial\Omega} = 0. \qquad (2.5)$$

To proceed further, let us introduce the following change of normalisation. The order parameter is defined according to $\psi = f(x)e^{i\theta(x)}$ so that f^2 measures the relative Cooper pair density $0 < f^2 < 1$. Space and time coordinates are measured in units of the penetration length:

$$\mathbf{u} = \frac{\mathbf{x}}{\lambda} \ , \quad \tau = \frac{ct}{\lambda}.$$

Similarly, magnetic and electric fields[2] are given in units of the magnetic field $\Phi_o/2\pi\lambda^2$ associated to one flux quantum Φ_o:

$$\mathbf{b} = \frac{\mathbf{B}}{\Phi_o/2\pi\lambda^2} \ , \quad \mathbf{e} = \frac{\mathbf{E}/c}{\Phi_o/2\pi\lambda^2}.$$

---

[2]The electric field is considered together with the velocity of light, so that the ratio $\mathbf{E}/c$ has indeed the same dimension as a magnetic field. In particular, $\mathbf{E}/c$ and $\mathbf{B}$ transform into one another under Lorentz boosts.

Finally, charge and current densities are re-parameterised through

$$j^0 = \frac{q}{\hbar} \frac{\lambda^3}{f^2} \frac{1}{c} \frac{\rho_{em}}{\varepsilon_o} , \quad \mathbf{j} = \frac{q}{\hbar} \frac{\lambda^3}{f^2} \mu_o \mathbf{J}_{em}.$$

Note that the newly defined variables are temperature dependent since λ is. The generalised GL equation then reduces to

$$(\partial_u^2 f - \partial_\tau^2 f) = f(\mathbf{j}^2 - j_0^2) - \kappa^2 f(1 - f^2) \qquad (2.6)$$

where the GL parameter $\kappa = \lambda/\xi$ has been introduced; ∂_u stands for the gradient with respect to the rescaled position. On the other hand, the inhomogeneous Maxwell equations (2.3) together with the generalised London equations (2.4) provide similar differential equations for the 4-supercurrent $(j^0, \mathbf{j})$:

$$\begin{aligned}
(\partial_u^2 j^0 - \partial_\tau^2 j^0) &= f^2 j^0 - \partial_\tau(\partial_\tau j_0 + \partial_u \mathbf{j}) , \\
(\partial_u^2 \mathbf{j} - \partial_\tau^2 \mathbf{j}) &= f^2 \mathbf{j} + \partial_u(\partial_\tau j_0 + \partial_u \mathbf{j}).
\end{aligned} \qquad (2.7)$$

The corresponding electric and magnetic fields are respectively given by

$$\begin{aligned}
\mathbf{e} &= \partial_\mathbf{u} j_0 + \partial_\tau \mathbf{j} , \\
\mathbf{b} &= \partial_\mathbf{u} \times \mathbf{j}.
\end{aligned} \qquad (2.8)$$

To conclude the general discussion, let us give the expression for the free energy of the system:

$$\begin{aligned}
\mathcal{E} &= \left(\frac{\lambda^3}{2\mu_o} \frac{\Phi_o}{2\pi\lambda^2} \right)^{-1} E = \int_{(\infty)} d^3\mathbf{u} \quad \{[\mathbf{e} - \mathbf{e}_{ext}]^2 + [\mathbf{b} - \mathbf{b}_{ext}]^2\} + \qquad (2.9) \\
&+ \int_\Omega d^3\mathbf{u} \quad \left\{ (\partial_\tau f)^2 + (\nabla_u f)^2 + f^2(j_0^2 + \mathbf{j}^2) + \frac{\kappa^2}{2}(1 - f^2)^2 - \frac{\kappa^2}{2} \right\} ,
\end{aligned}$$

where the normalisation has been chosen so that the energy be positive in the normal state and negative in the superconducting state, allowing an immediate identification of the phase transition at $\mathcal{E} = 0$.

2.2 Annular vortices in cylindrical topologies

We consider infinitely long mesoscopic samples with cylindrical symmetry, that is, a solid cylinder of radius $u_b = r_b/\lambda$ or an annulus with internal radius $u_a = r_a/\lambda$ and external radius $u_b = r_b/\lambda$ ($u_a, u_b \sim 1$). We further restrict to a static case with only a magnetic field along the axis of the sample; then the

electric field and the charge density j^0 vanish and the original GL equations are recovered. The order parameter is advantageously redefined as $\psi(u,\phi) = f(u)\, e^{-iL\phi} e^{i\theta_o}$ where θ_o is an arbitrary phase and L is the usual fluxoid quantum number[3]. It is also useful to introduce an additional function $g(u) = u \cdot j(u)$, so that the set of equations (2.6) and (2.7) reduce to the two differential equations [57, 35]:

$$\frac{1}{u}\frac{d}{du}\left[u\frac{d}{du}f(u)\right] = \frac{1}{u^2}f(u)g^2(u) - \kappa^2 f(u)[1 - f^2(u)] \,,$$

$$u\frac{d}{du}\left[\frac{1}{u}\frac{d}{du}g(u)\right] = f^2(u)g(u) \,,$$
(2.10)

associated to the following boundary conditions either obtained from (2.5) or from symmetry considerations:

disk case: $g(u)|_{u=0} = -L$; $\partial_u f(u)|_{u=0} = 0$ if $L = 0$

                                                 or $f(u)|_{u=0} = 0$ if $L \neq 0$

            $\frac{1}{u}\partial_u g(u)\big|_{u=u_b} = b_{ext}$; $\partial_u f(u)|_{u=u_b} = 0$

annulus case: $\frac{u_a}{2}\partial_u g(u)\big|_{u=u_a} = g(u_a) + L$; $\partial_u f(u)|_{u=u_a} = 0$

                 $\frac{1}{u}\partial_u g(u)\big|_{u=u_b} = b_{ext}$; $\partial_u f(u)|_{u=u_b} = 0 \,.$
(2.11)

In order to determine a solution uniquely, this pair of coupled second order differential equations requires a set of four boundary conditions which must be specified at the same point. Since we only have two conditions at each of the two boundaries, we must add two free conditions at one of the boundaries and then calculate the solution throughout the sample; the free boundary conditions will then be adjusted so as to meet the other two conditions at the opposite boundary. This procedure –known as the relaxation method of solving differential equations– has been implemented and resulted in solutions displayed in Fig. 2.1 for a disk case; those for the annulus are similar.

---

[3]The quantity u now describes the radial coordinate r/λ.
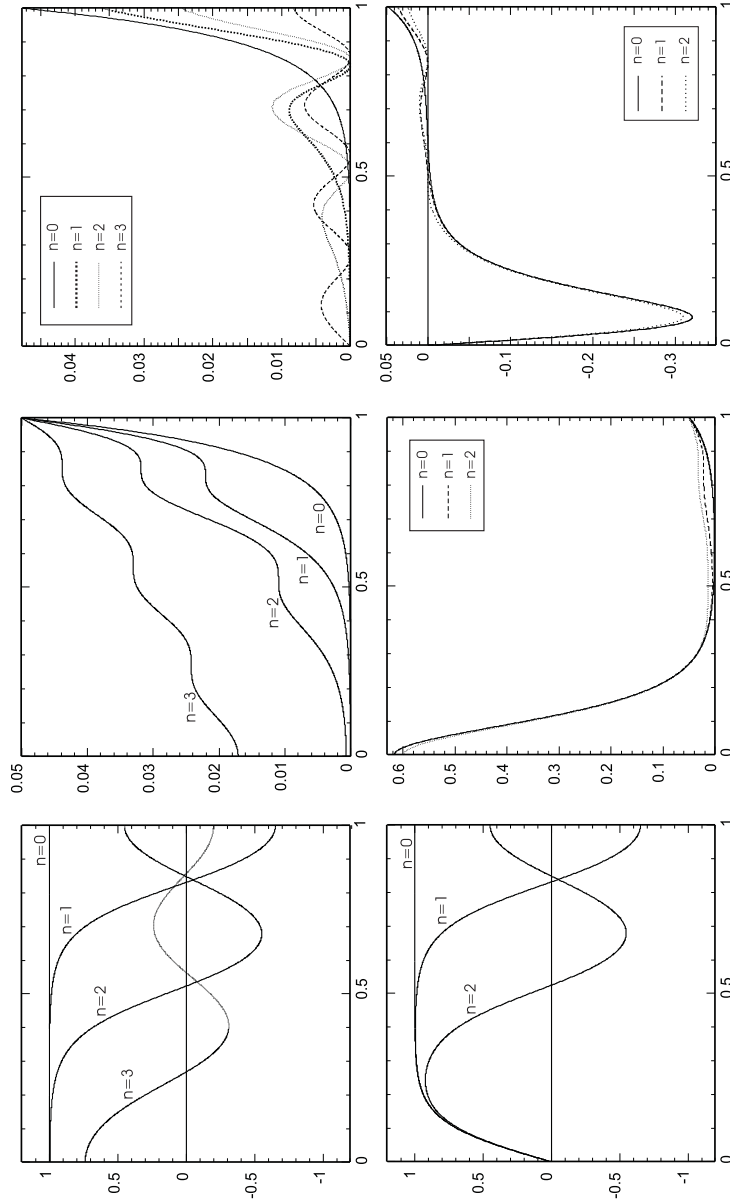
Figure 2.1: Numerical solutions to the GL equations for a disk with normalised radius $u_b = 11$ in a normalised magnetic field $b_{ext} = 0.05$, considering $\kappa = 1$. Top (resp. bottom) panel corresponds to a configuration with $L = 0$, $n = 0, 1, 2, 3$ (resp. $L = 1$, $n = 0, 1, 2$) and displays from left to right $f(u)$, $b(u)$ and $f^2(u)g(u) \sim J(u)$ as functions of $x = u/u_b$, $0 \le x \le 1$ [35].

Fig. 2.1 displays all possible solutions which can be found with $L = 0, 1$ for a disk with radius $r/\lambda = 11$ in an external magnetic field $b_{ext} = 0.05$, corresponding to a measurable value of about 66 gauss for a material[4] with $\lambda = 50$ *nm*. The first graph displays solutions denoted respectively $n = 0, 1, 2, 3$ associated to a novel quantum number n of cylindrical domains on which the order parameter vanishes, which we call "annular vortices". For the case $L = 1$, a solution with $n = 3$ cannot be found since the central vortex has pushed outwards the third vortex. As it may be seen on the graphs in the second column, a stabilisation of the magnetic field screening is observed where the annular vortices are located, confirmed by the fact that the supercurrents there also vanish (third column), enabling further penetration of the external field and thereby a partial anti-screening of the Meissner effect. The number of annular vortices which can be accommodated into the sample depends of course on the radius of the sample, but also on the GL parameter: a higher value of κ corresponds to a condensate with a lower rigidity (low value of the coherence length ξ) for which the Copper pair density may fluctuate over smaller distances, allowing therefore solutions with more closely packed annular vortices.

Unknown to us at that time, the existence of these oscillating solutions had already been demonstrated from a mathematical point of view [58], but they had never been constructed explicitly before. These solutions extend those in terms of the Bessel functions that may be found for the linearised equations, and more generally, they are close cousins to the familiar solitonic solutions for a Higgs-like potential in the context of particle physics [59]. After the publication of these results, such annular vortices have also been obtained from the usual GL theory using different numerical methods [60, 61].

Since these configurations solve the GL equations, they define local extrema of the free energy, but their stability has definitely not been established, leaving open the question of observing such solutions in mesoscopic devices. However, their free energy can be shown to increase with increasing n, suggesting a finite thermodynamic lifetime, but even if unstable these new solutions could contribute to the dynamics of the switching mechanism between different states.

---

[4]This situation models approximatively a niobium sample, for which $\lambda(0) = 44$ nm and $\xi_o = 40$ nm [14].

2.3   Validation of the covariant model

In the previous section, it has been shown that the Higgs mechanism could, under certain hypotheses, reproduce the Ginzburg-Landau equations for a phenomenological description of superconductivity. Among these hypotheses, a vanishing electric field has been assumed inside the superconducting sample in order to reproduce the property of infinite conductivity. As a motivation for the present covariant generalisation of the GL theory, we claim however that a vanishing electric field inside the superconducting sample raises a series of formal concerns. First, it is hardly believable that the electric field would discontinuously drop to zero when crossing the surface of the superconductor; even if we consider a screening over Thomas-Fermi typical length scales for normal metals, it would be interesting to know how this length scale is affected by the presence of a superconducting condensate.

More generally, another concern is the fact that the coupling of the GL and London equations with electromagnetism is not spacetime covariant. A self-consistent approach describing the coupling of an electron gas to the electromagnetic field should ensure that the relativistic covariance properties of the latter sector be also extended to the electronic sector. This description would advantageously extend this hybrid construct in which a non-relativistic electronic description is coupled to the relativistic covariant electromagnetic field. In that framework, under a Lorentz transform, the supercurrent density $\mathbf{J}$ should behave as the space component of a 4-vector, whose time component would be the supercharge density which appears in the London parameter Λ (1.3), while the electric and magnetic fields transform as the components of the field tensor $F^{\mu\nu}$.

To illustrate the possible consequence of a covariant approach, consider an infinite superconducting slab in a static homogeneous magnetic field parallel to its surface. In such a situation, the magnetic field penetrates the slab with a well-known characteristic length λ. If a Lorentz boost is performed in a direction both parallel to the surface of the slab and perpendicular to the magnetic field, according to the covariance of Maxwell equations, an electric field perpendicular to the surface of the slab appears in the boosted frame *even within the superconducting sample where the magnetic field in the rest frame is nonvanishing*. Obviously, one may argue that the superconducting sample defines itself a preferred rest-frame, but even if distinguished from other possible frames for describing physical properties of a superconductor, it remains true that

the coupling of GL and London equations with Maxwell equations should be consistent with the covariant description of electromagnetism. Furthermore, it provides a natural way of considering time varying properties as well as moving superconductors.

The infinite slab mentioned above provides a suitable geometry for discriminating experimentally between usual and covariant GL equations. In particular, we consider the case of an infinite slab in a static configuration, subjected to a homogeneous magnetic field parallel to its surface as well as a homogeneous electric field perpendicular to its surface. Obviously, this configuration for the electric and magnetic fields is not the only possible, but it has been shown to emphasise the very specific features of the phase diagram that will be described in the following. The slab is taken to be of thickness $2a$ (the origin of the coordinates is located at the centre of the slab), with the external electric field $\mathbf{e}_{ext}$ along the x axis and the magnetic field $\mathbf{b}_{ext}$ along the y axis. The screening supercurrent $\mathbf{j}$ shall thus develop only along the z axis (the previous rescaling of these quantities still applies). Symmetries of this situation imply that all functions only depend on the normalised coordinate $u = x/\lambda$ along the x axis.
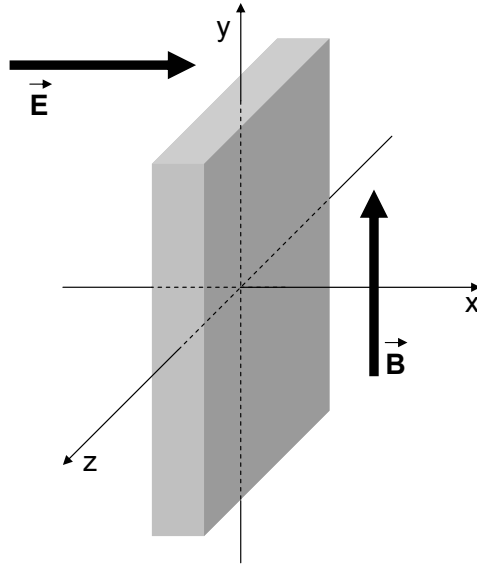
Figure 2.2: Infinite superconducting slab in crossed stationary electric and magnetic fields.

It proves possible to express both supercurrent $j^z(u)$ and supercharge $j^0(u)$ densities in terms of a single function $j(u)$

$$j^0(u) = -e_{ext}\, j(u) \,, \qquad j^z(u) = -b_{ext}\, j(u) \tag{2.12}$$

so that electric and magnetic fields (2.8) inside the superconducting sample are given by

$$e(u) = e_{ext}\, \frac{d}{du} j(u) \,, \qquad b(u) = b_{ext}\, \frac{d}{du} j(u). \tag{2.13}$$

The set of differential equations to be solved then reduces to

$$\frac{d^2}{du^2} j(u) = f^2(u)\, j(u) \,,$$

$$\frac{d^2}{du^2} f(u) = f(u) j^2(u) \left(b_{ext}^2 - e_{ext}^2 \right) - \kappa^2 f(u) \left(1 - f^2(u) \right) \,, \tag{2.14}$$

subjected to the boundary conditions (2.5) adapted to this specific setup:

$$\frac{d^2}{du^2} j(u) \bigg|_{u = \pm u_a} = 1 \,, \qquad \frac{d^2}{du^2} f(u) \bigg|_{u = \pm u_a} = 0. \tag{2.15}$$

In view of these equations, it appears that solutions for $f(u)$ and $j(u)$ are necessarily functions of the combination $(b_{ext}^2 - e_{ext}^2)$, indicating the nonvanishing contribution of the external electric field as a distinctive feature from the non-covariant model. This fact suggests to extend the phase diagram which characterises the superconducting transition in the (b, e) plane. Up to the contribution of the infinite surface of the slab as an overall factor, the free energy is given by

$$\begin{aligned} \mathcal{E} \;=\; & 2u_a \left\{ (b_{ext}^2 + e_{ext}^2) \left(1 - \frac{1}{u_a} j(u_a) \right) \right. \\ & - \frac{1}{u_a} \int_0^{u_a} du \left[\left(b_{ext}^2 - e_{ext}^2 \right) j^2(u) f^2(u) + \frac{1}{4} \kappa^2 f^4(u) \right] \right\} \end{aligned} \tag{2.16}$$

from which the critical curves of vanishing energy in the (b, e) plane, corresponding to the phase transition, are deduced [56, 62]:

$$b^2 + e^2 = \frac{1}{u_a - j(u_a)} \int_0^{u_a} du \left[\left(b^2 - e^2 \right) j^2(u) f^2(u) + \frac{1}{4} \kappa^2 f^4(u) \right]. \tag{2.17}$$

The corresponding expression in the non-covariant approach is obtained by fixing $j^0 = e = 0$ in the equations of motion and the free energy to be integrated. This leads to solutions for $f(u)$ and $j(u)$ in terms of b_{ext}^2 only, and

the critical curves of the phase diagram are modified to

$$b^2 + \frac{u_a}{u_a - j(u_a)} e^2 = \frac{1}{u_a - j(u_a)} \int_0^{u_a} du \left[b^2 j^2(u) f^2(u) + \frac{1}{4} \kappa^2 f^4(u) \right]. \qquad (2.18)$$

In a macroscopic limit $a \gg \lambda, \xi$, in which case we essentially have $j(u) = 0$ and $f(u) = 1$ throughout the material, the two critical curves (2.17) and (2.18) are identically given by

$$b^2 + e^2 = \frac{\kappa^2}{2}.$$

Normalised in units of the critical magnetic field in absence of electric field $b_o = \kappa/\sqrt{2}$, this criticality condition expressed in units of the critical magnetic field B_o is given by

$$\left(\frac{B}{B_o} \right)^2 + \left(\frac{E/c}{B_o} \right)^2 = 1, \quad a \gg \lambda, \xi. \qquad (2.19)$$

It is therefore impossible to distinguish the two approaches with a macroscopic device. However, considering a mesoscopic situation $a \ll \lambda, \xi$, it is then possible to expand the functions $j(u)$ and $f(u)$ in powers of u. In this case it would be necessary to expand $b(u)$ and $e(u)$ as well, since they appear in the r.h.s of the expressions. Hence it is more relevant to consider a weak field approximation and develop $j(u)$ and $f(u)$ in powers of $(b_{ext}^2 - e_{ext}^2)$ whatever the value of u_a; since the critical fields are on the order of $\kappa/\sqrt{2}$, this approximation remains valid for small values of κ, namely for type I superconductors.

A first order expansion of the functions in the squared fields leads to the following criticality condition in the (B, E) plane

$$\left(\frac{B}{B_o} \right)^2 + C \left(\frac{E/c}{B_o} \right)^2 = 1 \qquad (2.20)$$

with

$$C = \frac{1+\zeta}{1-\zeta} \qquad\qquad : \quad \text{covariant model,}$$

$$\qquad\qquad\qquad\qquad\qquad\qquad\qquad\qquad\qquad (2.21)$$

$$C = \frac{u_a}{u_a - \tanh u_a} \frac{1}{1-\zeta} \quad : \quad \text{non covariant model,}$$

$$\zeta = \frac{1}{16(\kappa^2 - 2)^2} \frac{u_a}{(u_a - \tanh u_a)^2} \left[8\kappa\sqrt{2} \frac{\tanh^2 u_a}{\tanh(\kappa\sqrt{2}u_a)} - (3\kappa^4 - 10\kappa^2 + 16)\tanh u_a + \right.$$

$$\left. + (3\kappa^2 - 4)(\kappa^2 - 2)\frac{u_a}{\cosh^4 u_a}(5\kappa^4 - 22\kappa^2 + 16)\tanh^3 u_a \right]$$

for any value of the slab thickness $u_a = a/\lambda(0)$. Taking the nanoscopic limit $a \ll \lambda, \xi$, one may simplify

$$\frac{u_a}{u_a - \tanh u_a} \sim \frac{3}{u_a^2}[1 + O(u_a^2)] \,, \qquad \zeta \sim \frac{1}{2}[1 + O(u_a^2)]$$

leading to distinct expressions of the criticality condition:

$$\left(\frac{B}{B_o}\right)^2 + 3\left(\frac{E/c}{B_o}\right)^2 = 1 \quad : \quad \text{covariant model, } a \ll \lambda, \xi$$

$$\text{(2.22)}$$

$$\left(\frac{B}{B_o}\right)^2 + 6\frac{\lambda^2}{a^2}\frac{1}{1 - \left(\frac{T}{T_c}\right)^4}\left(\frac{E/c}{B_o}\right)^2 = 1 \quad : \quad \text{non covariant model, } a \ll \lambda, \xi.$$

Numerical studies of a realistic situation close to the above mentioned cases allow for an explicit observation of those results. Here we present the analysis corresponding to an Al slab of thickness $u_a = 5$; tabulated values of the superconducting parameters give $T_c = 1.18$ K, $\kappa = 0.02$, $\lambda(0) = 50$ nm, and a critical magnetic field $B_c(0)$ of about 100 gauss, so that the required electric fields values lie around 3 MV/m, namely 3 V/μm, which is a reasonable range for nanoscopic devices.

Fig. 2.3 presents the phase diagram for the covariant (on the top) and non-covariant (on the bottom) models for a series of temperatures between 0 K and T_c. In particular, we observe that the critical electric field E_o in the absence of a magnetic field remains bounded below for any temperature in the covariant case, while it goes to zero when the temperature increases in the non-covariant case. Clearly, this major difference between the two approaches shows that it should be possible to discriminate between them by measuring the critical phase diagram of a corresponding device with properly oriented external electric and magnetic fields. The next chapter reports on the realisation of such a device.
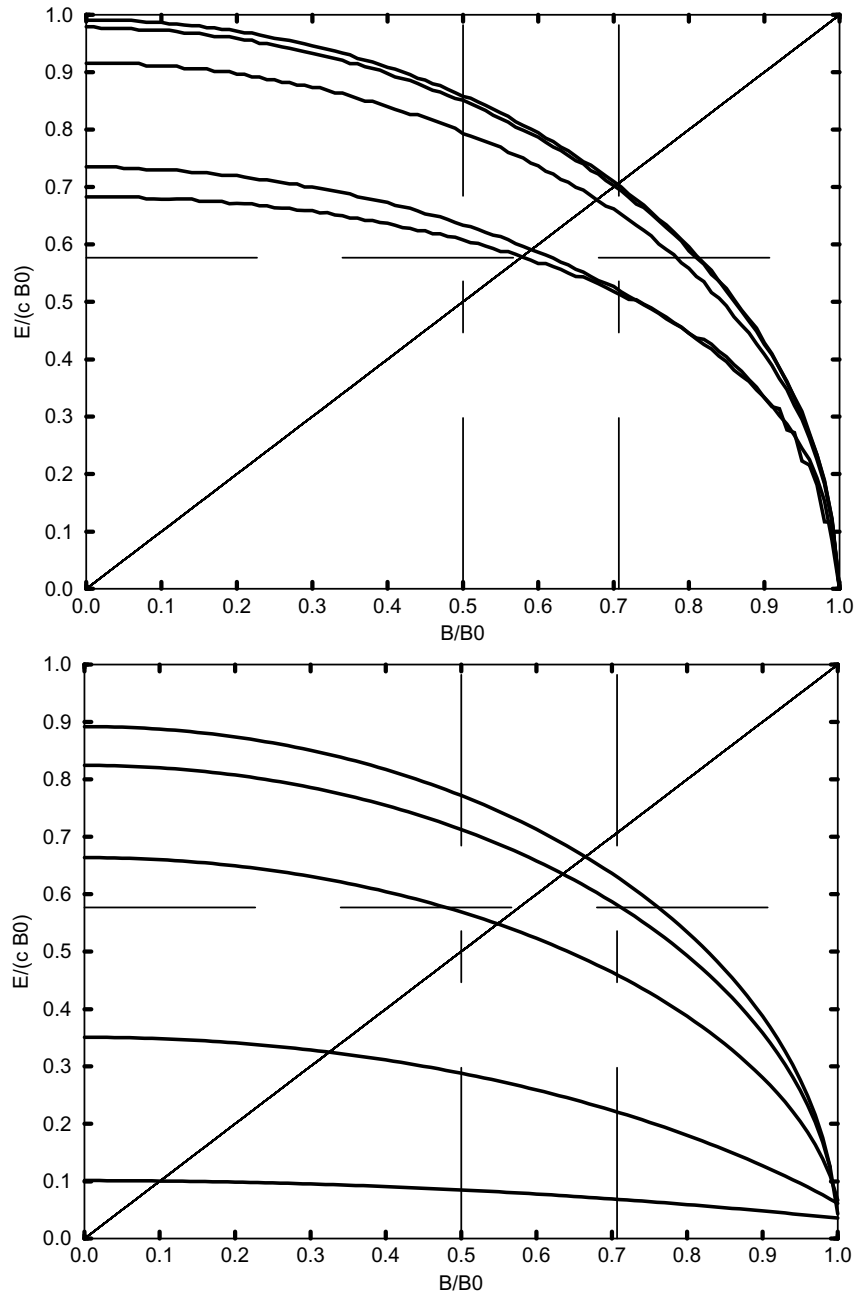
Figure 2.3: Phase diagram for the covariant (top) and non-covariant (bottom) models for an infinite slab of thickness $u_a = a/\lambda(0) = 5$ with $\kappa = 0.02$. On each graph, the curves shown from top to bottom are associated with increasing temperature values $T/T_c = 0$, 0.8766, 0.9659, 0.9935, 0.9996. For further characterisation of the above curves, see the original publication [56].

3

Experimental validation of the covariant model

In physics, you don't have to go around making trouble for yourself.
Nature does it for you.

Franck Wilczek, 2004 Nobel Laureate in Physics.

According to the relations (2.17) and (2.18), a discrimination between the usual and covariant Ginzburg-Landau equations should be possible based on the measurement of the temperature dependence of the phase diagram for a mesoscopic superconducting slab within a static magnetic field parallel to its surface and a static electric field perpendicular to it, assuming possible small variations from the calculated values due to the finite size of the experimental device. In particular, it should be possible to observe how the external electric field can break the superconducting state for sufficiently high critical value. This chapter presents the realisation of such a device and the results of the experimental measurements.

3.1   Sample fabrication

The Microelectronics Laboratory at Louvain-la-Neuve[1] provides extensive technology as well as the required know-how for the fabrication of integrated circuits on sub-micrometric devices in highly controlled clean rooms. With the help of the technical staff of the laboratory, several geometries were tested to approximate as well as possible the situation of an infinite slab in static electric and magnetic fields. In practice, the device should only contain the superconducting slab and the means for producing a perpendicular electric field, since a magnetic field can be produced by a superconducting solenoid enclosing the experimental chamber at the bottom of the cryostat that was used for the low-temperature measurements. The final design was a multilayer structure consisting of a 50-nm-thick Aluminum superconducting slab trapped between two metallic plates operating as a capacitor to produce the perpendicular electric field; two dielectric layers made of silicon nitride ensured the isolation between the capacitor and the slab. Four electrodes were connected to the central slab for the determination of its normal or superconducting state through a resistivity measurement: the advantage of this kind of probing is that one can then get rid of the contact resistances. A drawing of the device and its electrical connections is given in Fig. 3.1, together with the sizes of the slab and electric connections.
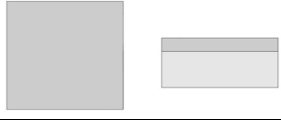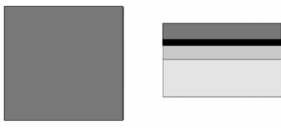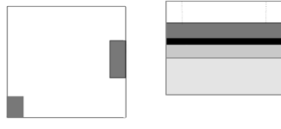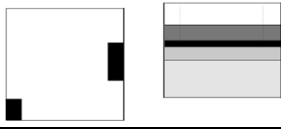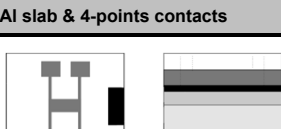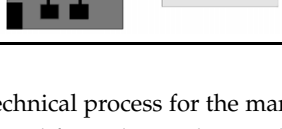
The complete process elaborated for the manufacturing of this multilayer device is displayed in Figs. 3.2 and 3.3 : experimental techniques are described in the next paragraphs [63, 57].

---
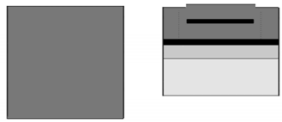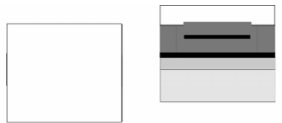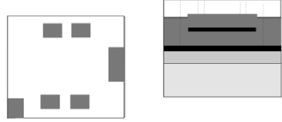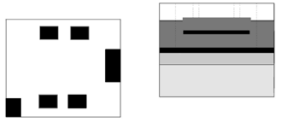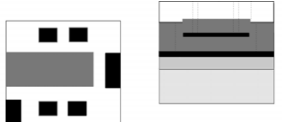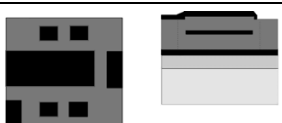
[1] Part of the FSA/ELEC/DICE entity at UCL; see detailed information at http://www.dice.ucl.ac.be.
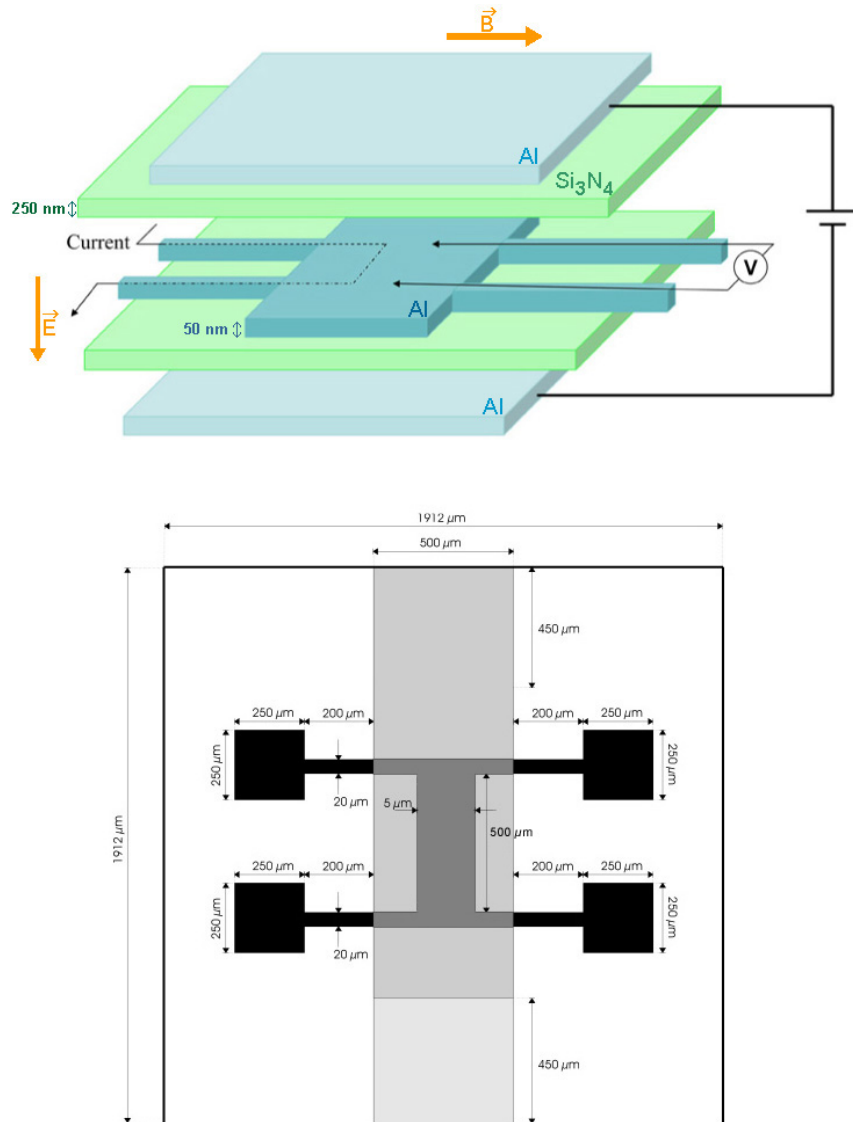
Figure 3.1: (Top) General layout of the experimental device: the superconducting aluminum device with four-points probing is shown in dark blue, insulating silicon nitride layers in green separate it from the aluminum plates of the capacitor, in light blue. (Bottom) Sizes of the various elements manufactured by lithography. Relative scales between the elements are not respected on the drawings.

		Nr	Substance (thickness)	Process
Preliminary isolation				
		1	SiO₂ (250 nm)	PECVD
Lower plate of the capacitor				
		2	Al (50 nm)	Evaporation
Dielectric layer				
		3	Si₃N₄ (250 nm)	PECVD
		4	PMMA (650 nm)	Spinning
		5		Baking
		6		e-beam litho. in PMMA
		7		Chemical cleaning
		8		RIE through dielectric
Al slab & 4-points contacts				
		9		e-beam litho.
		10		Chemical cleaning
		11	Al (50 nm)	Evaporation
		12		Chemical removing of remaining PMMA

Figure 3.2: Technical process for the manufacturing of the device. Step 1: A SiO₂ layer is deposited for isolating the Si substrate. Step 2: The Al lower plate of the capacitor is evaporated. Steps 3 to 8: The isolating layer of Si₃N₄ is deposited and two openings are performed by e-beam lithography for connecting the lower plate of the capacitor. Steps 9 to 12: The main structure is patterned by e-beam lithography and Al is evaporated; the excess layer of metal on top of the resist is chemically removed.

Dielectric layer				
		13	Si$_3$N$_4$ (250 nm)	PECVD
		14	PMMA (650 nm)	Spinning
		15		Baking
		16		e-beam litho. in PMMA
		17		Chemical cleaning
		18		RIE through dielectric
Upper plate of the capacitor				
		19		e-beam litho. in PMMA
		20		Chemical cleaning
		21	Al (50 nm)	Evaporation
		22		Chemical removing of remaining PMMA

Figure 3.3: Technical process for the manufacturing of the device (continued). Steps 13 to 18: The second dielectric layer of Si$_3$N$_4$ is deposited and the required apertures for the electrical contacts are released. Steps 19-22: the upper plate of the capacitor is realised by e-beam lithography and evaporation of Al.

The slab and the two capacitor plates were deposited by evaporation of Al using a standard e-gun evaporation technique. The thickness of the evaporated layer was controlled with a precision of several Angstroms by the change in the resonant frequency of an oscillating quartzite crystal.

Si_3N_4 layers were obtained by Plasma Enhanced Chemical Vapour Deposition: appropriate gases are ionised by a RF electric field and then recombined in a reacting chamber under controlled pressure and temperature conditions. PECVD provides a very reliable way of producing layers with a smooth surface and a precise control of the thickness. Tab. 3.1 displays adjusted parameter values[2] for the deposition of Si_3N_4 at a measured speed of 96 Å/min.

pressure (mTorr)	temp. (°C)	RF power (W)	NH_3 flow (sccm)	SiH_4 flow (sccm)	N_2 flow (sccm)	LCP	TCP	APC
675	300	20	300	600	900	87	104	33.4

Table 3.1: Parameters to be tuned on the ET Twin 310/340 furnace for PECVD deposition of Si_3N_4.

We used e-beam lithography for patterning specific geometries, namely for the opening of electrical leads and shaping of the superconducting structure. This has become a standard technique for manufacturing sub-micrometric devices. At first, an electro-sensitive resist (Poly-methyl-metacrylate –PMMA– diluted at 6% in chlorobenzene) is deposited on the wafer, which is kept spinning at 5000 rpm for 1 minute. After 5 minutes baking on a hot plate (160°C) for evaporating the chlorobenzene, we end up with a thickness of about 650 Å. In a second step, the PMMA resist is exposed to the beam of an electron microscope (Philips XL30 SFEG), the displacement of which is controlled by a specific software (Raith's ELPHY program). The electron beam damages polymeric chains, which become then more sensitive to the dissolution in an appropriate chemical developer. The PMMA irradiation depends on the dose of electric charge deposited by the electron beam, which is a function of the beam current, the surface exposed to the beam and the time spent on that surface. All those parameters are determined by adjusting the features of both the SFEG microscope and the ELPHY program: Tab. 3.2 displays the more efficient values of the exposure parameters after empiric adjustment

---

[2]In the following tables, the abbreviations LCP, TCP and APC stand respectively for *Load Capacitor Position*, *Tune Capacitor Position* and *Automatic Pressure Control*; the role of these controls is described in Ref. [57].

for optimal lithography of the presented geometries (see Fig. 3.1 for the dimensions of the elements to be exposed during lithography). Finally, dissolution of the exposed parts of the resist was performed in successive baths of methyl-isobutyl-ketone (MIBK)/isopropanol mixing in 1:3 proportion for 90 seconds, then pure isopropanol for 30 seconds and flowing de-ionised water for about 10 minutes.

SFEG parameters	magnification	field size (μm)	diaphragm	spotsize
	50	1750	5	5
ELPHY parameters	pixel dist.	stepsize (nm)	dwell time (μs)	current (μA)
	2	53.4	2.89	2.56

Table 3.2: Parameters for the e-beam lithography steps of our process.

Dry etching through Si_3N_4 was performed by Reactive Ion Etching (RIE): the etching is performed by a gas at low pressure ionised under RF electric field. This technique is less selective than other wet etching methods, but RIE is not very efficient on PMMA, therefore ensuring the protection of the regions not to be etched: the parameters displayed in Tab. 3.3 were used for etching the 250-nm-thick Si_3N_4 layers with a measured speed of 100 nm/minute, while the etching speed of PMMA was only 60 nm/minute [57]. On the other hand, RIE is rather anisotropic in the sense that the preferred etching direction is perpendicular to the surface, ensuring rather steep walls around etched regions; this is not a crucial concern however, since RIE was used only for the opening of electrical leads, for which the resolution is not very important.

pressure (mTorr)	RF power (°C)	SF_6 flow (W)	LCP	TCP
30	20	80	59	49

Table 3.3: Parameters for RIE etching of the Si_3N_4 layers.

Twenty devices were actually patterned on the same wafer. We measured the thickness of the central slab by profilometry and obtained values between 519 and 806 Å. Measurements of the electric resistance between two adjacent contact leads revealed values in the range 15-30 Ω. The differences between the samples may be explained by the granularity of the aluminum layer, together with a slight lack of reproducibility which was reported for the profilometer.

Once completed, the sample was mounted on a standard (dual inline multiple pin) DIP-header and the electrical leads were soldered by hand to the pins with gold wires and silver paint. The resulting device is shown in Fig. 3.4.
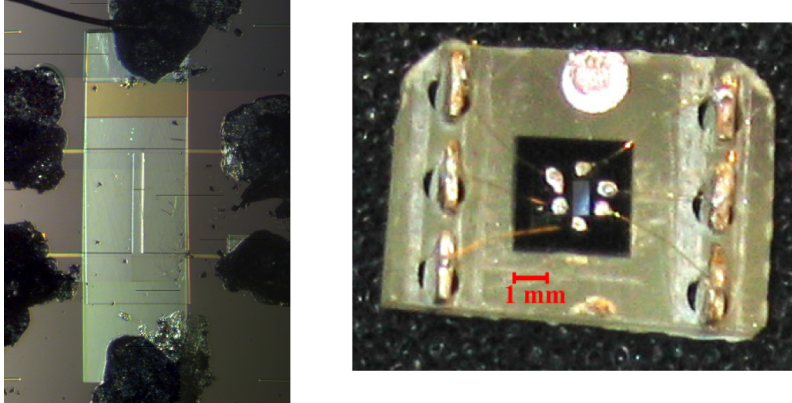
Figure 3.4: (Left) Microscope image of the completed device; in the last process, a fifth connection had been added on the slab for technical reasons, but it has not been used during the measurements. (Right) View of the device mounted on the DIP-header.

3.2   Experimental setup

For cooling the sample below the critical temperature at which Al becomes superconducting, namely around 1.17 K for a bulk device when no external field is applied [14], we used the ^{3}He Refrigerator of the PCPM Laboratory[3]. The refrigerator was used with a superconducting solenoid enclosing the measurement chamber, able to provide a central magnetic field oriented along the main axis of the cryostat up to 15 T. A rotating platform equipped with a DIP-socket was mounted at the end of the stick, allowing an appropriate orientation of the sample with respect to the magnetic field with a precision of about 0.1° [64]. Together with the sample holder, the DIP-socket was equipped with a carbon glass resistance thermometer calibrated against a RuO$_2$ thermistor to monitor the temperature as close as possible to the sample. Due to the small difference in the positions of the thermal probe and the sample in the ^{3}He bath, a small

---

[3]This device was adapted for transport experiments by Prof. V. Bayot *et al.* at UCL/FSA/MAPR/PCPM.

error on the temperature of the sample can occur: in comparison with other studies using the same equipment, this error is estimated to be around 40 mK, namely a raw 10 % uncertainty [65].

The complete experimental setup for low temperature measurements is depicted in Fig. 3.5: the right-hand part of the drawing displays the low temperature controls and the left-hand part shows the data measurement and acquisition system.
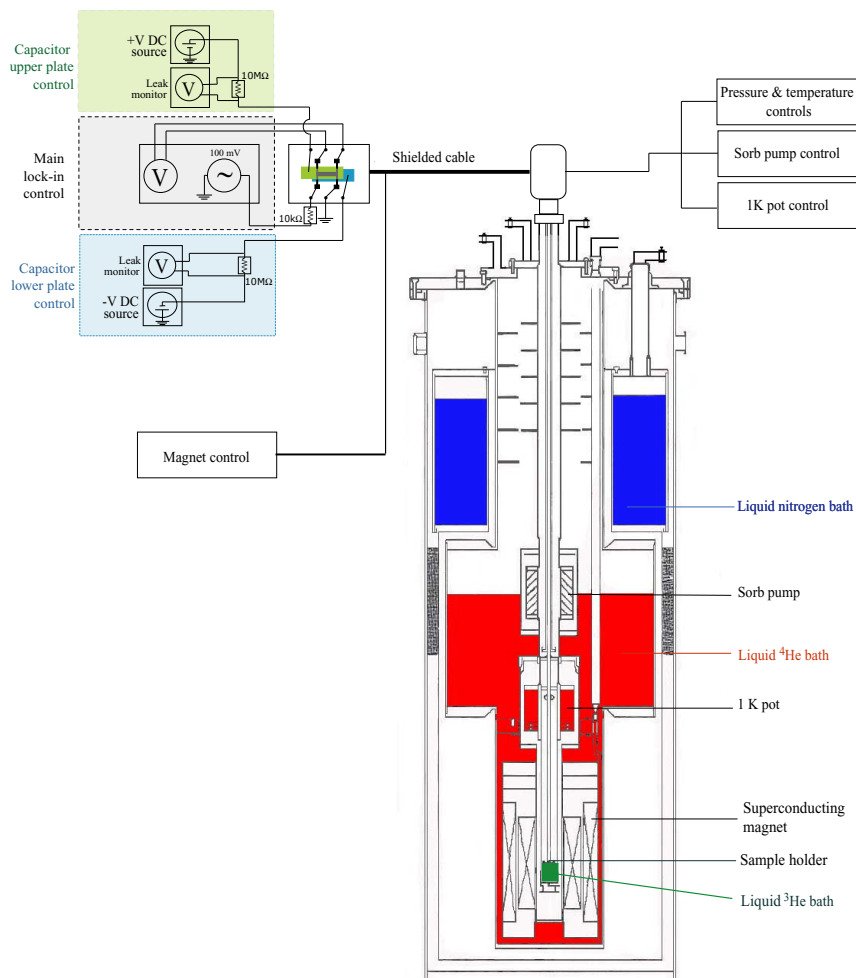
Figure 3.5: Simplified design of the measurement setup in ^{3}He cryostat.

The ^{3}He cryostat allows for low-temperature experiments down to 300 mK. After intermediate cooling in liquid nitrogen and liquid ^{4}He successively, the cooling to very low temperatures using ^{3}He is made in a two-steps cycle. In a first stage, ^{3}He is condensed along the walls of the so-called "1 K pot", which is a small chamber containing ^{4}He cooled to 1.2-2 K. When the experimental chamber at the bottom of the refrigerator contains enough liquid ^{3}He, then the pressure above the bath is lowered down to 10^{-3} mbar, corresponding to a temperature of about 0.3 K in the chamber. This pumping is achieved by a "sorb pump", which adsorbs gaseous ^{3}He on its surface when cooled below 4.2 K, and releases it when heated around 30 K. The experimental cycle is interrupted when all liquid ^{3}He has been evaporated and adsorbed on the sorb pump: it is then released and condensed again on the 1K pot. A precise control of the adsorption of ^{3}He allows for a fine tuning of the temperature of the bath between the base temperature and 1.8 K. Above 1.8 K, temperature is regulated by a heating resistor.

Resistivity measurements are performed by a four-probes method using a standard lock-in technique: the sample is biased by a (15.5 Hz) low-frequency current between two contacts, and the two others contacts allow for a measurement of the resulting AC voltage across the sample. The advantage of this technique is that we then get rid of the contact resistances: therefore, we expect a vanishing voltage when the sample enters its superconducting phase where it looses its resistivity. We limit excessive heating effects in the ^{3}He bath by biasing the sample with a current as low as possible, typically on the order of several μA. The lock-in is equipped with appropriate bandpass filter to reduce the noise on the signals. Measuring devices are connected to an acquisition and control computer where the resistance of the slab, the temperature and the magnetic field are recorded at 1 record/s.

DC voltages are applied on the two capacitor plates to adjust the electric field perpendicular to the slab. Any leak current from the plates (eventually observed if the disruptive voltage of the dielectric is reached, resulting in an irreversible damage of the sample) are monitored by measuring the voltage across a 10 MΩ resistance. To give an idea of the corresponding electric field, consider a plane capacitor filled with a 500-nm-thick dielectric layer (the thickness of the central Al slab is then negligible); since the relative dielectric constant of Si$_3$N$_4$ lies around 7.5 [66], a voltage difference of 1 V results in an electric field of approximatively 15 MV/m. In order to keep the applied electric field below the breakdown field of Si$_3$N$_4$ during the phase diagram measure-

ments, we progressively incremented the tensions on the capacitor plates on a test sample at 380 mK in absence of magnetic field: we reported leak currents through the capacitor plates when they were submitted to -38 V / +38 V.

Finally, the magnetic field is adjusted by injecting a current in the superconducting solenoid cooled at 4.2 K; the value of the field is deduced from a measure of this current using a Hall probe. In order to ensure sufficiently stable values of the magnetic field, we performed low speed sweeping at 50 gauss/min.

3.3   Resistance measurements

With the help of the setup described in the previous section, we performed a series of resistance measurements on two different samples. To identify the phase diagram of the superconducting slab, we cooled the sample below the critical temperature in the absence of any electric and magnetic field. Then for successive fixed values of the voltage between the plates of the capacitor, we swept the magnetic field up until we observed the critical magnetic field at which the sample becomes resistive.

3.3.1   First sample

For the experiments on the first sample (which was actually labelled as ♯ 3), we used 100 mV bias voltage on a 10 kΩ resistance (in series with the sample, with negligible resistance), resulting in a current of about 10 μA. In a resistive regime close to the critical temperature, this current resulted in a voltage of about 35 μV across the sample, from which we deduced its resistance, of the order of 3.5 Ω. In the absence of any external field, we measured a critical temperature of 1.438 K (Fig. 3.6).

Each series of measurements was carried out at fixed temperature. The magnetic field was then ramped upwards across its critical value along the surface of the sample, for a series of constant voltages symmetrically applied on the two plates of the capacitor by increasing steps of 5 volts. Fig. 3.7 (top graphic) displays the measured resistance as a function of the electric field (implicitly given by the voltage on the capacitor plates) and the magnetic field. The inset graph shows the temperature averaged over the complete sweep for each value of the capacitor voltage: the first point is significantly higher than the others because the base temperature was not reached at that time; if this
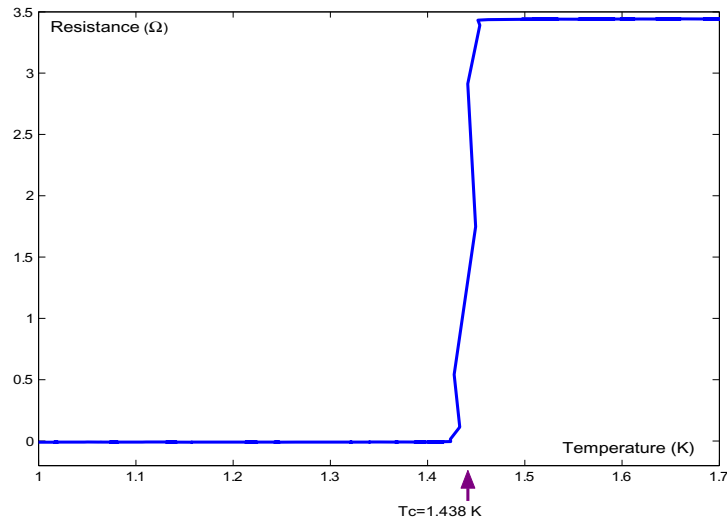
Figure 3.6: Electrical resistance of sample ♯ 3 as a function of the temperature, in absence of external electric and magnetic fields; the phase transition between normal and superconducting state is observed at ∼1.4 K.

point is excluded, the mean temperature for the complete range of measurements is 0.387 K with a standard deviation of 0.015 K. As it may be seen from the graph, there is no apparent dependence of the critical magnetic field on the electric field: its mean value is 80.6 gauss, with variations between 77.2 gauss and 81.7 gauss.

The same analysis was performed at a higher temperature, see Fig. 3.7 (middle graphic). The mean value of the temperature is 0.692 K with a standard deviation of 0.02 K (inset graph). The critical magnetic field is lower due to the change in temperature, but still it is not affected by the change in the applied electric field: all the critical values lie between 24.7 gauss and 25.0 gauss with an averaged value of 24.7 gauss.

Figure 3.7: (Next page) Electrical resistance of sample ♯ 3 as a function of the magnetic field and the capacitor voltage, analysed for 3 different values of the [3]He bath temperature from top to bottom: T∼ 0.4 K, T∼ 0.7 K, T∼ 1.1 K. The inset graphs show the averaged temperature over the whole magnetic sweep for each value of the capacitor voltage.
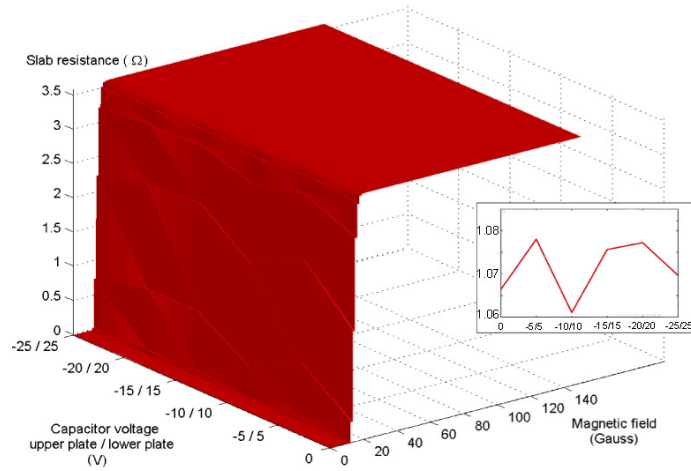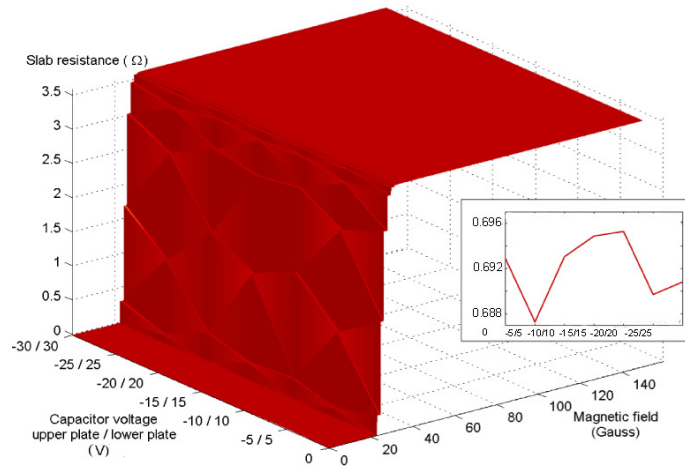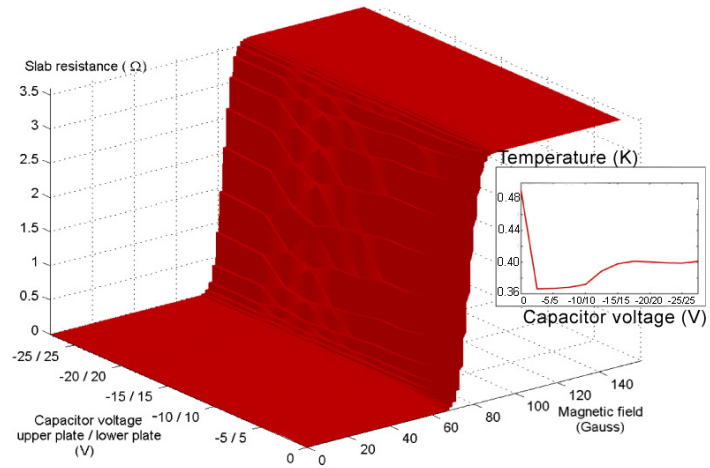
A third series of data was taken even closer to the critical temperature (Fig. 3.7, bottom graph). The measured temperature is 1.072 ± 0.007 K. Again, there is not any significant modification of the critical magnetic field when the capacitor voltage is increased: it remains around 14.1 gauss with all measured values between 13.6 gauss and 14.4 gauss.

3.3.2   Second sample

Another sample (labelled as $\sharp$ 4) was studied with the same methodology to confirm the results obtained with the previous device. We used identical lock-in parameters, namely a 100 mV bias voltage on a 10 kΩ resistance, corresponding to a bias current of 10 μA. In Fig. 3.8, we observe that the superconducting transition occurs at 1.539 K in the absence of external fields. The slab resistance at the critical temperature is 11.6 Ω. This difference with the resistance of sample $\sharp$3 may be explained by a small variation of the slab thickness[4] and by the addition of a fifth contact lead for characterisation purposes.
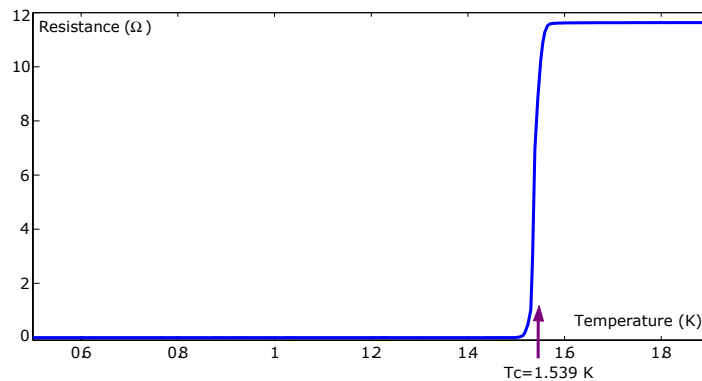
Figure 3.8: Electrical resistance of sample $\sharp$ 4 as a function of the temperature, in absence of external electric and magnetic fields; the phase transition between the normal and superconducting states is observed at $\sim$1.5 K.

Fig. 3.9 displays series of measurements operated with the previous method at two different temperatures. The upper graph was obtained at 0.385 K for symmetrical values of the voltage on the capacitor plates incremented by 2 V up to 10 V on each. All curves exhibit a critical magnetic field

---

[4]The exact thickness of both samples used for those measurements are unfortunately unknown: thickness characterisation was indeed performed on a limited number of samples to avoid possible damage by the tip of the profilometer.

between 61.3 gauss and 61.7 gauss. The data of the lower graph were taken at 1.470 K: again the critical magnetic field does not seem to be affected by the electric field and remains valued at around 5.6 gauss.
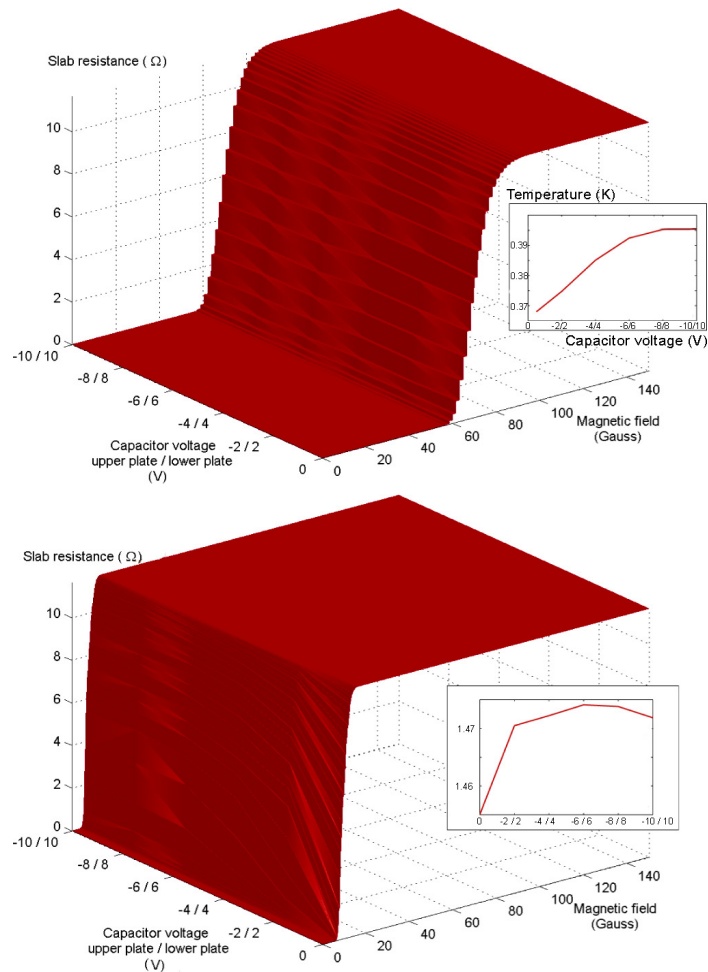
Figure 3.9: Electrical resistance of sample ♯ 4 as a function of the magnetic field and the capacitor voltage, analysed for two different values of the ^{3}He bath temperature: $T_{top} \sim 0.4$ K and $T_{bottom} \sim 1.4$ K. The inset graphs show the average temperature at each value of the capacitor voltage.

The analysis of all data presented in Figs. 3.7 and 3.9 suggests that an external electric field does not affect significantly the superconducting state. This conclusion seems in total contradiction with the expected behaviour based not only on the covariant theory, but also with the usual GL framework (see Fig. 1.5). Presumably, the explanation for this result is the fact that some non-paired *normal* electrons could play a crucial role against the electric field, whereas such contributions are not included in either model. Specifically, an electrostatic potential could combine with the thermodynamic potential in the superconductor, resulting in an effective potential acting on the condensate of Cooper pairs. The main consequence would be the formation of surface charge screening the external electric field, preventing it from penetrating the superconducting condensate. This interpretation will be discussed in the next chapter.

4

Relativistic BCS theory

I. Formulation

As a possible explanation for the observed phase diagram of the nanoscopic Al slab presented in the previous chapter, we assume that the external electric field could not penetrate the sample due to some screening by charge carriers. Since the phenomenological approach provided by the Ginzburg-Landau-Higgs action is in apparent contradiction with the experimental results, this screening mechanism is investigated by extending the microscopic BCS formulation of superconductivity in a relativistic formalism, enabling the covariant coupling of such systems to electric fields. This extension will be provided by a functional method, following an approach similar to that by which Gor'kov derived the non-relativistic Ginzburg-Landau theory from the non relativistic BCS theory [67].

4.1 Finite temperature field theory

A modern approach towards the microscopic understanding of superconductivity can be found using *equilibrium field theory at finite temperature*, or Thermal Field Theory (TFT) for short. This framework is the combination of two formalisms which have proved to be very successful on their own. TFT first includes Quantum Field Theory, which has been extensively developed for the description of fundamental particles and interactions and provides a wide

understanding of physical processes, including quantum fluctuations at various levels, classified and then calculated with the help of Feynman diagrams. The second element of TFT is Statistical Mechanics, particularly suitable for describing many-body problems, which involves the idea of statistical fluctuations as a consequence of the modification of Bose-Einstein or Fermi-Dirac distributions at non-zero temperature. TFT is therefore used in many-body problems where the underlying dynamics is described by quantum fields. Its first non-relativistic version was invented in the late 1950s for the purposes of nuclear matter; then a relativistic theory was developed for studying high temperature transitions occurring in the early universe; recent applications of TFT include the study of quark-gluon plasmas and general QCD processes at high density and/or high temperatures, as well as ultra-relativistic ion collisions. Since the domain of applications for TFT is wide, the literature devoted to it is extremely abundant; general considerations and structure of the formalism can be found in the books by Kapusta [68] and Le Bellac [69]. Explicit calculations in TFT can be either performed in the operator formalism or in the path integral formalism. We refer to Appendix D and to Ref. [69] for a detailed description of the two methods.

Before starting the description of TFT, we fix the choice of units by assuming $\hbar = c = 1$ (all notations and conventions are listed in the first Appendix). Let us introduce the partition function of a physical system of bosonic configuration space degrees of freedom q, described by a hamiltonian $\hat{H}$ in the operator formalism[1]

$$Z(\beta) = \text{Tr}\, e^{-\beta H} = \sum_n e^{-\beta E_n} \, , \quad \beta = \frac{1}{kT} \tag{4.1}$$

where the trace has been evaluated using a complete set of eigenvectors of the hamiltonian operator H. Since position eigenstates $\{|q\rangle\}$ define a complete set of states, it may be used to evaluate the trace and the partition function may alternatively be written

$$Z(\beta) = \int dq\, \langle q| e^{-\beta H} |q\rangle \tag{4.2}$$

from which it is clear that the partition function may be regarded as a propagator from 0 to β in imaginary time, subjected to the boundary condition

---

[1]Operators are generally denoted with a hat symbol to avoid confusion with observable values; since the forthcoming calculations do not contain misleading expressions, the hat notation shall be omitted from now on.

$q(\beta) = q(0)$. Assuming the hamiltonian admits the general form $H = p^2/2m + V(q)$ where p is the momentum operator conjugate to the position operator $[q, p] = i$, the partition function also admits the following path integral representation, where the integration over conjugate momenta has already been performed:

$$Z(\beta) = \int \mathcal{D}q(\tau) \, e^{-S_E(\beta)}, \quad \text{with} \qquad S_E(\beta) = \int_0^\beta d\tau \, L_E[q(\tau)],$$

$$L_E[q(\tau)] = \frac{m}{2}\left(\frac{dq}{d\tau}\right)^2 + V(q). \quad (4.3)$$

The remaining integral is to be performed over paths subjected to the aforementioned periodic boundary condition. The path integral formulation of the partition function is formally extended to the case of a Quantum Field Theory, for which the value of the field at every position of space defines an infinite set of degrees of freedom. The expression S_E is usually referred to as the euclidean action. In the case of QFT over Minkowski spacetime, the analytic continuation from real to imaginary time implies a change in the spacetime geometry, from Minkowski to an Euclidean space with the change of signature $t^2 - \mathbf{x}^2 \rightarrow -(\tau^2 + \mathbf{x}^2)$.

For the case of a complex fermionic field $\psi(\mathbf{x}, \tau)$, the quantum prescription is the equal time anticommutation relation between the field and its hermitian conjugate $\{\psi_r(\mathbf{x}, \tau_o), \psi_s^\dagger(\mathbf{y}, \tau_o)\} = \delta_{rs}\delta^{(3)}(\mathbf{x} - \mathbf{y})$ where r and s are spin indices. The path integral formulation of the partition function then becomes

$$Z(\beta) = \int \mathcal{D}\psi \mathcal{D}\psi^\dagger \, e^{-S_E(\beta)}$$

$$S_E(\beta) = \int_0^\beta d\tau \int d^3\mathbf{x} \, \mathcal{L}_E[\psi(\mathbf{x}, \tau), \psi^\dagger(\mathbf{x}, \tau)] \qquad (4.4)$$

$$\mathcal{L}_E = [\psi^\dagger(\mathbf{x}, \tau)\partial_\tau \psi(\mathbf{x}, \tau) + \mathcal{H}(\psi^\dagger, \psi)]$$

with *anti-periodical* boundary condition $\psi(\mathbf{x}, \beta) = -\psi(\mathbf{x}, 0)$ as demonstrated in Appendix D, since the field and its conjugate obey anti-commutation relations.

Assuming we can effectively construct and evaluate an expression of the partition function either through (4.1) or (4.4), the *effective action* S_{eff} is then defined as

$$S_{\text{eff}}(\beta) = -\frac{1}{\beta}\ln Z(\beta), \quad Z(\beta) = e^{-\beta S_{\text{eff}}}. \qquad (4.5)$$

The functional S_{eff} has the dimension of an energy and actually corresponds to the Helmholtz free energy in a thermodynamics formalism: it provides an

effective theory in the sense that an infinitesimal variation of external fields gives the usual equations of motion for these fields [70]. In theoretical superconductivity, this method was achieved for the first time by Gor'kov, who obtained the Ginzburg-Landau free energy from the microscopic BCS hamiltonian [67]. In the same way, we shall develop a phenomenological relativistic theory of superconductivity by showing that this effective action S_{eff} may be expanded into a form to be compared with the usual Ginzburg-Landau functional. To this end, the first step consists in identifying the relevant euclidean action which enters the partition function.

4.2   Effective coupling for a relativistic BCS theory

The present work is not the first attempt towards the formulation of a relativistic generalisation of the BCS theory: indeed, several authors already considered Dirac fermions within the BCS approach. In either cases, the starting point is the free relativistic Dirac hamiltonian augmented by an interaction term that models the attractive coupling between electrons. The major differences between the published papers lie with the motivations for the choice of the appropriate expression of the interaction. As is the case in the non-relativistic BCS theory, it is generally assumed that the exchange phonon carries no momentum, hence reducing the electron coupling to a local interaction between four fermions. To our knowledge, the first systematic treatment of all possible quadrilinear fermionic couplings was given by Capelle *et al.* [71, 72], who listed all bilinear order parameters consistent with the requirement of Lorentz covariance, and operated a classification of them according to their behaviour under the Lorentz transformation[2]. In particular, they restricted the possible choice for a relativistic BCS generalisation to the $(\bar{\psi}\psi)^2$ scalar coupling only by requiring a spin singlet structure with symmetry under parity. In a later paper [73], they completed the relativistic generalization of the Bogoliubov-de Gennes formulation of the BCS theory with their choice of order parameter, and examined the prospects for experimental detection of relativistic effects in superconductors through measurements of spin properties and specific kinds of fluctuations. In a more recent treatment, Ohsaku [74, 75] formulated a generalised BCS mechanism in relativistic quantum field theory, following the Gor'kov-Nambu functional method. In a systematic numerical

---

[2]The reader is referred to Appendix C for a detailed description of the Dirac equation and the properties of Dirac spinors under Lorentz transformations and other discrete symmetries.

treatment of all possible bilinear structures for the order parameter, that author discussed the form of the gap equation and the quasiparticle spectrum for all couplings. Similar treatments were used to develop a non-relativistic time-dependent Ginzburg-Landau theory [76]. In particle physics, functional methods based on the BCS theory have also become a standard in particle physics for the study of quark pairing, whose interaction has a strong similarity with BCS electron pairing up to an additional color index which justifies the now popular denomination of *color superconductivity*. The analogy between BCS superconductivity and quark matter has been given in a very pedagogical way by R. Casalbuoni in Ref. [77].

In the present analysis, the appropriate choice for the order parameter structure is performed by requiring that the BCS theory be reproduced in the non-relativistic limit. We start by writing the more general form of a Lorentz covariant lagrangian describing the pairing between two Grassmann odd Dirac spinor fields $\psi(x)$:

$$\mathcal{L}_{\text{int}} = g_1(\bar{\psi}\psi)^2 + g_2(\bar{\psi}\gamma_5\psi)^2 + g_3(\bar{\psi}\gamma^\mu\psi)^2 + g_4(\bar{\psi}\gamma^\mu\gamma_5\psi)^2 + g_5(\bar{\psi}\sigma^{\mu\nu}\psi)^2 \quad (4.6)$$

with $\bar{\psi} = \psi^\dagger\gamma^0$, considering respectively scalar, pseudo-scalar, vector, axial-vector and tensor structures under Lorentz transformations for the bilinear couplings. The interaction lagrangian (4.6) already assumes a local four-fermion interaction. This local coupling of four identical electron fields implies that the terms considered in (4.6) do not constitute a set of linearly independent couplings. This can be seen by operating a *Fierz transformation* [78, 79], which establishes a relation between products of bilinears when two of the constitutive spinors are exchanged. Denoting

$$
\begin{aligned}
s_1 &= \bar{\psi}_4\psi_2\ \bar{\psi}_3\psi_1 & s_2 &= \bar{\psi}_4\psi_1\ \bar{\psi}_3\psi_2 \\
v_1 &= \bar{\psi}_4\gamma^\mu\psi_2\ \bar{\psi}_3\gamma_\mu\psi_1 & v_2 &= \bar{\psi}_4\gamma^\mu\psi_1\ \bar{\psi}_3\gamma_\mu\psi_2 \\
t_1 &= \tfrac{1}{2}\bar{\psi}_4\sigma^{\mu\nu}\psi_2\ \bar{\psi}_3\sigma_{\mu\nu}\psi_1 & t_2 &= \tfrac{1}{2}\bar{\psi}_4\sigma^{\mu\nu}\psi_1\ \bar{\psi}_3\sigma_{\mu\nu}\psi_2 \\
a_1 &= \bar{\psi}_4\gamma_5\gamma^\mu\psi_2\ \bar{\psi}_3\gamma_\mu\gamma_5\psi_1 & a_2 &= \bar{\psi}_4\gamma_5\gamma^\mu\psi_1\ \bar{\psi}_3\gamma_\mu\gamma_5\psi_2 \\
p_1 &= \bar{\psi}_4\gamma_5\psi_2\ \bar{\psi}_3\gamma_5\psi_1 & p_2 &= \bar{\psi}_4\gamma_5\psi_1\ \bar{\psi}_3\gamma_5\psi_2
\end{aligned}
\quad (4.7)
$$

the Fierz identities take the explicit form

$$
\begin{pmatrix} s_1 \\ v_1 \\ t_1 \\ a_1 \\ p_1 \end{pmatrix} = -\frac{1}{4}
\begin{pmatrix}
1 & 1 & 1 & 1 & 1 \\
4 & -2 & 0 & 2 & -4 \\
6 & 0 & -2 & 0 & 6 \\
4 & 2 & 0 & -2 & -4 \\
1 & -1 & 1 & -1 & 1
\end{pmatrix}
\begin{pmatrix} s_2 \\ v_2 \\ t_2 \\ a_2 \\ p_2 \end{pmatrix}.
\quad (4.8)
$$

One shows that the transformation matrix admits the degenerate set of eigenvalues $\lambda_i = \{-1, -1, 1, 1, 1\}$, so that the following identities are proved:

$$
\begin{aligned}
(v_1 - a_1) &= (v_2 - a_2) \\
2(s_1 - p_1) - (v_1 + a_1) &= 2(s_2 - p_2) - (v_2 + a_2) \\
(s_1 + p_1) - t_1 &= (s_2 + p_2) - t_2 \\
2(s_1 - p_1) + (v_1 + a_1) &= (-1)[2(s_2 - p_2) + (v_2 + a_2)] \\
3(s_1 + p_1) + t_1 &= (-1)[3(s_1 + p_1) + t_1] \, .
\end{aligned}
\tag{4.9}
$$

In particular when considering four identical Dirac fermion fields $\psi_1 = \psi_2 = \psi_3 = \psi_4 = \psi$, then the quadrilinear expressions (4.7) with subscripts 1 and 2 are identical and the linear combinations associated to negative eigenvalues must vanish, leaving only three linearly independent combinations

$$
\begin{aligned}
v - a &= (\bar{\psi}\gamma^\mu\psi)(\bar{\psi}\gamma_\mu\psi) + (\bar{\psi}\gamma^\mu\gamma_5\psi)(\bar{\psi}\gamma_\mu\gamma_5\psi) \\
2(s - p) - (v + a) &= 2\left[(\bar{\psi}\psi)(\bar{\psi}\psi) - (\bar{\psi}\gamma_5\psi)(\bar{\psi}\gamma_5\psi)\right] \\
&\quad - \left[(\bar{\psi}\gamma^\mu\psi)(\bar{\psi}\gamma_\mu\psi) - (\bar{\psi}\gamma^\mu\gamma_5\psi)(\bar{\psi}\gamma_\mu\gamma_5\psi)\right] \\
(s + p) - t &= \left[(\bar{\psi}\psi)(\bar{\psi}\psi) + (\bar{\psi}\gamma_5\psi)(\bar{\psi}\gamma_5\psi)\right] - \frac{1}{2}(\bar{\psi}\sigma^{\mu\nu}\psi)(\bar{\psi}\sigma_{\mu\nu}\psi) \, .
\end{aligned}
\tag{4.10}
$$

It should be clear that these particular choices for the structure of the bilinears actually describe couplings of one fermion to one anti-fermion; hence the interaction of two fermions is most appropriately obtained by charge-conjugating one of the bilinears in the above linear combinations. One has:

$$
\begin{aligned}
\bar{\psi}\psi = \bar{\psi}_c\psi_c \, , \quad \bar{\psi}\gamma^\mu\psi = -\bar{\psi}_c\gamma^\mu\psi_c \, , \quad \bar{\psi}\sigma^{\mu\nu}\psi = -\bar{\psi}_c\sigma^{\mu\nu}\psi_c \, , \\
\bar{\psi}\gamma_5\psi = \bar{\psi}_c\gamma_5\psi_c \, , \quad \bar{\psi}\gamma^\mu\gamma_5\psi = \bar{\psi}_c\gamma^\mu\gamma_5\psi_c \, ,
\end{aligned}
\tag{4.11}
$$

with $\psi_c = \eta_c C\bar{\psi}^T$, $|\eta_c| = 1$ (see Appendix C). Considering again the Fierz identities with $\psi_1 = \psi_3 = \psi_c$ and $\psi_2 = \psi_4 = \psi$, all possible linearly independent combinations may then be constructed from

$$
\begin{aligned}
&\frac{1}{2}\alpha_1\left[(\bar{\psi}\gamma^\mu\psi)^2 + (\bar{\psi}\gamma^\mu\gamma_5\psi)^2\right] \\
+\quad &\frac{1}{2}\alpha_2\left[2[(\bar{\psi}\psi)^2 - (\bar{\psi}\gamma_5\psi)^2] - [(\bar{\psi}\gamma^\mu\psi)^2 - (\bar{\psi}\gamma^\mu\gamma_5\psi)^2]\right] \\
+\quad &\frac{1}{2}\alpha_3\left[[(\bar{\psi}\psi)^2 + (\bar{\psi}\gamma_5\psi)^2] - \frac{1}{2}(\bar{\psi}\sigma^{\mu\nu}\psi)^2\right] \\
=\quad &\beta_1(\bar{\psi}_c\psi)^\dagger(\bar{\psi}_c\psi) + \beta_2(\bar{\psi}_c\gamma_5\psi)^\dagger(\bar{\psi}_c\gamma_5\psi) + \beta_3(\bar{\psi}_c\gamma^\mu\gamma_5\psi)^\dagger(\bar{\psi}_c\gamma_\mu\gamma_5\psi)
\end{aligned}
\tag{4.12}
$$

with $\beta_1 = (\alpha_1 - \alpha_3)$, $\beta_2 = (\alpha_1 + \alpha_3)$ and $\beta_3 = \alpha_2$.

The identification of the appropriate coupling follows from the properties of these bilinears under discrete symmetry transformations.

Under **parity transformation**, the spinors transform according to

$$\psi'(\mathbf{x},t) = \eta_p \gamma^0 \psi(-\mathbf{x},t) , \quad \psi'_c(\mathbf{x},t) = -\bar{\eta}_p \gamma^0 \psi_c(-\mathbf{x},t) , \quad |\eta_p| = 1; \qquad (4.13)$$

hence the bilinears admit the following properties:

$$
\begin{aligned}
\bar{\psi}'_c \psi' &= -\eta_p^2 \bar{\psi}_c \psi \\
\bar{\psi}'_c \gamma_5 \psi' &= +\eta_p^2 \bar{\psi}_c \gamma_5 \psi \\
\bar{\psi}'_c \gamma^0 \gamma_5 \psi' &= +\eta_p^2 \bar{\psi}_c \gamma^0 \gamma_5 \psi \\
\bar{\psi}'_c \boldsymbol{\gamma} \gamma_5 \psi' &= -\eta_p^2 \bar{\psi}_c \boldsymbol{\gamma} \gamma_5 \psi .
\end{aligned}
\qquad (4.14)
$$

In either case, the transformation of the bilinears have an explicit dependence on the arbitrary choice of the transformation phase parameter η_p; therefore, the parity is not uniquely defined for these bilinears and may not constitute an argument towards the identification of the appropriate relativistic coupling, in contradiction with Capelle *et al.* [72].

Under **time reversal**, the Dirac spinor transforms according to

$$\psi'(\mathbf{x},t) = \eta_T i \gamma^1 \gamma^3 \psi(\mathbf{x},-t) = -\eta_T i C \gamma_5 \psi(\mathbf{x},-t) \qquad (4.15)$$

in the Dirac representation; on the other hand,

$$\bar{\psi}_c = \eta_c C \bar{\psi}^T \qquad (4.16)$$

so that one proves

$$
\begin{aligned}
\bar{\psi}_c \psi &= i\bar{\eta}_c \psi^T \gamma_5 (i\gamma^1 \gamma^3 \psi) = i\bar{\eta}_c \eta_T^{-1} \psi^T \gamma_5 \psi' \\
\bar{\psi}_c \gamma_5 \psi &= i\bar{\eta}_c \eta_T^{-1} \psi^T \psi' \\
\bar{\psi}_c \gamma^\mu \gamma_5 \psi &= -i\bar{\eta}_c \eta_T^{-1} \psi^T \gamma^{\mu T} \psi' .
\end{aligned}
\qquad (4.17)
$$

One should recall that the original non-relativistic BCS theory couples time-reversed states, as it has been shown by Anderson [80]; consequently, only the bilinear expression $\bar{\psi}_c \gamma_5 \psi$ couples an electron with its time-reversed state in the s-wave and is therefore considered as a valid candidate for the relativistic extension of the BCS theory.

This suggestion is further supported by the analysis of the spin structure of the above bilinears. From the mode expansion of the Dirac spinor

$$\psi(x) = \sum_s \int \frac{d^3 \mathbf{k}}{(2\pi)^3 \, 2\omega(\mathbf{k})} \left[b(\mathbf{k},s) u(\mathbf{k},s) e^{-ikx} + d^\dagger(\mathbf{k},s) v(\mathbf{k},s) e^{ikx} \right] \qquad (4.18)$$

one may calculate the expansion of the charge conjugate spinor. The spin structure of the bilinear couplings then follows from the analysis of the quantities

$$u^T(\mathbf{k}, s_1)\, C\, \Gamma\, u(-\mathbf{k}, s_2)\,, \quad \Gamma = 1, \gamma_5, \gamma^\mu \gamma_5\,.$$

Denoting all possible values by a 2×2 matrix such that one considers respectively the spin configurations

$$\begin{pmatrix} \uparrow\uparrow & \uparrow\downarrow \\ \downarrow\uparrow & \downarrow\downarrow \end{pmatrix},$$

then one has the following structures for the bilinears:

$$\Gamma = 1 \qquad 2\begin{pmatrix} k_1 + ik_2 & -k_3 \\ -k_3 & -k_1 + ik_2 \end{pmatrix} \tag{4.19}$$

$$\Gamma = \gamma_5 \qquad -2\omega(\mathbf{k})\begin{pmatrix} 0 & 1 \\ -1 & 0 \end{pmatrix} \tag{4.20}$$

$$\Gamma = \gamma^\mu \gamma_5 \qquad \mu = 0: \ 2m\begin{pmatrix} 0 & 1 \\ -1 & 0 \end{pmatrix} \tag{4.21}$$

$$\mu = 1: \ \begin{pmatrix} -k_3 & ik_2 \\ ik_2 & -k_3 \end{pmatrix}$$

$$\mu = 2: \ \begin{pmatrix} -ik_3 & -ik_1 \\ -ik_1 & ik_3 \end{pmatrix}$$

$$\mu = 3: \ \begin{pmatrix} k_1 + ik_2 & 0 \\ 0 & k_1 - ik_2 \end{pmatrix}$$

hence establishing again that $\bar{\psi}_c \gamma_5 \psi$ is the required coupling, since this is the only spin-singlet structure which couples states with opposite spins.

In conclusion, both arguments based on time reversal properties and the spin structure of the bilinear couplings support the choice of $\bar{\psi}_c \gamma_5 \psi$ as the relativistic generalisation of the BCS order parameter for s-wave pairing of electrons with opposite spins. As it will be shown in the following chapters, this particular order parameter leads to the identification of one energy gap which is a direct generalisation of the BCS gap; it would be interesting to investigate the two other bilinear structures $\bar{\psi}_c \psi$ and $\bar{\psi}_c \gamma^\mu \gamma_5 \psi$ in order to provide a description of materials with multiple gaps and other couplings (such as d-wave superconductivity, experimentally observed in some high-Tc oxides for

instance). This is however beyond the scope of this work, and we shall only concentrate on the interaction lagrangian

$$\mathcal{L}_{\text{int}} = -\frac{g}{2}(\bar{\psi}_c\gamma_5\psi)^\dagger(\bar{\psi}_c\gamma_5\psi) \tag{4.22}$$

where the normalisation of the coupling constant has been made for future convenience.

4.3 The effective action

In principle, we are now able to construct the complete expression of the Euclidean action. First, the dynamics of the free fermion field is naturally provided by the Dirac Lagrangian

$$L_D = i\bar{\psi}(x)(\slashed{\partial} - m)\psi(x) = \frac{i}{2}\left[\bar{\psi}(x)\gamma^\mu\partial_\mu\psi(x) - \partial_\mu\bar{\psi}(x)\gamma^\mu\psi(x)\right] - m\bar{\psi}(x)\psi(x). \tag{4.23}$$

The coupling of the Dirac field to the electromagnetic sector is performed through *minimal substitution* which ensures local U(1) gauge invariance $\partial_\mu \rightarrow \partial_\mu + ieA_\mu$, where $A_\mu = (\Phi, \mathbf{A})$ is the electromagnetic vector potential and $e = -|e| < 0$ is the electron charge. The complete lagrangian should also be augmented by the free electromagnetic lagrangian leading to the homogeneous Maxwell equations

$$L_{\text{em}} = -\frac{1}{4}F_{\mu\nu}F^{\mu\nu} \quad , \quad F_{\mu\nu} = \partial_\mu A_\nu - \partial_\nu A_\mu ; \tag{4.24}$$

however, the electromagnetic field is considered as an external field in the path integral over the fermions (4.4). Hence, the complete analysis of the effective action may be performed without considering the purely electromagnetic sector. The energy of the electromagnetic field shall eventually be added after the effective action is computed, in order to identify the appropriate screening lengths.

Finally, the interaction lagrangian between fermions has been proved to be of the form (4.22). All contributions are collected into the complete lagrangian density

$$\mathcal{L} = \frac{i}{2}\left[\bar{\psi}\gamma^\mu\partial_\mu\psi - \partial_\mu\bar{\psi}\gamma^\mu\psi\right] - m\bar{\psi}\psi - eA_\mu\bar{\psi}\gamma^\mu\psi - \frac{g}{2}(\bar{\psi}_c\gamma_5\psi)^\dagger(\bar{\psi}_c\gamma_5\psi) \tag{4.25}$$

so that we identify the hamiltonian density

$$\mathcal{H} = -\frac{i}{2}\left[\bar{\psi}\boldsymbol{\gamma}\cdot\boldsymbol{\nabla}\psi - \boldsymbol{\nabla}\bar{\psi}\cdot\boldsymbol{\gamma}\psi\right] + m\bar{\psi}\psi + eA_\mu\bar{\psi}\gamma^\mu\psi + \frac{g}{2}(\bar{\psi}_c\gamma_5\psi)^\dagger(\bar{\psi}_c\gamma_5\psi) . \tag{4.26}$$

From the U(1) phase symmetry of this hamiltonian, we infer the conservation of the number of fermions; in the thermodynamics language, this means working in the grand-canonical ensemble, in which the hamiltonian is shifted by a term $\mu_o N$ where μ_o is the *chemical potential* and N the number of conserved charges. In numerical analyses, we shall consider that the chemical potential is equal to the Fermi energy, which is strictly true at zero temperature only. However, one proves that the temperature dependence of the chemical potential is given by [81]

$$\mu_o(T) = E_F \left[1 - \frac{1}{3} \left(\frac{\pi k_B T}{2 E_F} \right)^2 \right] , \tag{4.27}$$

which leads only a shift from the Fermi level of about 0.01 percent at room temperature.
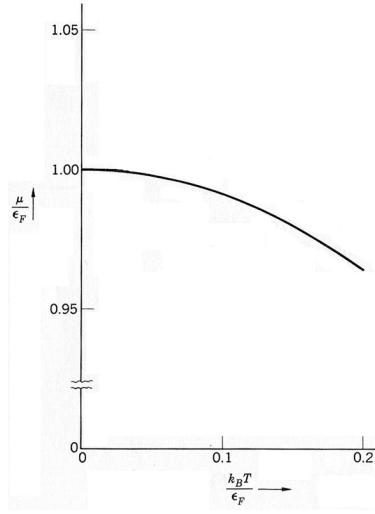
Figure 4.1: Temperature dependence of the chemical potential for a free electron gas (adapted form [82]).

The hamiltonian becomes

$$H \to H - \mu_o N = H - \mu_o \psi(x)^\dagger \psi(x)$$

and the Euclidean action then reads

$$S_E = \int_0^\beta d\tau \int_{(\infty)} d^3\mathbf{x} \left[\psi^\dagger \partial_\tau \psi + \mathcal{H} - \mu_o \psi^\dagger \psi \right] . \tag{4.28}$$

The quadrilinear interaction can be eliminated by inserting inside the action an additional term

$$\frac{1}{2g} \left(\Delta - g\eta_c \bar{\psi}_c \gamma_5 \psi \right)^\dagger \left(\Delta - g\eta_c \bar{\psi}_c \gamma_5 \psi \right) \tag{4.29}$$

introducing the auxiliary field $\Delta(\mathbf{x}, \tau) = g\eta_c \bar{\psi}_c \gamma_5 \psi$, where η_c is an arbitrary phase from the charge conjugation of one of the bilinears. In principle, this operation known as a Hubbard-Stratonovich transformation [83] would multiply the path integral measure for the effective action by

$$\int \mathcal{D}\Delta \mathcal{D}\Delta^\dagger \ e^{-\frac{1}{2g} \int_0^\beta d\tau \int d^3\mathbf{x} (\Delta - g\eta_c \bar{\psi}_c \gamma_5 \psi)^\dagger (\Delta - g\eta_c \bar{\psi}_c \gamma_5 \psi)} \ .$$

The above expression is recognised as a gaussian integral and acts only as a renormalisation of the partition function, with no consequence on the equations of motion resulting from the variational analysis of the euclidean action. By considering this gaussian integral, it should be clear that the auxiliary field $\Delta(x)$ actually describes the Cooper pair local density, the reason why it will be called from now on the *order parameter*. The advantage of this manipulation is that the auxiliary term cancels the quartic term of the interaction. The complete Euclidean lagrangian density now contains at most fermionic quadratic terms, and is finally given by

$$\begin{aligned}
\mathcal{L}_E &= \frac{1}{2} \left[\psi^\dagger \partial_\tau \psi - \partial_\tau \psi^\dagger \psi \right] - \frac{i}{2} \left[\bar{\psi} \boldsymbol{\gamma} \cdot \boldsymbol{\nabla} \psi - \boldsymbol{\nabla} \bar{\psi} \cdot \boldsymbol{\gamma} \psi \right] + m\bar{\psi}\psi + eA_\mu \bar{\psi} \gamma^\mu \psi - \mu_o \psi^\dagger \psi \\
&+ \frac{1}{2g} |\Delta|^2 - \frac{1}{2} \left[\Delta^\dagger (\bar{\psi}_c \gamma_5 \psi) + \Delta (\bar{\psi}_c \gamma_5 \psi)^\dagger \right]
\end{aligned} \tag{4.30}$$

where the arbitrary phase η_c has been absorbed into the complex field Δ. Considering the Euclidean action constructed from this lagrangian density and the Nambu-Gor'kov basis extended to the present covariant formalism

$$\Psi = \begin{pmatrix} \psi \\ \psi_c \end{pmatrix} \ ,$$

the partition function admits the matrix form

$$Z(\beta) = \int \mathcal{D}[\Psi, \overline{\Psi}, \Delta, \Delta^\dagger] \ e^{-\int_0^\beta d\tau \int d^3\mathbf{x} \left[\frac{1}{2g} |\Delta|^2 + \overline{\Psi} \mathcal{S} \Psi \right]} \tag{4.31}$$

with

$$S = \begin{pmatrix} \frac{1}{2} (\gamma^0 \partial_\tau - i\boldsymbol{\gamma} \cdot \boldsymbol{\nabla} + m - \mu_o \gamma^0 + eA_\nu \gamma^\nu) & \frac{1}{2} \Delta \gamma_5 \\ -\frac{1}{2} \Delta^\dagger \gamma_5 & \frac{1}{2} (\gamma^0 \partial_\tau - i\boldsymbol{\gamma} \cdot \boldsymbol{\nabla} + m + \mu_o \gamma^0 - eA_\nu \gamma^\nu) \end{pmatrix} \ . \tag{4.32}$$

Considering the fermionic nature of the field ψ, the Grassmann algebra is used for the evaluation of the path integral and yields

$$Z(\beta,\mu_o) = \int \mathcal{D}[\Delta,\Delta^\dagger] \, (\det \mathcal{S})^{1/2} \cdot e^{-\int_0^\beta d\tau \int_\infty d^3\mathbf{x} \, \frac{1}{2g}|\Delta|^2} . \tag{4.33}$$

We further consider the saddle-point approximation by which we avoid the explicit evaluation of the path integration over Δ and $\Delta^\dagger$: we shall restrict only to those values Δ_o which minimise the effective action and small fluctuations around this minimum. Incidentally, this is equivalent to Gor'kov's approach to the derivation of the Ginzburg-Landau effective action from the BCS theory. Denoting

$$Z(\beta,\mu) = e^{-\beta S_{\text{eff}}} , \tag{4.34}$$

the effective action may be evaluated perturbatively as

$$\beta S_{\text{eff}} = -\frac{1}{2} \ln \det \mathcal{S} + \int_0^\beta d\tau \int_\infty d^3\mathbf{x} \, \frac{1}{2g}|\Delta|^2 \tag{4.35}$$

$$= -\frac{1}{2} \ln \det \mathcal{S}_o - \frac{1}{2}\text{Tr}\,[\mathcal{S}_o^{-1}\Delta\mathcal{S}] + \frac{1}{4}\text{Tr}\,[\mathcal{S}_o^{-1}\Delta\mathcal{S}\mathcal{S}_o^{-1}\Delta\mathcal{S}] + \int_0^\beta d\tau \int d^3\mathbf{x} \, \frac{1}{2g}|\Delta|^2$$

where the operator $\mathcal{S}$ has been separated into two parts $\mathcal{S}_o + \Delta\mathcal{S}$. Accordingly, it is supposed that the order parameter may be separated as $\Delta(\mathbf{x}) = \Delta_o + \overline{\Delta}(\mathbf{x})$, assuming that it takes a constant homogeneous value Δ_o in the whole volume of the superconductor (London limit), up to small local fluctuations $\overline{\Delta}(\mathbf{x})$. The unperturbed matrix operator $\mathcal{S}_o$ is constructed by assuming a static situation with homogeneous density $\Delta_o = \text{constant}$ in the absence of any external electromagnetic field $A^\mu = 0$; then the remaining part of the operator $\Delta\mathcal{S}$ contains the local fluctuations of the order parameter as well as the possible nonvanishing values of the electromagnetic potential A^μ.

By definition, the inverse operator $\mathcal{S}_o^{-1}(x_1,x_2)$ acts as the Green's function for the differential operator $\mathcal{S}_o$. One shows that it corresponds to the propagator of the complex field ψ between $(\mathbf{x}_1,\tau_1)$ and $(\mathbf{x}_2,\tau_2)$ in imaginary time, which may also be expressed as the thermal average of the time-ordered product of the field at the two corresponding points of spacetime in the Heisenberg picture[3]. Assuming the exactly solvable part $\mathcal{S}_o$ is constructed from the hamiltonian H_o, we may thus write:

---

[3]The correspondence between the Green's function $\mathcal{S}_o^{-1}$, the propagator and the thermal averaged correlation functions $\langle\ \rangle_\beta$ is demonstrated in Appendix D for a system with one degree of freedom and may be generalised to the case of a field theory.

$$
\begin{aligned}
\mathcal{S}_o^{-1}(x_1, x_2) &= \frac{1}{Z_o(\beta)} \Big\langle T \, \psi(\mathbf{x}_1, \tau_1) \, \psi(\mathbf{x}_2, \tau_2) \Big\rangle_\beta \\
&= \frac{\mathrm{Tr} \left[\psi(\mathbf{x}_1, \tau_1) \psi(\mathbf{x}_2, \tau_2) e^{-\beta H_o} \right]}{\mathrm{Tr} \; e^{-\beta H_o}} \;, \quad \tau_1 > \tau_2 \; .
\end{aligned}
\tag{4.36}
$$

Let us now recall the usual Ginzburg-Landau free energy for an order parameter ψ, extended to its covariant expression in a static limit (Chapter 2) by considering both the gradients of the electrostatic and vector potentials Φ and $\mathbf{A}$ respectively,

$$
\mathcal{F}_{\mathrm{GL}}(T, \psi) = f |(\boldsymbol{\nabla} - 2ie\mathbf{A})\psi|^2 + V_{\mathrm{GL}}(|\psi|) + \frac{\varepsilon}{2} |\boldsymbol{\nabla}\Phi|^2 + \frac{1}{2\mu} |\boldsymbol{\nabla} \times \mathbf{A}|^2 \; .
\tag{4.37}
$$

It should be clear that, in the absence of external fields or gradients, the only remaining part is the Ginzburg-Landau potential. Consequently, the effective action for the unperturbed operator $\mathcal{S}_o$ identifies the effective potential $V_{\mathrm{eff}}(\Delta)$ for the particular case $\Delta = \Delta_o$. Once obtained for a homogeneous condensate of Cooper pairs, the expression of the effective potential must remain valid even for a space-dependent order parameter, since all orders of the series expansion of the potential for small fluctuations around the rigid condensate are expected to appear in the successive orders of perturbations of the effective action (4.35). On the other hand it appears that the chemical potential μ_o and the electrostatic potential Φ enter the differential operator (4.32) in the same manner, allowing the definition of the *electrochemical potential* $\mu_{\mathrm{ec}} = \mu_o - e\Phi$. Then we expect that the expression of the effective potential in absence of external fields would be extended by considering the fluctuations of the electrochemical potential, induced by corresponding space-homogeneous variations of the electrostatic potential around the chemical potential.

The other terms of interest are the gradients of the fields. Once the gradient of the order parameter is known, gauge invariance suggest the minimal substitution of the covariant derivative to identify the first term in (4.37). On the other hand, possible contributions to the electric and magnetic screening mechanisms should come by with gradients of the electrostatic potential Φ and the vector potential $\mathbf{A}$ respectively: this is the reason why the electric and magnetic permittivities in vacuum have *a priori* been replaced by some non-indexed effective values in (4.37). Since the electromagnetic potentials are contained in $\Delta\mathcal{S}$ and since squared gradients are needed, it should be sufficient to consider the expansion of the effective action to second order in the perturbation operator.

4.4   Gauge invariance and Wilson's prescription

We provide a description of relativistic fermions coupled to the electromagnetic field, the lagrangian is therefore invariant under the local U(1) gauge transformation

$$\psi(x) \to e^{iq\alpha(x)}\psi(x) , \quad A_\mu(x) \to A_\mu(x) - \partial_\mu\alpha(x) , \tag{4.38}$$

where q stands for the U(1) charge of the fermion ψ. This gauge invariance actually requires the minimal substitution of the ordinary gradient by the covariant derivative in the original lagrangian density. However, the separation of the effective action (4.35) in a homogeneous part S_o and ΔS containing small fluctuations of the condensate and electromagnetic potentials does *not* guarantee the gauge invariance of the successive terms of the perturbative expansion, since the two components S_o and ΔS are not gauge covariant separately for gauge fields $A_\mu(x)$ with an arbitrary space dependence: the prescription of gauge invariance can only be ensured after resummation to all orders of the perturbation series, while we shall restrict our expansion to the second order only. In consequence, since the gauge transformation (4.38) treats the electromagnetic field in a very specific way, we should be careful when trying to collect terms that contain definite powers of this field, and we would expect to miss some of those terms unless we carry out the explicit expansion to all orders, a task which is obviously impossible. Hopefully, that concern may be fixed by restoring the gauge invariance for the components chosen for S_o and ΔS. The method consists in integrating the vector potential **A** along a *Wilson line* in space whose extremities coincide with the origin and the end of the perturbation term [70]. In a stationary situation, the electrostatic potential Φ has the same form whatever gauge is chosen, and may therefore be considered without Wilson's construction.

Let the operator matrix ΔS be defined between two points in space x and y according to

$$\Delta S(x) = \delta^{(4)}(x-y)\Delta S(x,y). \tag{4.39}$$

Since the gauge transformation (4.38) has been defined locally, there is no guarantee that the transformations match at two neighbouring points; therefore a factor $\chi(x,y)$ is introduced to compensate for that possible change in the phase transformation between those points and hence verifies the following transformation:

$$e^{iq\chi'(y,x)} = e^{iq\alpha(y)}e^{iq\chi(y,x)}e^{-iq\alpha(x)} . \tag{4.40}$$

Essentially, the purpose of this compensating function is to cancel the gradient of the arbitrary gauge function $\alpha(\mathbf{x})$ affecting the gauge transformation of the vector potential: $\mathbf{A}' = \mathbf{A} + \boldsymbol{\nabla}\alpha$. Assuming we work in an equilibrium situation with no time dependence, it may be proved that the integration of the vector potential along a path between some initial position $\mathbf{x}_o$ and $\mathbf{x}$ fulfils this condition. Let us consider

$$\chi(\mathbf{x}) = - \int_{\mathbf{x}_o}^{\mathbf{x}} d\mathbf{y} \cdot \mathbf{A}(\mathbf{y}) = \int_0^1 du \, (\mathbf{x} - \mathbf{x}_o) \cdot \mathbf{A} \, (\mathbf{x}_o + u(\mathbf{x} - \mathbf{x}_o)) \ . \tag{4.41}$$

Without loss of generality, one may consider $\mathbf{x}_o = 0$. In preparation for the evaluation of $\boldsymbol{\nabla}\chi$, we observe

$$\chi(\mathbf{x} + \boldsymbol{\varepsilon}) = - \oint_{0 \to \mathbf{x} + \boldsymbol{\varepsilon} \to \mathbf{x} \to 0} d\mathbf{y} \cdot \mathbf{A}(\mathbf{y}) - \int_0^{\mathbf{x}} d\mathbf{y} \cdot \mathbf{A}(\mathbf{y}) - \int_{\mathbf{x}}^{\mathbf{x} + \boldsymbol{\varepsilon}} d\mathbf{y} \cdot \mathbf{A}(\mathbf{y}).$$

Using Stokes's theorem, the circulation of the vector potential along the closed loop is transformed into a flux integral through the surface defined by the corresponding contour: with appropriate sign for the oriented surface, one may write

$$\mathbf{S} = \frac{1}{2}\boldsymbol{\varepsilon} \times \mathbf{x} \ ; \ \int_S d\mathbf{S} = \frac{1}{2}\boldsymbol{\varepsilon} \times \mathbf{x} \int_0^1 du \int_0^1 dv \ . \tag{4.42}$$

Hence,

$$\begin{aligned} \chi(\mathbf{x} + \boldsymbol{\varepsilon}) - \chi(\mathbf{x}) &= -\frac{1}{2} \int_0^1 du \int_0^1 dv \, \boldsymbol{\varepsilon} \times \mathbf{x} \cdot \boldsymbol{\nabla} \times \mathbf{A}(u\mathbf{x} + v\boldsymbol{\varepsilon}) - \int_0^1 dv \, \boldsymbol{\varepsilon} \cdot \mathbf{A}(\mathbf{x} + v\boldsymbol{\varepsilon}) \\ &= -\boldsymbol{\varepsilon} \cdot \left\{ \int_0^1 dv \, \mathbf{A}(\mathbf{x} + v\boldsymbol{\varepsilon}) + \int_0^1 du \int_0^1 dv \, \mathbf{x} \times (\boldsymbol{\nabla} \times \mathbf{A}(u\mathbf{x} + v\boldsymbol{\varepsilon})) \right\} \\ &\simeq -\boldsymbol{\varepsilon} \cdot \left\{ \mathbf{A}(\mathbf{x}) + \int_0^1 du \, \mathbf{x} \times (\boldsymbol{\nabla} \times \mathbf{A}(u\mathbf{x})) \right\} \end{aligned} \tag{4.43}$$

to first order in ε. We end up with

$$\boldsymbol{\nabla}\chi(\mathbf{x}) = -\mathbf{A}(\mathbf{x}) - \frac{1}{2}\mathbf{x} \times \int_0^1 du \, \mathbf{B}(u\mathbf{x}) \ . \tag{4.44}$$

Back to the original field theory, we substitute in the matrix $\mathcal{S}$ the quantities defined as

$$\begin{aligned} \chi(\mathbf{x}) &= -\int_0^1 du \, (\mathbf{x} - \mathbf{x}_o) \cdot \mathbf{A} \, (\mathbf{x}_o + u(\mathbf{x} - \mathbf{x}_o)) \\ \mathbf{A}_p(\mathbf{x}) &= \mathbf{A}(\mathbf{x}) + \boldsymbol{\nabla}\chi(\mathbf{x}) = -\frac{1}{2}(\mathbf{x} - \mathbf{x}_o) \times \int_0^1 du \, \mathbf{B} \, (\mathbf{x}_o + u(\mathbf{x} - \mathbf{x}_o)) \\ \psi_p(\mathbf{x}, \tau) &= e^{ie\chi(\mathbf{x})} \psi(\mathbf{x}, \tau) \\ \psi_{cp}(\mathbf{x}, \tau) &= e^{-ie\chi(\mathbf{x})} \psi_c(\mathbf{x}, \tau) \\ \Delta_p(\mathbf{x}) &= e^{2ie\chi(\mathbf{x})} \Delta(\mathbf{x}) \ . \end{aligned} \tag{4.45}$$

The subscript "p" stands for *physical* and refers to the fact that the newly defined fields are now gauge invariant, namely physical, up to a global phase transformation related to the specific point $\mathbf{x}_o$ which may be chosen arbitrarily. In particular, we show that they transform under a local gauge transformation according to

$$
\begin{aligned}
\psi'_p(\mathbf{x}) &= e^{ie\alpha(\mathbf{x}_o)}\psi_p(\mathbf{x}) \\
\Delta'_p(\mathbf{x}) &= e^{2ie\alpha(\mathbf{x}_o)}\Delta_p(\mathbf{x}) \\
\mathbf{A}'_p(\mathbf{x}) &= \mathbf{A}_p(\mathbf{x}) ,
\end{aligned}
\tag{4.46}
$$

hence showing that the matrices $\mathcal{S}_o$ and $\Delta\mathcal{S}$ in (4.35) now contain invariant quantities and thus possess gauge covariant properties.

4.5 Summary

To summarise the main results of this chapter, we aim at calculating an effective theory of the relativistic BCS s-wave coupling of two electrons in an electromagnetic field. This coupling is expressed through a quadrilinear interaction which can be immediately converted into a quadratic expression by means of an auxiliary field $\Delta(\mathbf{x}, \tau) = g\bar{\psi}_c \gamma_5 \psi$ describing electron pairs. The partition function may be given a path integral formulation

$$Z(\beta) = \int \mathcal{D}[\Psi, \overline{\Psi}, \Delta, \Delta^\dagger] \, e^{-\int_0^\beta d\tau \int d^3\mathbf{x} \mathcal{L}_E(\Psi, \overline{\Psi}, \Delta, \Delta^\dagger)} \,, \quad \Psi = \begin{pmatrix} \psi \\ \psi_c \end{pmatrix} \,, \tag{4.47}$$

where the fermions are integrated over paths subjected to antiperiodic boundary conditions in imaginary time $\Psi(\mathbf{x}, 0) = -\Psi(\mathbf{x}, \beta)$ and likewise for $\overline{\Psi}$. The integrations over the auxiliary field Δ and its conjugate are not performed, but instead one considers the saddle-point approximation by which one is only interested in the value Δ_o which minimises the action, and small fluctuations around this minimum. This allows for the calculation of the effective action

$$S_{\text{eff}} = \frac{1}{\beta} \int_0^\beta d\tau \int_\infty d^3\mathbf{x} \, \frac{1}{2g} |\Delta|^2 - \frac{1}{2\beta} \ln \det \mathcal{S} \tag{4.48}$$

with

$$\mathcal{S} = \frac{1}{2} \begin{pmatrix} \gamma^0 \partial_\tau - i\boldsymbol{\gamma} \cdot \boldsymbol{\nabla} + m - e\mathbf{A} \cdot \boldsymbol{\gamma} - \mu_{\text{ec}} \gamma^0 & \Delta\gamma_5 \\ -\Delta^\dagger \gamma_5 & \gamma^0 \partial_\tau - i\boldsymbol{\gamma} \cdot \boldsymbol{\nabla} + m + e\mathbf{A} \cdot \boldsymbol{\gamma} + \mu_{\text{ec}} \gamma^0 \end{pmatrix} \,, \tag{4.49}$$

where the chemical potential μ and the electrostatic potential $\Phi = eA_0$ have been combined in the electrochemical potential $\mu_{\text{ec}}(\mathbf{x}) = \mu(\mathbf{x}) - eA_0(\mathbf{x})$. In order to perform a perturbative analysis which ensures gauge covariant properties for the effective action, we define

$$\begin{aligned} \chi(\mathbf{x}) &= -\int_0^1 du \, (\mathbf{x} - \mathbf{x}_o) \cdot \mathbf{A}(\mathbf{x}_o + u(\mathbf{x} - \mathbf{x}_o)) \\ \mathbf{A}_p(\mathbf{x}) &= \mathbf{A}(\mathbf{x}) + \boldsymbol{\nabla}\chi(\mathbf{x}) = -\frac{1}{2}(\mathbf{x} - \mathbf{x}_o) \times \int_0^1 du \, \mathbf{B}(\mathbf{x}_o + u(\mathbf{x} - \mathbf{x}_o)) \\ \psi_p(\mathbf{x}, \tau) &= e^{ie\chi(\mathbf{x})} \psi(\mathbf{x}, \tau) \\ \psi_{cp}(\mathbf{x}, \tau) &= e^{-ie\chi(\mathbf{x})} \psi_c(\mathbf{x}, \tau) \\ \Delta_p(\mathbf{x}) &= e^{2ie\chi(\mathbf{x})} \Delta(\mathbf{x}) \end{aligned} \tag{4.50}$$

and further separate

$$\begin{aligned} \mu_{\text{ec}}(\mathbf{x}) &= \mu_o + \overline{\mu}(\mathbf{x}) \\ \Delta_p(\mathbf{x}) &= \Delta_o + \overline{\Delta}(\mathbf{x}) \end{aligned} \tag{4.51}$$

where the "o" subscripts refers to a situation with homogeneous order parameter in the absence of any external field. In particular, the fluctuations of the electrochemical potential are clearly associated to the electrostatic potential: $\bar{\mu} = -eA_0$. In terms of the above defined quantities, one performs the gauge invariant split $S = S_o + \Delta S$ with

$$
S_o = \frac{1}{2} \begin{pmatrix} \gamma^0 \partial_\tau - i\boldsymbol{\gamma} \cdot \boldsymbol{\nabla} + m - \mu_o \gamma^0 & \Delta_o \gamma_5 \\ -\Delta_o^\dagger \gamma_5 & \gamma^0 \partial_\tau - i\boldsymbol{\gamma} \cdot \boldsymbol{\nabla} + m + \mu_o \gamma^0 \end{pmatrix}
$$

(4.52)

$$
\Delta S(\mathbf{x}) = \frac{1}{2} \begin{pmatrix} -\bar{\mu}(\mathbf{x})\gamma^0 - e\mathbf{A}_p(\mathbf{x}) \cdot \boldsymbol{\gamma} & \overline{\Delta}(\mathbf{x})\gamma_5 \\ -\overline{\Delta}^\dagger(\mathbf{x})\gamma_5 & \bar{\mu}(\mathbf{x})\gamma^0 + e\mathbf{A}_p(\mathbf{x}) \cdot \boldsymbol{\gamma} \end{pmatrix} .
$$

With this parametrisation, the effective action is to be expanded up to second order according to

$$
\beta S_{\text{eff}} = \int_0^\beta d\tau \int_\infty d^3\mathbf{x} \, \frac{1}{2g} |\Delta|^2 - \frac{1}{2} \ln \det S_o - \frac{1}{2} \text{Tr} \, [S_o^{-1} \Delta S] + \frac{1}{4} \text{Tr} \, [S_o^{-1} \Delta S S_o^{-1} \Delta S] + \dots
$$

(4.53)

5

Relativistic BCS theory

II. The effective action to second order

In our description of nature, the purpose is not to disclose the real essence
of the phenomena, but only to track down, so far as it is possible,
relations between the manifold aspects of our experience.

<div align="right">Niels Bohr (1885 - 1962).</div>

Recalling the results of the previous chapter, a phenomenological relativis-
tic model for s-wave superconductivity follows from the identification of the
effective action

$$S_{\text{eff}} = \frac{1}{\beta} \int_0^\beta d\tau \int_\infty d^3\mathbf{x} \, \frac{1}{2g} |\Delta|^2 - \frac{1}{2\beta} \ln \, \det \mathcal{S} \tag{5.1}$$

where the determinant of the differential operator is evaluated by separating
an exactly solvable part and some perturbations $\mathcal{S} = \mathcal{S}_o + \Delta\mathcal{S}$; the identification
of the fields gradients requires to expand the effective action up to second
order of the perturbations contained in $\Delta\mathcal{S}$.

5.1   Homogeneous situation

5.1.1   Lowest order effective action

Let us start with the contribution to lowest order in the expansion of the effective action

$$\beta S_{\text{eff}}^{(0)} = \int_0^\beta d\tau \int_\infty d^3\mathbf{x} \, \frac{1}{2g}|\Delta|^2 - \frac{1}{2}\ln \det \mathcal{S}_o \tag{5.2}$$

with

$$\mathcal{S}_o \;=\; \begin{pmatrix} \gamma^0\partial_\tau - i\boldsymbol{\gamma}\cdot\boldsymbol{\nabla} + m - \mu_o\gamma^o & \Delta_o\gamma_5 \\[2ex] -\Delta_o^\dagger\gamma_5 & \gamma^0\partial_\tau - i\boldsymbol{\gamma}\cdot\boldsymbol{\nabla} + m + \mu_o\gamma^0 \end{pmatrix} \tag{5.3}$$

where μ_o is the chemical potential and Δ_o is the density of Cooper pairs, assumed to be homogeneous over the whole volume of the sample (London limit). We further assume that no external electromagnetic field is applied, a contribution to be included subsequently in the higher order expansion. We work in a static situation, hence no time dependence will be considered throughout this chapter. A factor $1/2$ multiplying $\mathcal{S}_o$ in (4.52) has been omitted in (5.3) without loss of generality, since it simply adds a constant term to the effective action. The zeroth order fermionic contribution to the effective action may be computed directly from the corresponding fermionic partition function

$$\begin{aligned} Z_\Psi^{(0)} &= (\det \mathcal{S}_o)^{1/2} = \int \mathcal{D}[\psi,\psi^\dagger] \, e^{-\int_0^\beta d\tau \int_\infty d^3\mathbf{x} \, \overline{\Psi}\mathcal{S}_o\Psi} \\ &= \operatorname{Tr} e^{-\beta H_o} \end{aligned} \tag{5.4}$$

since it will appear that the corresponding hamiltonian can easily be diagonalised. The homogeneous hamiltonian density in the operator (5.3) is

$$\mathcal{H}_o = \overline{\Psi}(-i\boldsymbol{\gamma}\cdot\boldsymbol{\nabla} + m)\psi - \mu_o\psi^\dagger\psi - \frac{1}{2}\Delta_o^\dagger\overline{\Psi}_c\gamma_5\psi + \frac{1}{2}\Delta_o\overline{\Psi}\gamma_5\psi_c \,, \tag{5.5}$$

where the appropriate spinors have been inserted according to the original identification of the corresponding lagrangian density. The Dirac field is expanded as

$$\psi(\mathbf{x}) = \int \frac{d^3k}{(2\pi)^3 \, 2\omega(\mathbf{k})} \sum_{s=\pm1} [b(\mathbf{k},s)u(\mathbf{k},s)e^{i\mathbf{k}\cdot\mathbf{x}} + d^\dagger(\mathbf{k},s)v(\mathbf{k},s)e^{-i\mathbf{k}\cdot\mathbf{x}}], \tag{5.6}$$

in terms of the Fock operators $b^\dagger(\mathbf{k}, s)$ (respectively $b(\mathbf{k}, s)$) which create (resp. annihilate) electrons with momentum $\mathbf{k}$ and spin s, and likewise for the operators $d^\dagger$ and d for positrons; these operators obey the usual anticommutation relations $\{b(\mathbf{k}, s), b^\dagger(\mathbf{k}', s')\} = \{d(\mathbf{k}, s), d^\dagger(\mathbf{k}', s')\} = (2\pi)^3 \, 2\omega(\mathbf{k})\delta^{(3)}(\mathbf{k} - \mathbf{k}')\delta_{ss'}$ with all other anticommutators equal to zero. The spinors $u(\mathbf{k}, s)$ and $v(\mathbf{k}, s)$ are the corresponding plane wave solutions of the free Dirac equation with positive and negative energy respectively[1].

The hamiltonian density (5.5) then reads

$$
\begin{aligned}
\mathcal{H}_o \;=\; & \int \frac{d^3 k}{(2\pi)^3 \, 2\omega(\mathbf{k})} \sum_s \times \\[6pt]
& \left\{ [\omega(\mathbf{k}) - \mu_o] \, b^\dagger(\mathbf{k}, s)b(\mathbf{k}, s) + [\omega(\mathbf{k}) + \mu_o] \, d^\dagger(\mathbf{k}, s)d(\mathbf{k}, s) \right. \\[6pt]
& + \frac{1}{2} s\Delta_o^\dagger \, b(\mathbf{k}, s)b(-\mathbf{k}, -s) + \frac{1}{2} s\Delta_o^\dagger \, d^\dagger(\mathbf{k}, s)d^\dagger(-\mathbf{k}, -s) \\[6pt]
& \left. - \frac{1}{2} s\Delta_o \, b^\dagger(\mathbf{k}, s)b^\dagger(-\mathbf{k}, -s) - \frac{1}{2} s\Delta_o \, d(\mathbf{k}, s)d(-\mathbf{k}, -s) \right\}.
\end{aligned}
\tag{5.7}
$$

Following Bogoliubov's analysis of the original BCS hamiltonian, it is possible to define an appropriate transformation of the operators by which the hamiltonian has a manifest diagonal form. Let us introduce

$$
\begin{aligned}
B(\mathbf{k}, s) \;&=\; \cos\theta_B(\mathbf{k}) \, b(\mathbf{k}, s) - s\,e^{i\phi_o} \sin\theta_B(\mathbf{k}) \, b^\dagger(-\mathbf{k}, -s) \\
D(\mathbf{k}, s) \;&=\; \cos\theta_D(\mathbf{k}) \, d(\mathbf{k}, s) + s\,e^{-i\phi_o} \sin\theta_D(\mathbf{k}) \, d^\dagger(-\mathbf{k}, -s)
\end{aligned}
\tag{5.8}
$$

verifying the same anticommutation relations as the electron and positron operators. Without loss of generality, the relative phase $e^{i\phi_o}$ may be taken as the complex part of the order parameter, namely $\Delta_o = |\Delta_o|e^{i\phi_o}$. The value of the mixing angles $\theta_B(\mathbf{k})$ and $\theta_D(\mathbf{k})$ are obtained by requiring the terms of the type $B(\mathbf{k}, s)B(-\mathbf{k}, -s)$ and $B^\dagger(\mathbf{k}, s)B^\dagger(-\mathbf{k}, -s)$ (and analogous terms in the positron sector) to cancel. This condition yields

$$
\begin{aligned}
\cos 2\theta_B(\mathbf{k}) = \frac{\omega(\mathbf{k}) - \mu_o}{E_B(\mathbf{k})} \;, \quad & \sin 2\theta_B(\mathbf{k}) = \frac{|\Delta_o|}{E_B(\mathbf{k})} \;, \quad \tan 2\theta_B = \frac{|\Delta_o|}{\omega(\mathbf{k}) - \mu_o} \\[6pt]
\cos 2\theta_D(\mathbf{k}) = \frac{\omega(\mathbf{k}) + \mu_o}{E_D(\mathbf{k})} \;, \quad & \sin 2\theta_D(\mathbf{k}) = \frac{|\Delta_o|}{E_D(\mathbf{k})} \;, \quad \tan 2\theta_D = \frac{|\Delta_o|}{\omega(\mathbf{k}) + \mu_o} \;.
\end{aligned}
\tag{5.9}
$$

---

[1] The most useful properties of Dirac spinors with this choice of normalisation are summarised in Appendix C.

In terms of these operators, the hamiltonian takes the following diagonal form:

$$\mathcal{H}_o = \int \frac{d^3k}{(2\pi)^3\,2\omega(\mathbf{k})}\ \sum_s\ \left\{ E_B(\mathbf{k})\,B^\dagger(\mathbf{k},s)B(\mathbf{k},s) + E_D(\mathbf{k})\,D^\dagger(\mathbf{k},s)D(\mathbf{k},s) \right\} + E_o$$

$$\begin{aligned} \text{with}\qquad E_B(\mathbf{k}) &= \sqrt{(\omega-\mu_o)^2 + |\Delta_o|^2} \\ E_D(\mathbf{k}) &= \sqrt{(\omega+\mu_o)^2 + |\Delta_o|^2} \\ E_o\ &= (2\pi)^3\delta^{(3)}(0)\int \frac{d^3k}{(2\pi)^3}\left[2\omega(\mathbf{k}) - E_B(\mathbf{k}) - E_D(\mathbf{k})\right]. \end{aligned} \tag{5.10}$$

It appears that Δ_o, denoting the homogeneous density of Cooper pairs, also measures the gap in the energy spectrum of the fermions. This is a consequence of our choice of dimensions with $\hbar = c = 1$, from which densities and energies enter the equations with the same units; their exact numerical value is to be identified through multiplication by appropriate dimensional factors if necessary. Nevertheless, the pair density and the energy gap shall be denoted by the same variable Δ throughout the analysis.

Turning back to the expression of the partition function, the diagonal expression of the hamiltonian allows for an immediate evaluation of the trace

$$\begin{aligned} \text{Tr}\ e^{-\beta\mathcal{H}_o} &= e^{-\beta E_o}\ \text{Tr}\ \exp\left(-\beta\int \frac{d^3\mathbf{k}}{(2\pi)^3\,2\omega}\sum_s[E_B B^\dagger B + E_D D^\dagger D]\right) \\ &= e^{-\beta E_o}\ \prod_{\mathbf{k}}\left[1 + e^{-\beta E_B(\mathbf{k})}\right]^2\left[1 + e^{-\beta E_D(\mathbf{k})}\right]^2, \end{aligned} \tag{5.11}$$

This provides the total contribution of the fermionic fields to the partition function (5.4), still to be combined with the auxiliary field contribution. The integration over space has not been considered until now, but is straightforward since the whole expression is space-independent: it simply contributes an overall total volume factor and we end with the following effective action to lowest order:

$$\begin{aligned} S_{\text{eff}}^{(0)}(\Delta_o,\beta) &= \frac{V}{2g}|\Delta_o|^2 + V\int \frac{d^3\mathbf{k}}{(2\pi)^3}\left[2\omega(\mathbf{k}) - E_B(\mathbf{k}) - E_D(\mathbf{k})\right] \\ &\quad - \frac{2V}{\beta}\int \frac{d^3\mathbf{k}}{(2\pi)^3}\ln\left[1+e^{-\beta E_B(\mathbf{k})}\right] - \frac{2V}{\beta}\int \frac{d^3\mathbf{k}}{(2\pi)^3}\ln\left[1+e^{-\beta E_D(\mathbf{k})}\right] \\[6pt] E_B(\mathbf{k}) &= \sqrt{(\omega(\mathbf{k})-\mu_o)^2 + |\Delta_o|^2} \\ E_D(\mathbf{k}) &= \sqrt{(\omega(\mathbf{k})+\mu_o)^2 + |\Delta_o|^2} \end{aligned}$$

$$\tag{5.12}$$

where V denotes the whole volume of space.

5.1.2   Effective potential and the gap equation

As already pointed out in the previous chapter, the effective action (5.12) for a homogeneous order parameter in the absence of external electromagnetic fields corresponds to the Ginzburg-Landau free energy in the absence of the gradients, that is precisely the effective potential $V_{\text{eff}}(\Delta_o, \mu_o)$ for the order parameter evaluated at its minimum. Differentiating (5.12) with respect to the conjugate order parameter $\Delta_o^\dagger$ leads to the gap equation, whose solution provides the effective density of the rigid condensate of Copper pairs:

$$g \int \frac{d^3\mathbf{k}}{(2\pi)^3} \left\{ \frac{1}{E_B(\mathbf{k})} \tanh \frac{\beta E_B(\mathbf{k})}{2} + \frac{1}{E_D(\mathbf{k})} \tanh \frac{\beta E_D(\mathbf{k})}{2} \right\} = 1 \; . \tag{5.13}$$

This reproduces the original BCS gap equation (1.20) with an additional term for the positron sector as a consequence of the relativistic framework. In order to perform a numerical analysis of these relations, the momentum integration is converted into an energy integration. One must recall that the chemical potential is identified as the Fermi energy. As in the usual BCS theory, the domain of the integration is limited by considering that the energy range for the order parameter is bounded by the Debye frequency above and below the Fermi level, see (1.14). Hence we substitute

$$\int_{(\infty)} \frac{d^3\mathbf{k}}{(2\pi)^3} \quad \longrightarrow \quad \int_m^\infty \frac{d\omega}{2\pi^2} \omega \sqrt{\omega^2 - m^2} \; , \; \; \omega^2 = k^2 + m^2$$

$$\longrightarrow \quad \frac{N(0)}{2} \int_{-\xi_D}^{\xi_D} d\xi \; , \quad \xi = \omega - \omega_F \tag{5.14}$$

where we factorised the number of available energy states at the Fermi level $N(0) = k_F \omega_F / \pi^2$, since the range over which the integration is running is by far much smaller than the Fermi energy, namely $\xi_D = 0.037$ eV and $\omega_F = 511.012$ keV for the case of aluminum (see Appendix B). These orders of magnitude also give some information about the relative importance of the different terms in (5.12) and (5.13): in particular, it turns out that the positron sector (that is, the terms with energy E_D) constitutes a negligible relativistic correction and may be ignored to a very good approximation throughout the numerical analysis. Substituting the change of integration variable and taking these simplifications into account provides the following *effective potential per unit volume*

$$\mathcal{V}_{\text{eff}} = \frac{1}{2g} |\Delta_o|^2 - \frac{N(0)}{2} \int_{-\xi_c}^{\xi_c} d\xi \sqrt{\xi^2 + |\Delta_o|^2} - \frac{N(0)}{\beta} \int_{-\xi_c}^{\xi_c} d\xi \ln\left[1 + e^{-\beta\sqrt{\xi^2 + |\Delta_o|^2}} \right]$$

$$\tag{5.15}$$

as well as the gap equation

$$\frac{1}{2}\int_{-\xi_c}^{\xi_c}d\xi\left\{\frac{1}{\sqrt{\xi^2+|\Delta_o|^2}}\tanh\frac{\beta}{2}\sqrt{\xi^2+|\Delta_o|^2}\right\}=\frac{1}{gN(0)}\ . \tag{5.16}$$

In the previous relation, there appears the BCS coupling constant $gN(0)$ which is a standard feature for superconducting materials: numerical values for common substances are provided in Tab. 1.1 of Chapter 1. In the following, we shall restrict the discussion to *weakly coupled* materials, with a coupling constant between 0.18 and 0.39. Eliashberg developed a specific approach for the study of strongly coupled superconductors by which he identified some corrections to the gap energy [84]; the case of such materials will not be addressed here but could constitute an interesting extension of the present model.

The critical temperature and the maximal gap

In the limit of vanishing temperature $\beta\to\infty$, hyperbolic tangents tend to the unit value and the solution to the gap equation provides the maximal value of the gap

$$|\Delta_o(0)|=\frac{\xi_c}{\sinh\left(\frac{1}{gN(0)-\frac{\xi_c}{2\omega_F}\tanh(\beta|\omega_F|)}\right)}\ \sim\ \frac{\xi_c}{\sinh\left(\frac{1}{gN(0)}\right)}\ . \tag{5.17}$$

On the other hand, the critical temperature is inferred from the limit case at which the gap is completely closed: using the approximation [13]

$$\int_0^{\alpha/2}\frac{dx}{x}\ \tanh x\ \simeq\ \ln\left(\alpha\frac{2e^{\gamma}}{\pi}\right)\ ,\quad\gamma=0.577\dots\ (\text{Euler's constant})$$

valid for $\alpha=\beta_c\xi_c\gtrsim 5$, we obtain

$$\beta_c^{-1}=kT_c=\frac{2e^{\gamma}}{\pi}\xi_c e^{-1/gN(0)}\ . \tag{5.18}$$

Finally, combining (5.17) and (5.18) yields

$$|\Delta_o(0)|=\frac{\pi e^{-\gamma}}{\beta_c}\frac{1}{1-e^{-2/gN(0)}}. \tag{5.19}$$

Again, these values coincide with those of the usual non-relativistic BCS theory, since the positron contributions constitute perfectly negligible corrections that have been ignored.

Analytic approximations

The shape of the effective potential as a function of the order parameter and the temperature dependence of the gap equation are obtained by numerical integration of the two relations. We consider only the dimensionless $gN(0)$ external parameter as the sole input in our analysis, from which we calculate the critical temperature in our system of units using (5.18). The maximal gap $\Delta_o(0)$ is also evaluated, and then numerical integration of the effective potential is performed at a given temperature such that $0 < T/T_c < 1$, for a whole range of values of the gap parameter Δ_o in the vicinity of this maximal value. The curves on the following graphs display the modified potential

$$\frac{g}{\xi_c^2} \mathcal{V}(x) \quad \equiv \quad F(x) \tag{5.20}$$

$$= \quad \frac{1}{2}x^2 - gN(0) \int_0^1 du \left\{ \sqrt{u^2 + x^2} + \frac{2}{\beta\xi_c} \ln\left[1 + e^{-\beta\xi_c\sqrt{u^2+x^2}}\right] \right\}$$

as a function of the rescaled gap parameter $x = |\Delta_o|/\xi_c$; the integration is performed over $u = \xi/\xi_c$ and the value of the temperature is taken as a fraction $\tau_T = T/T_c$ of the critical temperature

$$(\beta\xi_c)^{-1} = \tau_T \, (\beta_c\xi_c)^{-1} = \tau_T \, \frac{k_B T_c}{\xi_c} = \tau_T \, \frac{2e^\gamma}{\pi} e^{-1/gN(0)} \quad 0 \le \tau_T \le 1 \,. \tag{5.21}$$

The effective potential is recovered simply by multiplying this expression by a scaling factor, up to an arbitrary constant shift V_o. As expected, there exists a minimum value of the potential for a finite value of x: this suggests to compare this effective potential with the fourth order polynomial of the original Ginzburg-Landau theory. By requiring identical values at zero density $F(0)$ and at the minimum $F(x_o)$, the GL approximation is given by

$$G_1(x) = F(x_o) + [F(0) - F(x_o)] \left(\frac{x^2}{x_o^2} - 1\right)^2 \,. \tag{5.22}$$

As expected from the GL theory, this quartic formula matches fairly well the effective potential close to the critical temperature and around the equilibrium value of the order parameter; it is however a rather poor approximation for the analysis of fluctuations with a significant amplitude or in a temperature range distant from the transition point.

An alternative analytic approximation to the integral representation (5.20) may be proposed using

$$G_2(x) = F(x_o) + [F(0) - F(x_o)] \left(\frac{\ln(x_o^2 + \lambda x_o^2) - \ln(x^2 + \lambda x_o^2)}{\ln(x_o^2 + \lambda x_o^2) - \ln(\lambda x_o^2)}\right)^2 \tag{5.23}$$
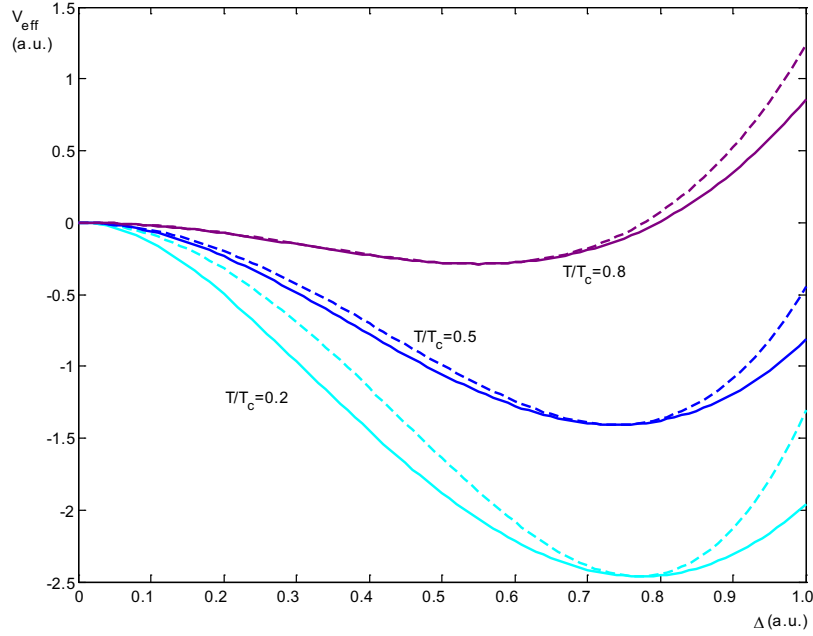
Figure 5.1: Rescaled effective potential (solid line) and Δ^4 approximation (dashed line) as a function of the order parameter for different values of the reduced temperature. The quantities V and Δ are given in arbitrary units.

where λ should be obtained by evaluating first and second derivatives of the potential as well in order to match the curves not only at the origin and the minimum value $x = x_o$, but also for the inflection point between them. Practically, this expression has been evaluated numerically with a range of plausible values for λ and then the best approximation in the sense of a least square fit has been kept. Reproducing the analysis for coupling parameters $gN(0) = 0.18$ and $gN(0) = 0.39$ in order to account for all Type I superconductors, it turns out that the parameter λ corresponding to the best fit of the potential admits an exponential temperature dependence

$$\lambda = 0.4 \, e^{4T/T_c} \ . \tag{5.24}$$

As shown in Fig. 5.2, the logarithmic function with this phenomenological parameter provides a better approximation than the fourth order polynomial for a much larger domain of order parameters x and for all temperatures below the critical transition.
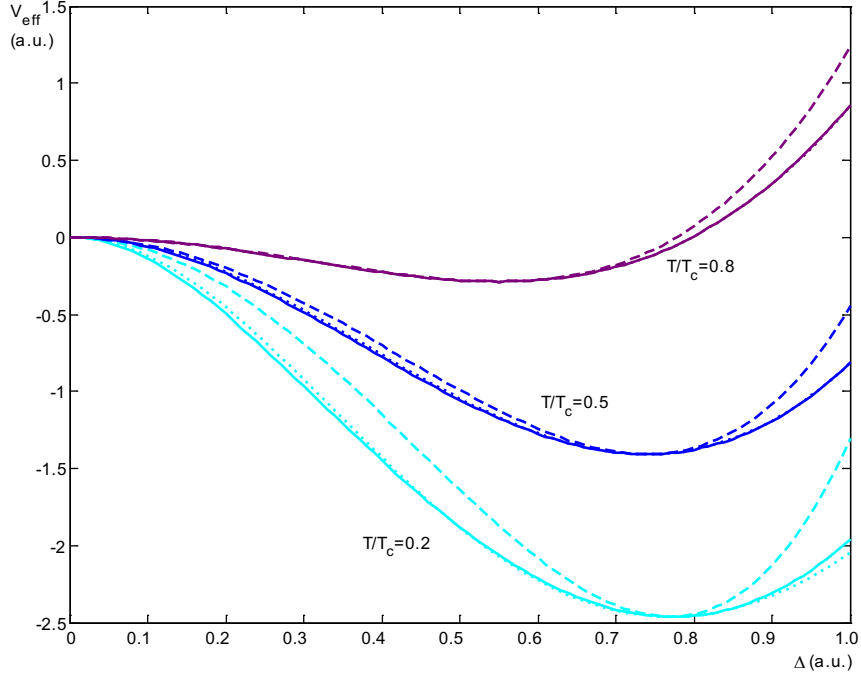
Figure 5.2: Rescaled effective potential (solid line) and logarithmic approximation (dotted line) as a function of the order parameter for different values of the reduced temperature. The Δ^4 approximation has also been displayed (dashed line) to show the increased precision using the logarithmic analytic approximation. The quantities V and Δ are given in arbitrary units.

Finally, we tried to write even better power approximations by considering possible polynomial exponents. We used the approximating function

$$G_3(x) = F(x_o) + [F(0) - F(x_o)] \left[1 - \left(\frac{\left[1 + \gamma \frac{x^2}{x_o^2} \right]^\alpha - 1}{[1 + \gamma]^\alpha - 1} \right)^2 \right] \quad (5.25)$$

with optimal values for the coefficients α and γ given by the temperature-dependent polynomial expressions

$$\alpha = 0.71 - 0.6\frac{T}{T_c} + \left(\frac{T}{T_c} \right)^2 - 1.3 \left(\frac{T}{T_c} \right)^3 + 1.1 \left(\frac{T}{T_c} \right)^4$$

$$\gamma = \frac{1}{4 \left(\frac{T}{T_c} \right)^2 - 0.25 \left(\frac{T}{T_c} \right)} \quad (5.26)$$

chosen to obtain the best fit for coupling constants $gN(0)$ again within the interval 0.18 to 0.39. Fig. 5.3 shows the effective potential and all approximations at half the critical temperature, so that one clearly notices the gain in precision in the successive analytic approximations. The relative improvement between all models is identical at all temperatures.
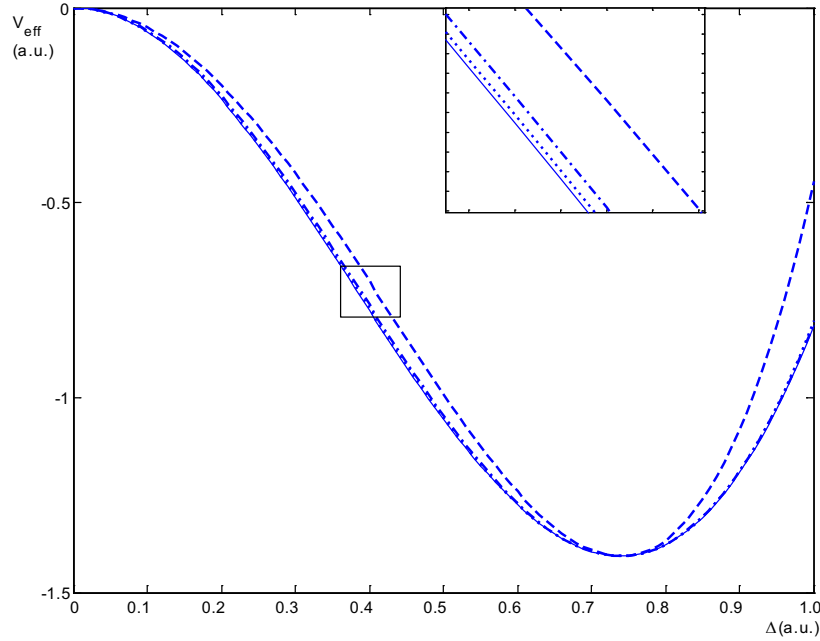
Figure 5.3: Rescaled effective potential (solid line), Δ^4 approximation (dashed line), logarithmic approximation (dash-dotted line) and approximation with rational exponents (dotted line) for $T/T_c = 0.5$ only. V and Δ are given in arbitrary units. Zoomed portion of the inset shows improvement of successive approximations.

This is actually the main result of this section: by considering the case of a homogeneous order parameter in the absence of any external electromagnetic field, it has been shown that the contribution of the positrons provides a negligible relativistic correction to the usual BCS gap equation, as should be expected. Furthermore, under these hypotheses, the effective action may be identified as the effective potential for the electron pairs. It is determined through an integral expression that can be evaluated numerically, and then approximated by several analytic functions. The fourth order polyno-

mial corresponding to the Ginzburg-Landau potential reproduces the conditions in which the GL theory is valid, namely close to the critical temperature and within small fluctuations of the order parameter; alternative power-like approximations are proposed, which give analytic expressions for the effective potential at all temperatures between 0 and T_c and which remain close to the integral expression even for large fluctuations (that is, significantly different from the order parameter value minimising the potential). In that sense, these approximations are definitely an improvement over the usual Ginzburg-Landau functional for the practical study of superconductivity away from equilibrium.

It would be interesting to consider, for example, what such improved analytic approximations to the effective potential entail for the order parameter radial profile of Abrikosov vortices, and more generally giant vortices and vortex arrays, as well as their stability as a function of the Ginzburg-Landau parameter.

5.2   First order effective action

We now turn to the first order correction in the expansion of the effective action in (4.53)

$$S_{\text{eff}}^{(1)} = -\frac{1}{2\beta} \text{Tr } S_o^{-1} \Delta S \; . \tag{5.27}$$

In general, we have

$$
\begin{aligned}
\text{Tr } S_o^{-1} \Delta S &= \int d^4x \int d^4y \text{ tr } S_o^{-1}(x,y) \Delta S(y,x) \\
&= \int d^4x \int d^4y \left(\int \frac{d^4k}{V_k} e^{-ik(x-y)} \text{tr } S_o^{-1}(k) \right) \left(\delta^{(4)}(y-x) \Delta S(x) \right) \\
&= \int d^4x \int \frac{d^4k}{V_k} \text{ tr } S_o^{-1}(k) \Delta S(x) \tag{5.28}
\end{aligned}
$$

where the small trace notation stands for the usual matrix trace over the diagonal elements of the 8×8 matrices, and V_k represents an elementary volume in k-space. Since the imaginary time $x^0 = \tau$ is (anti-)periodic over a period $[0, \beta]$, the zeroth component of the Fourier transform runs over discrete *Matsubara frequencies*, with even frequencies $\omega_n = 2n\pi/\beta$ for bosons with periodic condition in imaginary time and odd frequencies $\omega_n = (2n+1)\pi/\beta$ for fermions with

antiperiodic boundary conditions in τ. Consequently, we write in general

$$\text{Tr } S_o^{-1}\Delta S = \int_0^\beta d\tau \int d^3\mathbf{x} \frac{1}{\beta}\sum_n \int \frac{d^3\mathbf{k}}{(2\pi)^3}\, \text{tr } S_o^{-1}(i\omega_n,\mathbf{k})\Delta S(\mathbf{x})\,. \qquad (5.29)$$

In the present analysis, the homogeneous static part S_o is given by (5.3) and the deviations from this situation are contained into

$$\Delta S(\mathbf{x}) = \begin{pmatrix} -\bar{\mu}(\mathbf{x})\gamma^0 - e\mathbf{A}_p(\mathbf{x})\cdot\boldsymbol{\gamma} & \bar{\Delta}(\mathbf{x})\gamma_5 \\[2mm] -\bar{\Delta}^\dagger(\mathbf{x})\gamma_5 & \bar{\mu}(\mathbf{x})\gamma^0 + e\mathbf{A}_p(\mathbf{x})\cdot\boldsymbol{\gamma} \end{pmatrix} \qquad (5.30)$$

with

$$\begin{aligned} \bar{\mu}(\mathbf{x}) &= \mu_{\text{ec}}(\mathbf{x}) - \mu_o = -eA_p^0(\mathbf{x}) \\ \bar{\Delta}(\mathbf{x}) &= \Delta_p(\mathbf{x}) - \Delta_o \end{aligned} \qquad (5.31)$$

where the subscripts p refer to the physical fields after the transformation performed for a gauge invariant split. In order to simplify the notations, this subscript will be omitted until the end of the analysis.

5.2.1   Correlation functions

As already mentioned, the inverse operator S_o^{-1} is the Green's function of the differential operator S_o and can be obtained by evaluating the time-ordered correlation functions $\langle T\,\psi_i(\mathbf{x}_1,\tau_1)\psi_j(\mathbf{x}_2,\tau_2)\rangle_\beta$ for all combinations of the fields and their charge conjugates. Hence in principle, it may contain an explicit dependence in the imaginary time and we denote most generally

$$S_o^{-1}(\mathbf{x}_1,\tau_1;\mathbf{x}_2,\tau_2) = \begin{pmatrix} \left\langle \psi(\tau_1,\mathbf{x}_1)\,\overline{\psi}(\tau_2\mathbf{x}_2)\right\rangle_\beta & \left\langle \psi(\tau_1,\mathbf{x}_1)\,\overline{\psi}_c(\tau_2\mathbf{x}_2)\right\rangle_\beta \\[2mm] \left\langle \psi_c(\tau_1,\mathbf{x}_1)\,\overline{\psi}(\tau_2\mathbf{x}_2)\right\rangle_\beta & \left\langle \psi_c(\tau_1,\mathbf{x}_1)\,\overline{\psi}_c(\tau_2\mathbf{x}_2)\right\rangle_\beta \end{pmatrix},\ \ \tau_1 > \tau_2\,. \qquad (5.32)$$

To include the imaginary time dependence in the fields, they are provided in the Heisenberg picture

$$\psi_H(\mathbf{x},\tau) = e^{iH_o\tau}\,\psi_S(\mathbf{x})\,e^{-iH_o\tau}. \qquad (5.33)$$

If the fields are expressed in terms of the Bogoliubov operators $B(\mathbf{k},s), D(\mathbf{k},s)$ and their conjugates, the correlators

$$\langle T\,\psi_i(\mathbf{x}_1,\tau_1)\psi_j(\mathbf{x}_2,\tau_2)\rangle_\beta = \frac{\text{Tr}\left[T\,\psi_i(\mathbf{x}_1,\tau_1)\psi_j(\mathbf{x}_2,\tau_2)\,e^{-\beta H_o}\right]}{\text{Tr}\,e^{-\beta H_o}} \qquad (5.34)$$

are immediately computed and further converted into the Matsubara correlators; the detailed calculations are presented in Appendix E, which finally yields the inverse operator

$$
S_o^{-1}(\mathbf{x}_1, \tau_1; \mathbf{x}_2, \tau_2) = \frac{1}{\beta} \sum_n \int \frac{d^3\mathbf{k}}{(2\pi)^3} \, e^{-i\omega_n \Delta\tau + i\mathbf{k}\cdot\Delta\mathbf{x}} \, \frac{1}{a^2 - 4\mu_o^2\omega^2} \, *
$$

$$
* \begin{pmatrix} [2\mu_o\omega^2 - a(\mu_o - i\omega_n)]\gamma^\rho & \Delta_o\gamma^5[2\mu_o(\mathbf{k}.\boldsymbol{\gamma}+m)\gamma^\rho - a] \\ +[2\mu_o(\mu_o - i\omega_n) - a](\mathbf{k}.\boldsymbol{\gamma}-m) & \\ & \\ \Delta_o^\dagger\gamma^5[2\mu_o(\mathbf{k}.\boldsymbol{\gamma}+m)\gamma^\rho + a] & [a(\mu_o + i\omega_n) - 2\mu_o\omega^2]\gamma^\rho \\ & +[2\mu_o(\mu_o + i\omega_n) - a](\mathbf{k}.\boldsymbol{\gamma}-m) \end{pmatrix}
$$

(5.35)

with $a = \omega^2 + \mu_o^2 + |\Delta_o|^2 + \omega_n^2$. It is easy to verify that this is indeed the Green's function of the differential operator $\mathcal{S}_o$ (see Appendix E).

Once the propagator is known, the first order expansion of the effective action is easily computed: stationary configurations at equilibrium are considered, hence the matrix containing inhomogeneities does not depend on time and the τ integration can be readily performed, cancelling the factor $1/\beta$ from the Matsubara propagator. Using the standard properties of the γ^i matrices under the trace operation leads to the following first-order correction:

$$
S_{\text{eff}} = -\frac{1}{2\beta} \int d^3\mathbf{x} \int \frac{d^3\mathbf{k}}{(2\pi)^3} \sum_n *
$$

$$
* \frac{4}{a^2 - 4\mu_o^2\omega^2} \left\{ 2\mu_o\bar{\mu}(\mathbf{x})\left(a - 2\omega^2\right) + a\left(\Delta_o\overline{\Delta}^\dagger(\mathbf{x}) + \Delta_o^\dagger\overline{\Delta}(\mathbf{x})\right) \right\} \quad (5.36)
$$

At this point we need to evaluate the sum over the Matsubara frequencies.

5.2.2   Sum over Matsubara frequencies

Perturbative calculations in Thermal Field Theory often require the evaluation of infinite sums

$$
\sum_n M(i\omega_n)
$$

with even Matsubara frequencies $i\omega_n = 2n\pi/\beta$ in the case of bosonic fields and odd frequencies $i\omega_n = (2n+1)\pi/\beta$ for fermionic fields. There is a standard method for evaluating these sums, which consists in converting the sum into

a contour integral over the imaginary axis [69, 85]. Let $f_\beta(k^0)$ be a function with simple poles of residues unity at $k^0 = i\omega_n$; if the function $M(i\omega_n)$ has no singularity along the imaginary axis, then we may multiply it by $f_\beta(k^0)$ and convert the Matsubara sum into a contour integral in the complex plane

$$\sum_n M(i\omega_n) = \oint_C \frac{dk^0}{2\pi i}\, M(k^0) f_\beta(k^0) \tag{5.37}$$

where the contour C encloses all frequencies on the imaginary axis (Fig. 5.4-a). If the product $M(k^0)f_\beta(k^0)$ falls off sufficiently fast to zero at infinity, the contour may be deformed towards the two infinite loops C_1 and C_2 (Fig. 5.4-c), which have been reversed to consider the appropriate orientation for the contour integration. Generally, one chooses $f_\beta(k^0) = \frac{\beta}{2}\tanh\frac{\beta k^0}{2}$ for fermionic Matsubara frequencies and the corresponding $\coth\frac{\beta k^0}{2}$ when working with bosons. Hence in the present case, Matsubara sums are evaluated according to

$$\sum_n M(i\omega_n) = -\frac{\beta}{2}\oint_{C_1\cup C_2} \frac{dk^0}{2\pi i}\, M(k^0)\tanh\frac{\beta k^0}{2}. \tag{5.38}$$
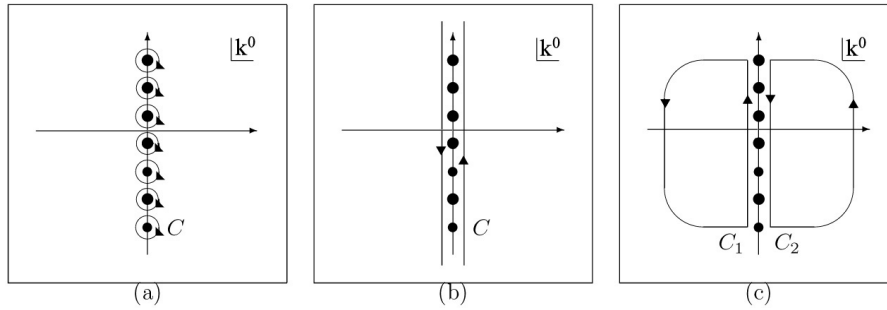
Figure 5.4: Step-by-step deformation of the contour integration in the evaluation of Matsubara sums. (a) The sum over the residues of a function along the imaginary axis (here we consider a fermion field with odd frequencies) corresponds to an integration around a contour that encloses every pole individually; (b) this contour can be deformed to run along the imaginary axis on either side; (c) if the function vanishes at the infinity, the contours can be closed and reversed so to end with C_1 and C_2.

The advantage of this analysis becomes clear when the original function $M(i\omega_n)$ has poles located somewhere inside the contours C_1 and C_2: in that case, the contour integrations are further transformed into sums over those poles and we are left with the final expression to be computed:

$$\sum_n M(i\omega_n) = -\frac{\beta}{2} \sum_{poles \; of \; M(k^0)} \text{Res}[M(k^0)\tanh\frac{\beta k^0}{2}]. \qquad (5.39)$$

All terms in (5.36) involving Matsubara frequencies may be re-expressed in terms of several functions having poles at the quasiparticles energies $\pm E_B$ and $\pm E_D$ from (5.12); performing the summations, the first order effective action is finally shown to be

$$
\begin{aligned}
S_{\text{eff}}^{(1)} \;=\; & \int d^3x \int \frac{d^3k}{(2\pi)^3} \;\times \qquad\qquad\qquad\qquad\qquad (5.40)\\
& \left\{ \; \bar{\mu}(\mathbf{x})\left[\frac{(\mu_o-\omega)}{E_B}\tanh(\tfrac{1}{2}\beta E_B) - \frac{(\mu_o+\omega)}{E_D}\tanh(\tfrac{1}{2}\beta E_D)\right] \right.\\
& \left. -\frac{1}{2}\left(\Delta_o\bar{\Delta}^\dagger(\mathbf{x}) + \Delta_o^\dagger\bar{\Delta}(\mathbf{x})\right)\left[\frac{1}{E_B}\tanh(\tfrac{1}{2}\beta E_B) + \frac{1}{E_D}\tanh(\tfrac{1}{2}\beta E_D)\right] \right\}.
\end{aligned}
$$

We observe that this expression is nothing but the first term of the series expansion of the lowest order effective action (5.3) around the homogeneous order parameter Δ_o and the constant chemical potential μ_o:

$$
\begin{aligned}
S_{\text{eff}}^{(1)} \;=\; & \int d^3x \int \frac{d^3k}{(2\pi)^3} \;\times \qquad\qquad\qquad\qquad\qquad (5.41)\\
& \left\{ (\mu-\mu_o)\frac{\partial}{\partial\mu}\left[[2\omega - E_B - E_D] - \frac{2}{\beta}\ln\left[1+e^{-\beta E_B}\right] - \frac{2}{\beta}\ln\left[1+e^{-\beta E_D}\right] \right]_{\mu=\mu_o} \right.\\
& \left. +(\Delta-\Delta_o)\frac{\partial}{\partial\Delta}\left[\quad\dots\quad \right]_{\Delta=\Delta_o} + (\Delta^\dagger - \Delta_o^\dagger)\frac{\partial}{\partial\Delta^\dagger}\left[\quad\dots\quad \right]_{\Delta^\dagger=\Delta_o^\dagger} \right\}.
\end{aligned}
$$

In consequence, the first order effective action extends the expression of the effective potential so that the order parameter and the electrochemical potential may now contain some space inhomogeneities; likewise, higher orders in the expansion of the effective action shall contribute to the other terms of the series expansion of the effective potential.

5.3   Second order effective action

5.3.1   Preparing the analysis of the effective action

Anticipating the analysis of the second order expansion of the effective action, we first consider the generalised Ginzburg-Landau free energy functional in the form

$$\mathcal{F} = \int d^3\mathbf{x} \; \left\{ f(\Delta,\mu)|(\boldsymbol{\nabla} - iq\mathbf{A})\Delta|^2 + V_{\text{eff}}(\Delta,\mu) + g(\Delta,\mu)|\boldsymbol{\nabla}\mu|^2 + h(\Delta,\mu)|\mathbf{B}|^2 \right\} \; .$$
(5.42)

In particular, we search for the specific form of the $f(\Delta,\mu)$ parameter which affects the squared gradient of the pair density, and the contributions to the electric and magnetic sectors in the parameters $g(\Delta,\mu)$ and $h(\Delta,\mu)$ respectively. For reasons that will become clear somewhat later, there is no need to provide the magnetic term as the curl of the vector potential. One further assumes that the pair density and the electrochemical potential may both be separated into a homogeneous part and some fluctuations, namely $\Delta = \Delta_o + \overline{\Delta}$ and $\mu = \mu_o + \overline{\mu}$. Introducing the Fourier transform of these two functions, we get, to lowest order in the fluctuations:

$$\int d^3\mathbf{x} \; f(\Delta,\mu)|\boldsymbol{\nabla}\Delta|^2 \quad \longrightarrow \quad \int \frac{d^3\mathbf{k}}{(2\pi)^3} \; f(\Delta_o,\mu_o) \; |\mathbf{k}|^2 \overline{\Delta}^\dagger(\mathbf{k})\overline{\Delta}(\mathbf{k})$$

$$\int d^3\mathbf{x} \; g(\Delta,\mu)|\boldsymbol{\nabla}\mu|^2 \quad \longrightarrow \quad \int \frac{d^3\mathbf{k}}{(2\pi)^3} \; g(\Delta_o,\mu_o) \; |\mathbf{k}|^2 \overline{\mu}(-\mathbf{k})\overline{\mu}(\mathbf{k}) \; .$$
(5.43)

On the other hand, we consider the second order corrections to the effective action given in terms of the Matsubara propagator $\mathcal{S}_o^{-1}(i\omega_n,\mathbf{k})$ calculated in the previous section, and the matrix containing variations of the fields $\Delta\mathcal{S}$. Actually, the analysis may be restricted to the terms with squared $\overline{\Delta}$, $\overline{\mu}$ and $\mathbf{A}$; other terms either contribute to the expansion of the effective potential, or they contain some corrections to higher orders in the order parameter, its fluctuations and those of the electromagnetic potentials, which should then be completed by a perturbative expansion of the effective action to higher orders.

We have

$$
\begin{aligned}
S_{\text{eff}}^{(2)} &= \frac{1}{4\beta} \, \text{Tr} \, [S_o^{-1} \Delta S S_o^{-1} \Delta S] \\
&= \frac{1}{4\beta} \int d^3\mathbf{x}_1 d^3\mathbf{x}_2 \int \frac{d^3\mathbf{k}_1}{(2\pi)^3} \frac{d^3\mathbf{k}_2}{(2\pi)^3} \sum_n e^{-i(\mathbf{k}_1-\mathbf{k}_2)\cdot(\mathbf{x}_2-\mathbf{x}_1)} \times \\
&\qquad\qquad \text{tr} \ \Delta S(\mathbf{x}_1) S_o^{-1}(i\omega_n,\mathbf{k}_1)\Delta S(\mathbf{x}_2) S_o^{-1}(i\omega_n,\mathbf{k}_2)
\end{aligned}
$$

$$(5.44)$$

$$
\begin{aligned}
&= \frac{1}{4\beta} \int d^3\mathbf{x}_1 d^3\mathbf{x}_2 \int \frac{d^3\mathbf{k}_1}{(2\pi)^3} \frac{d^3\mathbf{k}_2}{(2\pi)^3} \, e^{-i(\mathbf{k}_1-\mathbf{k}_2)\cdot(\mathbf{x}_1-\mathbf{x}_2)} \times \\
&\qquad \Big\{ \ \mathcal{F}_{\Delta\Delta}(i\omega_n,\mathbf{k}_1,\mathbf{k}_2) \left[\overline{\Delta}^{\dagger}(\mathbf{x}_1)\overline{\Delta}(\mathbf{x}_2) + \overline{\Delta}(\mathbf{x}_1)\overline{\Delta}^{\dagger}(\mathbf{x}_2) \right] \\
&\qquad + \ \mathcal{F}_{\mu\mu}(i\omega_n,\mathbf{k}_1,\mathbf{k}_2) \, \overline{\mu}(\mathbf{x}_1)\overline{\mu}(\mathbf{x}_2) \\
&\qquad + \ \mathcal{F}_{AA}(i\omega_n,\mathbf{k}_1,\mathbf{k}_2) \, \mathbf{A}(\mathbf{x}_1)\cdot\mathbf{A}(\mathbf{x}_2) \\
&\qquad + \ \mathcal{F}_{kA}(i\omega_n,\mathbf{k}_1,\mathbf{k}_2)\Big[\mathbf{A}(\mathbf{x}_1)\cdot\mathbf{k}_1\mathbf{A}(\mathbf{x}_2)\cdot\mathbf{k}_2 + \mathbf{A}(\mathbf{x}_1)\cdot\mathbf{k}_2\mathbf{A}(\mathbf{x}_2)\cdot\mathbf{k}_1\Big] \\
&\qquad + \ \text{irrelevant terms} \, \dots \ \Big\} \, .
\end{aligned}
$$

The exact content of the coefficients $\mathcal{F}_{\cdot\cdot}$ is not important for the present discussion. It is easy to see that the Fourier components of Δ, μ and $\mathbf{A}$ depend only on the momentum difference $\mathbf{k}_2 - \mathbf{k}_1$. Hence, in order to compare with the coefficients (5.43) which have a local form in momentum space, we provide a series expansion of $\mathbf{k}_1$ and $\mathbf{k}_2$ around their average position, namely

$$
\mathbf{k}_1 = \mathbf{K} - \frac{\mathbf{k}}{2}\,, \quad \mathbf{k}_2 = \mathbf{K} + \frac{\mathbf{k}}{2}\,. \tag{5.45}
$$

The coefficients (5.43) are then identified with specific terms of the series expansion of the corresponding terms in the effective action. The analogy between the contributions involving the order parameter is rendered more apparent by noting that the exact form of the coefficient $F_{\Delta\Delta}$ is not sensitive to the exchange of the momentum vectors $\mathbf{k}_1 \rightleftarrows \mathbf{k}_2$; we may therefore simplify

$$
[\overline{\Delta}^{\dagger}(\mathbf{k})\overline{\Delta}(\mathbf{k}) + \overline{\Delta}(-\mathbf{k})\overline{\Delta}^{\dagger}(-\mathbf{k})] \, F_{\Delta\Delta} = 2\overline{\Delta}^{\dagger}(\mathbf{k})\overline{\Delta}(\mathbf{k}) \, F_{\Delta\Delta}.
$$

The comparison between the electrochemical contributions is readily established. Finally, one has to recall that the vector potential has been subjected to a specific transformation to ensure gauge invariance of the corrections to the effective action (Section 4.4), and is given explicitly by

$$
\mathbf{A}(\mathbf{x}) = -\frac{1}{2}(\mathbf{x} - \mathbf{x}_o) \times \int_0^1 du \, \mathbf{B}\,(\mathbf{x}_o + u(\mathbf{x} - \mathbf{x}_o)) \, .
$$

This expression would obviously diverge if one considers the *x*-integration over the whole space. However, for a superconducting sample with finite dimensions, this space integration is limited by some boundary condition and the resulting vector potential is proportional to the magnetic field **B**. In consequence, the terms of the effective action involving a squared power of **A** should only be considered to the lowest level of the series expansion in order to identify the magnetic correction.

In summary, the required parameters are given by

$$
\begin{aligned}
f(\Delta_o, \mu_o) &= \frac{2}{4\beta} \int \frac{d^3\mathbf{K}}{(2\pi)^3} \left. \partial_{k^2} \mathcal{F}_{\Delta\Delta} \right|_{k=0} \\
g(\Delta_o, \mu_o) &= \frac{1}{4\beta} \int \frac{d^3\mathbf{K}}{(2\pi)^3} \left. \partial_{k^2} \mathcal{F}_{\mu\mu} \right|_{k=0} \\
h(\Delta_o, \mu_o) &= \frac{1}{4\beta} \int \frac{d^3\mathbf{K}}{(2\pi)^3} \left[\left. \mathcal{F}_{AA} \right|_{k=0} + \frac{2K^2}{3} \left. \mathcal{F}_{kA} \right|_{k=0} \right]
\end{aligned}
\tag{5.46}
$$

where $\partial_{k^2} \cdot |_{k=0}$ denotes the second order term of the series expansion in **k** around **K**. To establish the last identity, we considered the isotropic dependence of the effective action in momentum space, so that

$$
\int d^3\mathbf{K}\, F(|\mathbf{K}|)\, K^i K^j = \delta^{ij} \int d^3\mathbf{K}\, F(|\mathbf{K}|)\, \frac{K^2}{3} \,.
\tag{5.47}
$$

The complete scheme for the analysis of the second order corrections to the effective action is to be performed as follows: starting with the second order correction to the effective action expressed in matrix form, all terms involving squared powers of the fluctuations are collected separately. Then, the summations over the Matsubara frequencies are computed using contour integrations in the complex plane, as is the case for the first order corrections. Finally, the coefficient affecting the squared gradient of the order parameter and the contributions to the electric and magnetic energies are identified as specific terms of the series expansion in momentum space of the corresponding terms.

5.4   Explicit calculation of the coefficients

Considering the explicit form of the operator matrices as well as the trace properties of the Dirac matrices γ^i, we identify the relevant coefficients $\mathcal{F}_{\cdot\cdot}$ and perform the Matsubara summations: it turns out that these coefficients take then a very concise form. Anticipating the substitution $\mathbf{k}_1, \mathbf{k}_2 \rightarrow \mathbf{k}, \mathbf{K}$ and

subsequent series expansion in $\mathbf{k}$ around $\mathbf{K}$, we introduce the following notation:

$$\mathbf{k}_i^2 = \mathbf{K}^2 + \lambda\,\mathbf{k}\cdot\mathbf{K} + \frac{\mathbf{k}^2}{4}\,, \qquad \begin{cases} \lambda = -1 \Leftrightarrow i = 1 \\ \lambda = +1 \Leftrightarrow i = 2 \end{cases} \tag{5.48}$$

and

$$E_\lambda^\alpha = \sqrt{(\omega_\lambda + \alpha\mu_o)^2 + |\Delta_o|^2}\,, \qquad \begin{cases} \alpha = -1 \Leftrightarrow E_\lambda^\alpha = E_B(\mathbf{k}_i) \\ \alpha = +1 \Leftrightarrow E_\lambda^\alpha = E_D(\mathbf{k}_i) \end{cases} \tag{5.49}$$

Hence $\lambda = \pm 1$ is associated to the location of the corrections in momentum space, and $\alpha = \mp 1$ discriminates between electron and positron contributions respectively. With these notations, we have

$$\begin{aligned}
\mathcal{F}_{\Delta\Delta} &= \beta \sum_{\alpha=\pm 1}\sum_{\lambda=\pm 1} \frac{\omega_\lambda + \alpha\mu_o}{\omega_\lambda}\frac{1}{E_\lambda^\alpha}\tanh\frac{\beta E_\lambda^\alpha}{2}\left[\frac{\mathbf{k}_\lambda\cdot(\mathbf{k}_{-\lambda}-\mathbf{k}_\lambda)-2\alpha\mu_o\omega_\lambda}{(\omega_\lambda+2\alpha\mu_o)^2-\omega_{-\lambda}^2}\right] \\
\mathcal{F}_{\mu\mu} &= 2\beta \sum_{\alpha=\pm 1}\sum_{\lambda=\pm 1} \frac{\omega_\lambda + \alpha\mu_o}{\omega_\lambda}\frac{1}{E_\lambda^\alpha}\tanh\frac{\beta E_\lambda^\alpha}{2}\left[\frac{\mathbf{k}_\lambda\cdot(\mathbf{k}_{-\lambda}+\mathbf{k}_\lambda)+2m^2}{\omega_{-\lambda}^2-\omega_\lambda^2}\right] \\
\mathcal{F}_{AA} &= 2e^2\beta \sum_{\alpha=\pm 1}\sum_{\lambda=\pm 1} \frac{\omega_\lambda + \alpha\mu_o}{\omega_\lambda}\frac{1}{E_\lambda^\alpha}\tanh\frac{\beta E_\lambda^\alpha}{2}\left[\frac{\omega_\lambda^2-(\mathbf{k}_\lambda\cdot\mathbf{k}_{-\lambda}+m^2)}{\omega_\lambda^2-\omega_{-\lambda}^2}\right] \\
\mathcal{F}_{kA} &= 2e^2\beta \sum_{\alpha=\pm 1}\sum_{\lambda=\pm 1} \frac{\omega_\lambda + \alpha\mu_o}{\omega_\lambda}\frac{1}{E_\lambda^\alpha}\tanh\frac{\beta E_\lambda^\alpha}{2}\left[\frac{1}{\omega_\lambda^2-\omega_{-\lambda}^2}\right]\,.
\end{aligned} \tag{5.50}$$

Then the series expansions in $\mathbf{k}$ around $\mathbf{K}$ are performed for all the terms. The second order is considered only for the coefficients affecting squared $\overline{\Delta}$ and $\overline{\mu}$, and the lowest order for the coefficient of the squared vector potential. Defining

$$\begin{aligned}
\omega &= \sqrt{\mathbf{K}^2 + m^2} \\
E_\alpha &= \sqrt{(\omega + \alpha\mu_o)^2 + |\Delta_o|^2} \\
r_\alpha &= \frac{\omega + \alpha\mu_o}{\omega} \\
t_\alpha &= \tanh\frac{\beta E_\alpha}{2}\,,
\end{aligned} \tag{5.51}$$

we are left with

$$
\begin{aligned}
f(\Delta,\mu) &= \int \frac{d^3\mathbf{K}}{(2\pi)^3} \sum_{\alpha=\pm 1} \left\{ \frac{1}{8r_\alpha} \left[1 + \frac{2\mathbf{K}^2}{3\omega^2}\right] C_1^\alpha + \frac{\mathbf{K}^2}{6r_\alpha} C_2^\alpha \right. \\
&\qquad\qquad \left. - \frac{1}{E_\alpha} t_\alpha \frac{1}{8\alpha\mu_o\omega} \left[1 + \frac{\mu_o^2}{2\omega^2 r_\alpha}\right] \left[1 - \frac{\mathbf{K}^2}{3\omega^2}\right] \right\} \\
g(\Delta,\mu) &= \int \frac{d^3\mathbf{K}}{(2\pi)^3} \sum_{\alpha=\pm 1} \left\{ \frac{\omega^2}{2} \left[C_2^\alpha + \frac{2\mathbf{K}^2}{3} C_3^\alpha\right] + \frac{1}{8} \left[C_1^\alpha + \frac{4\mathbf{K}^2}{3} C_2^\alpha\right] \right\} \quad (5.52) \\
h(\Delta,\mu) &= \int \frac{d^3\mathbf{K}}{(2\pi)^3} \sum_{\alpha=\pm 1} \left\{ -\alpha(\mu_o^2 + \alpha\mu_o\omega) \frac{2\mathbf{K}^2 + 3m^2}{6\omega^3 E_\alpha} t_\alpha - \frac{\mathbf{K}^2}{6\omega^2} \frac{\beta}{2}(1 - t_\alpha^2) \right\}
\end{aligned}
$$

with

$$
C_1^\alpha = \left[\frac{\alpha\mu_o}{2\omega^3 E_\alpha} + \frac{r_\alpha^2}{2E_\alpha^3}\right] t_\alpha - \frac{r_\alpha^2}{2E_\alpha^2} \frac{\beta}{2}(1 - t_\alpha^2)
$$

$$
\begin{aligned}
C_2^\alpha = &\left[-\frac{3\alpha\mu_o}{8\omega^5 E_\alpha} - \frac{3r_\alpha\alpha\mu_o}{8\omega^3 E_\alpha^3} - \frac{3r_\alpha^3}{8E_\alpha^5}\right] t_\alpha \\
&+ \left[\frac{3r_\alpha\alpha\mu_o}{8\omega^3 E_\alpha^2} + \frac{3r_\alpha^3}{8E_\alpha^4}\right] \frac{\beta}{2}(1 - t_\alpha^2) \\
&+ \frac{3\beta r_\alpha^3}{8E_\alpha^3} \frac{\beta}{2}(1 - t_\alpha^2) t_\alpha \qquad\qquad (5.53)
\end{aligned}
$$

$$
\begin{aligned}
C_3^\alpha = &\left[\frac{5\alpha\mu_o}{16\omega^7 E_\alpha} + \frac{\mu_o^2}{16\omega^6 E_\alpha^3} + \frac{r_\alpha\alpha\mu_o}{4\omega^5 E_\alpha^3} + \frac{3r_\alpha^2\alpha\mu_o}{8\omega^3 E_\alpha^5} + \frac{5r_\alpha^4}{16E_\alpha^7}\right] t_\alpha \\
&- \left[\frac{\mu_o^2}{16\omega^6 E_\alpha^2} + \frac{r_\alpha\alpha\mu_o}{4\omega^5 E_\alpha^2} + \frac{3r_\alpha^2\alpha\mu_o}{8\omega^3 E_\alpha^4} + \frac{5r_\alpha^4}{16E_\alpha^6}\right] \frac{\beta}{2}(1 - t_\alpha^2) \\
&- \frac{\beta}{8}\left[\frac{\alpha\mu_o r_\alpha^2}{\omega^3 E_\alpha^3} + \frac{r_\alpha^4}{E_\alpha^5}\right] \frac{\beta}{2}(1 - t_\alpha^2) t_\alpha \\
&- \frac{\beta^2}{48} \frac{r_\alpha^4}{E_\alpha^4} \frac{\beta}{2}(1 - t_\alpha^2) t_\alpha^2 \\
&+ \frac{\beta r_\alpha^4}{48E_\alpha^4} \left[\frac{\beta}{2}(1 - t_\alpha^2)\right]^2 .
\end{aligned}
$$

Once these terms are identified, one provides an expression of the effective action which may be compared to the Ginzburg-Landau free energy functional. In particular, it is possible to identify the penetration lengths for the electric and the magnetic fields inside a superconducting sample. These two characteristic length scales should answer the question of the electric and magnetic screenings and explain the results of the experiment described in Chapter 3. This very point is the topic addressed in the last chapter.

6

Relativistic BCS theory

III. Electric and magnetic screenings

6.1 The results so far

6.1.1 The effective potential

In the previous chapter, the following expression was identified as the effective potential:

$$S_{\text{eff}}^{(0)} = \int d^3\mathbf{x} \left\{ \frac{1}{2g}|\Delta|^2 + \int \frac{d^3\mathbf{k}}{(2\pi)^3} \sum_{\alpha=\pm 1} \left[\omega(\mathbf{k}) - E_\alpha(\mathbf{k}) - \frac{2}{\beta} \ln\left(1 + e^{-\beta E_\alpha(\mathbf{k})} \right) \right] \right\}.$$

(6.1)

Indeed, this has been obtained from the exact evaluation of the partition function in the particular case of a superconducting sample with a homogeneous density of Cooper pairs, in the absence of external electromagnetic fields. The analysis of the first order corrections to the effective action then showed that the homogeneous effective potential could be extended to the more general case considering an order parameter with possible fluctuations around the homogeneous value $\Delta(\mathbf{x}) = \Delta_o + \overline{\Delta}(\mathbf{x})$ and variations of the electromagnetic potential. In particular, the chemical potential must be replaced by the electrochemical potential $\mu_{\text{ec}}(\mathbf{x}) = \mu_o - eA_0(\mathbf{x})$.

The general form of the energy in (5.12) is therefore

$$
\begin{aligned}
E_\alpha^2 &= (\omega + \alpha\mu)^2 + |\Delta|^2 \\
&= (\omega + \alpha(\mu_o - eA_0))^2 + |\Delta_o + \overline{\Delta}|^2 \\
&= \overline{E}_\alpha^2 - 2\alpha eA_0(\omega + \alpha\mu_o) + (eA_0)^2, \quad \overline{E}_\alpha^2 = (\omega + \alpha\mu_o)^2 + |\Delta_o|^2 \quad (6.2)
\end{aligned}
$$

ignoring the fluctuations of the order parameter. This allows for an expansion of the effective potential which renders explicit the dependence in the electrostatic potential:

$$
\begin{aligned}
S_{\text{eff}}^{(0)} &= \int d^3\mathbf{x} \left\{ \frac{1}{2g}|\Delta|^2 + \int \frac{d^3\mathbf{k}}{(2\pi)^3} \sum_{\alpha=\pm 1} \left[\omega - E_\alpha - \frac{2}{\beta} \ln\left(1 + e^{-\beta E_\alpha}\right) \right] \right\} \\
&+ \int d^3\mathbf{x} \, eA_0 \int \frac{d^3\mathbf{k}}{(2\pi)^3} \sum_{\alpha=\pm 1} \alpha \frac{\omega + \alpha\mu_o}{E_\alpha} t_\alpha \quad (6.3) \\
&+ \int d^3\mathbf{x} \, \frac{1}{2}(eA_0)^2 \int \frac{d^3\mathbf{k}}{(2\pi)^3} \sum_{\alpha=\pm 1} \left[-\frac{|\Delta_o^2|}{E_\alpha^3} t_\alpha - \frac{(\omega + \alpha\mu_o)^2}{E_\alpha^2} \frac{\beta}{2}(1 - t_\alpha) \right]
\end{aligned}
$$

where E_α must now be understood to stand for the value of the energy considering the chemical potential only: $E_\alpha = \sqrt{(\omega + \alpha\mu_o)^2 + |\Delta_o|^2}$; as previously, we used the shortened notation $t_\alpha = \tanh(\beta E_\alpha/2)$. This constitutes the major feature of the present work: to the best of our knowledge, the fluctuations of the effective potential in the electrostatic potential have never been studied before: even in the work by Koláček *et al* [42, 86], the electrostatic potential inside a superconducting material is considered without taking into account possible contributions coming from the superconducting potential. This however explains in a very natural way how the electric field is prevented from entering a superconductor, as it will be shown in the next section.

6.1.2 The quadratic contributions

From the analysis of the second order corrections, one identified the following contributions:

$$S_{\text{eff}}^{(2)} = \int d^3\mathbf{x} \, |(\boldsymbol{\nabla} - 2ie\mathbf{A})\Delta|^2 \int \frac{d^3\mathbf{k}}{(2\pi)^3} \times$$

$$\sum_{\alpha=\pm 1} \left\{ -\frac{1}{8\alpha\mu_o\omega} \left(1 - \frac{\mathbf{k}^2}{3\omega^2}\right) \frac{1}{E_\alpha} t_\alpha \right.$$

$$+ \frac{1}{E_\alpha^2} \left[\frac{r_\alpha}{16} + \frac{\mathbf{k}^2}{24\omega^2} \left(1 - \frac{\alpha\mu_o}{2\omega} - \frac{3r_\alpha^2\omega^2}{2E_\alpha^2}\right)\right] \left[\frac{t_\alpha}{E_\alpha} - \frac{\beta}{2}(1 - t_\alpha^2)\right]$$

$$\left. + \frac{\beta^2\mathbf{k}^2}{96E_\alpha^3} r_\alpha^2 \, t_\alpha(1 - t_\alpha^2) \right\} \tag{6.4}$$

$$+ \int d^3\mathbf{x} \, \frac{1}{2}(-\boldsymbol{\nabla} e A_0)^2 \int \frac{d^3\mathbf{k}}{(2\pi)^3} \sum_{\alpha=\pm 1} \left\{ \left[\frac{C_1^\alpha}{4} + \omega^2 C_2^\alpha\right] + \frac{\mathbf{k}^2}{3} \left[C_2^\alpha + 2\omega^2 C_3^\alpha\right] \right\}$$

$$+ \int d^3\mathbf{x} \, (e\mathbf{A})^2 \int \frac{d^3\mathbf{k}}{(2\pi)^3} \sum_{\alpha=\pm 1} \left\{ -\frac{2\mathbf{k}^2 + 3m^2}{6\alpha\mu_o\omega^3}(\mu_o^2 + \alpha\mu_o\omega)\frac{t_\alpha}{E_\alpha} - \frac{\mathbf{k}^2}{6\omega^2}\frac{\beta}{2}(1 - t_\alpha^2) \right\}$$

where the expression affecting the covariant gradient has been written in a somewhat different form compared to (5.52), in order to remove the apparent singularities $1/r_\alpha$ at the Fermi level. The meaning of all coefficients is given in the previous chapter.

6.1.3 The electromagnetic contribution

The question of the contribution of electromagnetic field to the effective action has not been addressed so far. This is done by identifying the hamiltonian density which corresponds to the free electromagnetic lagrangian $\mathcal{L}_{\text{em}} = -\frac{1}{4}F_{\mu\nu}F^{\mu\nu}$, $F_{\mu\nu} = \partial_\mu A_\nu - \partial_\nu A_\mu$. It yields the following contribution [87]:

$$\begin{aligned}
S_{\text{eff}}^{(\text{tot})} &= \int d^3\mathbf{x} \left\{ \frac{1}{2}\mathbf{E}^2 + \frac{1}{2}\mathbf{B}^2 - A_0(\boldsymbol{\nabla}\cdot\mathbf{E} - \rho_{\text{tot}}) \right\} \\
&= \int d^3\mathbf{x} \left\{ \frac{1}{2}(\mathbf{E} + \boldsymbol{\nabla}A_0)^2 + \frac{1}{2}\mathbf{B}^2 - \frac{1}{2}(\boldsymbol{\nabla}A_0)^2 + A_0\rho_{\text{tot}} \right\}
\end{aligned} \tag{6.5}$$

where ρ_{tot} represents the total charge density as it appears in Maxwell's equations, including not only the conduction electrons, but also the valence electrons and the charge of the ion lattice. In the following, we shall operate the distinction between the conduction electrons, to which the analysis of the effective action refers, and the remaining "static" charges that will be included in ρ_{lattice}.

6.1.4 The complete effective action

We now possess all the ingredients to establish the complete effective action to second order in the fluctuations of the electromagnetic field and the order parameter. One must recall that the effective action has been obtained in a completely general case by writing the general lagrangian density for a system of free electrons with a specific attractive coupling: hence no distinction has been operated to isolate *normal* electrons from those which take part in the superconducting condensate. This fact is mathematically translated by the fact that integral expressions cover the whole momentum space $-\infty \leq \mathbf{k} \leq \infty$, or equivalently, the whole energy domain starting from the mass energy $m_e \leq \omega \leq \infty$. The manifestation of superconductivity is the appearance of an energy gap $\Delta(\mathbf{k})$ which modifies the energy spectrum in a range $[-\omega_D, \omega_D]$ around the Fermi level E_F below the critical temperature. One may therefore separate this small interval from the remaining energy domain, where the gap is never present: one may write

$$S_{\text{eff}} = \int d^3\mathbf{x} \, \mathcal{L}_{\text{eff}}$$

with

$$\mathcal{L}_{\text{eff}} = \int_{m_e}^{\infty} d\omega \, L[\omega, \Delta] = \int_{\infty - 2\omega_D} d\omega \, L[\omega, \Delta = 0] + \int_{\omega_F - \omega_D}^{\omega_F + \omega_D} d\omega \, L[\omega, \Delta]$$

where "$\infty - 2\omega_D$" stands for the whole energy domain minus the small interval of width $2\omega_D$ around the Fermi energy. The contribution of $L[\omega, \Delta = 0]$ on this small integral may be added and then subtracted to close the whole energy domain and we have

$$\mathcal{L}_{\text{eff}} = \underbrace{\int_{m_e}^{\infty} d\omega \, L[\omega, \Delta = 0]}_{(n)} + \underbrace{\int_{\omega_F - \omega_D}^{\omega_F + \omega_D} d\omega \, [L[\omega, \Delta] - L[\omega, \Delta = 0]]}_{(s)}. \tag{6.6}$$

In the previous expression, a distinction has been operated between the contribution in the normal state and the remaining part which is non-vanishing only below the critical temperature, hence associated specifically to the superconducting state. In terms of the previous results, we separate

$$S_{\text{eff}} = \int d^3\mathbf{x}\, \mathcal{L}_{\text{eff}} = \int d^3\mathbf{x}\, [\mathcal{L}_{\text{eff}}^{(n)} + \mathcal{L}_{\text{eff}}^{(s)}]\,,$$

with

$$
\begin{aligned}
\mathcal{L}_{\text{eff}}^{(n)} =& \int \frac{d^3\mathbf{k}}{(2\pi)^3} \sum_\alpha \left[\omega - |\omega + \alpha\mu_o| - \frac{2}{\beta} \ln\left(1 + e^{-\beta|\omega + \alpha\mu_o|}\right) \right] \\
&+ eA_0 \int \frac{d^3\mathbf{k}}{(2\pi)^3} \sum_\alpha \alpha \frac{\omega + \alpha\mu_o}{|\omega + \alpha\mu_o|} \tanh\frac{\beta|\omega + \alpha\mu_o|}{2} + A_0\rho_{\text{lattice}} \\
&+ \frac{1}{2}(eA_0)^2 \int \frac{d^3\mathbf{k}}{(2\pi)^3} \sum_\alpha \left\{ -\frac{\beta}{2}\left(1 - \tanh^2\frac{\beta|\omega + \alpha\mu_o|}{2}\right) \right\} \\
&+ \frac{1}{2}(\boldsymbol{\nabla} eA_0)^2 \int \frac{d^3\mathbf{k}}{(2\pi)^3} \sum_\alpha \left\{ \left[\frac{C_1^\alpha}{4} + \omega^2 C_2^\alpha\right] + \frac{\mathbf{k}^2}{3}\left[C_2^\alpha + 2\omega^2 C_3^\alpha\right] \right\}_{\Delta=0} - \frac{1}{2}(\boldsymbol{\nabla} A_0)^2 \\
&+ (e\mathbf{A})^2 \int \frac{d^3\mathbf{k}}{(2\pi)^3} \sum_\alpha \left\{ -\frac{2\mathbf{k}^2 + 3m^2}{6\alpha\mu_o\omega^3}(\mu_o^2 + \alpha\mu_o\omega)\frac{1}{|\omega + \alpha\mu_o|}\tanh\frac{\beta|\omega + \alpha\mu_o|}{2} \right. \\
&\hspace{4cm} \left. -\frac{\mathbf{k}^2}{6\omega^2}\frac{\beta}{2}\left(1 - \tanh^2\frac{\beta|\omega + \alpha\mu_o|}{2}\right) \right\} + \frac{1}{2}\mathbf{B}^2
\end{aligned}
\tag{6.7}
$$

and

$$\mathcal{L}_{\text{eff}}^{(s)} = \frac{1}{2g}|\Delta|^2 + \int_{\xi_D} \frac{d^3\mathbf{k}}{(2\pi)^3} \sum_\alpha \left\{ -E_\alpha - \frac{2}{\beta} \ln\left(1 + e^{-\beta E_\alpha}\right) \right.$$

$$\left. + |\omega + \alpha\mu_o| + \frac{2}{\beta} \ln\left(1 + e^{-\beta|\omega + \alpha\mu_o|}\right) \right\}$$

$$+ eA_0 \int_{\xi_D} \frac{d^3\mathbf{k}}{(2\pi)^3} \sum_\alpha \left\{ \alpha \frac{\omega + \alpha\mu_o}{E_\alpha} \tanh \frac{\beta E_\alpha}{2} - \alpha \frac{\omega + \alpha\mu_o}{|\omega + \alpha\mu_o|} \tanh \frac{\beta|\omega + \alpha\mu_o|}{2} \right\}$$

$$+ \frac{1}{2}(eA_0)^2 \int_{\xi_D} \frac{d^3\mathbf{k}}{(2\pi)^3} \sum_\alpha \left\{ -\frac{|\Delta|^2}{E_\alpha^3} \tanh \frac{\beta E_\alpha}{2} - \frac{(\omega + \alpha\mu_o)^2}{E_\alpha^2} \frac{\beta}{2}\left(1 - \tanh^2 \frac{\beta E_\alpha}{2}\right) \right.$$

$$\left. + \frac{\beta}{2}\left(1 - \tanh^2 \frac{|\omega + \alpha\mu_o|}{2}\right) \right\}$$

$$+ \frac{1}{2}(\mathbf{\nabla} eA_0)^2 \int_{\xi_D} \frac{d^3\mathbf{k}}{(2\pi)^3} \sum_\alpha \left\{ \left[\frac{C_1^\alpha}{4} + \omega^2 C_2^\alpha\right] + \frac{\mathbf{k}^2}{3}\left[C_2^\alpha + 2\omega^2 C_3^\alpha\right] \right.$$

$$\left. - \left(\left[\,\cdot\,\right] + \left[\,\cdot\,\right]\right)_{\Delta=0} \right\}$$

$$+ (e\mathbf{A})^2 \int_{\xi_D} \frac{d^3\mathbf{k}}{(2\pi)^3} \sum_\alpha \left\{ -\left[\frac{2\mathbf{k}^2 + 3m^2}{6\alpha\mu_o\omega^3}(\mu_o^2 + \alpha\mu_o\omega)\frac{1}{E_\alpha} \tanh \frac{\beta E_\alpha}{2} \right.\right.$$

$$\left.\left. + \frac{\mathbf{k}^2}{6\omega^2} \frac{\beta}{2}\left(1 - \tanh^2 \frac{\beta E_\alpha}{2}\right)\right] + \left[\,\cdot\,\right]_{\Delta=0} \right\}$$

$$+ |(\mathbf{\nabla} - 2ie\mathbf{A})\Delta|^2 \int_{\xi_D} \frac{d^3\mathbf{k}}{(2\pi)^3} \sum_\alpha \left\{ -\frac{1}{8\alpha\mu_o\omega}\left(1 - \frac{\mathbf{k}^2}{3\omega^2}\right)\frac{1}{E_\alpha} t_\alpha \right.$$

$$+ \frac{1}{E_\alpha^2}\left[\frac{r_\alpha}{16} + \frac{\mathbf{k}^2}{24\omega^2}\left(1 - \frac{\alpha\mu_o}{2\omega} - \frac{3r_\alpha^2\omega^2}{2E_\alpha^2}\right)\right]\left[\frac{t_\alpha}{E_\alpha} - \frac{\beta}{2}(1 - t_\alpha^2)\right]$$

$$\left. + \frac{\beta^2\mathbf{k}^2}{96E_\alpha^3} r_\alpha^2 t_\alpha(1 - t_\alpha^2) \right\} \tag{6.8}$$

where integrals with a "bare" symbol run over the whole possible spectrum and those with a subscript ξ_D, once turned into an energy integration, are restricted to the small domain around the Fermi level bounded by the Debye energy. Considering the above equations, one may collect the contributions to the energy of the electromagnetic field in (6.7) and (6.8), and denote them as $|\mathbf{E}|^2\frac{1}{2}(1 + \varepsilon_e)$ and $|\mathbf{B}|^2\frac{1}{2}(1 + \varepsilon_m)$, with ε_e and ε_m being the integral expressions affecting $(\mathbf{\nabla} eA_0)^2$ and $(e\mathbf{A})^2$ respectively. However, performing a nume-

rical analysis of the integrals[1] shows that they do not contribute significantly ($\varepsilon_e \sim 10^{-7}$ and $\varepsilon_m \sim 10^{-9}$ respectively, hence negligible against unity) and may therefore be omitted. However, the remaining parts of the lagrangian density are sufficient to explain why the experiment did not show any dependence in the external electric field.

6.2 Electric and magnetic penetration lengths

In order to identify the relevant characteristic lengths, the complete lagrangian density is reformulated through a simplified expression

$$\mathcal{L} = f \, |(\boldsymbol{\nabla} - 2ie\mathbf{A})\Delta|^2 + A_0\rho_{\text{tot}} - \frac{1}{2}g \, A_0^2 - \frac{1}{2}(\boldsymbol{\nabla}A_0)^2 + \frac{1}{2}(\boldsymbol{\nabla} \times \mathbf{A})^2 \qquad (6.9)$$

where f and g are numerical coefficients that may be calculated using the corresponding integrated expressions in (6.7) and (6.8); it is important to keep in mind the fact that they both depend on the temperature and the chemical potential. Infinitesimal variations of the lagrangian density with respect to the fields provide the Euler-Lagrange equations of motion; in the London limit (Δ constant) and considering the Coulomb gauge ($\boldsymbol{\nabla} \cdot \mathbf{A} = 0$), these equations for the electromagnetic field take the form

$$\begin{aligned} \boldsymbol{\nabla}^2(A_0) - g \, (A_0) + \rho_{\text{tot}} &= 0 \;, \\ -\boldsymbol{\nabla}^2 \times (\mathbf{A}) + 8e^2|\Delta|^2 f \, \mathbf{A} &= 0 \;. \end{aligned} \qquad (6.10)$$

For an electrically neutral sample, the total charge is zero and both equations have the same structure, which leads naturally to the identification of the electric and magnetic penetration lengths. This is manifest when considering the case which was studied experimentally (Chapter 3), namely an infinite slab of thickness $2a$ in crossed stationary electric and magnetic fields. According to the axes system depicted in Fig. 6.1, the field configuration is

$$\begin{aligned} \mathbf{E} = E(x)\hat{x} &\quad, \quad E(x) = -\frac{dA_0}{dx} \;, \\ \mathbf{B} = B(x)\hat{y} &\quad, \quad B(x) = -\frac{dA_z}{dx} \;. \end{aligned} \qquad (6.11)$$

---

[1]One should take care of the choice of an appropriate cutoff for the evaluation of the integrals running over the whole momentum domain in the so-called normal effective lagrangian density; this question is also addressed for the evaluation of the characteristic lengths and shall be detailed in the next section.
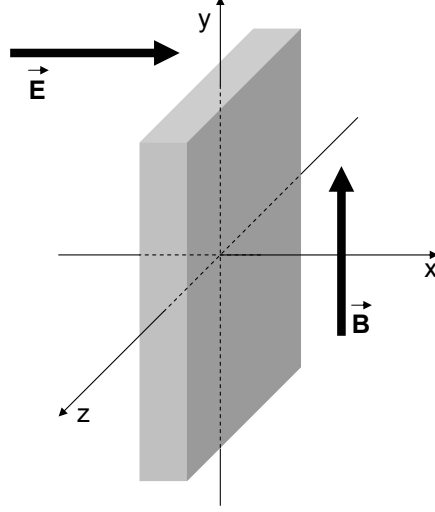
Figure 6.1: Infinite superconducting slab in crossed stationary electric and magnetic fields, as considered in Fig. 2.2.

For this particular configuration, the system (6.10) for a neutral sample becomes

$$
\begin{aligned}
\frac{d^2 A_0}{dx^2} - g\, A_0 &= 0 \,, \\
-\frac{d^2 A_z}{dx^2} + 8e^2 |\Delta|^2 f\, A_z &= 0 \,,
\end{aligned}
\tag{6.12}
$$

from which we infer an exponential decay of the electric and the magnetic fields inside the sample, over characteristic lengths λ_e and λ_m respectively given by

$$
\frac{1}{\lambda_e^2} = g \,, \qquad \frac{1}{\lambda_m^2} = 8e^2 |\Delta|^2 f \,.
\tag{6.13}
$$

In terms of the relevant integral coefficients in $\mathcal{L}_{\text{eff}}^{(n)}$ and $\mathcal{L}_{\text{eff}}^{(s)}$, ignoring the corrections to the electric and magnetic gradients, numerically shown to be negligible, the explicit relations defining the penetration lengths are finally:

$$
\frac{1}{\lambda_e^2} = e^2 \int_{\xi_D} \frac{d^3\mathbf{k}}{(2\pi)^3} \sum_\alpha \left\{ \frac{|\Delta|^2}{E_\alpha^3} \tanh \frac{\beta E_\alpha}{2} + \frac{(\omega + \alpha\mu_o)^2}{E_\alpha^2} \frac{\beta}{2} \left(1 - \tanh^2 \frac{\beta E_\alpha}{2}\right) \right.
$$
$$
\left. - \frac{\beta}{2}\left(1 - \tanh^2 \frac{\beta|\omega + \alpha\mu_o|}{2}\right) \right\} +
$$
$$
+ \; e^2 \int_\infty \frac{d^3\mathbf{k}}{(2\pi)^3} \sum_\alpha \left\{ \frac{\beta}{2}\left(1 - \tanh^2 \frac{\beta|\omega + \alpha\mu_o|}{2}\right) \right\}
$$

$$
\frac{1}{\lambda_m^2} = 8e^2|\Delta|^2 \int_{\xi_D} \frac{d^3\mathbf{k}}{(2\pi)^3} \sum_\alpha \left\{ -\frac{1}{8\alpha\mu_o\omega}\left(1 - \frac{\mathbf{k}^2}{3\omega^2}\right)\frac{1}{E_\alpha}t_\alpha \right.
$$
$$
+ \frac{1}{E_\alpha^2}\left[\frac{r_\alpha}{16} + \frac{\mathbf{k}^2}{24\omega^2}\left(1 - \frac{\alpha\mu_o}{2\omega} - \frac{3r_\alpha^2\omega^2}{2E_\alpha^2}\right)\right]\left[\frac{t_\alpha}{E_\alpha} - \frac{\beta}{2}(1 - t_\alpha^2)\right]
$$
$$
\left. + \frac{\beta^2\mathbf{k}^2}{96E_\alpha^3} r_\alpha^2 t_\alpha(1 - t_\alpha^2) \right\} .
$$

$$(6.14)$$

These two relations constitute the central theoretical result of the present work. One also identifies the electric charge as the terms which couple to the electro-static potential A_0 in (6.7) and (6.8):

$$
\rho_{\text{tot}} = \rho_{\text{lattice}} + e \int \frac{d^3\mathbf{k}}{(2\pi)^3} \sum_\alpha \alpha \frac{\omega + \alpha\mu_o}{|\omega + \alpha\mu_o|} \tanh|\omega + \alpha\mu_o| \tag{6.15}
$$
$$
+ e \int_{\xi_D} \frac{d^3\mathbf{k}}{(2\pi)^3} \sum_\alpha \left\{ \alpha \frac{\omega + \alpha\mu_o}{E_\alpha} \tanh \frac{\beta E_\alpha}{2} - \alpha \frac{\omega + \alpha\mu_o}{|\omega + \alpha\mu_o|} \tanh|\omega + \alpha\mu_o| \right\} .
$$

For practical purposes, one may have to regularise the possibly infinite integral in the expression of the electric penetration length, by choosing an appropriate cutoff so that the numerical integrations are possible without truncating the result. We first observe that the hyperbolic tangent rapidly tends to ± 1 outside a small domain such that its argument $(\omega + \alpha\mu) \approx 0$. Consequently, the function $[1 - \tanh^2 \frac{\beta(\omega + \alpha\mu)}{2}]$ always vanishes for $\alpha = +1$: we immediately conclude that positrons do not contribute significantly to this integral and may be ignored. Only the electrons ($\alpha = -1$) whose energies are close to the Fermi level ($x = \omega - \mu_o \approx 0$) shall therefore contribute. Then consider the integral

$$
\int_{-\infty}^\infty dx \left[1 - \tanh^2 \frac{\beta x}{2}\right] = \int_{-\infty}^\infty dx \frac{d}{dx}\left[\frac{2}{\beta}\tanh \frac{\beta x}{2}\right] = 2 * \frac{2}{\beta}
$$

to be compared to the integral of some rectangle function

$$
\int_{-\Lambda}^\Lambda dx = 2\Lambda .
$$

A reasonable approximation (see inset in Fig. 6.2 for the particular case $2/\beta = 1$) of the integral is provided by the rectangle function with

$$\Lambda = \frac{2}{\beta} \, . \tag{6.16}$$

On the other hand, the expression of the electric charge (6.15) also requires
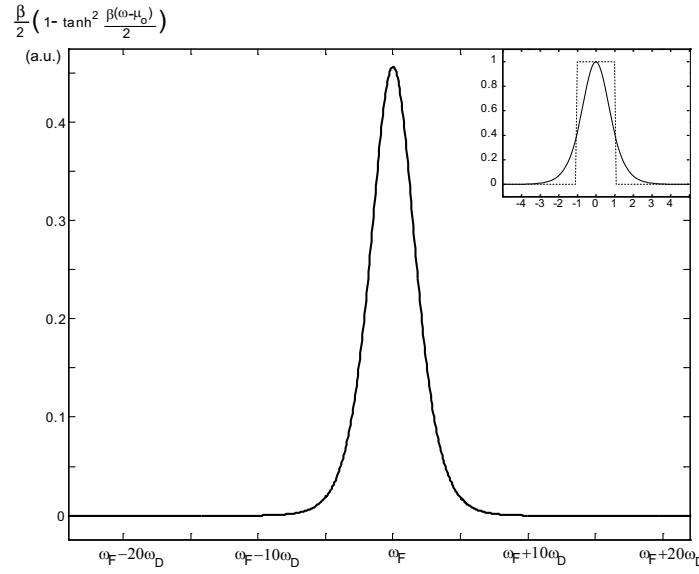
Figure 6.2: Numerical evaluation of the quantity $\frac{\beta}{2}(1 - \tanh^2[\beta(\omega - \mu_o)/2])$ to be integrated for obtaining the Thomas-Fermi length of a neutral sample ($\mu_o = \omega_F$). The value of $\beta = 1/k_B T$ corresponds to the room temperature. Inset: comparison of the expression $(1 - \tanh^2 x)$ (solid line) with the rectangle function $f(x) = 1$, $-1 \leq x \leq 1$ (dashed line).

the study of the function $\alpha \tanh \frac{\beta(\omega + \alpha\mu)}{2}$. This function is essentially unity over the whole domain when $\alpha = +1$ and rapidly reaches a plateau at ± 1 away from the Fermi energy when $\alpha = -1$, as shown in Fig. 6.3. The sign α affecting the function is of crucial importance. The lower integral bound is defined by the electron mass in either cases, and the upper bound may be chosen arbitrarily as long as the functions have reached their plateaus, since any additional contribution from the electrons when changing the cutoff $\Lambda \to \Lambda + \delta\Lambda$ is then balanced by an identical contribution of the positrons with opposite sign. Hence, one is free of choosing a symmetrical interval around the Fermi level; considering the Fermi kinetic energy $K_F = \omega_F - mc^2 = \omega_F - m_e$ ($c^2 = 1$), the

interval $[\omega_F - K_F, \omega_F + K_F] = [m_e, \omega_F + K_F]$ certainly covers the whole energy domain over which the function takes non-trivial values and may be used for the numerical evaluation of the unbounded integrations. Actually, this is by far too much, as an interval delimited by a few times the Debye energy, which is much smaller than K_F, would be sufficient[2]. However, the domain over which the hyperbolic tangent is non-trivial broadens when temperature is decreased and K_F constitutes then a natural choice for the limit over which the function certainly vanishes at any temperature.
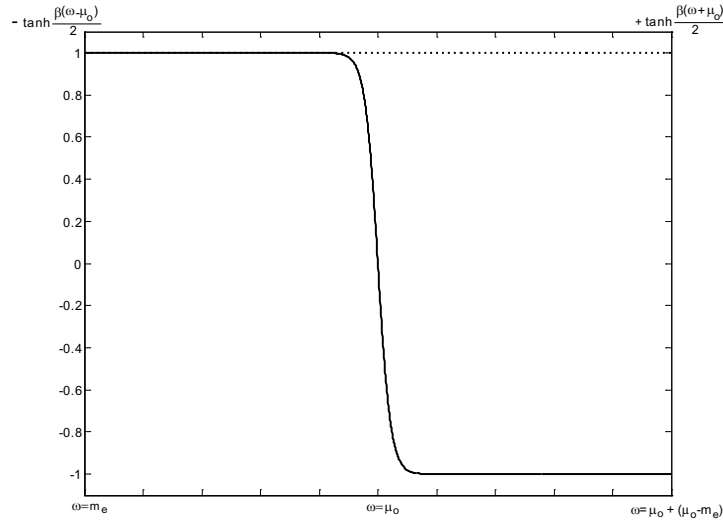
Figure 6.3: Numerical evaluation of the quantities $(-\tanh[\beta(\omega - \mu_o)/2])$ (solid curve) and $(\tanh[\beta(\omega + \mu_o)/2])$ (dashed curve) for a neutral sample ($\mu_o = \omega_F$) at room temperature.

6.2.1 The Thomas-Fermi length

Above the critical temperature, one considers normal electrons only and λ_e should in principle reproduce the usual Thomas-Fermi length, which describes how the electrostatic potential is screened by the free electrons in metals [82]. For most common metals, the Thomas-Fermi length λ_{TF} does not exceed a few angstroms. From the electric penetration length in (6.14), the electric screening

---

[2]It is useful to keep the orders of magnitudes in mind for all these quantities: for aluminum, $E_F = 511.012$ keV, $K_F = 11.65$ eV and $\omega_D = 0.037$ eV.

above the critical temperature is given by

$$\frac{1}{\lambda_{TF}^2} = e^2 \frac{\beta}{2} \int_\infty \frac{d^3\mathbf{k}}{(2\pi)^3} \sum_\alpha \left(1 - \tanh^2 \frac{\beta|\omega + \alpha\mu|}{2} \right) \ . \tag{6.17}$$

An analytical approximate analysis of (6.17) may be performed: as it has been shown previously, the contribution of the positrons ($\alpha = +1$) may be ignored and the remaining electron contribution may be approximated by

$$\begin{aligned}
e^2 \frac{\beta}{2} \int_{-\infty}^{\infty} \frac{d^3\mathbf{k}}{(2\pi)^3} \left(1 - \tanh^2 \frac{\beta|\omega - \mu|}{2} \right) &\approx e^2 \frac{\beta}{2} \frac{N(0)}{2} \int_{\mu-\Lambda}^{\mu+\Lambda} d\omega \ , \quad \Lambda = \frac{2}{\beta} \\
&= e^2 N(0) \ . \tag{6.18}
\end{aligned}$$

Using $N(0) = \frac{3n}{2K_F}$ (see Appendix B), one obtains an analytical expression for the Thomas-Fermi length

$$\lambda_{TF}^2 = \frac{2K_F}{3e^2 n} \tag{6.19}$$

which agrees with the usual expression $\frac{2\varepsilon_o E_F}{3e^2 n}$ in the non relativistic limit [76].

Finally, numerical integration is performed over the interval $[\omega_F - K_F, \omega_F + K_F]$. One should observe that the above expressions provide the quantity $1/\lambda^2$ in units of squared energy; this is a direct consequence of the initial choice of units $\hbar = c = 1$. According to this choice, the electric and magnetic permittivities are also equal to unity, and the value of the electron charge becomes $e^2 = 4\pi\alpha$, with $\alpha = 1/137$ the fine structure constant. Consequently, to obtain a numerical values in SI units, one should divide this relation by $(\hbar c)^2$. At room temperature (T=293 K) for a neutral sample ($\mu = \mu_o = \omega_F$) one obtains the Thomas-Fermi length $\lambda_{TF} = 4.84 \cdot 10^{-11}$ m, in agreement with the tabulated value for aluminum.

6.2.2   Temperature dependence of the penetration lengths

Once the Thomas-Fermi length for normal electrons is obtained, one has to study how it is affected in presence of the superconducting condensate. In particular, the penetration of external electric field inside the sample, as it was assumed in Chapter 2, would require a total electric penetration length comparable to the dimensions of the sample, namely a few tens of nanometres. On the other hand, it is also interesting to study how the magnetic penetration length is affected by the relativistic corrections. Both electric and magnetic aspects are studied by performing the numerical integration of the expressions (6.14) below T_c.
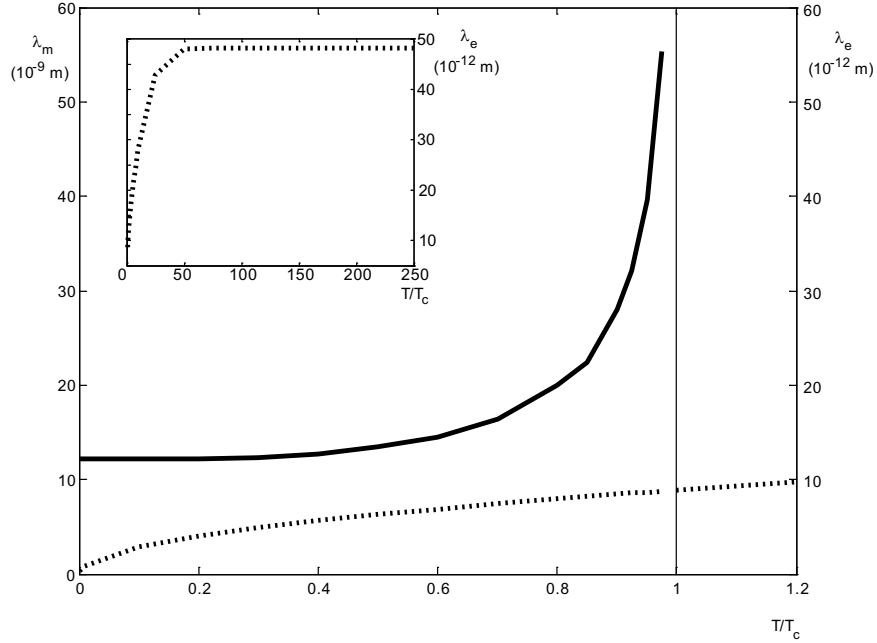
Figure 6.4: Numerical evaluation of the electric (dotted curve) and magnetic (solid curve) penetration lengths as a function of the reduced temperature. The input parameters are those for aluminum (see text for numerical values). Inset: electric penetration length (Thomas-Fermi length) evaluated up to room temperature.

The results of the numerical integrations are displayed in Fig. 6.4. The order parameter Δ is taken homogeneous (London limit), considering the value Δ_o which minimises the effective potential and numerical external parameters are those for aluminum, namely $gN(0) = 0.18$, $\omega_F = 511.012$ keV, $\xi_c = \omega_D = 0.037$ eV. The integrated expressions are further converted in SI units by dividing the quantities in (6.14) by $(\hbar c)^2$.

The magnetic penetration length is of the order of the nanometric scale, as expected. At $T = 0$ K, it tends to some finite value $\lambda_o = 1.22 \cdot 10^{-8} m$, which matches perfectly with the London penetration length (1.3) for aluminum:

indeed, considering the density of free electrons per unit volume in Al $n = 1.81 \cdot 10^{29}$ m^{-3}, one gets

$$\lambda_L = \sqrt{\frac{m_e}{\mu_o n e^2}} = 1.25 \cdot 10^{-8} \text{ m} . \tag{6.20}$$

This value does not correspond to the tabulated value for Al, which has been verified experimentally to be approximatively 50 nm; however, one must recall that the expression of the penetration length must be extended beyond London's homogeneous limit for the order parameter, by taking into account specific features of the sample such as its purity. It was shown by Pippard [9] that the following effective expression holds in general:

$$\lambda_{\text{eff}} = \lambda_L \left(1 + c \frac{\xi_o}{l} \right)^{1/2} , \quad \begin{cases} c = 1 & \text{at } T = 0 \text{ K} , \\ c = 0.75 & \text{close to } T_c , \end{cases} \tag{6.21}$$

where ξ_o is the coherence length in Pippard's theory and l is the mean free path of a free electron between two collisions. A complete discussion of the effective penetration length as a function of the purity, but also of the geometry and dimensions of the sample can be found in Refs. [11, 13].

The temperature dependence of the magnetic penetration length also reproduces the generally admitted empirical dependencies. Considering the London limit and extremely pure materials, the most widely used empirical dependence had been proposed by Gorter and Casimir [8] in the framework of their two-fluid model; on the other hand, from the BCS theory, one may also identify an expression which is valid close to T_c only: these two expressions are respectively given by [13]

$$\begin{aligned} \text{Gorter-Casimir:} \quad & \frac{\lambda_L(0)}{\lambda(T)} = \sqrt{1 - \left(\frac{T}{T_c} \right)^4} , \\ \text{BCS:} \quad & \frac{\lambda_L(0)}{\lambda(T)} = \sqrt{2 \left(1 - \frac{T}{T_c} \right)} . \end{aligned} \tag{6.22}$$

As shown in Fig. 6.5, our expression of the magnetic penetration length matches fairly well with these two models, at least considering their respective hypotheses of validity.

Turning to the analysis of the electric penetration length in the vicinity of the critical temperature, the values obtained just below this temperature do not differ from those just above which correspond to the Thomas-Fermi screening length, namely a fraction of an angstrom: hence, any external electric field is screened just as if the sample would be in the normal state.
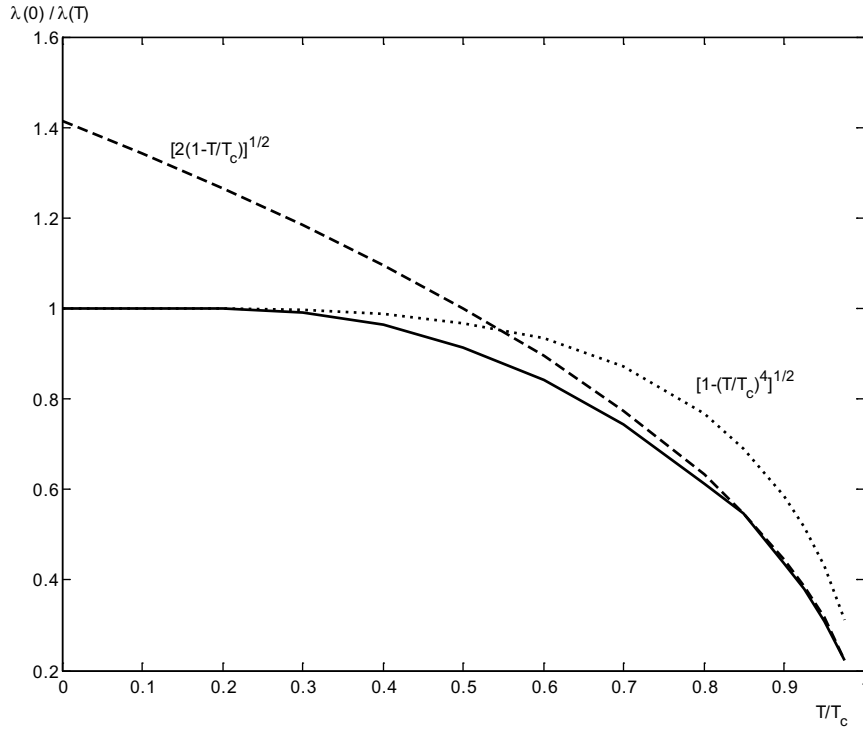
Figure 6.5: Inverse magnetic penetration length (solid curve) as a function of the reduced temperature, compared to the two-fluid model (dotted curve) and the BCS model close to T_c (dashed curve). The input parameters are those for aluminum.

One must admit that the Cooper pair condensate does not play a significant role in the enhancement or screening of electric fields inside the sample.

This observation provides a microscopic answer to a long-lasting debate which was raised in a series of contradictory articles, over the electrostatic response of a superconductor. J.E. Hirsch theoretically studied the surface charge inside a superconductor, and obtained some results related to our early guess, namely the exponential decay of electric field over a distance of the order of the magnetic penetration length [88]. In a comment to Hirsch's publication, T. Koyama pointed out a misleading gauge choice and proposed a more appropriate gauge condition to reproduce the qualitative assumption that the electric screening length is still given by the Thomas-Fermi length in the superconducting phase [89]. This comment is further rejected by Hirsch,

who develops several arguments to support his claims; in particular he distinguishes the role played by the superconducting condensate and the normal electrons in the screening of an external electric field [90]. Our model provides the definite answer to the debate between the two authors: since we start from a microscopic description of all conducting electrons, we naturally take into account the electrodynamics of all charge carriers inside the superconductor, whatever their superconducting or normal behaviour. Our theory provides a firm argument supporting the qualitative claim that the Thomas-Fermi length still describes the electric penetration, hence confirming Koyama's argument without need of any particular gauge choice.
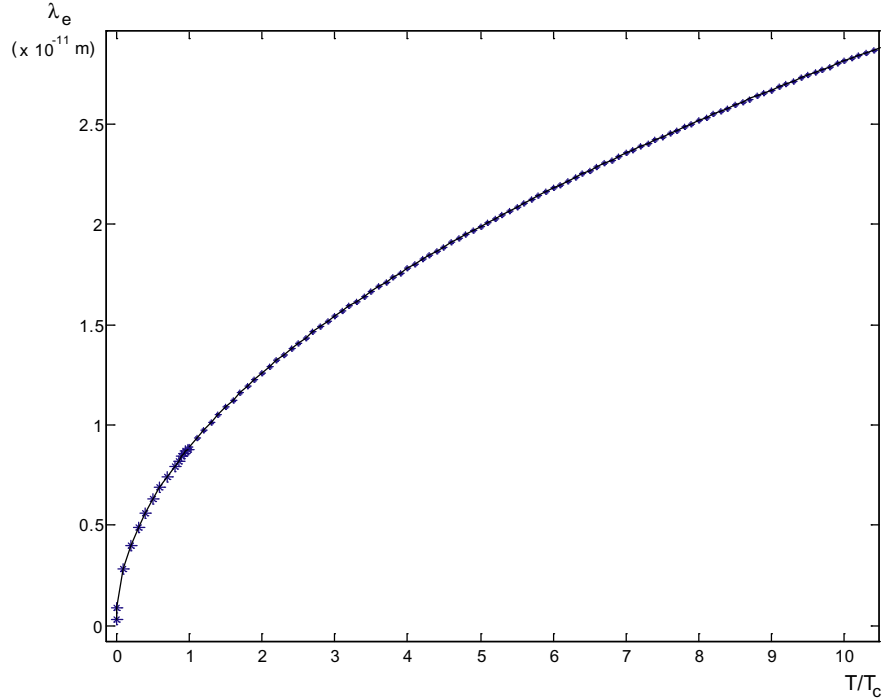
Figure 6.6: Electric penetration length (asterisks) as a function of the reduced temperature, compared to the $\sqrt{T}$ model (solid curve). The input parameters are those for aluminum.

Finally, the temperature dependence of the electric penetration length has been identified to be

$$\frac{\lambda_e(T)}{\lambda_e(T_C)} = \sqrt{\frac{T}{T_c}}$$

(6.23)

close to the critical temperature (Fig. 6.6). This dependence in $\sqrt{T}$ agrees with that of the Debye-Hückel screening length, which is analogous to the Thomas-Fermi screening, but was obtained in an earlier treatment using the Maxwell-Boltzmann distribution for the electron gas instead of the Fermi-Dirac distribution [91].

6.2.3 Depleted superconducting sample

In order to investigate their possible modification with charge depletion, the electric and magnetic penetration lengths (6.14) are studied as functions of the chemical potential μ. At this point, one has to recall that the chemical potential enters the hamiltonian of the system together with the number of conserved charges in a term $\mu N = \mu \langle \psi^\dagger \psi \rangle$; in a neutral sample at zero temperature, all free electrons are arranged on successive energy levels from the mass level $\omega = m_e$ ($c^2 = 1$) up to the Fermi level ω_F (the situation at non-zero temperature is analogous, but for a fuzzy limit around the Fermi energy due to the thermal excitations of some electrons close to that level). When a negative voltage is applied, part of the free electrons are removed from the sample and the Fermi level is progressively lowered.

All electrons will be removed when the Fermi level reaches the mass energy, which is a non-physical limit but constitutes anyway the theoretical lower limit for the numerical investigations of the characteristic lengths. It would also be arguable to apply the present model to a situation in which the total number of free electrons has been lowered to a very small number, that is when the chemical potential has been lowered close to the electron rest-mass energy: indeed, the whole theory has been constructed on the basis of a thermodynamic formalism, for which the number of particles is assumed to be large. Consequently, the limit $\mu \rightarrow m_e$ in Figs. 6.7 and 6.8 must be taken with great care.

The complete numerical procedure was reproduced for three different temperatures, namely $T/T_c = 0.2$, $T/T_c = 0.5$ and $T/T_c = 0.8$. Starting from the Fermi energy $\mu = \mu_o = \omega_F$, the chemical potential was progressively lowered as $\mu = \mu_o - \alpha K_F$, $0 \leq \alpha \leq 1$. The integrals in (6.15) were also evaluated to identify the total charge $\rho_n + \rho_s$; they confirmed that the total number of freely moving charges goes to zero as $\mu \rightarrow m_e$. All results are summarised in Fig. 6.7. By looking at the different curves, it is clear that the two penetration lengths increase when the sample is progressively depleted, which is not surprising since the
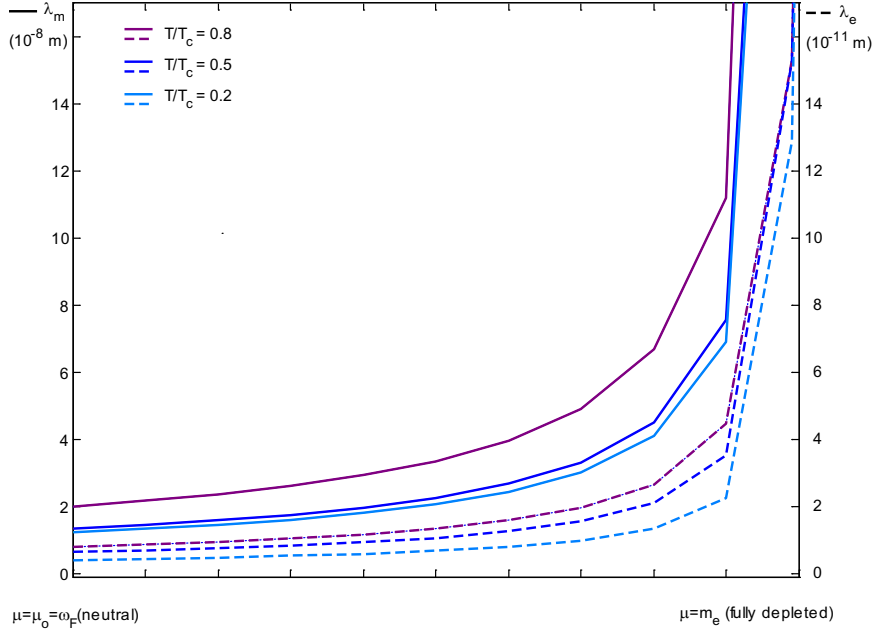
Figure 6.7: Numerical evaluation of the electric (dotted lines) and magnetic (solid lines) penetration lengths as a function of chemical potential, which is progressively lowered from the Fermi level down to the mass energy. Expressions are evaluated for three different temperatures: $T = 0.2\,T_c$ (cyan), $T = 0.5\,T_c$ (blue) and $T = 0.2\,T_c$ (magenta). Required input parameters are those for aluminum.

number of charges that take part in the screening mechanism is then smaller. In particular, the magnetic penetration length diverges rapidly. However, the electric penetration length increase is less than an order of magnitude and the curves corresponding to different values of temperature all converge towards a same finite value when $\rho_{\text{free}} = 0$. This graph shows that the experimental phase diagram obtained in Chapter 3 would not have been significantly affected by the external electric field, even if we had applied a constant voltage on the superconducting slab to remove part of the free electrons.

The dependence of both characteristic lengths with decreasing chemical potential could actually have been predicted from the approximate expressions of the energy gap at zero temperature and the Thomas-Fermi length

$$\Delta_o(0) \sim \frac{1}{\sinh(1/gN(0))} \,, \quad \lambda_{TF}^2 \sim \frac{1}{e^2 N(0)} \qquad (6.24)$$

as functions of the density of energy states at the Fermi level $N(0) = k_F \omega_F / \pi^2$. Indeed, the magnetic penetration length is inversely proportional to the squared gap, while the electric penetration length is essentially unaffected by the condensate of Cooper pairs. Since the density of states decreases when the sample is progressively depleted, the energy gap also decreases, so that λ_m is progressively increased. Above 0 K, the gap is only a fraction of $\Delta_o(0)$ but the qualitative evolution with a lowered potential is unchanged. On the other hand, the electric screening length is also raised up to a finite value (Fig. 6.8).
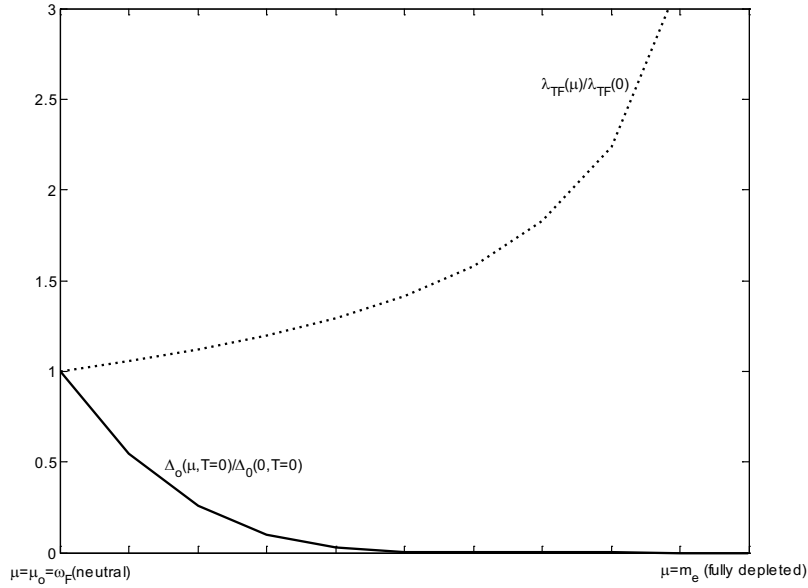
Figure 6.8: Evolution of the energy gap and the Thomas-Fermi length with decreasing chemical potential. Both quantities are normalised to their value in a neutral sample, when the chemical potential is at the Fermi level.

It is important to note that the distinction between the so-called normal and superconducting electrons cannot be given a precise technical definition from such a microscopic model which basically accounts for all conducting

electrons, in this case considered as a gas of free relativistic electrons whose density is fixed by the choice of the chemical potential. The variation of the effective potential with respect to the order parameter could determine the density of Cooper pairs, namely essentially the order parameter itself. The local Cooper pair density could in turn lead to the local density of the remaining free "normal" electrons; in particular, this would help understanding better how the condensation of Cooper pairs leads to a redistribution of charges within the material and thereby generate some surface electric fields. Studies of such issues are available in the literature (see [86] and references therein); however, since they are based on phenomenological or even empirical models, it remains to be seen how they would compare with our microscopic approach and which physical properties the latter implies.

6.3   A few words on the coherence length

In addition to the electromagnetic penetration lengths, the obtained effective action allows for the calculation of the coherence length, which is a measure of the rigidity of the condensate. An infinitesimal variation with respect to Δ^* yields an expression comparable with the relations (6.10) for the electromagnetic potentials, namely

$$-f(\Delta_o, \mu_o)\boldsymbol{\nabla}^2\Delta + \Delta \frac{\partial V_{\text{eff}}(|\Delta|^2)}{\partial|\Delta|^2} = 0 \, . \tag{6.25}$$

Considering the fluctuations $\overline{\Delta}$ of the order parameter around its homogeneous value Δ_o, we may expand this equation of motion to first order in the fluctuations; we get

$$f(\Delta_o, \mu_o)\boldsymbol{\nabla}^2\overline{\Delta} - (\Delta_o + \overline{\Delta})\left[\frac{\partial V_{\text{eff}}(|\Delta_o|^2)}{\partial|\Delta|^2} + (\Delta_o\overline{\Delta}^* + \Delta_o^*\overline{\Delta})\frac{\partial^2 V_{\text{eff}}(|\Delta_o|^2)}{\partial|\Delta|^4}\right] = 0 \tag{6.26}$$

where $\partial^2 \, . \, /\partial|\Delta|^4$ stands for the second-order derivative with respect to the squared order parameter density. The first-order derivative of the effective potential is nothing but the gap equation and vanishes identically; taking all quantities real in the remaining terms, and keeping only terms linear in $\overline{\Delta}$, yields

$$f(\Delta_o, \mu_o)\boldsymbol{\nabla}^2\overline{\Delta} - 2\overline{\Delta}|\Delta_o^2|\frac{\partial^2 V_{\text{eff}}(|\Delta_o|^2)}{\partial|\Delta|^4} = 0 \, , \tag{6.27}$$

from which we identify the coherence length:

$$\frac{1}{\xi^2(T)} = 2\frac{|\Delta_o|^2}{f(\Delta_o,\mu_o)}\frac{\partial^2 V_{\text{eff}}(|\Delta_o|^2)}{\partial|\Delta|^4} \ . \tag{6.28}$$

The integral expression for $f(\Delta_o,\mu_o)$ has already been used for the magnetic penetration length in (6.14) and the following expression is easily obtained:

$$\frac{\partial^2 V_{\text{eff}}(|\Delta_o|^2)}{\partial|\Delta|^4} = \int_{\xi_D}\frac{d^3\mathbf{k}}{(2\pi)^3}\sum_\alpha\left\{\frac{1}{2E_\alpha^3}\tanh\frac{\beta E_\alpha}{2} + \frac{1}{2E_\alpha^2}\frac{\beta}{2}\left(1-\tanh^2\frac{\beta E_\alpha}{2}\right)\right\} \ . \tag{6.29}$$

It is therefore possible to evaluate the coherence length (6.28) within the whole range between 0 K and the critical temperature with the numerical input parameters corresponding to aluminum: the results are displayed in Fig. 6.9. At $T = 0$ K, one obtains $\xi_o = 1556$ nm, in agreement with the tabulated value of 1600 nm [14]; furthermore, the coherence length is essentially constant close to this limit, as it is generally admitted [13]. However, the simple-minded dependence in $1/\sqrt{1-T/T_c}$ obtained from the Ginzburg-Landau theory is not recovered in the vicinity of the critical temperature, and one observes an intriguing change in concavity which still needs to be fully explored and understood.
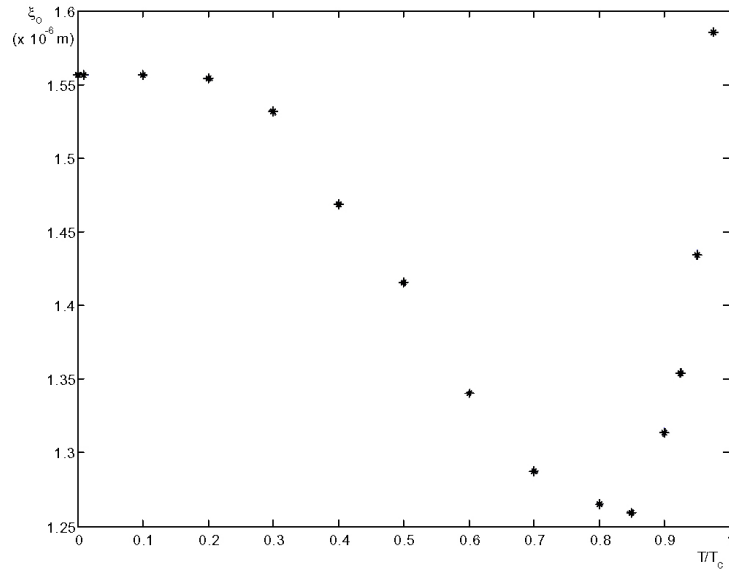
Figure 6.9: Temperature dependence of the coherence length; the input parameters are those for aluminum.

6.4   Summary

To summarise the results of the present chapter, we have shown that the effective potential may be given as a function of the electrostatic fluctuations that affect the chemical potential. Then the second order corrections to the effective action of the relativistic BCS model, expanded around the homogeneous density of Cooper pairs and considering possible fluctuations of the electromagnetic potential inside the sample, have led to the identification of the characteristic screening lengths for the electric and the magnetic fields, the relative contribution of the normal electrons and the Cooper pair condensate remaining an open issue. In particular, the electric penetration length extends the usual expression of the Thomas-Fermi length and exhibits a negligible contribution of the superconducting condensate. Even if the sample is depleted of nearly all its free charge carriers, the penetration of the electric field remains essentially unaffected. Both these conclusions explain why the experiment conducted with the Al slab was not sensitive to the external electric field. Finally, the coherence length may also be calculated and matches the tabulated values at 0 K; however, it exhibits an unexpected temperature dependence which still need to be fully analysed.

It is important to note that all these results have been obtained for the specific case of aluminum, that is, in the limit of a weak coupling ($gN(0) = 0.18$). It would certainly be interesting to extend the present analysis to some materials in a strong coupling regime: presumably the relativistic effects would then become more important and eventually lead to some observable but albeit small effects.

Conclusion

The important thing is not to stop questioning...

<div align="right">Albert Einstein (1879 - 1955).</div>

Motivated by the desire of understanding nanoscopic superconducting phenomena for relativistic time scales, a Lorentz-covariant extension of the phenomenological Ginzburg-Landau theory has been developed initially on basis of the $U(1)$ local gauge invariant Higgs model.

It has first be shown that the variational principle applied to the Higgs action for stationary configurations in the absence of external electric fields results in a set of equations of motion equivalent to the Ginzburg-Landau equations which minimize the thermodynamic free energy. These equations have been studied in the case of mesoscopic samples with cylindrical symmetries, namely for infinitely long cylinders and annuli. For such geometries, we identified particular solutions for which the order parameter describing the density of Cooper pairs vanishes on closed surfaces within the sample: these topologies were called *annular vortices* of order n and vorticity L, n referring to the number of cylindrical domains on which the order parameter vanishes and L to the fluxoid quantum number, namely the total number of magnetic flux quanta carried by the complete system of vortices. The maximal number of annular vortices which can be accommodated within the sample has also been studied as a function of the sample dimensions and of the characteristic superconducting parameters of the material.

Since these configurations solve the Ginzburg-Landau equations, they define local extrema of the free energy, but it has not been established under which circumstances these are minima or maxima, thus leaving open the question of the stability of such solutions; however, even if unstable, these particular topologies could possibly play a role in the dynamics of the switching mechanisms between different states.

In a second stage of our analysis, we identified a criterion which could confirm or invalidate the covariant extension Ginzburg-Landau theory through experimental measurements: this possible discrimination between the usual and the covariant Ginzburg-Landau models relies on the possible penetration of an electric field inside the superconducting sample. Considering an infinite slab of mesoscopic thickness submitted to a static electric field perpendicular to its surface as well as a static magnetic field parallel to the slab, the study of the phase diagram which characterises the superconducting transition in terms of its critical parameters has led to a definite and clear-cut distinction between the two models: in a weak field approximation for the external electric and magnetic fields, we observed that the critical electric field in the absence of a magnetic field remains bounded below for any temperature in the covariant model, while it goes to zero with increasing temperatures in the non-covariant model.

This major difference with this particular choice for the configuration of the external electromagnetic fields opened the possibility of discriminating the two approaches simply by measuring the critical phase diagram for a superconducting device whose dimensions are of the order of a few tens of nanometres and which approximates as well as possible the situation of an infinite slab in crossed static electric and magnetic fields. To this end, we identified a complete process for manufacturing such a device using e-beam lithography techniques. Then, resistivity measurements were carried out at low temperatures in various configurations of the external electric and magnetic fields. Surprisingly, they did not show any dependence of the phase diagram on the external electric field whatever the magnetic field and for all temperatures between some hundreds of millikelvins up to the critical temperature T_c. These experimental results are in complete opposition not only with the numerical simulations based on the covariant model, but also with the usual Ginzburg-Landau theory. They suggested a possible screening of the electric field by surface charges, to be studied from a microscopic point of view.

In the third stage of the present work, through a microscopic approach to superconductivity, we extended the standard BCS theory into a relativistic framework using a functional integral method exploiting techniques of quantum field theory at finite temperature. First we showed that all possible ways of describing a local phonon-mediated attractive interaction between pairs of electrons may be restricted to a linear combination involving only three of the five quadrilinear structures that can be constructed from the basic Dirac bilinears. Amongst these three, given their time reversal properties and their spin structure, we identified the only bilinear coupling which reproduces the usual BCS order parameter for s-wave pairing of electrons with opposite spins in the non-relativistic limit.

Within the formalism of Finite Temperature Field Theory in imaginary time, we identified the euclidean action describing the dynamics of a relativistic fermion field coupled to the electromagnetic sector in a gauge invariant manner, considering the relevant relativistic BCS coupling mentioned above. This euclidean action was studied exactly in the limiting case corresponding to a homogeneous density for the order parameter in the absence of any external electric and magnetic field. This particular situation provides an expression of the effective potential under these specific hypotheses, which can be extended to all situations with possible fluctuations of the order parameter and when an electrostatic potential couples to the chemical potential. From the effective action, we deduced the critical temperature and the maximal value of the energy gap at zero temperature, whose numerical values are in perfect agreement with the commonly admitted and experimentally measured values. Also, numerical simulations proved that the positron sector provides a perfectly negligible relativistic correction. Finally, power-like analytic approximations were proposed to fit the integral expression of the effective potential at all temperatures between 0 K and T_c: in that sense, these approximations constitute an improvement over the usual Ginzburg-Landau quartic potential for practical study of superconductivity away from the critical temperature. These analytical approximations should certainly be studied further; in particular, it would be interesting to consider what they entail for the profile of Abrikosov vortices, for instance.

Building on the knowledge of the effective potential, the expansion of the effective action up to second order in the perturbation around the exactly solved part was performed in order to identify the squared gradients of the fields. In particular, numerical values of the corrections to the electric and

magnetic field energies –namely corrections to the effective electric and magnetic permittivities of the material– were shown to be negligible.

The term containing the squared gradient of the order parameter leads to the expression of the magnetic penetration length as a function of the temperature and the chemical potential. On the other hand, the dependence of the effective potential in the electrostatic potential provides the integral expression of the electric penetration length, which also depends on the temperature and the chemical potential. Our results for the magnetic penetration length in the limit of vanishing temperature and the electric penetration length at room temperature, which then correspond to the usual Thomas-Fermi length, both reproduce the generally admitted numerical values for the case of a neutral aluminum sample. We also showed that, below the critical temperature, electric screening remains, for all practical purposes, unaffected by the superconducting phase and the electric penetration length remains close to the Thomas-Fermi screening length. Finally, even if the sample is depleted from nearly all free charge carriers, which is modelled by lowering the chemical potential from the Fermi level down to the electron rest-mass energy, the electric screening remains essentially unaffected and in no way does it reach the order of magnitude of the magnetic screening. Both these conclusions explain why the experiment conducted with the superconducting slab did not show any manifest dependence of the phase diagram on the external electric field.

In retrospect, the main question which motivated most of this work, namely "How does an electric field get expelled from a superconductor, and over which length scale?", finds its answer in the effective potential, and more specifically in its dependence on the chemical potential. To the best of our knowledge, such a dependence of the effective potential, which corresponds to the Ginzburg-Landau potential in the phenomenological theories of superconductivity, has not been explored in the literature to any great extent. Nevertheless, by separating the electrostatic contributions through a power series expansion of the effective potential, one identifies, first, the charge distribution of the conducting electrons in the superconducting phase, and second, the electric penetration length of the Thomas-Fermi type, but inclusive of the condensate contributions. As such, both so-called superconducting and normal electrons contribute at once to these phenomena, as well as to the magnetic penetration and condensate coherence lengths, but the only expression of the total electric charge could not allow for explicit identification of the electrons which take part in the superconducting condensate. It would be worth

studying these specific issues further, for instance in order to understand better how the condensation of Cooper pairs could lead to a redistribution of charges within the material and thereby generate some electric field on its surface, albeit small, and then of which order of magnitude. In particular, it would be interesting to study how this microscopic model compares with other approaches existing in the literature and dealing with related issues. By extension, such questions of charge redistribution through Cooper pair condensation are of even greater interest when it comes to magnetic vortices and their arrays, possibly even more when the sample is no longer neutral.

Still, the present work has put to rest the main question which it raised, in the case of a simple s-wave BCS superconductor. Nevertheless, it also points to further avenues of potential interest for exploration. Besides those mentioned above and related to charge redistribution at the phase transition, one may also wonder what kind of superconducting properties would be implied by the two other types of order parameters which our classification scheme identified. A general analysis could include two or even three order parameters, corresponding to models for materials with more than one gap in their energy spectrum, with at least one which no longer is purely s-wave. Clearly, this fact raises the possibility that such models could be of relevance to some of the superconducting materials discovered over the recent past.

APPENDIX

A

Notations and conventions

This appendix is by no means a complete listing of all symbols used in this thesis: it collects symbols that may be confused with each other as well as the main conventions which are commonly used in Field Theory. The numerical values of the fundamental constants used in the calculations have also been included.

Constants

e	electron charge $e = -|e| < 0$	$|e| = 1.602 \times 10^{-19}$ Cb
q	Cooper pair electric charge	$q = 2e < 0$
$\hbar$	Reduced Planck's constant	$1.055 \cdot 10^{-34}$ J.s
k_B	Boltzmann's constant	$1.38 \cdot 10^{-23}$ J/K $= 8.617 \cdot 10^{-5}$ eV/K
m_e	electron mass	$9.109 \cdot 10^{-31}$ kg $= 511$ keV/c^2
Φ_o	Magnetic flux quantum	$2.07 \, 10^{-15}$ Wb $= 2.07 \, 10^{-7}$ gauss/cm^2

Variables

β Inverse temperature, defined as $\beta = \frac{1}{k_B T}$

E_F Relativistic Fermi energy (inclusive the rest-mass energy)
         if $\hbar = 1$, then $E_F = \omega_F$

n Number of free electrons per unit volume

$N(0)$ Density of energy states at the Fermi level

Φ Electrostatic potential

τ Imaginary time, related to the real time through $t = -i\tau$

ξ Energy relative to the Fermi level: $\xi = \omega - \omega_F$

ξ_D or ω_D: Debye energy, which fixes the cutoff of the phonon energy spectrum

Possible confusions

- E_F is used for the relativistic Fermi energy, except in the description of the non-relativistic electron gas (App.B) where it does not include the rest-mass energy.

- λ is used for the magnetic penetration lengths, except in Sec. 5.4 where it is associated to the location of the fluctuations in momentum space.

- μ_o stands in general for the chemical potential; in Chaps. 1 and 2 however, it represents the vacuum magnetic permittivity.

- ξ generally describes the energy relative to the Fermi level (see above); it may also stand for the superconducting coherence length when explicitly stated.

Conventions

Einstein's rule: Einstein's implicit summation is used for repeated crossed indices:

$$a_i b^i \equiv \sum_{i=1}^{3} a_i b^i \tag{A.1}$$

Fourier transformations: in general, the Fourier transformation of a function $F(\mathbf{x})$ in configuration space will be used with the following normalisation:

$$F(\mathbf{x}) = \int \frac{d^3 k}{(2\pi)^3} \, e^{i\mathbf{k}\cdot\mathbf{x}} \, \widetilde{F}(\mathbf{k}) \, , \quad \widetilde{F}(\mathbf{k}) = \int d^3 x \, e^{-i\mathbf{k}\cdot\mathbf{x}} \, F(\mathbf{x}). \tag{A.2}$$

The tilde notation will often be omitted when no confusion arises. For time-dependent quantities, (anti-)periodicity with period β in imaginary time leads to a similar transformation with a discrete variable in frequency space: the Matsubara sum is then defined as

$$F(\tau) = \frac{1}{\beta} \sum_n e^{-i\omega_n \tau} \widetilde{F}(i\omega_n) , \quad \widetilde{F}(i\omega_n) = \int_0^\beta d\tau \, e^{i\omega_n \tau} F(\tau) \tag{A.3}$$

with even Matsubara frequencies $\omega_n = n\pi/\beta$ for periodic boundary conditions (boson field) and odd frequencies $\omega_n = (2n+1)\pi/\beta$ for anti-periodic boundary conditions (fermion field).

Indices: Greek indices refer to four-dimensional vector indices running from 0 to 3 and latin indices describe three-dimensional indices running from 1 to 3; e.g. the position vector

$$x^\mu = (x^0, x^i) = (ct, \mathbf{x}). \tag{A.4}$$

Metric: We use the Minkowski metric $g^{\mu\nu}$ with signature (1 -1 -1 - 1).

Units: Unless explicitly stated, Field Theory is studied in a system of natural units such that $\hbar = c = 1$. The electric and magnetic permittivities in vacuum are related to each other and to the velocity of light according to $\varepsilon_o \mu_o = c^{-2}$; in natural units, we shall further assume that $\varepsilon_o = \mu_o = 1$. On the other hand, the fine structure constant is given by

$$\alpha = \frac{e^2}{4\pi\varepsilon_o \hbar c} \simeq \frac{1}{137} \, ;$$

consequently, in the natural system of units, the fundamental electric charge is dimensionless and takes the numerical value $e^2 = 4\pi/137 \simeq 0.1$.

APPENDIX

B

Elements of Solid State Physics

Since several fundamental notions such as the *Fermi level* or the *density of states* are constantly used in this work, it may be useful to briefly review them in their original context, with special attention to the framework –be it relativistic or not– in which one works.

At a macroscopic level, current transport in electrically conducting materials is governed by Ohm's law $V = R\,I$, which simply states that the electric current I carried through a conducting material is proportional to the potential difference V causing the charge motion, the proportionality coefficient being the (electric) resistance R.

In the simplest picture, electric current is seen as a flow of nearly free electrons through a regular lattice formed by the positively charged atomic cores. The erratic motion of the electrons results in stochastic collisions with the ions through which they loose part of their kinetic energy: the macroscopic manifestation of this energy exchange is the heating of the conductor –namely the Joule effect– with a thermal dissipated power given by $W = RI^2$. Electric resistance is therefore a measure of the energy loss incurred through collisions of the electron flow in the material. Alternatively, to factor out any dependence on the geometry of the conductor, one introduces the notion of *resistivity* ρ, which accounts only for the electric resistive properties of the material.

Its inverse, the *conductivity* σ, enters the constitutive equation

$$\mathbf{J} = \sigma \mathbf{E} \; , \quad \sigma = \frac{1}{\rho} \tag{B.1}$$

setting the relation between the local current density $\mathbf{J}$ induced by an applied electric field $\mathbf{E}$. Table B.1 lists values for the resistivity of some typical conductors, semiconductors and isolating materials.

Material	Resistivity ($\Omega \cdot m$)	Material	Resistivity ($\Omega \cdot m$)
Conductors		*Semiconductors*	
Silver - Ag	$1.51 \ 10^{-8}$	Germanium - Ge	0.60
Copper - Cu	$1.56 \ 10^{-8}$	Silicon - Si	2300
Gold - Au	$2.04 \ 10^{-8}$	*Insulators*	
Aluminum - Al	$2.45 \ 10^{-8}$	Rubber	10^3 - 10^6
Niobium - Nb	$15.2 \ 10^{-8}$	Wood	10^8 - 10^{11}
Lead - Pb	$19.0 \ 10^{-8}$	Glass	10^{10} - 10^{14}

Table B.1: Resistivity of typical isolating, semiconducting and conducting materials at room temperature [81, 92].

At the microscopic scale, conductivity is modeled by analyzing the dynamics of individual electrons. At this point, it must be emphasized that the whole discussion is henceforth restricted to the so-called DC conductivity, *i.e.* induced by a constant voltage. The reader should refer to Refs. [81] and [82] for a detailed discussion of both AC and DC conductivity.

The classical Drude model

The first model of electrical conductivity was given by P. Drude only three years after the discovery of the electron. As already mentioned, Drude assumes that the current is composed of a flow of electrons moving through a network of regularly arranged ions with which they may collide occasionally. Two successive collisions are separated by a *mean relaxation time* τ, during which the electrons are considered as freely moving. Resistivity is related to τ through

$$\rho = \frac{m}{ne^2\tau} \tag{B.2}$$

where m is the electron mass, e its electric charge, and n the average number of free electrons per unit volume in the sample. The relaxation time τ is also

inversely proportional to another typical parameter, the *mean free path* λ between two successive collisions, which will turn to be of crucial importance for the determination of the purity of a sample. This purity has a non negligible role in superconductivity, since it appears to influence the formation and dynamics of vortices [11, 25].

At this point there is no apparent dependence of the resistivity on the temperature. Drude simply introduced it by requiring that the distribution of the electron velocities be coherent with the kinetic theory of gases, through the Maxwell-Boltzmann distribution.

The Drude model was rapidly accepted and remained for a long time a standard for the physics community, since it could account well for conductivity measurements, until it appeared that it failed to explain thermal conductivity satisfactorily. This is the point where quantum mechanics took over from where the Drude model failed: the temperature distribution of free electrons follows the Fermi-Dirac statistics, instead of the one described by Maxwell and Boltzmann. This was the first argument that compelled A. Sommerfeld to include quantum features into the description of conducting electrons.

Semi-classical theory of solids

Starting from the same hypothesis that conductivity is related to the motion of free incoherent electrons, Sommerfeld required that each electron obeys Schrödinger's equation, resulting in the quantisation of its energy levels:

$$E(\mathbf{k}) = \frac{p^2}{2m} = \frac{\hbar^2 k^2}{2m} \tag{B.3}$$

in terms of discrete values for the wave vector $\mathbf{k}$:

$$k_x = n_x \frac{2\pi}{L_x}, \quad k_y = n_y \frac{2\pi}{L_y}, \quad k_z = n_z \frac{2\pi}{L_z}, \quad n_x, n_y\, n_z \text{ integers}$$

having assumed a finite-size rectangular box of dimensions L_x, L_y and L_z. However, since the number of free electrons is large, one may approximate the discrete wave vector spectrum by a continuous one in k-space, leading to an analytic expression for the *density of states per unit energy*

$$2\frac{d^3\mathbf{k}}{(2\pi)^3} = dE\, g(E) \ , \quad g(E) = \frac{1}{2\pi^2}\frac{2m}{\hbar^3}\sqrt{2mE} \ , \tag{B.4}$$
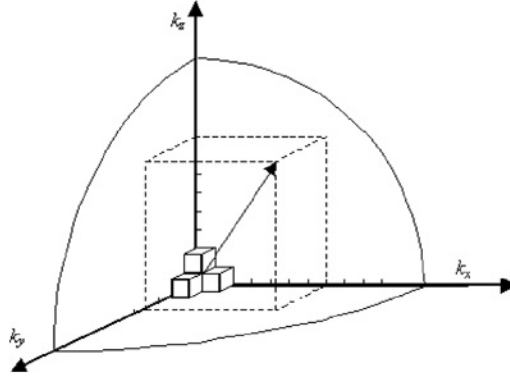
Figure B.1: Graphical representation of wave vectors in k-space. Energy levels are associated to unit cells that are piled up isotropically; for a large number of unit cells, one can approximate the volume by a sphere [93].

where the overall factor 2 accounts for Pauli's exclusion principle, so that each energy state can contain at most two electrons with opposite spins.

Since there is no thermal energy at zero kelvin, all energy levels are filled from the lowest one up to some highest level: this upper state is called the *Fermi level* and defines a sphere in k-space with a radius related to the number of electrons per unit volume n:

$$E_F = \frac{\hbar^2}{2m}(3\pi^2 n)^{2/3} . \tag{B.5}$$

Once the Fermi level is known, one can compute the density of states at the Fermi level, usually denoted $N(0)$:

$$N(0) = g(E_F) = \frac{(2m)^{3/2}}{2\pi^2\hbar^3}\sqrt{E_F} = \frac{3n}{2E_F} . \tag{B.6}$$

In some circumstances, it may be useful to know the Fermi temperature, which follows from the identity

$$E_F = k_B T_F \tag{B.7}$$

where k_B is Boltzmann's constant.

At non-zero temperature, electrons may be thermally excited into levels above the Fermi energy; their energy distribution is then given by the Fermi-Dirac statistics

$$f(E) = \frac{1}{e^{(E-E_F)/k_B T} + 1} . \tag{B.8}$$
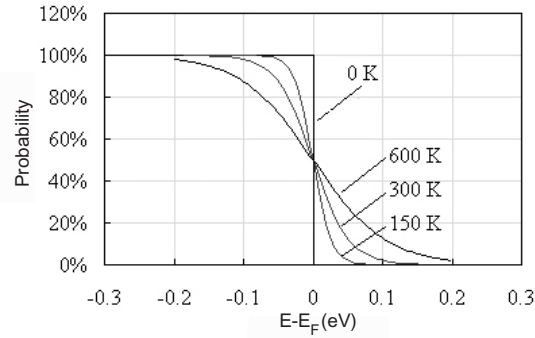
Figure B.2: Fermi-Dirac distribution of the energy states at zero and higher temperatures [93].

We conclude this section by providing numerical values for the main relevant variables in a standard metal. Considering the case of aluminum, with density $\rho = 2700$ kg/m^3 and atomic weight $M = 26.98$, each atom contributes to the electron gas three conduction electrons and the average number of free electrons per unit volume is $n = 1.81 \cdot 10^{29}$ m^{-3}. It follows that

$$
\begin{aligned}
E_F &= 1.86 \cdot 10^{-18} \text{ J} = 11.67 \text{ eV} \\
N(0) &= 1.46 \cdot 10^{47} \text{ J}^{-1}.\text{m}^{-3} \\
T_F &= 1.35 \cdot 10^{5} \text{ K} \\
\beta_F &= \frac{1}{T_F} = 6.77 \cdot 10^{-3} \text{ K}^{-1} .
\end{aligned}
\tag{B.9}
$$

Relativistic electron gas

The discussion of the previous section can be extended to the description of a relativistic free fermion gas; in that case, the energy levels are modified so to include the mass energy:

$$
E = \sqrt{(pc)^2 + (mc^2)^2} .
\tag{B.10}
$$

In order to compare with the non-relativistic limit, it is useful to separate the mass contribution to the energy, defining the kinetic energy

$$
K = E - mc^2 .
\tag{B.11}
$$

The Fermi level is re-expressed in terms of the above quantities, and in particular the density of states at the Fermi level becomes

$$N(0) = \frac{1}{\pi^2 \hbar^3 c3} E_F \sqrt{E_F^2 - (mc^2)^2} = \frac{1}{\pi^2 \hbar^2 c^2} E_F (3\pi^2 n)^{1/3} . \tag{B.12}$$

In the system of units such that $\hbar = c = 1$, the previous relation simply writes $N(0) = k_F \omega_F / \pi^2$. For the case of aluminum, the values of $N(0)$ and T_F do not differ significantly from their non-relativistic values, but we have to consider instead

$$E_F = 511.735 \, keV \tag{B.13}$$

$$K_F = 11.68 \, eV . \tag{B.14}$$

In comparison, the Debye energy is

$$\omega_D = k_B \theta_D = 0.037 \, eV \tag{B.15}$$

and usual BCS quantities are evaluated to be

$$k_B T_c = 1.012 \cdot 10^{-4} \, eV \tag{B.16}$$

$$\Delta_o = 1.76 \, k_B T_c = 1.76 \cdot 10^{-4} \, eV . \tag{B.17}$$
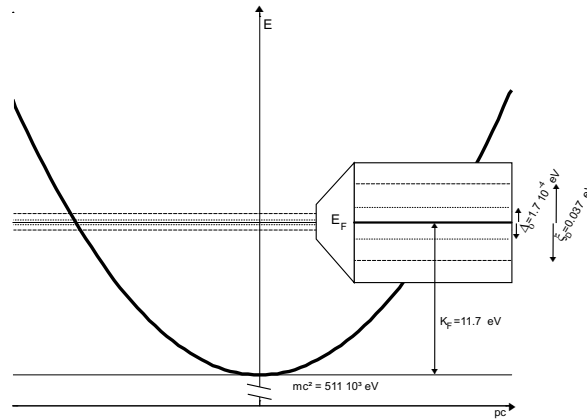
Figure B.3: Relative orders of magnitudes of the different energy scales for a relativistic free electron gas in aluminum.

Band structures

Although Sommerfeld's model matched fairly well with a number of experimental verifications, theorists knew that it had to be refined, simply because the hypothesis of free electrons was too strong. Considering the crystallographic classification of ionic lattices –the so-called Bravais lattices–, F. Bloch considered electrons submitted to a periodic potential. This leads to the description of energy levels in terms of families of solutions, continuously extended to *energy bands* usually separated by forbidden areas, or *gaps*, in the energy spectrum.

In the modern picture of conductivity, the electrical features of materials depend on the way the energy bands are filled (Fig. B.4) for an electric current can emerge only in partially filled bands –where electrons can then jump along adjacent levels. If the Fermi level is located inside one band, then conduction will be possible, but if the electrons perfectly fill a band separated from the next one by a gap larger than the thermal energy, then it will never be possible to observe an electric current. Semiconductors correspond to a special class of materials for which several energy bands are partially filled and separated by a gap less than the thermal energy: under certain circumstances it is possible for some electrons to hop from one band to the next and develop conduction mechanisms.
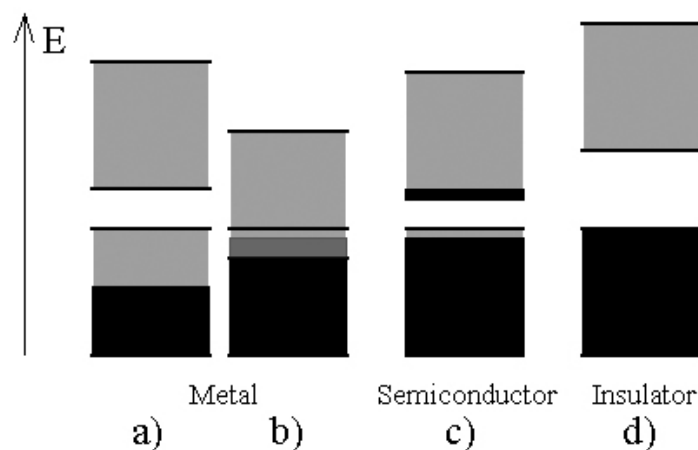
Figure B.4: The electrical properties of materials depend on their band structure and the way they are filled [93].

APPENDIX

C

Elements of Classical and Relativistic Field Theory

Probably the best known equation of Modern Physics is Einstein's relation $E = mc^2$ which allows for the transformation between mass and energy. One consequence is the impossibility of maintaining a description of Nature in terms of (classical or relativistic) dynamical systems with a fixed number of particles, even at a quantum level, since particles may be created or annihilated provided the energetic content of the system is preserved. This is one of the arguments supporting the development of Field Theory, which provides a natural framework to account for multiparticle states. Whether at a classical or quantum level, the dynamical description of a field can be inferred from a lagrangian or a hamiltonian formulation [79, 94].

C.1 Relativistic invariance

Before addressing any consideration about fields, we first review the basic properties of Lorentz transformations, which underlie the mathematical expression of relativistic invariance [70, 94]. We consider a system of units such that $\hbar = c = 1$.

Two observers in different inertial frames may describe a same physical event within their own system of space-time coordinates, say x^μ for the first observer and $(x^\mu)'$ for the second, both systems being related through a *Lorentz transformation* such that

$$(x^\nu)' = \Lambda^\nu{}_\mu x^\mu \tag{C.1}$$

where Λ is determined in terms of six parameters associated to three space rotations and three Lorentz boosts. The basic Minkowski space invariant is the *proper time interval*

$$ds^2 = dx^\mu dx_\mu. \tag{C.2}$$

From these relations, it follows that the transformation coefficients should verify

$$\Lambda_\rho{}^\mu \Lambda^\rho{}_\nu = \delta^\mu{}_\nu \ , \tag{C.3}$$

which in particular implies that $\det|\Lambda| = \pm 1$. The positive value $det|\Lambda| = +1$ is associated to so-called proper (or *orthochronous*) Lorentz transformations, while the negative value corresponds to improper transformations. More generally, the Lorentz group is defined as the group of all 4×4 matrices preserving the spacetime invariant, thus satisfying the restriction

$$g_{\mu\nu} = \Lambda^\rho{}_\mu g_{\rho\sigma} \Lambda^\sigma{}_\nu \tag{C.4}$$

where the Minkowski metric is conventionally taken to be $g_{\mu\nu} = \text{diag}(1 - 1 - 1 - 1)$. If these signature signs were all the same, the group would be $O(4)$, but since a sign difference distinguishes time from spatial coordinates, the Lorentz group is usually denoted $O(3,1)$.

Equipped with these transformations, one defines some specific classes of objects, such as scalars and vector fields defined by the following transformation properties:

$$\text{scalar:} \quad s'(x') = s(x) \tag{C.5}$$

$$\text{vector:} \quad v^{\mu\prime}(x') = \Lambda^\mu{}_\nu v^\nu(x); \tag{C.6}$$

namely, scalars are invariant under Lorentz transforms whereas vectors transform as the coordinates do. Finally, the formulation of a dynamical system is said to be Lorentz covariant if the relations between its physical observables remain unchanged under Lorentz transformations. One must distinguish between covariant and contravariant quantities, such as x_μ and x^ν respectively

in the case of four-vectors (note the position of their indices), which are connected by raising and lowering indices with the help of the Minkowski metric; for instance

$$x^\mu = g^{\mu\nu} x_\nu.$$

Thus, one has for example

$$
\begin{aligned}
x^\mu &= (t, \mathbf{x}) , & x_\mu &= (t, -\mathbf{x}) \\
\partial_\mu &= \frac{\partial}{\partial x^\mu} = (\frac{d}{dt}, \mathbf{\nabla}) , & \partial^\mu &= (\frac{d}{dt}, -\mathbf{\nabla}).
\end{aligned}
$$

The Lorentz invariant contraction of four-vectors thus also reads

$$p \cdot q = p_\mu q^\mu = p_\mu q_\nu g^{\mu\nu} = p^0 q^0 - \mathbf{p} \cdot \mathbf{q}. \tag{C.7}$$

C.2   Field dynamics

Considering a classical system described by a *field* $\phi(x)$ over the time and the space coordinates $x = (t, \mathbf{x})$, the dynamics of the system is governed by the action integral built from the lagrangian density $\mathcal{L}(\phi, \partial_\mu \phi)$, which is a functional of the field and its derivatives:

$$S[\phi] = \int d^4x \, \mathcal{L}(\phi, \partial_\mu \phi). \tag{C.8}$$

Applying the variational principle to such an action leads to the Euler-Lagrange equation of motion

$$\partial_\mu \left(\frac{\partial \mathcal{L}}{\partial(\partial_\mu \phi)} \right) - \frac{\partial \mathcal{L}}{\partial \phi} = 0. \tag{C.9}$$

Within the hamiltonian formulation, phase space consists of the field configurations $\phi(x)$ and their conjugate momenta

$$\pi(x) = \frac{\partial \mathcal{L}}{\partial \dot{\phi}(x)} \tag{C.10}$$

where $\dot{\phi}$ denotes the time derivative of the field. The hamiltonian density is then given by

$$\mathcal{H}(\pi, \phi) = \pi(x)\dot{\phi}(x) - \mathcal{L} \tag{C.11}$$

leading to the hamiltonian

$$H = \int d^3x \, \mathcal{H}.$$

When one deals with relativistic theories, the advantage of the first formulation is clear since the lagrangian and the equations of motion are manifestly

covariant under Lorentz transformations. On the other hand, the hamilto-
nian formulation is more directly related to some physical observables, such
as for example the energy as an eigenvalue of the hamiltonian spectrum in
the case of stationary states. Furthermore, canonical quantization follows the
hamiltonian formulation since the (anti-)commutation relations are just in di-
rect correspondence with the Poisson brackets which define an algebra over
the phase space spanned by the field and its conjugate momentum.

C.3   The Dirac field

C.3.1   Dirac equation

In the spacetime described by the four-components coordinates x, the tradi-
tional form of the Dirac lagrangian which describes the dynamics of a free
relativistic fermion field is

$$\mathcal{L} = \frac{i}{2}[\bar{\psi}\gamma^{\mu}(\partial_{\mu}\psi) - (\partial_{\mu}\bar{\psi}\gamma^{\mu}\psi)] - m\bar{\psi}\psi \ . \tag{C.12}$$

The Dirac spinor field $\psi(x)$ admits the following Fourier decomposition:

$$\psi(x) = \sum_{s=1,2}\int \frac{d^3k}{(2\pi)^3 \, 2k^0} \, [b(\mathbf{k},s)u(\mathbf{k},s)e^{-ikx} + d^{\dagger}(\mathbf{k},s)v(\mathbf{k},s)e^{ikx}] \tag{C.13}$$

with $k^0 = \omega(\mathbf{k}) = (\mathbf{k}^2 + m^2)^{1/2}$, $k \cdot x = k^0 x^0 - \mathbf{k} \cdot \mathbf{x}$ and the plane wave spinors
being solutions to

$$\begin{cases} (\gamma^{\mu}k_{\mu} - m)u(k) = 0 \\ (\gamma^{\mu}k_{\mu} + m)v(k) = 0. \end{cases}$$

In the Dirac representation of the Clifford algebra for the γ^{μ} matrices, these
solutions admit the following form:

$$u(\mathbf{k},s) = \frac{1}{\sqrt{\omega+m}}\begin{pmatrix} (\omega+m) \, \varphi_s \\ \mathbf{k} \cdot \boldsymbol{\sigma} \, \varphi_s \end{pmatrix} \ , \ v(\mathbf{k},s) = \frac{1}{\sqrt{\omega+m}}\begin{pmatrix} \mathbf{k} \cdot \boldsymbol{\sigma} \, \varphi_s \\ (\omega+m) \, \varphi_s \end{pmatrix} \tag{C.14}$$

$$\text{where } \omega^2 = \mathbf{k}^2 + m^2 \ , \ \varphi_+ = \begin{pmatrix} 1 \\ 0 \end{pmatrix} \ , \ \varphi_- = \begin{pmatrix} 0 \\ 1 \end{pmatrix} \ .$$

The quantum prescription for the components of the Dirac field is the equal
time anti-commutation relation verified by the operators $b(\mathbf{k},s)$ and $d(\mathbf{k},s)$:

$$\{b(\mathbf{k},r),b^{\dagger}(\mathbf{k}',s)\} = \{d(\mathbf{k},r),d^{\dagger}(\mathbf{k}',s)\} = (2\pi)^3 \, 2\omega(\mathbf{k}) \, \delta^{rs} \, \delta^{(3)}(\mathbf{k}-\mathbf{k}') \tag{C.15}$$

with all other anticommutators vanishing. This yields the hamiltonian, in normal ordered form

$$H = \sum_s \int d^3k\, k_0 [b^\dagger(\mathbf{k},s)b(\mathbf{k},s) + d^\dagger(\mathbf{k},s)d(\mathbf{k},s)].$$ (C.16)

In terms of individual particles, each Fourier component of the spinor has an immediate interpretation: for instance

$b(\mathbf{k},s)u(\mathbf{k},s)e^{-ikx}$ annihilates a positive energy electron with momentum k and spin s

$d^\dagger(\mathbf{k},-s)v(\mathbf{k})e^{ikx}$ creates a positive energy positron with momentum k and spin $-s$.

C.3.2 Dirac algebra

The Dirac lagrangian (C.12) involves a set of 4×4 matrices which define the Dirac (or Clifford) algebra: these are the γ^μ matrices satisfying the anticommutation relations

$$\{\gamma^\mu, \gamma^\nu\} = 2g^{\mu\nu}.$$ (C.17)

Traditionally, the following notations are introduced:

$$\bar{\psi} = \psi^\dagger \gamma^0 \quad , \quad \not{a} = a_\mu \gamma^\mu .$$ (C.18)

In this thesis, we consider exclusively the Dirac representation for this algebra, in which the γ^μ matrices admit the following explicit realisation:

$$\gamma^0 = \begin{pmatrix} I & 0 \\ 0 & -I \end{pmatrix} \quad , \quad \gamma^j = \begin{pmatrix} 0 & \sigma^i \\ -\sigma^i & 0 \end{pmatrix}$$ (C.19)

where I is the 2×2 identity matrix and the σ^is are the Pauli matrices

$$\sigma^1 = \begin{pmatrix} 0 & 1 \\ 1 & 0 \end{pmatrix} \quad , \quad \sigma^2 = \begin{pmatrix} 0 & -i \\ i & 0 \end{pmatrix} \quad , \quad \sigma^3 = \begin{pmatrix} 1 & 0 \\ 0 & -1 \end{pmatrix} .$$ (C.20)

It proves useful to introduce two further Dirac objects, whose utility will appear below:

$$\gamma^5 = i\gamma^0\gamma^1\gamma^2\gamma^3 = \begin{pmatrix} 0 & I \\ I & 0 \end{pmatrix}$$ (C.21)

and

$$\sigma^{\mu\nu} = \frac{i}{2}[\gamma^\mu, \gamma^\nu],$$ (C.22)

where the square brackets denote the commutator of the two matrices; the explicit form in the Dirac representation is:

$$\sigma^{0i} = \begin{pmatrix} 0 & \sigma^i \\ \sigma^i & 0 \end{pmatrix} \qquad \sigma_{ij} = \varepsilon^{ijk} \begin{pmatrix} \sigma^k & 0 \\ 0 & \sigma^k \end{pmatrix}. \tag{C.23}$$

The most essential properties of those matrices are summarised below:

$$\begin{aligned}
(\gamma^\mu)^\dagger &= \gamma^0 \gamma^\mu \gamma^0 \\
(\gamma^0)^\dagger &= \gamma^0 \\
(\gamma^i)^\dagger &= -\gamma^i, \quad i = 1,2,3 \\
(\gamma^5)^\dagger &= \gamma^5 \\
(\gamma^5)^2 &= I \\
\{\gamma^5, \gamma^\mu\} &= 0 \\
[\gamma^5, \sigma^{\mu\nu}] &= 0
\end{aligned} \tag{C.24}$$

showing that γ^0 and γ^5 are hermitian and γ^i are anti-hermitian. They also verify the following contraction identities:

$$\begin{aligned}
\gamma^\mu \gamma_\mu &= 4 \\
\gamma^\nu \gamma^\mu \gamma_\nu &= -2\gamma^\mu \\
\gamma^\rho \gamma^\mu \gamma^\nu \gamma_\rho &= 4g^{\mu\nu},
\end{aligned} \tag{C.25}$$

and some of their essential trace properties are

$$\begin{aligned}
\text{tr } \gamma^\mu &= 0 \\
\text{tr } \gamma_5 &= 0 \\
\text{tr } (\gamma^\mu \gamma_5) &= 0 \\
\text{tr } (\gamma^\mu \gamma^\nu) &= 4g^{\mu\nu} \\
\text{tr } \sigma^{\mu\nu} &= 0
\end{aligned} \tag{C.26}$$

and in general the trace of an odd number of γ^μ matrices vanishes.

The γ^μ matrices and their products provide a natural sixteen-dimensional basis of the full Clifford-Dirac algebra: this basis is constructed from

$$\Gamma = \{I, \gamma^5, \gamma^\mu, \gamma^\mu \gamma^5, \sigma^{\mu\nu}\}. \tag{C.27}$$

Moreover, this basis introduces a classification of all possible Dirac bilinears $\bar{\psi}\Gamma\psi$ according to their behaviour under a Lorentz transformation $S(\Lambda) = \Lambda^\mu{}_\nu$:

I	scalar	$\bar{\psi}'(x')\psi'(x') = \bar{\psi}(x)\psi(x)$
γ^5	pseudo-scalar	$\bar{\psi}'(x')\gamma^5\psi'(x') = \det\Lambda\ \bar{\psi}(x)\gamma^5\psi(x)$
γ^μ	vector	$\bar{\psi}'(x')\gamma^\mu\psi'(x') = \Lambda^\mu{}_\nu\ \bar{\psi}(x)\gamma^\nu\psi(x)$
$\gamma^\mu\gamma^5$	pseudo-vector	$\bar{\psi}'(x')\gamma^\mu\gamma^5\psi'(x') = \det\Lambda\ \Lambda^\mu{}_\nu\ \bar{\psi}(x)\gamma^\nu\gamma^5\psi(x)$
$\sigma^{\mu\nu}$	tensor	$\bar{\psi}'(x')\sigma^{\mu\nu}\psi'(x') = \Lambda^\mu{}_\alpha\Lambda^\nu{}_\beta\ \bar{\psi}(x)\sigma^{\alpha\beta}\psi(x)$

Table C.1: Classification of Dirac bilinears.

C.3.3   Symmetries of Dirac spinors

It is instructive to consider how Dirac spinors transform under discrete transformations such as charge conjugation, parity and time reversal [94].

Parity: an explicit form of the parity operator performing the transformation $\psi'(-\mathbf{x},t) = \mathcal{P}\psi(\mathbf{x},t)$ is found by recalling that parity is nothing but a π-rotation followed by a specular transformation; then the operator is simply given by

$$\mathcal{P} = e^{i\theta}\gamma^0 \tag{C.28}$$

where θ is an arbitrary phase factor.

Charge conjugation: charge conjugation $\psi'_c = C\psi(\mathbf{x},t)$ takes the explicit form

$$\psi_c = \eta_c C\bar{\psi}^T \ , \quad C = i\gamma^2\gamma^0 \tag{C.29}$$

with an arbitrary phase factor such that $\eta_c^\dagger\eta_c = 1$. The charge conjugation matrix has following properties:

$$C^T = C^\dagger = -C = C^{-1} \ . \tag{C.30}$$

We have in general

$$\begin{aligned} \psi &= \eta_c\ C\ \bar{\psi}_c^T & \psi_c &= \eta_c\ C\ \bar{\psi}^T \\ \bar{\psi} &= \eta_c^{-1}\ \psi_c^T\ C & \bar{\psi}_c &= \eta_c^\dagger\ \psi^T\ C \end{aligned} \tag{C.31}$$

Time reversal: the transformation $\psi'(\mathbf{x},-t) = \mathcal{T}\psi(\mathbf{x},t)$ is performed through a transformation operator such that

$$\mathcal{T}\psi(\mathbf{x},t)\mathcal{T}^{-1} = e^{i\theta}T\psi(\mathbf{x},-t). \tag{C.32}$$

The T matrix is given by the explicit representation

$$T = i\gamma^1\gamma^3 \tag{C.33}$$

and verifies

$$
\begin{aligned}
T\gamma^\mu T^{-1} &= (\gamma^\mu)^T = (\gamma^\mu)^* \\
T &= T^{-1} = T^\dagger = -T^* \ .
\end{aligned}
\tag{C.34}
$$

Now that we have established how spinors behave under those transformations, we could prove that Dirac bilinears transform according to $\bar\psi \Gamma^i \psi = s\, \bar\psi \Gamma^i \psi$, with $s = \pm 1$, namely they remain either unchanged or acquire a minus sign when submitted to one of those transformations separately or the combination of them three (CPT transformation); Table C.2 summarises these properties.

	$\bar\psi\psi$	$\bar\psi\gamma^\mu\psi$	$\bar\psi\sigma^{\mu\nu}\psi$	$\bar\psi\gamma_5\psi$	$\bar\psi\gamma_5\gamma^\mu\psi$
C	1	-1	-1	1	1
P	1	1	1	-1	-1
T	1	1	-1	-1	1
CPT	1	-1	1	1	-1

Table C.2: Behaviour of the Dirac bilinears under C, P, T and CPT transformations.

C.3.4 Algebra of Fock operators

The mode expansion (C.13) introduces the Fock operators $b(\mathbf{k}, s)$ and $d(\mathbf{k}, s)$ and their conjugates, whose action on a physical state is to raise or lower the number of particles, whether electrons or positrons. It is worth recalling some interesting relations associated to the Fock algebra. In simplified notations, let us consider a single Fock operator for a fermion verifying the anticommutation relations

$$
\{b, b^\dagger\} = c > 0 \ , \qquad \{b, b\} = \{b^\dagger, b^\dagger\} = 0 \ .
\tag{C.35}
$$

Its action on physical states is given by

$$
\begin{array}{lll}
b\,|0\rangle = 0 & \frac{1}{\sqrt{c}}\,b\,|1\rangle = |0\rangle & b^\dagger b\,|0\rangle = 0 \\[4pt]
\frac{1}{\sqrt{c}}\,b^\dagger\,|0\rangle = |1\rangle & b^\dagger\,|1\rangle = 0 & b^\dagger b\,|1\rangle = c\,|1\rangle
\end{array}
\tag{C.36}
$$

with $\langle 0|0\rangle = \langle 0|0\rangle = 1$. Since at most one fermion may occupy any given state, the trace of any given operator $\hat{A}$ simply consists in the contributions

$$
Tr\hat{A} = \langle 0|\hat{A}|0\rangle + \langle 1|\hat{A}|1\rangle \ .
$$

In particular, let us consider a basic operator of the form $\hat{A} = e^{-\beta \frac{1}{c} \omega b^\dagger b} = 1 - \beta \frac{1}{c} \omega b^\dagger b$. Then the observable value of this operator are

$$
\begin{aligned}
\langle 0 | \hat{A} | 0 \rangle &= e^{-\beta \frac{1}{c} \omega \langle 0 | b^\dagger b | 0 \rangle} = 1 \\
\langle 1 | \hat{A} | 1 \rangle &= e^{-\beta \frac{1}{c} \omega \langle 1 | b^\dagger b | 1 \rangle} = e^{-\beta \omega}
\end{aligned}
$$

so that

$$
\text{Tr } e^{-\beta \frac{1}{c} \omega b^\dagger b} = 1 + e^{-\beta \omega}. \tag{C.37}
$$

The normalisation constant c has been reabsorbed into the trace operation and does not appear any more in the final result; this will have important consequences in the following. By expanding the exponential, it is easy to show:

$$
\begin{aligned}
\text{Tr } \left(b^\dagger b \, e^{-\beta \frac{1}{c} \omega b^\dagger b} \right) &= e^{-\beta \omega} \\
\text{Tr } \left(b b^\dagger \, e^{-\beta \frac{1}{c} \omega b^\dagger b} \right) &= 1.
\end{aligned} \tag{C.38}
$$

Now consider two kinds of fermionic creation and annihilation operators obeying identical anticommutation relations (for the sake of simplicity, we normalize them to unity):

$$
\{b, b^\dagger\} = \{d, d^\dagger\} = 1 \; ; \tag{C.39}
$$

then any state is obtained as a tensor product of two states referring to each of the fermionic sectors, for example

$$
|1, 0\rangle = |1\rangle_b \otimes |0\rangle_d
$$

so that the full trace operation factorizes as follows:

$$
\text{Tr } e^{-\beta(\omega_b b^\dagger b + \omega_d d^\dagger d)} = (\text{Tr } e^{-\beta \omega_b b^\dagger b})(\text{Tr } e^{-\beta \omega_d d^\dagger d}) = (1 + e^{-\beta \omega_b})(1 + e^{-\beta \omega_d}). \tag{C.40}
$$

APPENDIX

D

Thermal Field Theory

D.1 Path integral formulation

This Appendix provides a detailed construction of the path integral formulation of quantum dynamics following Feynman's method [95] but in a slightly more modern approach [96, 97]. First, it is useful to recall that a quantum system can either be described in the Schrödinger or in the Heisenberg picture. In the former, operators are defined at constant time and the physical states may evolve in time; in particular, they verify Schrödinger's equation of motion

$$i\hbar \frac{\partial}{\partial t} |\psi, t\rangle_S = \hat{H} |\psi, t\rangle_S \ .$$ (D.1)

In the Heisenberg picture, physical states are considered at one given time, while the Heisenberg operators are dynamical variable which obey the equation of motion

$$i\hbar \frac{d}{dt} \hat{O}_H(t) = \left[\hat{O}_H(t), \hat{H} \right] \ .$$ (D.2)

The relation between operators in these two pictures is determined through the time evolution operator defined in term of the hamiltonian:

$$\hat{O}_H(t) = e^{i\hat{H}(t - t_o)/\hbar} O_S e^{-i\hat{H}(t - t_o)/\hbar}$$ (D.3)

where t_o refers to the reference time at which the Schrödinger picture is considered.

On the other hand, the transition amplitude describing a system at a position q' at time t' coming from an initial position q at time t, also called the *propagator* from (q,t) to (q',t'), is obtained by evaluating the overlap between the physical states at q and q' enclosing the time evolution operator[1]:

$$P(q',t';q,t) = \langle q' | e^{-iH(t'-t)} | q \rangle .$$ (D.4)

The philosophy of the path integral formalism is to derive an expression for this amplitude considering all possible ways of getting from the starting point to the other. To this end, we first divide the evolution of the system into two sub-intervals by considering an intermediate position in space and time (q_1, t_1). The propagator is then factorised as

$$P = \langle q' | e^{-iH(t'-t_1)} e^{-iH(t_1-t)} | q \rangle .$$

Since the $\{|q\rangle\}$ define a complete set of eigenvectors, the closing relation may be inserted into the propagator, which becomes

$$P = \langle q' | e^{-iH(t'-t_1)} \int dq_1 |q_1\rangle \langle q_1 | e^{-iH(t_1-t)} | q \rangle = \int dq_1 P(q',t';q_1,t_1) P(q_1,t_1;q,t).$$ (D.5)

The integration simply means that we walk between q and q' through an intermediate position q_1, considering all possible positions of this intermediate point. Of course we can repeat this process and divide the time interval $t'-t$ into a large number N of intervals of width $\varepsilon = (t'-t)/N$ in order to obtain a probability amplitude represented in terms of all N-legged paths between the initial and final positions:

$$P = \int dq_1 \cdots dq_{N-1} P(q_N,t_N;q_{N-1},t_{N-1}) P(q_{N-1},t_{N-1};q_{N-2},t_{N-2})\ldots P(q_1,t_1;q_0,t_0)$$

where

$$q_N = q',\, t_N = t';\, \ldots ;\, q_0 = q,\, t_0 = t .$$

Of course no integration is performed over q_0 and q_N since they determine the initial and final positions, which are fixed. It is clear that this amplitude can be considered as a sum over all possible paths from q_0 to q_N moving in succession through $q_1, q_2, \ldots q_{N-1}$, this sum being performed by the multiple integration.

---

[1]From now on the hat notation for the operators will be omitted, and we will assume $\hbar = 1$ unless explicitly given.
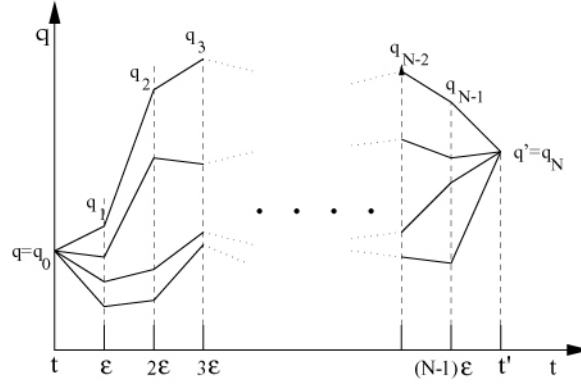
Figure D.1: Propagator between (q,t) and (q',t') as a sum over all N-legged paths [97].

We can pursue further through a detailed analysis of the expression for one given path by performing an expansion for each small time interval ε; there are N such factors, each of the form:

$$
\begin{aligned}
P(q_{j+1},t_{j+1};q_j,t_j) &= \langle q_{j+1}|e^{-iH\varepsilon}|q_j\rangle \\
&= \langle q_{j+1}|q_j\rangle - i\varepsilon\langle q_{j+1}|H|q_j\rangle + O(\varepsilon^2).
\end{aligned}
$$

Normalising the overlap expression between position and conjugate momentum as $\langle q|p\rangle = e^{iqp}$ and introducing the closure relation in momentum space, we have

$$
\langle q_{j+1}|q_j\rangle = \delta(q_{j+1} - q_j) = \int \frac{dp}{2\pi} e^{i(q_{j+1}-q_j)p} .
$$

and

$$
\begin{aligned}
\langle q_{j+1}|H|q_j\rangle &= \langle q_{j+1}|\int \frac{dp_j}{2\pi}|p_j\rangle\langle p_j|H|q_j\rangle \\
&= \int \frac{dp_j}{2\pi} H(q_j,p_j) e^{i(q_{j+1}-q_j)p_j},
\end{aligned}
$$

so that we may write

$$
P(q_{j+1},t_{j+1};q_j,t_j) = \int \frac{dp_j}{2\pi} e^{i\varepsilon[p_j\dot{q}_j - H(q_j,p_j)]} \tag{D.6}
$$

where we defined $\dot{q}_j = (q_{j+1} - q_j)/\varepsilon$. Combining the N such factors that deter-

mine one path, the propagator is then given by

$$
\begin{aligned}
P(q',t';q,t) &= \int dq_1 \ldots dq_{N-1} \quad \int \frac{dp_0}{2\pi} \ldots \frac{dp_{N-1}}{2\pi} \exp i\varepsilon \sum_j [p_j \dot{q}_j - H(p_j,q_j)] \\
&\equiv \int \mathcal{D}p(t)\mathcal{D}q(t) \, \exp\left[i \int_t^{t'} dt'' \left(p\,\partial_{t''}q - H(p,q) \right) \right] .
\end{aligned}
\tag{D.7}
$$

The last expression is known as the *phase space path integral*. This is the more general expression for the path integral formalism. Assuming the momentum integrals can be performed, we are left with a more compact form known as the *configuration space path integral*:

$$
P = \int \mathcal{D}q(t)e^{iS[q(t)]}
\tag{D.8}
$$

where $S[q(t)]$ is the action for the system moving along each path between q and q'. Infinitesimal variation of this action provides the usual Euler-Lagrange equation of motion, which simply states that the system shall effectively choose to walk along the path between initial and final positions that minimises the action.

D.2   Path integrals in statistical mechanics

Equilibrium statistical mechanics is constructed from one fundamental expression known as the *partition function*

$$
Z(\beta) = Tr[e^{-\beta H}] , \quad \beta = 1/kT.
\tag{D.9}
$$

Expanded in the configuration space basis, the partition function reads

$$
Z(\beta) = \int dq \, \langle q| e^{-\beta H} |q\rangle ,
\tag{D.10}
$$

and can be compared to the definition of the propagator (D.4): performing a transformation over the time variable $t \to -i\tau$, the expression of the partition function corresponds to a propagator between 0 and β in imaginary time, with the additional boundary condition $q(\beta) = q(0)$. The partition function may therefore be given a path integral formulation. To illustrate the features of this partition function, consider the hamiltonian for the classical one-dimensional harmonic oscillator

$$
H_{ho} = \frac{p^2}{2m} + \frac{m\omega^2 q^2}{2}
\tag{D.11}
$$

where $p = m\dot{q}$ is the momentum conjugate to the coordinate q; the algebraic structure of phase space is derived from the canonical Poisson bracket at equal time

$$\{q(t_o), p(t_o)\} = 1 .$$

The dynamics of the system may alternatively be formulated in terms of the lagrangian L, related to the hamiltonian by the general Legendre transform $H = \dot{q}p - L$; for the harmonic oscillator,

$$L_{ho} = \frac{p^2}{2m} - \frac{m\omega^2 q^2}{2} = \frac{m\dot{q}^2}{2} - \frac{m\omega^2 q^2}{2} . \tag{D.12}$$

We may then calculate the partition function (D.8) for that specific hamiltonian. In particular, the gaussian integral over momentum is readily performed; in the statistical mechanics case, we are left with

$$Z(\beta) = \int \mathcal{D}q(\tau) \, e^{-S_E(\beta)} \tag{D.13}$$

where the time dependence of the coordinate has been turned to imaginary time $t = -i\tau$, and the path integration is performed over paths with period β in imaginary time. The functional

$$S_E(\beta) = \int_0^\beta d\tau \, L_E[\dot{q}(\tau), q(\tau)]$$

is usually referred to as the euclidean action, with now $\dot{q}(\tau) = \frac{dq}{q\tau}$.

The generalisation to quantum field theory follows the considerations of the previous section: the dynamics of a complex **bosonic field** $\phi(x)$ may be inferred from its hamiltonian

$$H = \int d^3\mathbf{x} \, \mathcal{H}[\phi(\mathbf{x}), \pi(\mathbf{x})]$$

where $\pi(\mathbf{x})$ denotes the conjugate momentum field. Alternatively, one may start from the lagrangian density, which is related to the hamiltonian density through $\mathcal{L} = \pi\dot{\phi} - \mathcal{H}$. Then the partition function becomes

$$Z(\beta) = \int \mathcal{D}\phi(x)\mathcal{D}\phi^\dagger(x)\, e^{-S_E(\beta)} \, , \quad S_E(\beta) = \int_0^\beta d\tau \int d^3\mathbf{x} \, \mathcal{L}_E(\partial_\mu\phi, \phi) \tag{D.14}$$

with periodicity of the field in imaginary time $\phi(\mathbf{x}, \beta) = \phi(\mathbf{x}, 0)$.

For a **fermionic field** $\psi(x)$ however, the formal path integral representation of $Z(\beta)$ given in (D.14) still holds, but the field is subject to the *anti-periodic* boundary condition $\psi(\mathbf{x}, \beta) = -\psi(\mathbf{x}, 0)$. To understand the origin of

this anti-periodic condition, recall that a field ψ describes particles which obey Fermi-Dirac statistics; at a quantum level, this field obeys (equal time) anti-commutation relations of the form $\{\psi, \psi^\dagger\} = 1$ which generalises the classical Poisson bracket. This defines a two-dimensional Hilbert space spanned by $|0\rangle$ and $|1\rangle$, with

$$\begin{aligned} \psi|0\rangle &= 0 \\ \psi^\dagger|0\rangle &= |1\rangle \ . \end{aligned} \tag{D.15}$$

(With this notation, the field $\psi^\dagger$ is naturally identified as the creation operator for a fermionic particle and the basis vectors represent physical states of the Fock space labelled by the number of particles they contain.)

We may then define "coherent fermionic states"

$$|\eta\rangle = e^{-\eta\psi^\dagger}|0\rangle = |0\rangle - \eta|1\rangle \ ; \tag{D.16}$$

by convention, $\langle\eta| = \langle 0|e^{-\eta^*\psi^\dagger}$. Those states are such that $\psi|\eta\rangle = \eta|\eta\rangle$ where the eigenvalue η is now a Grassmann number [79]. Grassmann variables are anticommuting numbers $\{\theta_i, \theta_j\} = 0$ leading to the obvious consequence $\theta_i^2 = 0$. Any polynomial series constructed from two of those numbers is thus truncated to the form:

$$P(\theta_i, \theta_j) = p_0 + p_1\theta_i + p_2\theta_j + p_{12}\theta_i\theta_j.$$

This results in a very unusual set of definitions:

$$\int d\theta = 0 \ , \quad \int d\theta\,\theta = 1,$$

introducing the very special property that the left integral of a Grassmann variable equals its left derivative:

$$\int d\theta = \frac{\partial}{\partial\theta}.$$

Finally, let us mention the complex conjugation rule $(\theta_i\theta_j)^* = \theta_j^*\theta_i^*$.

Therefore, the following resolution of the identity is easily proved:

$$1 = \int d\eta^* d\eta \ e^{-\eta^*\eta}|\eta\rangle\langle\eta| \ . \tag{D.17}$$

Turning to the question of the trace of an operator $\mathcal{A}$, which should by definition correspond to

$$\text{Tr}\,\mathcal{A} = \langle 0|\mathcal{A}|0\rangle + \langle 1|\mathcal{A}|1\rangle, \tag{D.18}$$

we would naively try the following η integral

$$\int d\eta^* d\eta \, e^{-\eta^*\eta} \langle \eta | \mathcal{A} | \eta \rangle = \langle 0 | \mathcal{A} | 0 \rangle - \langle 1 | \mathcal{A} | 1 \rangle \tag{D.19}$$

which manifestly differs from (D.18) by a minus sign; this can be avoided by defining the trace of an operator $\mathcal{A}$ over fermionic states as

$$\text{Tr} \, \mathcal{A} \equiv \int d\eta^* d\eta \, e^{-\eta^*\eta} \langle -\eta | \mathcal{A} | \eta \rangle . \tag{D.20}$$

Recalling the definition of the partition function (D.9), a corresponding integral expression may be given as a starting point for constructing its path integral representation, but the opposite sign in the bra $\langle -\eta |$ leads to the anti-periodic condition in imaginary time.

D.3 Correlation function

In general, the generating functional associated to the partition function (D.10) is defined through

$$Z(\beta; j) = \int \mathcal{D}q(\tau) \exp \left[-S_E(\beta) + \int_0^\beta d\tau \, j(\tau) q(\tau) \right] \tag{D.21}$$

or the alternative operator form

$$Z(\beta; j) = \text{Tr} \left[e^{-\beta H} T(e^{\int_0^\beta d\tau \, j(\tau) q(\tau)}) \right] . \tag{D.22}$$

Functional derivation of the integral expression yields the propagator in imaginary time

$$P(\tau_1, \tau_2) = \frac{1}{Z(\beta)} \frac{\delta^2 Z(\beta; j)}{\delta j(\tau_1) \delta j(\tau_2)} \bigg|_{j=0} = \frac{1}{Z(\beta)} \int \mathcal{D}q(\tau) \, q(\tau_1) q(\tau_2) \, e^{-S_E(\beta)} . \tag{D.23}$$

Recalling the general definition for the thermal average of an operator A at a temperature $1/\beta$

$$\langle A \rangle_\beta = \frac{1}{Z(\beta)} \text{Tr} \left[A e^{-\beta H} \right] ,$$

it is straightforward to show that the propagator $P(\tau_1, \tau_2)$ is also the thermal average of the correlation operator with ordered time $\langle T \, q(\tau_1) q(\tau_2) \rangle_\beta$ between time-dependent (Heisenberg) position operators $q(\tau_i) = e^{H\tau_i} q e^{-H\tau_i}$. Indeed,

the generating functional (D.21) for the harmonic oscillator is easily computed and then integrated by parts, leading to

$$Z(\beta; j) = \int \mathcal{D}q(\tau) \exp\left[-\int_0^\beta d\tau \left(q(\tau)\left(-\frac{m}{2}\frac{d^2}{d\tau^2} + \frac{m\omega^2}{2}\right)q(\tau) - j(\tau)q(\tau)\right)\right] \; ; \tag{D.24}$$

completing the square in the exponential factor, the resulting exponential is gaussian and may be integrated, leaving

$$Z(\beta; j) = Z(\beta) \, \exp\left[\frac{1}{2}\int d\tau d\tau' \; j(\tau)G(\tau,\tau')j(\tau')\right] \tag{D.25}$$

where the Green function $G(\tau,\tau')$ is the inverse of the differential operator. Differentiating this last expression with respect to $j(\tau)$ achieves to prove the identity between the Green function of the differential operator and the time-ordered correlator in imaginary time:

$$G(\tau,\tau') = \langle T\, q(\tau)q(\tau')\rangle_\beta = \frac{1}{Z(\beta)}\text{Tr}\,\left[e^{-\beta H} T\, q(\tau)q(\tau')\right] \;. \tag{D.26}$$

This relation generalises immediately to the case of complex fields.

APPENDIX

E

Relativistic BCS model

Detailed calculations

In this Appendix are detailed the calculations leading to the identification of the first and second order corrections to the effective action.

E.1 First order corrections

E.1.1 Correlation functions

The identification of the first order corrections to the effective action requires the calculation of the inverse matrix $\mathcal{S}_o^{-1}$. As shown in Appendix D, this matrix is the Green's function of the differential operator matrix $\mathcal{S}_o$ and may be identified with the time-ordered correlation function of the spinors in the Heisenberg picture $\langle T\ \psi_i(\mathbf{x}_1,\tau_1)\bar\psi_j(\mathbf{x}_2,\tau_2)\rangle$. Hence we start by expressing the Dirac spinor (5.6) and other relevant spinors in terms of the Bogoliubov operators $B(\mathbf{k},s)$ and $D(\mathbf{k},s)$ and their conjugates, defined as

$$
\begin{aligned}
B(\mathbf{k},s) &= b(\mathbf{k},s)\ \cos\theta_B(\mathbf{k}) - b^\dagger(-\mathbf{k},-s)\ s\,e^{i\phi_o}\sin\theta_B(\mathbf{k}) \\
D(\mathbf{k},s) &= d(\mathbf{k},s)\ \cos\theta_D(\mathbf{k}) + d^\dagger(-\mathbf{k},-s)\ s\,e^{-i\phi_o}\sin\theta_D(\mathbf{k})\ ,
\end{aligned}
\tag{E.1}
$$

where ϕ_o is the phase of the order parameter, $\Delta_o = |\Delta_o|e^{i\phi_o}$.

We further convert them in the Heisenberg picture

$$\psi_H(\mathbf{x}, \tau) = e^{iH_o t} \psi_S(\mathbf{x}) e^{-iH_o t} = e^{H_o \tau} \psi_S(\mathbf{x}) e^{-H_o \tau}$$

with the homogeneous hamiltonian (5.10) used as the evolution operator in imaginary time; to this end, we recall the Baker-Campbell-Hausdorff (BCH) formula

$$e^A B e^{-A} = B + [A, B] + \frac{1}{2!}[A, [A, B]] + \dots .$$

After some algebra, one obtains (for the sake of simplicity, the dependence of the mixing angles in the momentum vectors is omitted):

$$
\begin{aligned}
\psi(\mathbf{x}, \tau) = \int \frac{d^3k}{(2\pi)^3 \, 2\omega(\mathbf{k})} \sum_s \Big\{ \ & B(\mathbf{k}, s) \, e^{-E_B \tau + i\mathbf{k}\cdot\mathbf{x}} \, u(\mathbf{k}, s) \cos\theta_B \\
+ \ & B^\dagger(\mathbf{k}, s) \, e^{E_B \tau - i\mathbf{k}\cdot\mathbf{x}} \, u(-\mathbf{k}, -s) \, \sin\theta_B \, (-s e^{i\phi_o}) \\
+ \ & D^\dagger(\mathbf{k}, s) \, e^{E_D \tau - i\mathbf{k}\cdot\mathbf{x}} \, v(\mathbf{k}, s) \, \cos\theta_D \\
+ \ & D(\mathbf{k}, s) \, e^{-E_D \tau + i\mathbf{k}\cdot\mathbf{x}} \, v(-\mathbf{k}, -s) \, \sin\theta_D \, (s e^{i\phi_o}) \Big\} \ ;
\end{aligned}
$$

$$
\begin{aligned}
\overline{\psi}(\mathbf{x}, \tau) = \int \frac{d^3k}{(2\pi)^3 \, 2\omega(\mathbf{k})} \sum_s \Big\{ \ & B^\dagger(\mathbf{k}, s) \, e^{E_B \tau - i\mathbf{k}\cdot\mathbf{x}} \, \overline{u}(\mathbf{k}, s) \cos\theta_B \\
+ \ & B(\mathbf{k}, s) \, e^{-E_B \tau + i\mathbf{k}\cdot\mathbf{x}} \, \overline{u}(-\mathbf{k}, -s) \, \sin\theta_B \, (-s e^{-i\phi_o}) \\
+ \ & D(\mathbf{k}, s) \, e^{-E_D \tau + i\mathbf{k}\cdot\mathbf{x}} \, \overline{v}(\mathbf{k}, s) \, \cos\theta_D \\
+ \ & D^\dagger(\mathbf{k}, s) \, e^{E_D \tau - i\mathbf{k}\cdot\mathbf{x}} \, \overline{v}(-\mathbf{k}, -s) \, \sin\theta_D \, (s e^{-i\phi_o}) \Big\} \ ;
\end{aligned}
$$

$$
\begin{aligned}
\psi_c(\mathbf{x}, \tau) = \int \frac{d^3k}{(2\pi)^3 \, 2\omega(\mathbf{k})} \sum_s \Big\{ \ & B^\dagger(\mathbf{k}, s) \, e^{E_B \tau - i\mathbf{k}\cdot\mathbf{x}} \, (+s) \, v(\mathbf{k}, -s) \cos\theta_B \\
+ \ & B(\mathbf{k}, s) \, e^{-E_B \tau + i\mathbf{k}\cdot\mathbf{x}} \, (-s) \, v(-\mathbf{k}, s) \, \sin\theta_B \, (-s e^{-i\phi_o}) \\
+ \ & D(\mathbf{k}, s) \, e^{-E_D \tau + i\mathbf{k}\cdot\mathbf{x}} \, (-s) \, u(\mathbf{k}, -s) \, \cos\theta_D \\
+ \ & D^\dagger(\mathbf{k}, s) \, e^{E_D \tau - i\mathbf{k}\cdot\mathbf{x}} \, (+s) \, u(-\mathbf{k}, s) \, \sin\theta_D \, (s e^{-i\phi_o}) \Big\} \ ;
\end{aligned}
$$

$$
\begin{aligned}
\overline{\psi}_c(\mathbf{x}, \tau) = \int \frac{d^3k}{(2\pi)^3 \, 2\omega(\mathbf{k})} \sum_s \Big\{ \ & B(\mathbf{k}, s) \, e^{-E_B \tau + i\mathbf{k}\cdot\mathbf{x}} \, (+s) \, \overline{v}(\mathbf{k}, -s) \cos\theta_B \\
+ \ & B^\dagger(\mathbf{k}, s) \, e^{E_B \tau - i\mathbf{k}\cdot\mathbf{x}} \, (-s) \, \overline{v}(-\mathbf{k}, s) \, \sin\theta_B \, (-s e^{i\phi_o}) \\
+ \ & D^\dagger(\mathbf{k}, s) \, e^{E_D \tau - i\mathbf{k}\cdot\mathbf{x}} \, (-s) \, \overline{u}(\mathbf{k}, -s) \, \cos\theta_D \\
+ \ & D(\mathbf{k}, s) \, e^{-E_D \tau + i\mathbf{k}\cdot\mathbf{x}} \, (+s) \, \overline{u}(-\mathbf{k}, s) \, \sin\theta_D \, (s e^{i\phi_o}) \Big\} \ .
\end{aligned}
$$

$$(E.2)$$

Indeed, one easily proves the following identities under charge conjugation:

$$u_c(\mathbf{k},s) = s\, v(\mathbf{k},-s)\,, \quad v_c(\mathbf{k},s) = -s\, u(\mathbf{k},-s)\,.$$

The arbitrary phase η_c has been absorbed into the order parameter Δ_o. From these expressions it is possible to calculate the relevant correlation functions, for instance

$$\left\langle T\,\psi_r(\mathbf{x}_1,\tau_1)\,\psi_s(\mathbf{x}_2,\tau_2)\right\rangle = \frac{1}{\mathrm{Tr}\ e^{-\beta H_o}}\mathrm{Tr}\ \left[e^{-\beta H_o}\psi_r(\mathbf{x}_1,\tau_1)\psi_s(\mathbf{x}_2,\tau_2)\right]\,,\quad \tau_1 > \tau_2\,.$$

Denoting $\Delta\mathbf{x} = \mathbf{x}_1 - \mathbf{x}_2$ and $\Delta\tau = \tau_1 - \tau_2$, we have

$$
\begin{aligned}
\left\langle T\,\psi(\mathbf{x}_1,\tau_1)\,\overline{\psi}(\mathbf{x}_2,\tau_2)\right\rangle_{ij} &= \\
= \int \frac{d^3\mathbf{k}}{(2\pi)^3\,2\omega}\sum_s \Bigg\{ & e^{-E_B\Delta\tau + i\mathbf{k}\cdot\Delta\mathbf{x}}\ \frac{1}{1+e^{-\beta E_B}}\ u_i(\mathbf{k},s)\bar{u}_j(\mathbf{k},s)\ \cos^2\theta_B \\
& + e^{E_B\Delta\tau - i\mathbf{k}\cdot\Delta\mathbf{x}}\ \frac{e^{-\beta E_B}}{1+e^{-\beta E_B}}\ u_i(-\mathbf{k},-s)\bar{u}_j(-\mathbf{k},-s)\ \sin^2\theta_B \\
& + e^{E_D\Delta\tau - i\mathbf{k}\cdot\Delta\mathbf{x}}\ \frac{e^{-\beta E_D}}{1+e^{-\beta E_D}}\ v_i(\mathbf{k},s)\bar{v}_j(\mathbf{k},s)\ \cos^2\theta_D \\
& + e^{-E_D\Delta\tau + i\mathbf{k}\cdot\Delta\mathbf{x}}\ \frac{1}{1+e^{-\beta E_D}}\ v_i(-\mathbf{k},-s)\bar{v}_j(-\mathbf{k},-s)\ \sin^2\theta_D \Bigg\}
\end{aligned}
$$

$$
\begin{aligned}
\left\langle T\,\psi(\mathbf{x}_1,\tau_1)\,\overline{\psi}_c(\mathbf{x}_2,\tau_2)\right\rangle_{ij} &= \\
= \int \frac{d^3\mathbf{k}}{(2\pi)^3\,2\omega}\sum_s \Bigg\{ & e^{-E_B\Delta\tau + i\mathbf{k}\cdot\Delta\mathbf{x}}\ \frac{1}{1+e^{-\beta E_B}}\ u_i(\mathbf{k},s)\bar{v}_j(-\mathbf{k},s)e^{i\phi_o}\ \sin\theta_B\cos\theta_B \\
& - e^{E_B\Delta\tau - i\mathbf{k}\cdot\Delta\mathbf{x}}\ \frac{e^{-\beta E_B}}{1+e^{-\beta E_B}}\ u_i(-\mathbf{k},-s)\bar{v}_j(\mathbf{k},-s)e^{i\phi_o}\ \sin\theta_B\cos\theta_B \\
& + e^{E_D\Delta\tau - i\mathbf{k}\cdot\Delta\mathbf{x}}\ \frac{e^{-\beta E_D}}{1+e^{-\beta E_D}}\ v_i(\mathbf{k},s)\bar{u}_j(-\mathbf{k},s)e^{i\phi_o}\ \sin\theta_D\cos\theta_D \\
& - e^{-E_D\Delta\tau + i\mathbf{k}\cdot\Delta\mathbf{x}}\ \frac{1}{1+e^{-\beta E_D}}\ v_i(-\mathbf{k},-s)\bar{u}_j(\mathbf{k},-s)e^{i\phi_o}\ \sin\theta_D\cos\theta_D \Bigg\}
\end{aligned}
$$

$$
\begin{aligned}
\left\langle T\,\psi_c(\mathbf{x}_1,\tau_1)\,\overline{\psi}(\mathbf{x}_2,\tau_2)\right\rangle_{ij} &= \\
= \int \frac{d^3\mathbf{k}}{(2\pi)^3\,2\omega(k)}\sum_s \Bigg\{ & -e^{E_B\Delta\tau - i\mathbf{k}\cdot\Delta\mathbf{x}}\ \frac{e^{-\beta E_B}}{1+e^{-\beta E_B}}\ v_i(\mathbf{k},-s)\bar{u}_j(-\mathbf{k},-s)e^{-i\phi_o}\ \sin\theta_B\cos\theta_B \\
& + e^{-E_B\Delta\tau + i\mathbf{k}\cdot\Delta\mathbf{x}}\ \frac{1}{1+e^{-\beta E_B}}\ v_i(-\mathbf{k},s)\bar{u}_j(\mathbf{k},s)e^{-i\phi_o}\ \sin\theta_B\cos\theta_B \\
& - e^{-E_D\Delta\tau + i\mathbf{k}\cdot\Delta\mathbf{x}}\ \frac{1}{1+e^{-\beta E_D}}\ u_i(\mathbf{k},-s)\bar{v}_j(-\mathbf{k},-s)e^{-i\phi_o}\ \sin\theta_D\cos\theta_D \\
& + e^{E_D\Delta\tau - i\mathbf{k}\cdot\Delta\mathbf{x}}\ \frac{e^{-\beta E_D}}{1+e^{-\beta E_D}}\ u_i(-\mathbf{k},s)\bar{v}_j(\mathbf{k},s)e^{-i\phi_o}\ \sin\theta_D\cos\theta_D \Bigg\}
\end{aligned}
$$

$$\ldots/\ldots$$

$$\left\langle T \, \psi_c(\mathbf{x}_1, \tau_1) \, \overline{\psi}_c(\mathbf{x}_2, \tau_2) \right\rangle_{ij} =$$

$$
\begin{aligned}
= \int \frac{d^3\mathbf{k}}{(2\pi)^3 \, 2\omega} \sum_s \Big\{ & e^{E_B \Delta\tau - i\mathbf{k}\cdot\Delta\mathbf{x}} \, \frac{e^{-\beta E_B}}{1+e^{-\beta E_B}} \, v_i(\mathbf{k}, -s)\bar{v}_j(\mathbf{k}, -s)\cos^2\theta_B \\
& + e^{-E_B \Delta\tau + i\mathbf{k}\cdot\Delta\mathbf{x}} \, \frac{1}{1+e^{-\beta E_B}} \, v_i(-\mathbf{k}, s)\bar{v}_j(-\mathbf{k}, s)\sin^2\theta_B \\
& + e^{-E_D \Delta\tau + i\mathbf{k}\cdot\Delta\mathbf{x}} \, \frac{1}{1+e^{-\beta E_D}} \, u_i(\mathbf{k}, -s)\bar{u}_j(\mathbf{k}, -s)\cos^2\theta_D \\
& + e^{E_D \Delta\tau - i\mathbf{k}\cdot\Delta\mathbf{x}} \, \frac{e^{-\beta E_D}}{1+e^{-\beta E_D}} \, u_i(-\mathbf{k}, s)\bar{u}_j(-\mathbf{k}, s)\sin^2\theta_D \Big\}.
\end{aligned}
$$

$$(\text{E.3})$$

The tensor products of the free spinors $u(\pm\mathbf{k}, \pm s)$ and $v(\pm\mathbf{k}, \pm s)$ are to be considered together with the spin sums according to the following properties:

$$
\begin{aligned}
\sum_s u(\mathbf{k}, s) \otimes \bar{u}(\mathbf{k}, s) &= \slashed{k} + m \quad , \quad \sum_s u(\mathbf{k}, s) \otimes \bar{v}(-\mathbf{k}, s) = (\slashed{k} + m)\gamma_5\gamma_0 \\
\sum_s v(\mathbf{k}, s) \otimes \bar{v}(\mathbf{k}, s) &= \slashed{k} - m \quad , \quad \sum_s v(-\mathbf{k}, s) \otimes \bar{u}(\mathbf{k}, s) = \gamma_0(\slashed{k} - m)\gamma_5
\end{aligned}
$$

$$(\text{E.4})$$

Then the inverse Fourier transforms over the imaginary time are performed, in order to obtain the Matsubara propagators

$$
P(i\omega_n) = \int_0^\beta d\tau \, e^{i\omega_n \tau} P(\tau) \quad , \quad P(\tau) = \frac{1}{\beta}\sum_n e^{-i\omega_n \tau} P(i\omega_n) \quad , \quad \omega_n = \frac{2n+1}{\beta}\pi \, , \, n \in \mathbb{Z} \, .
$$

$$(\text{E.5})$$

Finally, the values of the mixing angles θ_B and θ_D are substituted using (5.9). One ends up with the correlation functions

$$
S_o^{-1}(x_1, x_2) = \begin{pmatrix} \left\langle T \, \psi(\mathbf{x}_1, \tau_1) \, \overline{\psi}(\mathbf{x}_2, \tau_2) \right\rangle & \left\langle T \, \psi(\mathbf{x}_1, \tau_1) \, \overline{\psi}_c(\mathbf{x}_2, \tau_2) \right\rangle \\ \left\langle T \, \psi_c(\mathbf{x}_1, \tau_1) \, \overline{\psi}(\mathbf{x}_2, \tau_2) \right\rangle & \left\langle T \, \psi_c(\mathbf{x}_1, \tau_1) \, \overline{\psi}_c(\mathbf{x}_2, \tau_2) \right\rangle \end{pmatrix} \quad (\text{E.6})
$$

where

$$\left\langle T \, \psi(\mathbf{x}_1, \tau_1) \, \overline{\psi}(\mathbf{x}_2, \tau_2) \right\rangle = \frac{1}{\beta} \sum_n \int \frac{d^3\mathbf{k}}{(2\pi)^3 \, 2\omega} \, e^{-i\omega_n \Delta\tau + i\mathbf{k} \cdot \Delta\mathbf{x}}$$

$$\left\{ -\frac{2\omega}{a^2 - 4\omega^2 \mu_o^2} \, \left[\gamma_o \left[a(\mu_o - i\omega_n) - 2\mu_o \omega^2 \right] + \left[a - 2\mu_o(\mu_o - i\omega_n) \right] (\mathbf{k} \cdot \boldsymbol{\gamma} - m) \right] \right\}$$

$$\left\langle T \, \psi(\mathbf{x}_1, \tau_1) \, \overline{\psi}_c(\mathbf{x}_2, \tau_2) \right\rangle = \frac{1}{\beta} \sum_n \int \frac{d^3\mathbf{k}}{(2\pi)^3 \, 2\omega} \, e^{-i\omega_n \Delta\tau + i\mathbf{k} \cdot \Delta\mathbf{x}}$$

$$\left\{ -\frac{2\omega}{a^2 - 4\omega^2 \mu_o^2} \, \Delta_o \gamma_5 \left[a + 2\mu_o \gamma_o (\mathbf{k} \cdot \boldsymbol{\gamma} - m) \right] \right\}$$

$$\left\langle T \, \psi_c(\mathbf{x}_1, \tau_1) \, \overline{\psi}(\mathbf{x}_2, \tau_2) \right\rangle = \frac{1}{\beta} \sum_n \int \frac{d^3\mathbf{k}}{(2\pi)^3 \, 2\omega} \, e^{-i\omega_n \Delta\tau + i\mathbf{k} \cdot \Delta\mathbf{x}}$$

$$\left\{ \frac{2\omega}{a^2 - 4\omega^2 \mu_o^2} \, \Delta_o^\dagger \gamma_5 \left[a - 2\mu_o \gamma_o (\mathbf{k} \cdot \boldsymbol{\gamma} - m) \right] \right\}$$

$$\left\langle T \, \psi_c(\mathbf{x}_1, \tau_1) \, \overline{\psi}_c(\mathbf{x}_2, \tau_2) \right\rangle = \frac{1}{\beta} \sum_n \int \frac{d^3\mathbf{k}}{(2\pi)^3 \, 2\omega} \, e^{-i\omega_n \Delta\tau + i\mathbf{k} \cdot \Delta\mathbf{x}}$$

$$\left\{ -\frac{2\omega}{a^2 - 4\omega^2 \mu_o^2} \, \left[-\gamma_o \left[a(\mu_o + i\omega_n) - 2\mu_o \omega^2 \right] + \left[a - 2\mu_o(\mu_o + i\omega_n) \right] (\mathbf{k} \cdot \boldsymbol{\gamma} - m) \right] \right\}$$

with $a = \omega^2 + \mu_o^2 + |\Delta_o|^2 + \omega_n^2$.

E.1.2   The Green's function of the differential operator

It is now possible to check that $\mathcal{S}_o^{-1}$ provides indeed the Green's function of the homogeneous differential operator: let us evaluate[1]

$$\mathcal{S}_o \mathcal{S}_o^{-1} \; : \qquad \int d^4 x_3 \mathcal{S}_o(x_1, x_3) \mathcal{S}_o^{-1}(x_3, x_1)$$

$$= \int d^4 x_3 \delta^{(4)}(x_1 - x_3) \overline{\mathcal{S}}_o(x_3) \mathcal{S}_o^{-1}(x_3, x_2)$$

$$= \overline{\mathcal{S}}_o(x_1) \mathcal{S}_o^{-1}(x_1, x_2) \,,$$

$$\overline{\mathcal{S}}_o(x_1) \mathcal{S}_o^{-1}(x_1, x_2) \;\; = \;\; \begin{pmatrix} \gamma^0 \partial_{\tau_1} - i\boldsymbol{\gamma} \cdot \boldsymbol{\nabla}_{\mathbf{x}_1} + m - \mu_o \gamma^0 & \Delta_o \gamma_5 \\[2mm] -\Delta_o^\dagger \gamma_5 & \gamma^0 \partial_{\tau_1} - i\boldsymbol{\gamma} \cdot \boldsymbol{\nabla}_{\mathbf{x}_1} + m + \mu_o \gamma^0 \end{pmatrix} \times$$

$$\begin{pmatrix} \left\langle T \, \psi(\mathbf{x}_1, \tau_1) \, \overline{\psi}(\mathbf{x}_2, \tau_2) \right\rangle & \left\langle T \, \psi(\mathbf{x}_1, \tau_1) \, \overline{\psi}_c(\mathbf{x}_2, \tau_2) \right\rangle \\[2mm] \left\langle T \, \psi_c(\mathbf{x}_1, \tau_1) \, \overline{\psi}(\mathbf{x}_2, \tau_2) \right\rangle & \left\langle T \, \psi_c(\mathbf{x}_1, \tau_1) \, \overline{\psi}_c(\mathbf{x}_2, \tau_2) \right\rangle \end{pmatrix} \,.$$

---

[1] The operator $\overline{\mathcal{S}}_o$ is defined through the identity $\mathcal{S}_o(x_1, x_2) = \delta^{(4)}(x_1 - x_2) \overline{\mathcal{S}}_o(x_2)$.

Considering the upper-left element:

$$(\mathcal{S}_o\mathcal{S}_o^{-1})_{11} = \frac{1}{\beta}\sum_n \int \frac{d^3k}{(2\pi)^3}\, e^{-i\omega_n\Delta\tau + i\mathbf{k}\cdot\Delta\mathbf{x}}\, \frac{1}{a^2 - 4\omega^2\mu_o^2}\, \times$$

$$\left\{ -\left[\mathbf{k}\cdot\boldsymbol{\gamma} + m - (\mu_o + i\omega_n)\gamma_o\right]\, \times \right.$$

$$\left[\gamma_o\left[a(\mu_o - i\omega_n) - 2\mu_o\omega^2\right] + \left[a - 2\mu_o(\mu_o - i\omega_n)\right]\left(\mathbf{k}\cdot\boldsymbol{\gamma} - m\right)\right]$$

$$\left. + |\Delta_o|^2\left[a - 2\mu_o\gamma_o(\mathbf{k}\cdot\boldsymbol{\gamma} - m)\right]\right\}. \qquad (E.7)$$

The properties of the γ matrices greatly simplify the term between brackets and we are left with

$$(\mathcal{S}_o\mathcal{S}_o^{-1})_{11} = \frac{1}{\beta}\sum_n \int \frac{d^3k}{(2\pi)^3}\, e^{-i\omega_n\Delta\tau + i\mathbf{k}\cdot\Delta\mathbf{x}} = \delta^{(3)}(\Delta\mathbf{x})\sum_n (-1)^n\delta(\Delta\tau + n\beta) \qquad (E.8)$$

where we have used the Poisson resummation formula in the antiperiodic case

$$\frac{1}{L}\sum_n e^{-i\pi\frac{2n+1}{L}x}\, \tilde{f}(\pi\frac{2n+1}{L}) = \sum_n (-1)^n f(x + nL)$$

for the special case $\tilde{f}(k) = 1$, $f(x) = \delta(x)$ and $L = \beta$. The sum $\sum_n(-1)^n\delta(\Delta\tau + n\beta)$ hence represents the antiperiodic delta function over a variable τ running on a circle with circumference β. The term $(\mathcal{S}_o\mathcal{S}_o^{-1})_{22}$ provides the same result, and the off-diagonal terms are shown to cancel exactly.

E.1.3   Trace evaluation and the Matsubara sums

Once the correlation functions are known, we have to evaluate the trace

$$\text{Tr}\, \mathcal{S}_o^{-1}\Delta\mathcal{S} = \int_0^\beta d\tau \int d^3x \frac{1}{\beta}\sum_n \int \frac{d^3k}{(2\pi)^3} e^{-i\omega_n\tau + i\mathbf{k}\cdot\mathbf{x}}\, \text{tr}\, \mathcal{S}_o^{-1}(i\omega_n,\mathbf{k})\Delta\mathcal{S}(x). \qquad (E.9)$$

The matrix $\Delta\mathcal{S}(x)$ does not contain any explicit time dependency and the τ integration is immediately performed to cancel the $1/\beta$ factor. Since we are interested in the trace of this product, only the diagonal terms are evaluated; the γ matrices with a non-vanishing trace provide an additional factor of 4 and

we are left with

$$
\text{Tr} \begin{pmatrix} \left\langle T\, \psi\, \overline{\psi} \right\rangle_\beta & \left\langle T\, \psi\, \overline{\psi}_c \right\rangle_\beta \\ \left\langle T\, \psi_c\, \overline{\psi} \right\rangle_\beta & \left\langle T\, \psi_c\, \overline{\psi}_c \right\rangle_\beta \end{pmatrix} \begin{pmatrix} -\overline{\mu}(\mathbf{x})\gamma^0 - e\mathbf{A}(\mathbf{x})\cdot\boldsymbol{\gamma} & \overline{\Delta}(\mathbf{x})\gamma_5 \\ -\overline{\Delta}^\dagger(\mathbf{x})\gamma_5 & \overline{\mu}(\mathbf{x})\gamma^0 + e\mathbf{A}(\mathbf{x})\cdot\boldsymbol{\gamma} \end{pmatrix}
$$

$$
= \int d^3x \sum_n \int \frac{d^3k}{(2\pi)^3} \frac{4}{a^2 - 4\omega^2\mu_o^2} \times
$$

$$
\left\{ 2\mu_o\overline{\mu}(\mathbf{x})\left(a - 2\omega^2\right) - 4\mu_o e\, i\omega_n\, \mathbf{k}\cdot\mathbf{A}(\mathbf{x}) + a\left(\Delta_o\overline{\Delta}^\dagger(\mathbf{x}) + \Delta_o^\dagger\overline{\Delta}(\mathbf{x})\right) \right\} \quad \text{(E.10)}
$$

with $a = \omega^2 + \mu_o^2 + |\Delta_o|^2 + \omega_n^2$. By reason of isotropy, the term in $\mathbf{k}\cdot\mathbf{A}(\mathbf{x})$ does not survive the d^3k integration. For the other terms, we need to perform the Matsubara summations. Referring back to (5.36), one has to evaluate expressions involving one of the following sums:

$$
\sum_n \frac{a}{a^2 - 4\mu_o^2\omega^2} = \frac{1}{2}\sum_n\left[\frac{1}{E_B^2 + \omega_n^2} + \frac{1}{E_D^2 + \omega_n^2}\right]
$$

$$
\sum_n \frac{1}{a^2 - 4\mu_o^2\omega^2} = \frac{1}{4\mu_o\omega}\sum_n\left[\frac{1}{E_B^2 + \omega_n^2} - \frac{1}{E_D^2 + \omega_n^2}\right]
$$

for which we evaluate in a general case

$$
\sum_n \frac{1}{E^2 + \omega_n^2} = -\frac{\beta}{2}\oint\frac{dk^0}{2\pi i}\frac{1}{(E^2 - k^{0\,2})}\tanh(\frac{1}{2}\beta k^0)
$$

$$
= -\frac{\beta}{2}\,\text{Res}\left[\frac{1}{(E - k^0)(E + k^0)}\tanh(\frac{1}{2}\beta k^0)\right]_{\pm E}
$$

$$
= \frac{\beta}{2E}\tanh(\frac{1}{2}\beta E). \quad \text{(E.11)}
$$

Hence we have

$$
\sum_n \frac{a}{a^2 - 4\omega^2\mu_o^2} = \frac{\beta}{4}\left[\frac{1}{E_B}\tanh(\frac{1}{2}\beta E_B) + \frac{1}{E_D}\tanh(\frac{1}{2}\beta E_D)\right] \quad \text{(E.12)}
$$

$$
\sum_n \frac{a - 2\omega^2}{a^2 - 4\omega^2\mu_o^2} = -\frac{\beta}{4\mu_o}\frac{(\omega - \mu_o)}{E_B}\tanh(\frac{1}{2}\beta E_B) + \frac{\beta}{4\mu_o}\frac{(\mu_o + \omega)}{E_D}\tanh(\frac{1}{2}\beta E_D)\,. \quad \text{(E.13)}
$$

Substituting in the previous expressions and then in the trace of the matrix product, we obtain finally the first-order term of the effective action

$$
S_{\text{eff}} = -\frac{1}{2\beta} \int d^3x \int \frac{d^3k}{(2\pi)^3} \times \tag{E.14}
$$

$$
\left\{ -2\beta\overline{\mu}(\mathbf{x}) \left[\frac{(\omega - \mu_o)}{E_B} \tanh(\frac{1}{2}\beta E_B) - \frac{(\mu_o + \omega)}{E_D} \tanh(\frac{1}{2}\beta E_D) \right] \right.
$$

$$
\left. + \beta \left(\Delta_o \overline{\Delta}^\dagger(\mathbf{x}) + \Delta_o^\dagger \overline{\Delta}(\mathbf{x}) \right) \left[\frac{1}{E_B} \tanh(\frac{1}{2}\beta E_B) + \frac{1}{E_D} \tanh(\frac{1}{2}\beta E_D) \right] \right\} .
$$

E.2   Second order corrections

E.2.1   Identification of the relevant terms

We consider the generalised Ginzburg-Landau free energy functional

$$
\mathcal{F} = \int d^3\mathbf{x} \left\{ f(\Delta,\mu) |(\boldsymbol{\nabla} - iq\mathbf{A})\Delta|^2 + V_{\text{eff}}(\Delta,\mu) + g(\Delta,\mu)|\boldsymbol{\nabla}\mu_{\text{ec}}|^2 + h(\Delta,\mu)|\mathbf{B}|^2 \right\} . \tag{E.15}
$$

For reasons that will become clear somewhat later, there is no need to express the magnetic contribution in terms of the vector potential. We expand the order parameter around its homogeneous value $\Delta = \Delta_o + \overline{\Delta}$ and the electrochemical potential around the chemical potential $\mu = \mu_o + \overline{\mu}$; we may then identify the specific form of $f(\Delta,\mu)$ and some contributions to $g(\Delta,\mu)$ and $h(\Delta,\mu)$ by considering the perturbations to the lowest order in the Fourier transformations of the fields $\mathbf{A}(\mathbf{x})$, $\mu_{\text{ec}}(\mathbf{x})$ and $\Delta(\mathbf{x})$ according to the general parametrisation

$$
F(\mathbf{x}) = \int \frac{d^3\mathbf{k}}{(2\pi)^3} e^{-i\mathbf{k}\cdot\mathbf{x}} \tilde{F}(\mathbf{k}) . \tag{E.16}
$$

The specific terms of the free energy become[2]:

$$
\int d^3\mathbf{x} \, f(\Delta,\mu) \boldsymbol{\nabla}\Delta^\dagger \cdot \boldsymbol{\nabla}\Delta
$$

$$
= \int d^3\mathbf{x} \, f(\Delta_o,\mu_o) \int \frac{d^3\mathbf{k}_1}{(2\pi)^3} \int \frac{d^3\mathbf{k}_2}{(2\pi)^3} e^{i(\mathbf{k}_1 - \mathbf{k}_2)\cdot\mathbf{x}} (i\mathbf{k}_1)\cdot(-i\mathbf{k}_2) \, \overline{\Delta}^\dagger(\mathbf{k}_1)\overline{\Delta}(\mathbf{k}_2)
$$

$$
= \int \frac{d^3\mathbf{k}_1}{(2\pi)^3} \int \frac{d^3\mathbf{k}_2}{(2\pi)^3} f(\Delta_o,\mu_o) (2\pi)^3\delta^{(3)}(\mathbf{k}_1 - \mathbf{k}_2)(\mathbf{k}_1\cdot\mathbf{k}_2)\overline{\Delta}^\dagger(\mathbf{k}_1)\overline{\Delta}(\mathbf{k}_2)
$$

$$
= \int \frac{d^3\mathbf{k}}{(2\pi)^3} f(\Delta_o,\mu_o) |\mathbf{k}|^2 \overline{\Delta}^\dagger(\mathbf{k})\overline{\Delta}(\mathbf{k}) . \tag{E.17}
$$

---

[2]The variable on which the fields depend are sufficient to identify the configuration or Fourier space and the tilde notations is therefore omitted.

Likewise,

$$\int d^3\mathbf{x}\, g(\Delta,\mu)|\nabla\mu|^2 = \int \frac{d^3\mathbf{k}}{(2\pi)^3}\, g(\Delta_o,\mu_o)\,|\mathbf{k}|^2\mu(-\mathbf{k})\mu(\mathbf{k}) \tag{E.18}$$

since the electrochemical potential is supposed to be real. Finally, the corrections to the magnetic term simply come through

$$\int d^3\mathbf{x}\ h(\Delta_o,\mu_o)|\mathbf{B}|^2\ . \tag{E.19}$$

These expression may be compared to specific terms of the second order corrections to the effective action.

E.2.2   Evaluation of the matrix product

The second order corrections to the effective action are

$$
\begin{aligned}
S_{\text{eff}}^{(2)} &= \frac{1}{4\beta}\, \text{Tr}\, [S_o^{-1}\Delta S S_o^{-1}\Delta S] \tag{E.20}\\
&= \frac{1}{4\beta}\int d^4x_1 d^4x_2 d^4x_3 d^4x_4\, \text{tr}\, S_o^{-1}(x_1,x_2)\Delta S(x_2,x_3)S_o^{-1}(x_3,x_4)\Delta S(x_4,x_1)\\
&= \frac{1}{4\beta}\int d^4x_1 d^4x_2\, \text{tr}\, \Delta S(\mathbf{x}_1)S_o^{-1}(x_1,x_2)\Delta S(\mathbf{x}_2)S_o^{-1}(x_2,x_1)\\
&= \frac{1}{4\beta}\int_0^\beta d\tau_1 d\tau_2 \int d^3\mathbf{x}_1 d^3\mathbf{x}_2\, \frac{1}{\beta^2}\sum_{n1,n2}\int \frac{d^3\mathbf{k}_1}{(2\pi)^3}\frac{d^3\mathbf{k}_2}{(2\pi)^3}\ \times\\
&\qquad\qquad e^{-i\omega_{n1}(\tau_1-\tau_2)+i\mathbf{k}_1\cdot(\mathbf{x}_1-\mathbf{x}_2)}\, e^{-i\omega_{n2}(\tau_2-\tau_1)+i\mathbf{k}_2\cdot(\mathbf{x}_2-\mathbf{x}_1)}\ \times\\
&\qquad\qquad \text{tr}\, \Delta S(\mathbf{x}_1)S_o^{-1}(i\omega_{n1},\mathbf{k}_1)\Delta S(\mathbf{x}_2)S_o^{-1}(i\omega_{n2},\mathbf{k}_2)\\
&= \frac{1}{4\beta}\int d^3\mathbf{x}_1 d^3\mathbf{x}_2 \int \frac{d^3\mathbf{k}_1}{(2\pi)^3}\frac{d^3\mathbf{k}_2}{(2\pi)^3}\sum_n\ \times\\
&\qquad\qquad e^{-i(\mathbf{k}_1-\mathbf{k}_2)\cdot(\mathbf{x}_2-\mathbf{x}_1)}\, \text{tr}\ \Delta S(\mathbf{x}_1)S_o^{-1}(i\omega_n,\mathbf{k}_1)\Delta S(\mathbf{x}_2)S_o^{-1}(i\omega_n,\mathbf{k}_2)
\end{aligned}
$$

where the cyclicity of the trace operation has been used to modify the order of the matrix product. As previously, the small trace is used to denote the usual sum over diagonal matrix elements.

The operator matrices are

$$S_o^{-1}(i\omega_n, \mathbf{k}) = \frac{1}{a^2 - 4\mu_o^2\omega^2} \times \tag{E.21}$$

$$\begin{pmatrix} [2\mu_o\omega^2 - a(\mu_o - i\omega_n)]\gamma^o & \Delta_o\gamma^5[2\mu_o(\mathbf{k}.\boldsymbol{\gamma}+m)\gamma^o - a] \\ +[2\mu_o(\mu_o - i\omega_n) - a](\mathbf{k}.\boldsymbol{\gamma}-m) & \\ & \\ \Delta_o^\dagger\gamma^5[2\mu_o(\mathbf{k}.\boldsymbol{\gamma}+m)\gamma^o + a] & [a(\mu_o + i\omega_n) - 2\mu_o\omega^2]\gamma^o \\ & +[2\mu_o(\mu_o + i\omega_n) - a](\mathbf{k}.\boldsymbol{\gamma}-m) \end{pmatrix}$$

with $a = \omega^2 + \mu_o^2 + \Delta_o^2 + \omega_n^2$, and

$$\Delta S(\mathbf{k}) = \begin{pmatrix} -\overline{\mu}(\mathbf{k})\gamma^o - e\mathbf{A}(\mathbf{k}).\boldsymbol{\gamma} & \overline{\Delta}(\mathbf{k})\gamma^5 \\ -\overline{\Delta}^\dagger(\mathbf{k})\gamma^5 & \overline{\mu}(\mathbf{k})\gamma^o + e\mathbf{A}(\mathbf{k}).\boldsymbol{\gamma} \end{pmatrix}. \tag{E.22}$$

We may calculate explicitly the whole collection of terms, taking into account the trace properties of the γ matrices and ignoring the terms odd in $i\omega_n$ in the numerator, since they do not contribute to the summation over the Matsubara frequencies.

In order to simplify the notations, we denote Δ_i for $\Delta(\mathbf{x}_i)$ and identically for μ_i and $\mathbf{A}_i$. We also have $a_1 = \omega_1^2 + \mu_o^2 + \Delta_o^2 + \omega_n^2$, $a_2 = \omega_2^2 + \mu_o^2 + \Delta_o^2 + \omega_n^2$, and $N_1 = a_1^2 - 4\mu_o^2\omega_1^2$, $N_2 = a_2^2 - 4\mu_o^2\omega_2^2$. The total second order correction to the effective action is then:

$$
S_{\text{eff}}^{(2)} = \frac{1}{4\beta} \int d^3\mathbf{x}_1 d^3\mathbf{x}_2 \int \frac{d^3\mathbf{k}_1}{(2\pi)^3} \frac{d^3\mathbf{k}_2}{(2\pi)^3} \sum_n e^{-i(\mathbf{k}_1-\mathbf{k}_2)\cdot(\mathbf{x}_2-\mathbf{x}_1)} \frac{4}{N_1 N_2} \times
$$

$$
\left\{ \quad [\overline{\Delta}_1^\dagger \overline{\Delta}_2 + \overline{\Delta}_1 \overline{\Delta}_2^\dagger] \right.
$$

$$
\left\{ \left[-\mu_o^2(a_1 - 2\omega_1^2)(a_2 - 2\omega_2^2) - a_1 a_2(\omega_n^2 + |\Delta_o|^2) \right] \right.
$$

$$
\left. + (\mathbf{k}_1 \cdot \mathbf{k}_2 + m^2) \left[-(a_1 - 2\mu_o^2)(a_2 - 2\mu_o^2) - 4\mu_o^2(\omega_n^2 + |\Delta_o|^2) \right] \right\}
$$

$$
+ [\Delta_o^\dagger \overline{\Delta}_1 + \Delta_o \overline{\Delta}_1^\dagger][\Delta_o^\dagger \overline{\Delta}_2 + \Delta_o \overline{\Delta}_2^\dagger] \left[a_1 a_2 + 4\mu_o^2(\mathbf{k}_1 \cdot \mathbf{k}_2 + m^2) \right]
$$

$$
+ 2\overline{\mu}_1 \overline{\mu}_2 \left\{ \left[\mu_o^2(a_1 - 2\omega_1^2)(a_2 - 2\omega_2^2) - a_1 a_2(\omega_n^2 + |\Delta_o|^2) \right] \right.
$$

$$
\left. + (\mathbf{k}_1 \cdot \mathbf{k}_2 + m^2) \left[(a_1 - 2\mu_o^2)(a_2 - 2\mu_o^2) - 4\mu_o^2(\omega_n^2 + |\Delta_o|^2) \right] \right\}
$$

$$
+ 2e^2 \mathbf{A}_1 \cdot \mathbf{A}_2 \left\{ \left[\mu_o^2(a_1 - 2\omega_1^2)(a_2 - 2\omega_2^2) - a_1 a_2(\omega_n^2 - |\Delta_o|^2) \right] \right.
$$

$$
\left. + (\mathbf{k}_1 \cdot \mathbf{k}_2 + m^2) \left[-(a_1 - 2\mu_o^2)(a_2 - 2\mu_o^2) + 4\mu_o^2(\omega_n^2 - |\Delta_o|^2) \right] \right\}
$$

$$
+ 2e^2 \left(\mathbf{A}_1 \cdot \mathbf{k}_1 \mathbf{A}_2 \cdot \mathbf{k}_2 + \mathbf{A}_1 \cdot \mathbf{k}_2 \mathbf{A}_2 \cdot \mathbf{k}_1 \right)
$$

$$
\left[(a_1 - 2\mu_o^2)(a_2 - 2\mu_o^2) - 4\mu_o^2(\omega_n^2 - |\Delta_o|^2) \right]
$$

$$
+ 2\mu_o [\mu_1 (\Delta_o^\dagger \Delta_2 + \Delta_o \Delta_2^\dagger) + \mu_2 (\Delta_o^\dagger \Delta_1 + \Delta_o \Delta_1^\dagger)]
$$

$$
\left\{ \left[(a_1 - \omega_1^2)(a_2 - \omega_2^2) - \omega_1^2 \omega_2^2 \right] + (\mathbf{k}_1 \cdot \mathbf{k}_2 + m^2) \left[4\mu_o^2 - a_1 - a_2 \right] \right\}
$$

$$
+ \left[e\mathbf{A}_1 (\Delta_o^\dagger \Delta_2 - \Delta_o \Delta_2^\dagger) - e\mathbf{A}_2 (\Delta_o^\dagger \Delta_1 - \Delta_o \Delta_1^\dagger) \right] \cdot
$$

$$
\left. \cdot \left[\mathbf{k}_2 (4\mu_o^2 \omega_1^2 - a_1 a_2) - \mathbf{k}_1 (4\mu_o^2 \omega_2^2 - a_1 a_2) \right] \quad \right\} . \tag{E.23}
$$

Let us concentrate only on the first contribution. Introducing the coefficient $\mathcal{F}_{\Delta\Delta}$ which involves all the terms between the brackets as well as the summation over the Matsubara frequencies, we perform the Fourier transformation over the fields $\Delta(\mathbf{x}_1)$ and $\Delta(\mathbf{x}_2)$:

$$
\begin{aligned}
S_{\text{eff}}^{(2)}[\Delta\Delta] \;=\;& \frac{1}{4\beta} \int d^3\mathbf{x}_1 d^3\mathbf{x}_2 \int \frac{d^3\mathbf{k}_1}{(2\pi)^3} \frac{d^3\mathbf{k}_2}{(2\pi)^3} \times \\
& e^{-i(\mathbf{k}_1-\mathbf{k}_2)\cdot(\mathbf{x}_2-\mathbf{x}_1)} \; \mathcal{F}_{\Delta\Delta}(i\omega_n,\mathbf{k}_1,\mathbf{k}_2) \left[\overline{\Delta}^\dagger(\mathbf{x}_1)\overline{\Delta}(\mathbf{x}_2) + \overline{\Delta}(\mathbf{x}_1)\overline{\Delta}^\dagger(\mathbf{x}_2) \right] \\[2mm]
=\;& \frac{1}{4\beta} \int d^3\mathbf{x}_1 d^3\mathbf{x}_2 \int \frac{d^3\mathbf{k}_1}{(2\pi)^3} \frac{d^3\mathbf{k}_2}{(2\pi)^3} \frac{d^3\mathbf{l}_1}{(2\pi)^3} \frac{d^3\mathbf{l}_2}{(2\pi)^3} \; e^{i\mathbf{l}_1\cdot\mathbf{x}_1 - i\mathbf{l}_2\cdot\mathbf{x}_2} \times \\
& e^{-i(\mathbf{k}_1-\mathbf{k}_2)\cdot(\mathbf{x}_2-\mathbf{x}_1)} \; \mathcal{F}_{\Delta\Delta}(i\omega_n,\mathbf{k}_1,\mathbf{k}_2) \left[\overline{\Delta}^\dagger(\mathbf{l}_1)\overline{\Delta}(\mathbf{l}_2) + \overline{\Delta}(-\mathbf{l}_1)\overline{\Delta}^\dagger(-\mathbf{l}_2) \right] \\[2mm]
=\;& \frac{1}{4\beta} \int \frac{d^3\mathbf{k}_1}{(2\pi)^3} \frac{d^3\mathbf{k}_2}{(2\pi)^3} \; \mathcal{F}_{\Delta\Delta}(i\omega_n,\mathbf{k}_1,\mathbf{k}_2) \times \\
& \left[\overline{\Delta}^\dagger(\mathbf{k}_2-\mathbf{k}_1)\overline{\Delta}(\mathbf{k}_2-\mathbf{k}_1) + \overline{\Delta}(\mathbf{k}_1-\mathbf{k}_2)\overline{\Delta}^\dagger(\mathbf{k}_1-\mathbf{k}_2) \right] \\[2mm]
=\;& \frac{1}{4\beta} \int \frac{d^3\mathbf{k}_1}{(2\pi)^3} \frac{d^3\mathbf{k}_2}{(2\pi)^3} \; 2\overline{\Delta}^\dagger(\mathbf{k}_2-\mathbf{k}_1)\overline{\Delta}(\mathbf{k}_2-\mathbf{k}_1) \; \mathcal{F}_{\Delta\Delta}(i\omega_n,\mathbf{k}_1,\mathbf{k}_2) , \qquad \text{(E.24)}
\end{aligned}
$$

the last step resulting from the fact that the coefficient $\mathcal{F}_{\Delta\Delta}$ is not affected by the exchange $\mathbf{k}_1 \rightleftarrows \mathbf{k}_2$. Then we assume that second order corrections are located close to each other in momentum space and we expand $\mathbf{k}_1$ and $\mathbf{k}_2$ around their average position:

$$
\begin{cases} \mathbf{K} = \frac{1}{2}(\mathbf{k}_1 + \mathbf{k}_2) \\ \mathbf{k} = \mathbf{k}_2 - \mathbf{k}_1 \end{cases} \quad \text{or equivalently} \quad \begin{cases} \mathbf{k}_1 = \mathbf{K} - \frac{\mathbf{k}}{2} \\ \mathbf{k}_2 = \mathbf{K} + \frac{\mathbf{k}}{2} \end{cases} . \qquad \text{(E.25)}
$$

The term of the effective action involving the squared Δ becomes

$$
S_{\text{eff}}^{(2)}[\Delta\Delta] = \frac{1}{4\beta} \int \frac{d^3\mathbf{K}}{(2\pi)^3} \frac{d^3\mathbf{k}}{(2\pi)^3} \; 2\overline{\Delta}^\dagger(-\mathbf{k})\overline{\Delta}(\mathbf{k}) \; \mathcal{F}_{\Delta\Delta}(i\omega_n,\mathbf{K},\mathbf{k}) . \qquad \text{(E.26)}
$$

Comparing with (E.17), we conclude that the parameter $f(\Delta_o,\mu_o)$ corresponds to the series expansion of $\mathcal{F}_{\Delta\Delta}$ to second order in $\mathbf{k}$ around $\mathbf{K}$, which we denote

$$
f(\Delta_o,\mu_o) = \frac{2}{4\beta} \int \frac{d^3\mathbf{K}}{(2\pi)^3} \; \partial_{k^2} \mathcal{F}_{\Delta\Delta}|_{k=0} . \qquad \text{(E.27)}
$$

Likewise, we may collect all terms of the matrix product involving squared corrections in the electrochemical potential and further perform the Fourier transform; we obtain

$$
S_{\text{eff}}^{(2)}[\mu\mu] = \frac{1}{4\beta} \int \frac{d^3\mathbf{k}}{(2\pi)^3} \frac{d^3\mathbf{K}}{(2\pi)^3} \; \overline{\mu}(-\mathbf{k}) \, \overline{\mu}(\mathbf{k}) \; \mathcal{F}_{\mu\mu}(i\omega_n,\mathbf{k},\mathbf{K}) . \qquad \text{(E.28)}
$$

Comparing with (E.18), we identify the parameter of the correction to the electric term of the free energy as the second order term of the series expansion of $\mathcal{F}_{\mu\mu}$ in $\mathbf{k}$ around $\mathbf{K}$:

$$g(\Delta_o,\mu_o) = \frac{1}{4\beta} \int \frac{d^3\mathbf{K}}{(2\pi)^3} \, \partial_{k^2} \mathcal{F}_{\mu\mu}\big|_{k=0} \,. \tag{E.29}$$

Finally, terms with squared vector potential are collected in two distinct expressions:

$$S_{\text{eff}}^{(2)}[AA] = \frac{1}{4\beta} \int \frac{d^3\mathbf{k}}{(2\pi)^3} \frac{d^3\mathbf{K}}{(2\pi)^3} \, \mathcal{F}_{AA}(i\omega_n,\mathbf{k},\mathbf{K}) \, \mathbf{A}(-\mathbf{k})\mathbf{A}(\mathbf{k}) \tag{E.30}$$

$$S_{\text{eff}}^{(2)}[kA] = \frac{1}{4\beta} \int \frac{d^3\mathbf{k}}{(2\pi)^3} \frac{d^3\mathbf{K}}{(2\pi)^3} \, \mathcal{F}_{kA}(i\omega_n,\mathbf{k},\mathbf{K}) \, \times$$
$$2\left[\mathbf{A}(-\mathbf{k})\cdot\mathbf{K}\mathbf{A}(\mathbf{k})\cdot\mathbf{K} + \frac{1}{4}\mathbf{A}(-\mathbf{k})\cdot\mathbf{k}\mathbf{A}(\mathbf{k})\cdot\mathbf{k} \right] \tag{E.31}$$

Recalling the expression of the vector potential after Wilson integration

$$\mathbf{A}(\mathbf{x}) = -\frac{1}{2}\int_0^1 du \, [(\mathbf{x}-\mathbf{y})\times\mathbf{B}\,(\mathbf{y}+u(\mathbf{x}-\mathbf{y}))]$$

and assuming we may effectively perform this integration, we deduce that only the zeroth order term of the series expansion in $\mathbf{k}$ around $\mathbf{K}$ is required to identify the correction to the magnetic sector of the free energy, namely

$$h(\Delta,\mu) = \frac{1}{4\beta} \int \frac{d^3\mathbf{K}}{(2\pi)^3} \left[\mathcal{F}_{AA}\big|_{k=0} + \frac{2K^2}{3} \, \mathcal{F}_{kA}\big|_{k=0} \right] \,. \tag{E.32}$$

E.2.3 Matsubara sums

Before giving the series expansion of the coefficients multiplying the terms with squared gradients of the fields, we perform the summations over the Matsubara frequencies, using the same method as in the case of the first order corrections. Let us define

$$T_1(E_1,E_2) = \frac{1}{E_2^2-E_1^2}\left[\frac{\beta}{2E_1}\tanh\frac{\beta E_1}{2} - \frac{\beta}{2E_2}\tanh\frac{\beta E_2}{2} \right] \tag{E.33}$$

$$T_2(E_1,E_2) = \frac{1}{E_2^2-E_1^2}\left[\frac{\beta E_1}{2}\tanh\frac{\beta E_1}{2} - \frac{\beta E_2}{2}\tanh\frac{\beta E_2}{2} \right]$$

where $E_i \equiv E(\mathbf{k}_i)$ represents either electron or positron energies. With these notations, all Matsubara sums follow from one of the expressions hereafter:

$$\sum_n \frac{1}{N_1 N_2} = \frac{1}{16\mu_o^2 \omega_1 \omega_2} \left\{ T_1(E_{B1}, E_{B2}) - T_1(E_{D1}, E_{B2}) - T_1(E_{B1}, E_{D2}) + T_1(E_{D1}, E_{D2}) \right\}$$

$$\sum_n \frac{a_1}{N_1 N_2} = \frac{1}{8\mu_o \omega_2} \left\{ T_1(E_{B1}, E_{B2}) + T_1(E_{D1}, E_{B2}) - T_1(E_{B1}, E_{D2}) - T_1(E_{D1}, E_{D2}) \right\}$$

$$\sum_n \frac{a_2}{N_1 N_2} = \frac{1}{8\mu_o \omega_1} \left\{ T_1(E_{B1}, E_{B2}) - T_1(E_{D1}, E_{B2}) + T_1(E_{B1}, E_{D2}) - T_1(E_{D1}, E_{D2}) \right\}$$

$$\sum_n \frac{a_1 a_2}{N_1 N_2} = \frac{1}{4} \left\{ T_1(E_{B1}, E_{B2}) + T_1(E_{D1}, E_{B2}) + T_1(E_{B1}, E_{D2}) + T_1(E_{D1}, E_{D2}) \right\}$$

$$\sum_n \frac{\omega_n^2}{N_1 N_2} = \frac{-1}{16\mu_o^2 \omega_1 \omega_2} \left\{ T_2(E_{B1}, E_{B2}) - T_2(E_{D1}, E_{B2}) - T_2(E_{B1}, E_{D2}) + T_2(E_{D1}, E_{D2}) \right\}$$

$$\sum_n \frac{\omega_n^2 a_1 a_2}{N_1 N_2} = \frac{-1}{4} \left\{ T_2(E_{B1}, E_{B2}) + T_2(E_{D1}, E_{B2}) + T_2(E_{B1}, E_{D2}) + T_2(E_{D1}, E_{D2}) \right\} .$$
$$(E.34)$$

The coefficient affecting the second order term in Δ then become

$$\mathcal{F}_{\Delta\Delta}(i\omega_n, \mathbf{k}_1 \mathbf{k}_2)$$

$$= \sum_n \frac{4}{N_1 N_2} \left\{ \left[-\mu_o^2 (a_1 - 2\omega_1^2)(a_2 - 2\omega_2^2) - a_1 a_2 (\omega_n^2 + |\Delta_o|^2) \right] \right.$$

$$\left. + (\mathbf{k}_1 \cdot \mathbf{k}_2 + m^2) \left[-(a_1 - 2\mu_o^2)(a_2 - 2\mu_o^2) - 4\mu_o^2 (\omega_n^2 + |\Delta_o|^2) \right] \right\}$$

$$= \left\{ T_1(E_{B1}, E_{B2}) \left[-(\omega_1 - \mu_o)(\omega_2 - \mu_o) - |\Delta_o|^2 \right] \right.$$

$$+ T_1(E_{D1}, E_{B2}) \left[(\omega_1 + \mu_o)(\omega_2 - \mu_o) - |\Delta_o|^2 \right]$$

$$+ T_1(E_{B1}, E_{D2}) \left[(\omega_1 - \mu_o)(\omega_2 + \mu_o) - |\Delta_o|^2 \right]$$

$$+ T_1(E_{D1}, E_{D2}) \left[-(\omega_1 + \mu_o)(\omega_2 + \mu_o) - |\Delta_o|^2 \right]$$

$$\left. + \left[T_2(E_{B1}, E_{B2}) + T_2(E_{D1}, E_{B2}) + T_2(E_{B1}, E_{D2}) + T_2(E_{D1}, E_{D2}) \right] \right\}$$

$$- \frac{\mathbf{k}_1 \cdot \mathbf{k}_2 + m^2}{\omega_1 \omega_2} \left\{ T_1(E_{B1}, E_{B2}) \left[(\omega_1 - \mu_o)(\omega_2 - \mu_o) + |\Delta_o|^2 \right] \right.$$

$$+ T_1(E_{D1}, E_{B2}) \left[(\omega_1 + \mu_o)(\omega_2 - \mu_o) - |\Delta_o|^2 \right]$$

$$+ T_1(E_{B1}, E_{D2}) \left[(\omega_1 - \mu_o)(\omega_2 + \mu_o) - |\Delta_o|^2 \right]$$

$$+ T_1(E_{D1}, E_{D2}) \left[(\omega_1 + \mu_o)(\omega_2 + \mu_o) + |\Delta_o|^2 \right]$$

$$\left. - \left[T_2(E_{B1}, E_{B2}) - T_2(E_{D1}, E_{B2}) - T_2(E_{B1}, E_{D2}) + T_2(E_{D1}, E_{D2}) \right] \right\} .$$
$$(E.35)$$

At this point, the whole expression may advantageously be simplified by collecting all terms involving hyperbolic tangents of the same type. Anticipating

the series expansion in $\mathbf{k}$ around $\mathbf{K}$, we introduce the following notation:

$$\mathbf{k}_i^2 = \mathbf{K}^2 + \varepsilon_\lambda \,, \qquad \varepsilon_\lambda = \lambda\, \mathbf{k}\cdot\mathbf{K} + \frac{\mathbf{k}^2}{4} \,, \qquad \begin{cases} \lambda = -1 \Leftrightarrow i = 1 \\ \lambda = +1 \Leftrightarrow i = 2 \end{cases} \qquad \text{(E.36)}$$

and

$$E_i^\alpha = \sqrt{(\omega_i + \alpha\mu_o)^2 + |\Delta_o|^2} \,, \qquad \begin{cases} \alpha = -1 \Leftrightarrow E_i^\alpha = E_B(\mathbf{k}_i) \\ \alpha = +1 \Leftrightarrow E_i^\alpha = E_B(\mathbf{k}_i) \end{cases} \qquad \text{(E.37)}$$

Hence $\lambda = \pm 1$ is associated with the location of the corrections in momentum space, and $\alpha = \pm 1$ distinguishes between electron and positron sectors respectively. With these notations, it turns out that the order parameter contribution takes a very concise form:

$$\mathcal{F}_{\Delta\Delta} = \beta \sum_{\alpha=\pm 1}\sum_{\lambda=\pm 1} \frac{\omega_\lambda + \alpha\mu_o}{\omega_\lambda} \frac{1}{E_\lambda^\alpha} \tanh\frac{\beta E_\lambda^\alpha}{2} \left[\frac{\mathbf{k}_\lambda\cdot(\mathbf{k}_{-\lambda} - \mathbf{k}_\lambda) - 2\alpha\mu_o\omega_\lambda}{(\omega_\lambda + 2\alpha\mu_o)^2 - \omega_{-\lambda}^2} \right] \,. \qquad \text{(E.38)}$$

The factor affecting the squared electrochemical potential is treated in exactly the same way:

$$\begin{aligned} \mathcal{F}_{\mu\mu} &= 2\sum_n \frac{4}{N_1 N_2} \Big\{ \big[\mu_o^2(a_1 - 2\omega_1^2)(a_2 - 2\omega_2^2) - a_1 a_2(\omega_n^2 + |\Delta_o|^2)\big] \\ &\qquad + (\mathbf{k}_1\cdot\mathbf{k}_2 + m^2)\big[(a_1 - 2\mu_o^2)(a_2 - 2\mu_o^2) - 4\mu_o^2(\omega_n^2 + |\Delta_o|^2)\big] \Big\} \\[2mm] &= 2\beta \sum_{\alpha=\pm 1}\sum_{\lambda=\pm 1} \frac{\omega_\lambda + \alpha\mu_o}{\omega_\lambda} \frac{1}{E_\lambda^\alpha} \tanh\frac{\beta E_\lambda^\alpha}{2} \left[\frac{\mathbf{k}_\lambda\cdot(\mathbf{k}_{-\lambda} + \mathbf{k}_\lambda) + 2m^2}{\omega_{-\lambda}^2 - \omega_\lambda^2} \right] \,. \qquad \text{(E.39)} \end{aligned}$$

The coefficient of the squared vector potential is:

$$\begin{aligned} \mathcal{F}_{AA} &= 2e^2 \sum_n \frac{4}{N_1 N_2} \big[\mu_o^2(a_1 - 2\omega_1^2)(a_2 - 2\omega_2^2) - a_1 a_2(\omega_n^2 - |\Delta_o|^2)\big] \\ &\qquad + (\mathbf{k}_1\cdot\mathbf{k}_2 + m^2)\big[-(a_1 - 2\mu_o^2)(a_2 - 2\mu_o^2) + 4\mu_o^2(\omega_n^2 - |\Delta_o|^2)\big] \\[2mm] &= 2e^2\beta \sum_{\alpha=\pm 1}\sum_{\lambda=\pm 1} \frac{\omega_\lambda + \alpha\mu_o}{\omega_\lambda} \frac{1}{E_\lambda^\alpha} \tanh\frac{\beta E_\lambda^\alpha}{2} \left[\frac{\omega_\lambda^2 - (\mathbf{k}_\lambda\cdot\mathbf{k}_{-\lambda} + m^2)}{\omega_\lambda^2 - \omega_{-\lambda}^2} \right] \end{aligned}$$
$$\text{(E.40)}$$

with an additional term including $|\Delta_o|^2$ that may be omitted.

The last expression to be considered is

$$\begin{aligned} \mathcal{F}_{kA} &= 2e^2 \big[(a_1 - 2\mu_o^2)(a_2 - 2\mu_o^2) - 4\mu_o^2(\omega_n^2 - |\Delta_o|^2)\big] \\[2mm] &= 2e^2\beta \sum_{\alpha=\pm 1}\sum_{\lambda=\pm 1} \frac{\omega_\lambda + \alpha\mu_o}{\omega_\lambda} \frac{1}{E_\lambda^\alpha} \tanh\frac{\beta E_\lambda^\alpha}{2} \left[\frac{1}{\omega_\lambda^2 - \omega_{-\lambda}^2} \right] \qquad \text{(E.41)} \end{aligned}$$

where the additional term in $|\Delta_o|^2$ is also omitted.

E.2.4   Series expansion

We now turn to the expansion of the previous expressions in power series of **k** around **K**. Depending on the coefficients to be identified, the expansions should be performed up to the lowest or the second order, which means that some functions must be expanded up to third order in order to cancel one singularity sometimes appearing in the denominators. Let us define

$$
\begin{aligned}
\omega &= \sqrt{\mathbf{K}^2 + m^2} \\
E_\alpha &= \sqrt{(\omega + \alpha\mu_o)^2 + |\Delta_o|^2} \\
r_\alpha &= \frac{\omega + \alpha\mu_o}{\omega} \\
t_\alpha &= \tanh\frac{\beta E_\alpha}{2} \ .
\end{aligned}
\tag{E.42}
$$

In terms of these variables, we prove the following expansions:

(a) The common factor

$$
\frac{\omega_\lambda + \alpha\mu_o}{\omega_\lambda}\frac{1}{E_\lambda^\alpha}\tanh\frac{\beta E_\lambda^\alpha}{2} = r_\alpha\frac{1}{E_\alpha}\tanh\frac{\beta E_\alpha}{2} - C_1^\alpha\varepsilon_\lambda - C_2^\alpha\varepsilon_\lambda^2 - C_3^\alpha\varepsilon_\lambda^3
\tag{E.43}
$$

comes with the coefficients

$$
C_1^\alpha = \left[\frac{\alpha\mu_o}{2\omega^3 E_\alpha} + \frac{r_\alpha^2}{2E_\alpha^3}\right]t_\alpha - \frac{r_\alpha^2}{2E_\alpha^2}\frac{\beta}{2}(1 - t_\alpha^2)
$$

$$
\begin{aligned}
C_2^\alpha ={}& \left[-\frac{3\alpha\mu_o}{8\omega^5 E_\alpha} - \frac{3r_\alpha\alpha\mu_o}{8\omega^3 E_\alpha^3} - \frac{3r_\alpha^3}{8E_\alpha^5}\right]t_\alpha \\
&+ \left[\frac{3r_\alpha\alpha\mu_o}{8\omega^3 E_\alpha^2} + \frac{3r_\alpha^3}{8E_\alpha^4}\right]\frac{\beta}{2}(1 - t_\alpha^2) \\
&+ \frac{3\beta r_\alpha^3}{8E_\alpha^3}\frac{\beta}{2}(1 - t_\alpha^2)\,t_\alpha
\end{aligned}
\tag{E.44}
$$

$$
\begin{aligned}
C_3^\alpha ={}& \left[\frac{5\alpha\mu_o}{16\omega^7 E_\alpha} + \frac{\mu_o^2}{16\omega^6 E_\alpha^3} + \frac{r_\alpha\alpha\mu_o}{4\omega^5 E_\alpha^3} + \frac{3r_\alpha^2\alpha\mu_o}{8\omega^3 E_\alpha^5} + \frac{5r_\alpha^4}{16E_\alpha^7}\right]t_\alpha \\
&- \left[\frac{\mu_o^2}{16\omega^6 E_\alpha^2} + \frac{r_\alpha\alpha\mu_o}{4\omega^5 E_\alpha^2} + \frac{3r_\alpha^2\alpha\mu_o}{8\omega^3 E_\alpha^4} + \frac{5r_\alpha^4}{16E_\alpha^6}\right]\frac{\beta}{2}(1 - t_\alpha^2) \\
&- \frac{\beta}{8}\left[\frac{\alpha\mu_o r_\alpha^2}{\omega^3 E_\alpha^3} + \frac{r_\alpha^4}{E_\alpha^5}\right]\frac{\beta}{2}(1 - t_\alpha^2)\,t_\alpha \\
&- \frac{\beta^2}{48}\frac{r_\alpha^4}{E_\alpha^4}\frac{\beta}{2}(1 - t_\alpha^2)\,t_\alpha^2 \\
&+ \frac{\beta r_\alpha^4}{48E_\alpha^4}\left[\frac{\beta}{2}(1 - t_\alpha^2)\right]^2 \ .
\end{aligned}
$$

(b) The term from the Δ^2 contribution

$$\frac{\mathbf{k}_\lambda \cdot (\mathbf{k}_{-\lambda} - \mathbf{k}_\lambda) - 2\alpha\mu_o\omega_\lambda}{(\omega_\lambda^2 + 2\alpha\mu_o)^2 - \omega_{-\lambda}^2}$$

$$= -\frac{1}{r_\alpha}\left[1 + \lambda\,\frac{\mathbf{k}\cdot\mathbf{K}}{2\omega^2} + \frac{1}{4\alpha\mu_o\omega}\left(1 + \frac{\mu_o^2}{1\omega^2 r_\alpha}\right)\left(\mathbf{k}^2 - \frac{(\mathbf{k}\cdot\mathbf{K})^2}{\omega^2}\right)\right] \quad \text{(E.45)}$$

(c) The term from the μ^2 contribution

$$\frac{\mathbf{k}_\lambda \cdot (\mathbf{k}_{-\lambda} + \mathbf{k}_\lambda) + 2m^2}{\omega_{-\lambda}^2 - \omega_\lambda^2} = \frac{2\omega^2 + \lambda\,\mathbf{k}\cdot\mathbf{K}}{-2\lambda\,\mathbf{k}\cdot\mathbf{K}}. \quad \text{(E.46)}$$

(d) The term from the $\mathbf{A}^2$ contribution

$$\frac{\omega_\lambda^2 - (\mathbf{k}_\lambda \cdot \mathbf{k}_j + m^2)}{\omega_\lambda^2 - \omega_{-\lambda}^2} = \frac{1}{2} + O(\mathbf{k})\ . \quad \text{(E.47)}$$

(e) The $(\mathbf{k}\cdot\mathbf{A})^2$ contribution

$$\frac{1}{\omega_\lambda^2 - \omega_{-\lambda}^2} = \frac{1}{2\lambda\,\mathbf{k}\cdot\mathbf{K}}\ . \quad \text{(E.48)}$$

Finally, we retain the following contributions:

$$S_{\text{eff}}^{(2)}[\Delta\Delta]\ :\ \int \frac{d^3\mathbf{k}}{(2\pi)^3}\,\mathbf{k}^2\,\overline{\Delta}^\dagger(\mathbf{k})\overline{\Delta}(\mathbf{k})\ \times$$

$$\int \frac{d^3\mathbf{K}}{(2\pi)^3} \sum_{\alpha=\pm 1}\left\{\frac{1}{8r_\alpha}\left[1 + \frac{2\mathbf{K}^2}{3\omega^2}\right]C_1^\alpha + \frac{\mathbf{K}^2}{6r_\alpha}C_2^\alpha\right.$$

$$\left. -\frac{1}{E_\alpha}t_\alpha\,\frac{1}{8\alpha\mu_o\omega}\left[1 + \frac{\mu_o^2}{2\omega^2 r_\alpha}\right]\left[1 - \frac{\mathbf{K}^2}{3\omega^2}\right]\right\}$$

$$S_{\text{eff}}^{(2)}[\mu\mu]\ :\ \int \frac{d^3\mathbf{k}}{(2\pi)^3}\,\mathbf{k}^2\,\overline{\mu}(-\mathbf{k})\overline{\mu}(\mathbf{k})\ \times$$

$$\int \frac{d^3\mathbf{K}}{(2\pi)^3} \sum_{\alpha=\pm 1}\left\{\frac{\omega^2}{2}\left[C_2^\alpha + \frac{2\mathbf{K}^2}{3}C_3^\alpha\right] + \frac{1}{8}\left[C_1^\alpha + \frac{4\mathbf{K}^2}{3}C_2^\alpha\right]\right\}$$

$$S_{\text{eff}}^{(2)}[AA]\ :\ \int \frac{d^3\mathbf{k}}{(2\pi)^3}\,e^2\mathbf{A}(-\mathbf{k})\mathbf{A}(\mathbf{k})\ \times$$

$$\int \frac{d^3\mathbf{K}}{(2\pi)^3} \sum_{\alpha=\pm 1}\left\{-\alpha(\mu_o^2 + \alpha\mu_o\omega)\frac{2\mathbf{K}^2 + 3m^2}{6\omega^3 E_\alpha}\,t_\alpha - \frac{\mathbf{K}^2}{6\omega^2}\frac{\beta}{2}(1 - t_\alpha^2)\right\}\ . \quad \text{(E.49)}$$

BIBLIOGRAPHY

[1] H. Kamerlingh Onnes. *Leiden Comm.* **120b, 122b, 124c** (1911).

[2] Nobel Foundation Ed. *Nobel Lectures. Physics 1901-1921.* Elsevier, Amsterdam (1967).

[3] G. Vidali. *Superconductivity, the Next Revolution?* Cambridge University Press, Cambridge (1993).

[4] W. Meissner and R. Oschenfeld. *Naturwiss.* **21**, 787 (1933).

[5] J.D. Jackson. *Classical Electrodynamics, 2nd ed.* J. Wiley & sons, New York (1975).

[6] F. London and H. London. *Proc. R. Soc. London* **A149**, 71 (1935).

[7] C.G. Kuper. *An Introduction to the Theory of Superconductivity.* Clarendon Press, Oxford (1968).

[8] C.J. Gorter and H.B.G. Casimir. *Phys. Z.* **35**, 963 (1934).

[9] A.B. Pippard. *Proc. Roy.Soc. London* **A 216**, 547 (1953).

[10] V.L. Ginzburg and L.D. Landau. *Zh. Eksp. Teor. Fiz.* **20**, 1064 (1950).

[11] G. Stenuit. *Configuration de Vortex Magnétiques dans des Cylindres Supraconducteurs.* PhD thesis, UCL, Louvain-la-Neuve, (2004).

[12] J. Tate, S.B. Felch, and B. Cabrera. *Phys. Rev.* **B 42**, 7885 (1990).

[13] M. Tinkham. *Introduction to Superconductivity, 2nd ed.* McGraw-Hill Inc., New York (1996).

[14] J.R. Waldram. *Superconductivity of Metals and Cuprates*. IOP Publishing, Bristol (1996).

[15] A.A. Abrikosov. *Zh. Eksp. Teor. Fiz.* **32**, 1442 (1957). English trad. in Sov. Phys. JETP, **5**, 1174 (1957).

[16] U. Essmann and H. Träuble. *Phys. Lett.* **A 24**, 526 (1967).

[17] J. Bardeen, L.N. Cooper, and J.R. Schrieffer. *Phys. Rev.* **108**, 1175 (1957).

[18] H. Fröhlich. *Phys. Rev.* **79**, 845 (1950).

[19] N.N. Bogoliubov. *Zh. Eksp. Teor. Fiz.* **34**, 58 (1958). English trad. in Sov. Phys. JETP, **7**, 41 (1958).

[20] J.G. Bednorz and K.A. Müller. *Z. Phys.* **B64**, 189 (1986).

[21] J. Nagamatsu, N. Nakagawa, T. Muranaka, Y. Zenitani, and J. Akimitsu. *Nature* **410**, 63 (2001).

[22] A.K. Geim, I.V. Gregorieva, S.V. Dubonos, J.G.S. Lok, J.C. Maan, A.E. Filippov, and F.M. Peeters. *Nature* **390**, 259 (1997).

[23] V.A. Schweigert and F.M. Peeters. *Phys. Rev.* **B 57**, 13 817 (1998).

[24] G. Stenuit, S. Michotte, J. Govaerts, L. Piraux, and D. Bertrand. In *Proceedings of the International Conference on Modern Problems in Superconductivity, Mod. Phys. Lett.*, **B 17**, 537 (2003).

[25] S. Michotte. *Elaboration et Propriétés Physiques de Nanofils Supraconducteurs de Plomb et d'Etain Electrodéposés*. PhD thesis, UCL, Louvain-la-Neuve, (2005).

[26] G. Stenuit, S. Michotte, J. Govaerts, and L. Piraux. *Supercond. Sci. Technol.* **18**, 174 (2005).

[27] W.A. Little and R.D. Parks. *Phys. Rev. Lett.* **9**, 9 (1962).

[28] D. Saint-James. *Phys. Rev.* **15**, 13 (1965).

[29] P. Singha Deo, V.A. Schweigert, F.M. Peeters, and A.K. Geim. *Phys. Rev. Lett.* **79**, 4653 (1997).

[30] V.A. Schweigert, F.M. Peeters, and P. Singha Deo. *Phys. Rev. Lett.* **81**, 2783 (1998).

[31] J.J. Palacios. *Phys. Rev.* **B 58**, R5948 (1998).

[32] J.J Palacios. *Physica* **B 256-258**, 610 (1998).

[33] E.H. Brandt. *Phys. Rev. Lett.* **78**, 2208 (1997).

[34] V. Bruyndoncx, L. Van Look, M. Verschuere, and V.V. Moschalkov. *Phys. Rev.* **B 60**, 10468 (1999).

[35] J. Govaerts, G. Stenuit, D. Bertrand, and O. van der Aa. *Phys. Lett.* **A 267**, 56 (2000).

[36] G. Stenuit, J. Govaerts, D. Bertrand, and O. van der Aa. In *Proceedings of the 1st European Conference on Vortex Matter in Superconductors, Physica*, **C 332**, 277 (2000).

[37] F. London and H. London. *Proc. R. Soc. London* **A155**, 102 (1936).

[38] F. Bopp. *Zeit. f. Physik* **107**, 623 (1937).

[39] A.G. van Vijfeijken and F.S. Staas. *Phys. Lett.* **12**, 175 (1964).

[40] E. Jakeman and E.R. Pike. *Proc. Phys. Soc.* **91**, 422 (1967).

[41] G. Rickayzen. *J. Phys.* **C 2**, 1334 (1969).

[42] P. Lipavský, J. Koláček, K. Morawetz, and E.H. Brandt. *Phys. Rev.* **B 65**, 144 511 (2002).

[43] H. Lewis. *Phys. Rev.* **92**, 1149 (1953).

[44] R. Jaggi and R. Sommerhalder. *Hel. Phys. Acta* **32**, 167 (1959).

[45] J. Bok and J. Klein. *Phys. Rev. Lett.* **20**, 660 (1968).

[46] J.B. Brown and T.D. Morris. *Proc. 11th Int. Conf. Low Temp. Phys.* **2**, 768 (1968). see also T.D. Morris and J.B. Brown, *Physica* **55**, 760 (1971).

[47] Y.N. Chiang and O.G. Schevchenko. *Fiz. Nizk. Temp.* **22**, 669 (1996).

[48] D.I. Khomskii and A. Freimuth. *Phys. Rev. Lett.* **75**, 1384 (1995).

[49] K. Kumagai, K. Nokazi, and Y. Matsuda. *Phys. Rev.* **B 63**, 144 502 (2001).

[50] S.V. Yampolskii, B.J. Baelus, and F.M. Peeters. *Phys. Rev.* **B 64**, 144 511 (2001).

[51] R.E. Glover and D.M. Sherill. *Phys. Rev. Lett.* **5**, 248 (1960).

[52] T. Frey, J. Manhart, J.G. Bendorz, and E.J. Williams. *Phys. Rev.* **B 51**, 3257 (1995).

[53] B.Y. Shapiro. *Phys. Lett.* **A 197**, 361 (1995).

[54] T.J. Yang and W.D. Lee. *Physica* **C 341-348**, 291 (2000).

[55] H.B. Nielsen and P. Olesen. *Nucl. Phys.* **B 61**, 45 (1973).

[56] J. Govaerts, D. Bertrand, and G.Stenuit. *Supercond. Sci. Technol.* **14**, 463 (2001).

[57] D. Bertrand. *Propriétés Critiques de Supraconducteurs Mésoscopiques sous Champs Électromagnétiques Stationnaires*. Master thesis, UCL, Louvain-la-Neuve, (2000).

[58] R.-M. Hervé and M. Hervé. *Ann. Inst. H. Poincaré* **11**, 427 (1994).

[59] J. Govaerts. *J. Phys.* **A 34**, 8955 (2001).

[60] S.V. Yampolskii and F.M. Peeters. *Phys. Rev.* **B 62**, 9663 (2000).

[61] H. Zhao, V.M. Fomin, J.T. Devreese, and V.V. Moshchalkov. *Solid State Comm.* **125**, 59 (2003).

[62] D. Bertrand, J. Govaerts, and G. Stenuit. In *Proceedings of the 2nd European Conference on Vortex Matters in Superconductors, Physica*, **C 369**, 339 (2002).

[63] D. Bertrand. *Etude des États Quantiques d'Anneaux Mésoscopiques Supra-conducteurs*. Diploma thesis, UCL, Louvain-la-Neuve, (1999).

[64] S. Melinte. *Quantum Hall Effect Skyrmions: Nuclear Magnetic Resonance and Heat Capacitiy Measurements*. PhD thesis, UCL, Louvain-la-Neuve, (2001).

[65] B. Hackens. *Coherent and Ballistic Transport in InGaAs and Bi Mesoscopic Devices*. PhD thesis, UCL, Louvain-la-Neuve, (2005).

[66] http://www.semiconfareast.com/sio2si3n4.htm.

[67] L.P. Gor'kov. *Zh. Eksp. Teor. Fiz.* **36**, 1364 (1959).

[68] J.I. Kapusta. *Finite Temperature Field Theory*. Cambridge University Press, Cambridge (1989).

[69] M. Le Bellac. *Thermal Field Theory*. Cambridge University Press, Cambridge (1996).

[70] M.E. Peskin and D.V. Schroeder. *An introduction to Quantum Field Theory*. Addison-Wesley, Reading (1995).

[71] K. Capelle and E.K.U Gross. *Phys. Rev.* **B 59**, 7140 (1999).

[72] K. Capelle and E.K.U Gross. *Phys. Rev.* **B 59**, 7154 (1999).

[73] M. Marques K. Capelle and E.K.U. Gross. *Cond. Matt. Theories* **16**, 253 (2001).

[74] T. Ohasaku. *Phys. Rev. B* **65**, 024 512 (2002).

[75] T. Ohasaku. *Phys. Rev.* **B 66**, 054 518 (2002).

[76] H.T.C. Stoof. *Phys. Rev.* **B 47**, 7979 (1993).

[77] R. Casalbuoni. *Rev. Mod. Phys.* **76**, 263 (2004).

[78] M. Fierz. *Z. Physik* **104**, 553 (1937).

[79] C. Itzykson and J.-B. Zuber. *Quantum Field Theory*. McGraw-Hill, New York (1980).

[80] P.W. Anderson. *J. Phys. Chem. Solids* **11**, 26 (1959).

[81] N.W. Ashcroft and N.D. Mermin. *Solid State Physics*. Holt, Rinehart & Winston, New York (1976).

[82] C. Kittel. *Introduction to Solid State Physics*. John Wiley & sons, New York3rd edition (1966).

[83] J. Hubbard. *Pys. Rev. Lett.* **3**, 77 (1959).

[84] G.M. Eliashberg. *Zh. Eksp. Theor. Fiz.* **38**, 966 (1960). eng. transl. *Sov. Phys. JETP* **11** (1960) 696.

[85] A. Nieto. *Comput. Phys. Commun.* **92**, 54 (1995).

[86] J. Koláček, P. Lipavský, and E.H. Brandt. *Physica* **C 369**, 55 (2002).

[87] J. Govaerts. *Hamiltonian Quantisation and Constrained Dynamics*. Leuven University Press, Leuven (1991).

[88] J.E. Hirsch. *Phys. Rev.* **B 68**, 184 502 (2003).

[89] T. Koyama. *Phys. Rev.* **B 70**, 226 503 (2004).

[90] J.E. Hirsch. *Phys. Rev.* **B 70**, 226 504 (2004).

[91] P. Debye and E. Hückel. *Phys. Z.* **24**, 185 (1923).

[92] H.D. Young. *University Physics, 8th ed.* Addison Wesley, Boston (1992).

[93] B. Van Zeghbroeck. *Principles of semiconductor devices*. Online textbook available for download at
`http://ece-www.colorado.edu/˜bart/book/` (2004).

[94] M. Kaku. *Quantum Field Theory, a Modern Introduction*. Oxford University Press, New York (1993).

[95] R.P. Feynman. *Rev. Mod. Phys.* **20**, 367 (1948).

[96] E. Fradkin, *General Field Theory*. Notes from lectures given at the University of Illinois at Urbana-Champaign, available for download at
`http://w3.physics.uiuc.edu/ efradkin`.

[97] R. McKenzie. quant-ph/0004090, (27 December 1999 - 8 January 2000). Lectures given at the VIth Vietnam School of Physics, Vung Tau, Vietnam.